# AN ANALYSIS OF THERMAL ANHARMONICITY IN SOME CUBIC PEROVSKITES

THESIS

SUBMITTED BY

JOHN HUTTON

FOR THE DEGREE OF

DOCTOR OF PHILOSOPHY

UNIVERSITY OF EDINBURGH

1979

Except where otherwise stated, the research undertaken in this thesis was the unaided work of the author. Where the work was done in collaboration with others, a significant contribution was made by the author.

ACKNOWLEDGEMENTS

I would like to record my thanks to all those who have helped me in the course of this work. In particular, the following :

Dr R J Nelmes, for his conscientious and very able supervision and unflagging interest throughout ;

Professors W Cochran and R A Cowley, for extending to me the facilities of the Department of Physics ;

Dr A D Bruce, for his highly valued and often timely comments ;

Professor K Kurki-Suonio and his colleagues at the University of Helsinki, who introduced me to the methods of Fourier-invariants ;

Mr J Allibon of the Institut Laue-Langevin, Grenoble, Mr G Proudfoot of A.E.R.E., Harwell and Mr T Ryan of this Department, for their excellent technical support and advice ;

The Science Research Council, for financial support ;

Mrs Linda Halstead, for the excellent way she has typed this manuscript ;

My parents, for their encouragement at all times ;

and my wife, Linda, who has been my greatest source of encouragement and support throughout.

ABSTRACT

High-resolution neutron elastic-diffraction data have been collected for the cubic perovskites $CsPbCl_3$, $RbCaF_3$, $KMnF_3$ and $SrTiO_3$ at a few degrees above their cubic → tetragonal phase transition temperatures, $T_c$. Similar data have also been collected for $RbCaF_3$ and $KMnF_3$ at room temperature - well above the transition.

Use of both cumulant- and Fourier-invariant-expansion formalisms in the characterisation of anharmonic temperature factors is examined. The relative merits of each formalism are compared with particular reference to computational aspects and to the ease with which reliable descriptions of atomic probability density functions may be derived. It is found that the regimes of validity of both formalisms fall considerably short of systems displaying classically disordered microstructure. The superiority of Fourier-invariant techniques in the regime of relatively small anharmonic thermal motion is, however, clearly established.

Cumulant and Fourier-invariant expressions have been used in the analysis of the data collected for the cubic perovskites. It is found that such anharmonicity as does exist in these crystals just above $T_c$ is predominantly associated with the thermal motion of the cations; that the magnitude and significance of this anharmonicity varies considerably between the different cations; but that its structure shows similar features in each. The motion of the cations is shown to be preferentially in the plane of the cubic unit cell face; a further slight preference is established for motion in the directions along which the ions are known to displace on passing to the lower-temperature phase. Clear evidence is found, for $RbCaF_3$ and $KMnF_3$, that the thermal anharmonicity of the cations is anomalously enhanced just above $T_c$, while that of the anions is qualitatively as expected.

Suggestions are made as to the nature of further work which will be required in order to clarify the full range of anharmonic atomic distributions susceptible to meaningful analysis by elastic-diffraction techniques.

TABLE OF CONTENTS

# CHAPTER 1 : INTRODUCTION

# CHAPTER 1 : INTRODUCTION

## 1.1 OBJECTIVES

The overall aim of this thesis is to carry out an examination of the methods and problems associated with the collection and analysis of high-resolution neutron elastic-diffraction data. In particular, attention is focused on systems falling in the region between those describable in terms of purely harmonic thermal motions and those in which the atoms are classically and unambiguously disordered over spacially distinct sites. An attempt is made to probe the suitability and potential yield of general anharmonic temperature-factor formalisms over a wide range of anharmonicity and, in particular, to examine the ease with which reliable descriptions of the corresponding real-space probability density function (p.d.f.) may be extracted.

The systems studied all undergo structural phase transitions and the p.d.f.'s derived from these analyses are examined in the light of recent theoretical ('cluster' model) thinking as to possible types of non-linear atomic motion near the transition temperature, $T_c$.

Considerable effort is put throughout into the identification of spurious effects arising from model inadequacies and into an examination of the statistical justification for the conclusions reached.

## 1.2 CLUSTER MODELS

In the last ten years or so it has become apparent that the long-serving phenomenology of the soft mode (Cochran (1960); Anderson (1960)) cannot explain various observed features of quasi-elastic response. The experiments which aroused much of the initial interest were those performed by Riste et al (1971) and Shapiro et al (1972) in which a two-component response was observed

in the spectral functions of $SrTiO_3$ and $KMnF_3$ above their high-temperature phase transitions. One component was found to soften as expected but to saturate above $T_c$. In the case of $KMnF_3$, the soft phonons were overdamped 40°K above the transition. The other component - the so-called *central peak* - at zero energy transfer, was observed to form at temperatures well above $T_c$ and to grow critically as the transition was approached. Qualitatively similar features have since been reported in many compounds, for example, lead germanate (Cowley et al (1976)).

Considerable theoretical interest has been shown in the problem although no rigorous or universally accepted solution has yet been formulated (see the review by Bruce and Cowley (1979)). What does seem clear is that a significant part of the additional, non-classical response can be attributed to extrinsic effects such as strain fields set up by crystal defects (Halperin and Varma (1976)); however, it is now generally held that intrinsic effects are at least partly responsible.

One particularly interesting line of approach has grown around the proposition that just above $T_c$ there occurs a change in the collective motion of the atoms in the crystal (Bruce (1978)); that, as the short-range order increases in the critical region, there is a crossover from a system displaying a predominantly displacive form to one which is of a classical order-disorder type. The concept of universality is therefore a central feature of this type of thinking, linking as it does two regimes which have often previously been treated as conceptually (and intrinsically) distinct.

Is is not the intention here to give a resume of the current theoretical status of this very complex and continually evolving field; rather it is hoped to illustrate some of the more easily interpreted experimental results which may be of use in formulating models for the test refinements of Chapter 2.5, and which may in themselves suggest plausible models for the crystals studied (Chapter 4).

The most illuminating manifestations of the crossover from 'displacive' to 'order-disorder' regimes, referred to above, have emerged from studies of low-dimensional model systems. Using a one-dimensional model Hamiltonian, Krumhansl and Schrieffer (1975) obtained solutions to the resulting non-linear equation of motion which may be interpreted as travelling 'cluster' waves. Computer-simulation techniques have been used by Schneider and Stoll (1976) to demonstrate the formation of regions with non-zero local order parameter (clusters) whose spacial extent is found to increase as $T_c$ is approached from above. Within each cluster the atoms are displaced towards one of their possible positions in the low-temperature phase (below $T_c$), the displacement (called the local order parameter and denoted $\delta$) being constant throughout the cluster but changing at the cluster wall. (However, the vector sum of all such displacements above $T_c$ must be zero in a homogeneous crystal.) It is further postulated (Bruce et al (1979)) that the change from one configuration to another within a cluster occurs on a timescale much longer than typical inverse phonon frequencies. A series of 'snap-shots' taken just above $T_c$ at small time intervals, $\delta t$, will then reveal spacially distinct regions of non-zero $\delta$ which will change their configuration over some time interval of many $\delta t$. The atomic p.d.f. will therefore be intrinsically multi-peaked at any instant.

Until recently, direct experimental support for this type of microstructure in real three-dimensional systems has been lacking; however, the EPR results of Bruce et al (1979) for monodomain transforming $SrTiO_3$ (see Section 4) are at least highly indicative of such underlying two-timescale dynamics. Moreover, their findings do in fact suggest evidence of a simple type of ordering similar to that obtained by Krumhansl and Schrieffer (1975) for their highly idealised, one-dimensional model system. For the sake of definiteness, any further reference in this thesis to a 'cluster model' will imply a system displaying the simple intrinsic manifestations of disorder outlined in the previous paragraph. It should be borne in mind, though, and is reiterated, that the theoretical justification for the existence of such behaviour in a

real three-dimensional system has not yet been unambiguously established.

It must also be realised that the existence of two-timescale dynamics constitutes the only *absolute* distinction between the cluster model and a model based on anharmonic (one-timescale) phonon theory. It is possible (if unlikely) to envisage within the latter, the existence of regions with non-zero $\delta$. Clearly then, experimental verification of cluster-model dynamics is only strictly possible by suitable discrimination between frequencies - as in the EPR experiment of Bruce et al (1979). However, the observation of such intrinsic multi-peaking in any atomic p.d.f. just above a structural phase transition could be taken as highly suggestive of a plausible interpretation within the cluster formalism (as it is outlined here).

## 1.3 ANHARMONICITY

It has been, and still is in many cases, assumed that atoms in a real crystal can be treated in elastic-diffraction analyses as though they vibrate in harmonic potential wells : in other words that they can be treated as independent, Einsteinian, harmonic oscillators. This led to a great simplification of the analysis required in the refinement of crystal structures (as outlined in Chapter 2.2), and it is only comparatively recently (Lonsdale (1962)), with the availability of large-scale digital computers, that progress has been made in taking account of non-harmonic interactions.

The approximate nature of the above assumption has been recognised for a long time. It is apparent that many observed physical properties of real crystals (for example, thermal expansion) are incompatible with purely harmonic models. Of particular relevance from the point of view of the present study, is the fact that a system undergoing a structural phase transition *must* be anharmonic (Bruce (1978)). Recently, direct evidence of

anharmonicity has been obtained from a variety of experiments : the determination of non-zero third-order elastic constants in Zn (Schwartz and Elbaum (1970)), the occurrence of 'forbidden' reflections in white tin (Merisalo and Järvinen (1978)), among many others.

Details of the modifications to the temperature factor due to thermal expansion - the so-called quasi-harmonic contribution - have been summarised by Willis (1969). It is assumed that the force constants soften when the crystal expands and that the relative change in frequency of the normal modes is the same for each mode. This change in frequency is proportional to $-T(^{o}K)$, the proportionality constant being the product of the Gruneisen constant, $\gamma_G$, and the volume coefficient of expansion, $\chi$. The quasi-harmonic temperature factor is then obtained from the harmonic one by multiplication by $(1 + 2\ \gamma_G\ \chi T)$. Using the KCl X-ray diffraction data of James and Brindley (1928), Willis shows that most of the anharmonicity observed in the temperature dependence of the Bragg intensities (for KCl) can be accounted for in terms of thermal expansion.

For the cases in which it can not, two principal methods of approaching the problem have been investigated. The first, and more rigorous, involves the estimation of anharmonic contributions to the measured Bragg intensities by a lattice dynamical calculation. However, such calculations are extremely difficult and virtually intractable for all but the simplest structures (see, for example, Maradudin and Flinn (1963)). The second type of approach, and the one with which this thesis is mainly concerned, involves the parameterisation of the anharmonic effects in some discernable atomic quantity such as the p.d.f. or the effective single-particle potential. It is then possible to refine the corresponding anharmonic parameters in the modified temperature factor together with those of the conventional (harmonic) thermal model.* This approach, in contrast to the first, does not, therefore, presuppose any knowledge of the microscopic interactions within the crystal.

---

* Much of the pioneering theoretical work, and the first applications to the refinement of crystal structures, were carried out by Dawson and his coworkers (Dawson (1967, 1967a); Dawson et al (1967); Dawson and Willis (1967)). Using temperature factors based on their formalism, successful analyses have since been carried through for a variety of compounds (see, for example, the study of $BaF_2$ by Cooper et al (1968)).

Following Willis (1969), the atomic temperature factor, $W_j(\underline{Q})$, is given by the ensemble average of the quantity $\exp(i\underline{Q} \cdot \underline{r}_j)$, where $\underline{r}_j$ denotes the thermal displacement of the $j^{th}$ atom from its mean position and $\underline{Q}$ is a reciprocal lattice vector. $\langle \exp(i\underline{Q} \cdot \underline{r}_j) \rangle$ can be calculated by assigning to each $\exp(i\underline{Q} \cdot \underline{r}_j)$ a thermodynamic probability based on the form chosen for the atomic potential. Usually (see, for example, Merisalo and Larsen (1977); Prager and Harvey (1975)), the potential is expanded as a power series in terms of $r_1$, $r_2$ and $r_3$, the Cartesian coordinates of the atomic displacement.

It is common practice to partition the anharmonic temperature factor, and expressions derived therefrom such as the atomic p.d.f., into constituent parts : '*the* harmonic part' and '*the* anharmonic part' are used in the literature in a rather arbitrary (although consistent and mathematically well defined) way. This essentially derives from the fact that any anharmonic contribution is usually considered as a perturbation to be added to an underlying, dominant, harmonic distribution. Such a division may be made for one or both of the following reasons. First, the analysis technique may be inadequate unless some artificial division is made. For example, depending upon the size and range of the sample space (the list of observed structure amplitudes - see Chapter 3.6), it may prove impossible to refine simultaneously parameters describing second- (harmonic) and higher-order effects. Johnson (1970) suggests that an observation/parameter ratio of at least 5:1 be maintained in the refinements and many authors (Merisalo and Larsen (1977); Kurki-Suonio et al (1979)) have encountered insuperable parameter correlation problems. Second, it may seem conceptually beneficial to do so. A situation, in many ways analogous, exists in the division of a distribution into isotropic and anisotropic components (Willis (1969)). This division is often made so that the anisotropic contributions sum to zero over the sphere defining the isotropic distribution, and assuming proper normalisation, can only be made when the best-fitting isotropic distribution is found first. The difference

between the two distributions then gives an immediate indication of the way in which 'the' isotropic (or harmonic) part is modified by the presence of anisotropic (or anharmonic) components. In their discussion, Merisalo and Larsen (1977) point to the fact that the refined parameters which they obtain in their expression for the anharmonic potential in Zn can take widely different sets of values and still result in identical fits to their data. They contend that this is due to parameter correlation and conclude, for one of the sets of refined parameters, that 'part of the anharmonic contribution is included in the harmonic parameters'. Implicitly recognising the difficulties involved in making any absolute division, they go on to examine the effects due to anharmonicity in terms of so-called integral parameters (presumably meaning those likely to be independent of parameter correlation effects) such as thermal mean-square amplitudes (m.s.a.'s). This theme is taken up later by Kurki-Suonio et al (1979).

From the limited number of examples discussed here, and from a study of the available literature, several points emerge.

(i) It seems that, although the problem of thermal anharmonicity is demonstrably a real one to be faced in crystallographic refinements, few estimates have been made of the range over which the methods presently available are expected to be satisfactory.

(ii) Results derived using different methods have seldom been compared - the work of Kurki-Suonio et al (1979) is an exception.

(iii) There appears to be some doubt as to whether anharmonic parameters *can* be meaningfully and unambiguously interpreted.

(iv) Care must be taken to ensure that any conclusions reached as regards possible anharmonic thermal motion are physically reasonable. As pointed out by Merisalo and Järvinen (1978), the observation of 'forbidden' reflections in white tin by Field (1976) cannot result from anharmonic atomic vibration as suggested by Field (since then the true crystal symmetry would be violated); rather, it must be due to either multiple scattering or higher-order wavelength contamination.

## 1.4 PEROVSKITES

Although the name 'perovskite' has been given specifically to the substance with chemical formula $CaTiO_3$, it is also commonly used to denote the family of ionic compounds with general formula $ABX_3$. Here, A and B are monovalent and divalent metal ions respectively and X are halogen or oxygen ions. In the high-temperature phase, the structure is simple cubic with each ion occupying a site of high symmetry in the unit cell as shown in Figure 1.4.1. *The* perovskite structure will hereafter be used to denote this particular structure.

Quite apart from recent, potentially useful applications in industry (Mel'nikova et al (1977)) these compounds have been well studied because of many characteristics of theoretical interest which they exhibit. Many are found to undergo structural or magnetic phase transitions, often accompanied by drastic, anomalous behaviour in their physical properties.

The sequence $CsPbCl_3 \rightarrow RbCaF_3 \rightarrow KMnF_3 \rightarrow SrTiO_3$ is the subject of the present study. Each of these compounds has been found to undergo an antiferroelectric cubic$\rightarrow$tetragonal phase transition (at temperatures ranging from $325^oK$ for $CsPbCl_3$ to $105^oK$ for $SrTiO_3$) characterised by a small rotation of the $BX_6$ octahedra about one of the $\langle 1,0,0 \rangle$ axes (see Figure 1.4.2). The metal-ion

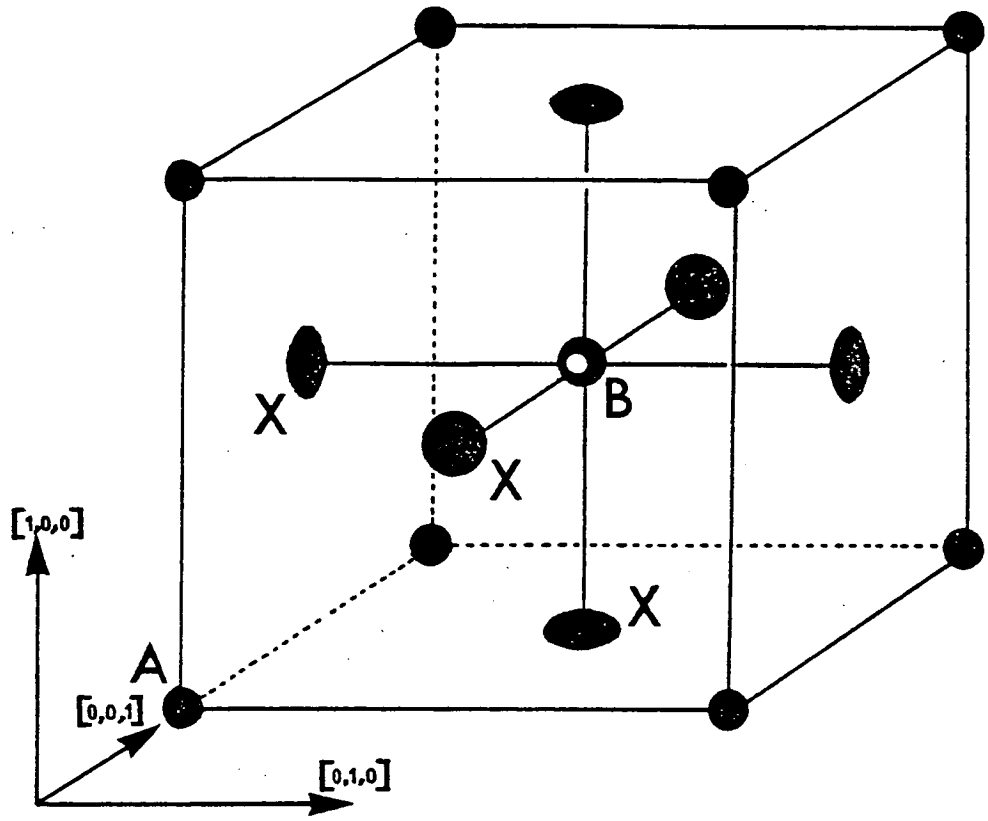


Figure 1.4.1 The sites occupied in the standard perovskite structure. One cubic unit cell is shown. The (arbitrary) labelling of the axes is to establish a consistent convention between diagram and diagram, and between diagram and text.

| Ion Type | Site Symmetry | Coordinates |
|---|---|---|
| A | m3m | (0,0,0) |
| B | m3m | $(\frac{1}{2},\frac{1}{2},\frac{1}{2})$ |
| X | 4/mmm | $(\frac{1}{2},\frac{1}{2},0)$; $(0,\frac{1}{2},\frac{1}{2})$; $(\frac{1}{2},0,\frac{1}{2})$ |

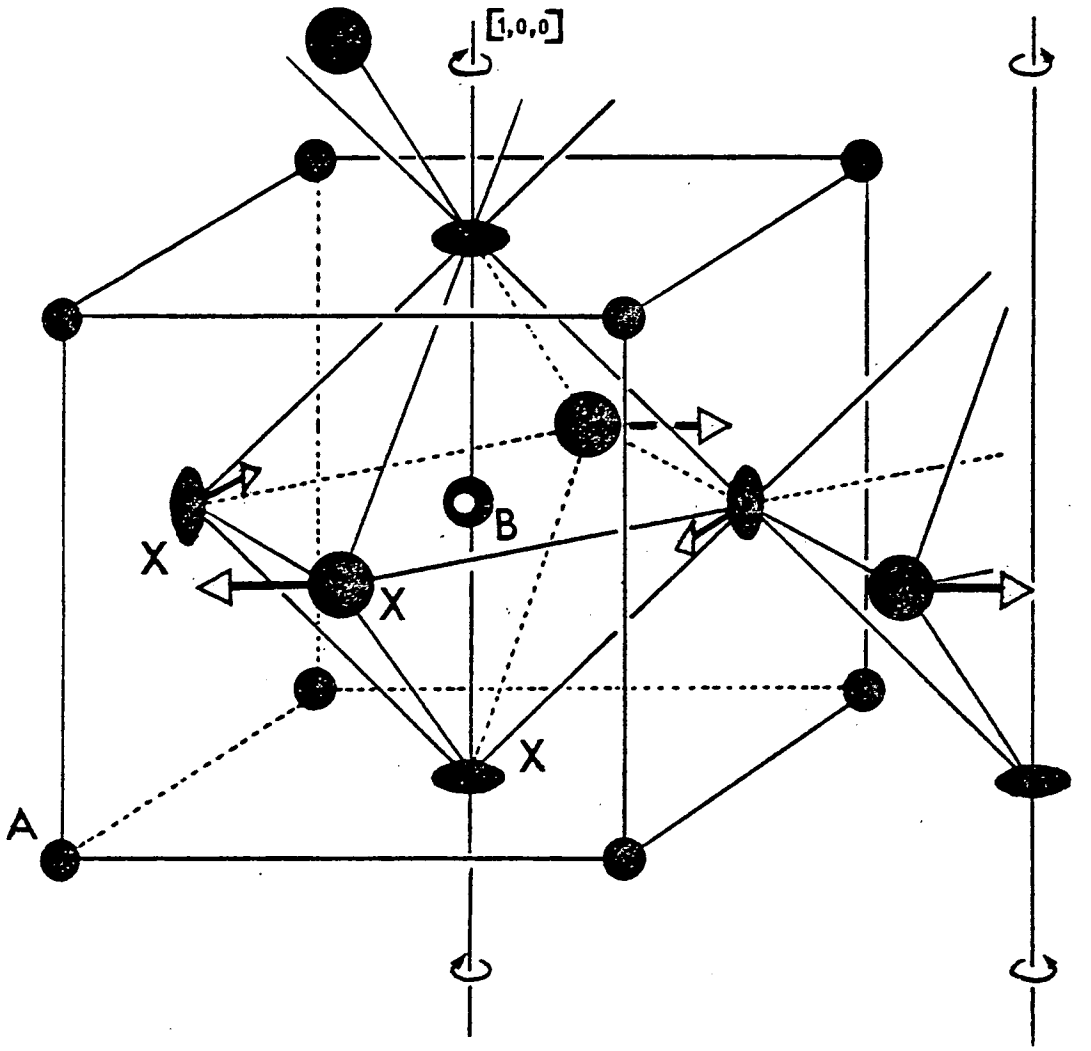


Figure 1.4.2 The displacement patterns of the X ions in the cubic perovskite $ABX_3$ arising from $M_3$- and $R_{25}$- mode vibration. For the $M_3$ mode, the $BX_6$ octahedra oscillate about one of the $\langle 1,0,0 \rangle$ directions - here denoted [1,0,0] - and are in phase along their oscillation axis as shown; the rotations about nearest-neighbour parallel axes are in antiphase. When the mode condenses, the X ions move to new positions in the directions shown arrowed. For the $R_{25}$ mode (not explicitly illustrated here), the successive $BX_6$ octahedra oscillate in *antiphase* along [1,0,0].

sublattice remains essentially rigid on passing through $T_c$. Bearing in mind the equivalence of the three principal crystal axes above $T_c$, it is clear that below the transition the X ion may take up one of several positions (see Figure 1.4.3) : to sites 1 or 2 if the rotation is about [ 1,0,0 ] , to sites 3 or 4 if the rotation is about [ 0,1,0 ] and to sites 5 or 6 (coincident and undisplaced) if the rotation is about [ 0,0,1 ] - using the arbitrary axes adopted in the diagram. The low-temperature phase is thus characterised by an order parameter, $\delta_o$, the displacement of the X ion from its high-symmetry position to one of the sites 1, 2, 3 or 4.

In the spirit of the simplified cluster model as developed in Section 2 - and neglecting effects due to domain walls (Cowley et al (1976)) - a homogeneous perovskite crystal just above $T_c$ is then composed equally of regions in which the X ion is displaced to sites 1/2, or to sites 3/4, or undisplaced at sites 5/6. (So, for these perovskites, *three* distinguishable clusters are 'predicted', though any one unit cell may assume six different configurations.) It seems intuitively clear that the magnitude of the displacement, $\delta$ , will be less than that of $\delta_o$. It is also not unreasonable to expect that the size of $\delta$ will increase with $\delta_o$ and with the strength of the anharmonic interactions present (Bruce and Schneider (1977)).

$SrTiO_3$ has been the subject of extensive study over the last decade. The crystal is found to undergo a second-order (continuous) phase transition at $T_c \approx 105^oK$. ($T_c$ is found to be rather sensitive to the sample purity - see, for example, Hastings et al (1978).) Just above $T_c$, the primary instability, against rotation of the $TiO_6$ octahedra about [ 1,0,0 ] , is in strong competition with an instability against rotation about [ 1,1,1 ] (Bruce and Cowley (1973)). From EPR (Müller and Berlinger (1971)) and birefringence (Courtens (1972)) measurements, a value of about 0.07 Å has been obtained for $\delta_o$. Hirotsu and Sawada (1973) have confirmed this value down to $4.2^oK$. From very recent EPR measurements just above $T_c$, Bruce et al (1979) extract a value $\delta \approx 0.008$ Å. In their

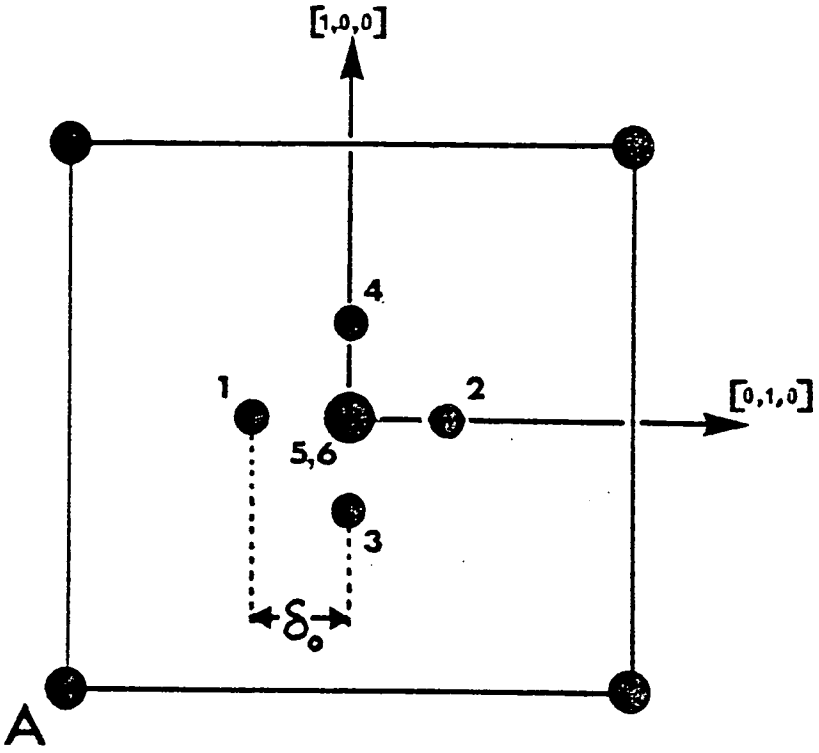


Figure 1.4.3 The X sites obtained by the $M_3$-mode rotation of the $BX_6$ octahedron about the [1,0,0] axis (sites 1 and 2) the [0,1,0] axis (sites 3 and 4) and the [0,0,1] axis (sites 5 and 6). Sites 5 and 6 are coincident (and undisplaced) so that the resulting single site has twice the 'occupancy' of the others. The axes established here are those used in the X-ion p.d.f. maps throughout this thesis. [1,0,0] and [0,1,0] will often be referred to as the X and Y axes respectively.

experiment, the existence of motional narrowing was used to discriminate between the predominant, harmonic (short-timescale) vibrations and the non-linear (comparatively long-timescale) fluctuations. The linewidth from the $Fe^{3+}$ - $V_o$ centre, caused by a charge misfit resulting from substitution of the $Ti^{4+}$ ion, was observed to change from a purely Lorentzian shape far above $T_c$ , through a Gaussian shape to a 'flattened' Gaussian near $T_c$. By showing that two spacially separated Gaussians can be made to fit this shape better than a single one, Bruce et al thereby extract evidence of separated clusters whose frequency fluctuations match that of their EPR probe.

$KMnF_3$ is found to undergo a first-order (discontinuous) phase transition at $T_c \approx 186^oK$ (Minkiewicz et al (1970)), caused by a condensation of the $R_{25}$ mode of the cubic phase. The soft phonons are found to be overdamped well above the transition, unlike those in $SrTiO_3$ (Shapiro et al (1972)), but similar anisotropic dispersion has been observed along the R-T direction in both crystals (Kjems et al (1973)). A finite displacement, $\delta_c$, is stabilised at $T_c$ and is of the order 0.13 Å (Minkiewicz et al (1970) ; Shirane et al (1970)). Bruce et al (1979a) obtain an upper limit for $\delta_o$ of the order 0.12 Å. Although a value for $\delta_o$ has not yet been measured, it is expected to be at least as large as that derived for $RbCaF_3$ - about 0.4 Å (Hirotsu and Sawada (1973)).

The dynamics of $RbCaF_3$ have been extensively studied by Rousseau and his co-workers and bear many similarities to those of $KMnF_3$ (Rousseau et al (1977)): a weak discontinuous transition can be observed at $T_c = 193^oK$; the central peak first starts to form about $60^o$ above $T_c$, at which point the soft-phonon side bands are already overdamped; and the temperature dependence of the soft mode (given by the relation $\omega^2(\underline{0},T) = a(T-T_o)$, $T_o=212^oK$) holds to within $+60^o$ of the transition where deviations start to become significant (Almairac et al (1977)). Values obtained for $\delta_c$ from the works of Buzaré et al (1977) and Maetz et al (1978) are in accord : both give a value of about 0.08 Å. From their recent detailed study of Raman activity just above $T_c$, Bruce et al

(1979a) can assign an upper bound of about 0.11 Å for $\delta$.

$CsPbCl_3$ is found to undergo three structural phase transitions at 320°K, 315°K and 310°K : that at 315°K is continuous, and the others discontinuous (Hirotsu and Sawada (1969); Törberg-Jensen (1969)). From inelastic neutron-scattering studies, Fujii et al (1974) have established the space group in each of the four phases and have shown that the successive transitions may be understood in terms of soft $M_3$ and $R_{25}$ modes of the cubic phase. In particular, they show that the cubic$\rightarrow$tetragonal transition at 320°K is associated with a condensation of the $M_3$ mode, in which the $PbCl_6$ octahedra oscillate about a $\langle 100 \rangle$ direction and are in phase along that direction (see Figure 1.4.2). The existence of several closely separated transitions suggests that there may be competing instabilities in the cubic phase, similar to those witnessed in $SrTiO_3$. For example, one of the low-temperature phases corresponds to a rotation of the $PbCl_6$ octahedra about [1,1,0] (Fujii et al (1974)). Any significant development of clusters characterised by such (possibly) competing instabilities would render the Cl-ion distribution more isotropic than that suggested by Figure 1.4.3. Because of the successive phase transitions below $T_c$ it is impossible to obtain an estimate for $\delta_o$; however, Mel'nikova et al (1977) have determined a value $\delta_c \approx 0.33$ Å (compared with about 0.1 Å in both $RbCaF_3$ and $KMnF_3$) so that $\delta$ might be expected to be correspondingly higher than that obtaining in the other perovskites (if indeed it exists in any of them).

In fact, disorder above $T_c$ in $CsPbCl_3$ has already been proposed by Møller (1959) on the basis of results obtained with X-ray diffraction data. Since then, however, Harada et al (1976) have shown that the approximations made by Møller in his analysis are not valid with displacements as large as those he obtained. With their own data, Harada et al carried out refinements of parameters describing the disordered models proposed by Møller, and showed that a better fit could be obtained with the standard perovskite structure. Recently (Sakata et al (1979)), the functional forms

of the ionic potentials have been examined in a series of elastic neutron-diffraction experiments covering the range of temperatures from $T_c$ up to $623^oK$. From their analysis, Sakata et al conclude that the anharmonic components in the potential are large for the Cs and Cl ions but insignificant for the Pb ions. They also find that the temperature factor of the Cl ion, in the plane perpendicular to the unique axis and containing the principal axes of the harmonic thermal ellipsoid, shows anomalous behaviour which they connect with the softening of the phonon mode.

From the point of view of the objectives set out in Section 1, it is clear that the perovskites discussed here constitute an ideal subject for investigation. Their structure and dynamics have been well studied both theoretically and experimentally, enabling objective comparisons to be made with any conclusions reached from the results of further study. Because the standard perovskite structure is so simple it might be expected (or at least hoped with some justification) that the fine detail sought in the description of the atomic thermal motions will not be masked by uncertainties in other crystal characteristics such as, for example, atomic positions within the unit cell. Furthermore, the strength of anharmonic interactions within the series $CsPbCl_3 \rightarrow RbCaF_3 \rightarrow KMnF_3 \rightarrow SrTiO_3$ appears to extend over a wide range of the anharmonic spectrum, thus establishing a reasonable basis for using the series to probe the generality of the anharmonic thermal treatments to be investigated.

## 1.5 THE PRESENT WORK AND OUTLINE OF THE THESIS

Since elastic neutron diffraction yields the time- and space-averaged crystal structure, it is clear that no direct information about two-timescale dynamics can be extracted. However, the cluster model - as presented in Section 2 - necessarily predicts intrinsic disorder of the X ions in these perovskites above $T_c$. If that is accepted, and if it is also accepted that an anharmonic phonon theory would be extremely

unlikely to predict such disorder, then in principle elastic diffraction may be used to reveal highly suggestive evidence for cluster-type disordering. Whether or not such evidence is accessible in practice will clearly depend upon the relative magnitudes of $\delta$ and the thermal m.s.a. about each of the separated sites. It is clear that intrinsic disorder will only be *resolvable* (in a time-averaged situation) if $\delta \gtrsim \sqrt{\text{m.s.a.}}$ ; if it is not then the equilibrium p.d.f. will be single-peaked (although perhaps markedly non-Gaussian). Certainly no resolvable disorder can be expected to be found in $SrTiO_3$ where the value of $\delta$ (Bruce et al (1979)) is very small compared with the known thermal amplitudes. However, in this case, and in the cases of the other crystals examined in this study, the shape of the p.d.f. derived from elastic-scattering data should at least be *compatible* with any other results purporting to demonstrate intrinsic disorder (or the lack of it).

For this reason, high-resolution neutron-scattering data have been collected for the perovskites $CsPbCl_3$, $RbCaF_3$, $KMnF_3$ and $SrTiO_3$ at a few degrees above $T_c$. Similar data have also been collected for both $RbCaF_3$ and $KMnF_3$ at room temperature - considerably above $T_c$ where collective motion is not expected to be so important. The latter will therefore act as a form of 'control' data against which the lower-temperature data will be compared.

The rest of this thesis is organised as follows :

Chapter 2 contains a detailed account of the mathematical formalisms used to characterise the ionic thermal motions and a discussion of the validity of each. Chapter 3 gives an account of the general features associated with the collection and analysis of neutron elastic-diffraction data. Details of the experimental work undertaken are described in Chapter 4 together with the results of the refinements. Finally, Chapter 5 examines the results obtained for features of interest and relevance vis à vis the objectives set out in Section 1.

# CHAPTER 2 : TREATMENT OF THERMAL MOTION

# CHAPTER 2 : TREATMENT OF THERMAL MOTION

## 2.1 INTRODUCTION

An atom in a crystal is not fixed rigidly : it has vibrational energy so that at any given instant it may be displaced from its mean position. From a diffraction point of view, the electron (or nuclear) density around any atomic site is then the convolution of the density of the atom at rest with a 'smearing' function characteristic of the nature of the vibrational motion. This assumes the validity of treating the atomic sites as separable - usually a good approximation. The three-dimensional smearing function will be called the probability density function (p.d.f.) of the atom, and will be denoted $P_i(\underline{r}) = P_i(\underline{r}_1 - \underline{r}_o)$ where $\underline{r}_1 - \underline{r}_o$ denotes displacements from the mean positon $\underline{r}_o$ and i labels the atoms in the unit cell. The value of $P_i(\underline{r})$ gives the probability that at any time the atom is displaced to a specified position $\underline{r}$ relative to its mean position.

As a consequence of the convolution of the atomic density in direct space, the corresponding atomic scattering factor, $f_i$ (or coherent neutron scattering length, $b_i$), must be modified by multiplication by the temperature factor, $W_i(\underline{Q})$, which is the Fourier transform (F.T.) of $P_i(\underline{r})$. (This is a standard result of F.T. theory - see for example, Lipson and Cochran (1966).) The products $f_iW_i(\underline{Q})$ (or $b_iW_i(\underline{Q})$) can then be used (see Chapter 3.7) in the calculation of structure amplitudes, $F_{calc}(\underline{Q})$, which may be compared with those derived from the measured diffracted intensities. (The structure *amplitude* is the modulus of the structure *factor* (see, for example, Lipson and Cochran (1966)). Most references in this thesis will be to structure amplitudes because the imaginary part of the structure factor is identically zero for the crystal symmetries considered here.) The parameters used to characterise $W_i(\underline{Q})$ are therefore among those to be optimised in the refinements.

There is no unique mathematical form for $W_i(\underline{Q})$; the actual choice is governed by a variety of factors such as

(i) computational ease, particularly with large data sets;

(ii) Fourier transformability, since often (and certainly in the cases considered here ) it is the direct-space p.d.f. which is of more interest; and

(iii) the 'expected' form of the p.d.f. : that is, because the expansion used will always be an approximation to the transform of $P_i(\underline{r})$, one particular approximation might offer a better description in a given case.

Nevertheless, certain similarities must exist between the functional forms of any temperature-factor expressions used to parameterise the motion of a given atom. In particular, they must satisfy the symmetry of the atomic site (Kurki-Suonio (1977)). An important corollary is then that the number of independent parameters required to specify $W_i(\underline{Q})$ is greatly reduced for highly symmetric sites compared with the number required for a general (symmetry 1) site. The specific forms used for $W_i(\underline{Q})$ in this analysis are now described (Sections2, 3 and 4) and their suitability tested (Section 5).

## 2.2 HARMONIC TREATMENT OF THERMAL MOTION

This treatment is based on the assumption that the restoring force acting upon an atom is proportional to the magnitude of the atom's displacement from its mean position in any given direction (Hooke's Law). $P_i(\underline{r})$ can then be written in tensor notation (Johnson (1969, 1970)) as

$$P_i(\underline{r}) = \frac{|\underline{\underline{p}}|^{\frac{1}{2}}}{(2\pi)^{3/2}} \exp\left\{-\tfrac{1}{2} \sum_{j,k=1}^{3} p_{jk}\, r_j\, r_k\right\} \qquad \ldots (2.2.1)$$

where p is a second-rank tensor and the components $r_j$ of $\underline{r}$ are based on the crystal axes. (The label i will frequently be dropped for clarity.) The integral of $P_i(\underline{r})$ over space is normalised to unity as required.

Use of the harmonic p.d.f. as given by expression (2.2.1) offers the advantage that $P_i(\underline{r})$ can be transformed analytically giving the conventional, harmonic approximation to the temperature factor,

$$W_i(\underline{Q}) = \exp\left\{-\sum_{j,k=1}^{3} 2\pi^2 u^{jk} h_j h_k\right\} \quad \ldots (2.2.2)$$

where $h_j = h_j^B/a_j$, $h_j^B$ being the Bragg indices and $a_j$ the lattice constants. $u^{jk}$ are the elements of the mean-square vibrational amplitude tensor.

## 2.3 CUMULANT TREATMENT OF ANHARMONIC THERMAL MOTION

### 2.3.1 Introduction

In this treatment the second-order, harmonic approximation to the p.d.f. as given by expression (2.2.1) is used as a developing function about which higher-order approximations may be expanded. The most general p.d.f. so obtained, when rearranged to give the best possible approximation with a finite number of terms, is called the Edgeworth Series Expansion (Edgeworth expansion). This expansion was first used by Edgeworth (1905) and its development has been reviewed by Wallace (1958). More recently, the formalism has been applied specifically in the treatment of p.d.f.'s (Chambers (1967) and references therein).*

As discussed by Johnson (1970), it is most convenient for the purposes of thermal vibration analysis and subsequent least-squares refinement, to express the Edgeworth expansion as a series of differential operators acting on the harmonic approximation to the p.d.f.. Set out explicitly, a more general,

* The theoretical development of cumulant methods is still evolving (Rae (1975)) and the application of cumulants in studies of thermal anharmonicity is now quite common (see, for example, Cooper and Sakata (1979)).

higher-order p.d.f. can then be written (adopting for convenience a notation based on that of Johnson (1970))

$$P(\underline{r}_1;\ {}^1_{=}\kappa,\ {}^2_{=}\kappa,\ {}^3_{=}\kappa,\ \ldots;\ \text{general}) = \left\{1 + Q_1(\underline{r}_1) + Q_2(\underline{r}_2) + \ldots\right\} P(\underline{r}_1;$$

$$\underline{r}_o,\ \underline{\underline{\sigma}};\ \text{harmonic}) \qquad \ldots (2.3.1)$$

where ${}^n_{=}\kappa$ are tensors of rank n, $\underline{\underline{\sigma}}$ is the variance-covariance matrix $(\underline{\underline{\sigma}}^{-1} = \{p_{jk}\}\ j,k = 1, 2, 3$, the matrix of covariant components of the second-rank tensor $\underline{\underline{p}}$) and $Q_m(\underline{r}_1)$ are terms involving products of the differential operators, $\partial/\partial(\underline{r}_1)_j$, with the elements of the tensors, ${}^n_{=}\kappa$. The rank of the highest-rank tensor included in the term $Q_m(\underline{r}_1)$ increases with m.

The anharmonic temperature factor (the F.T. of expression (2.3.1)) may then be written as a product of exponentials, the arguments of which contain progressively higher-order terms in $h_j$ :

$$W_i(\underline{Q}) = \exp\left\{ \sum_{j,k=1}^{3} \frac{i^2}{2!}\ 4\pi^2\ {}^2\kappa^{jk}\ h_j\ h_k \right.$$

$$\left. + \sum_{j,k,l=1}^{3} \frac{i^3}{3!}\ 8\pi^3\ {}^3\kappa^{jkl}\ h_j\ h_k\ h_l + \ldots \right\} \qquad \ldots (2.3.2)$$

$W_i(\underline{Q})$ could be used in this form and values refined for the independent non-zero elements of the tensors, ${}^n_{=}\kappa$; however, it is conventional to eliminate the factors of $\pi$ by the substitutions

$$b^{jk} = 2\pi^2\ {}^2\kappa^{jk},\ c^{jkl} = \frac{4\pi^3}{3}\ {}^3\kappa^{jkl},\ d^{jklm} = \frac{2\pi^4}{3}\ {}^4\kappa^{jklm} \ldots$$

$$\ldots (2.3.3)$$

($b^{jk}$ is therefore related to $u^{jk}$ by $u^{jk} = b^{jk}/2\pi^2$.)

Because $^{n}\underline{\underline{\kappa}}$ contains in the symmetry 1 case $\frac{n^2+3n+2}{2}$ unique elements (the parameters to be optimised in the refinements), it is clear that the temperature-factor expansion will have to be truncated after a few terms so that an acceptable parameter/observation ratio can be maintained in the refinements.

The distinction between the *rank* and the *order* of a tensor is a possible source of confusion. Following the terminology common in the literature (see, for example, Willis (1969)) $n^{th}$-order anharmonicity will be used here to mean anharmonicity specified by terms involving reciprocal-space dimensions of power n. Clearly then, in expression (2.3.2), the term involving the $n^{th}$-rank tensor specifies $n^{th}$-order anharmonicity. The order of the tensors, $^{n}\underline{\underline{\kappa}}$, is always three here, irrespective of the rank, n.

## 2.3.2 Features of the Cumulant Treatment

The ease of computer implementation is an obvious advantage of using this formalism: any order of anharmonicity may be incorporated into the refinement model by the straightforward addition of terms to the temperature-factor expansion (expression (2.3.2)). The resulting series is then divided into two component series - one involving only even tensors, $^{2n}\underline{\underline{\kappa}}$, and the other involving only odd tensors, $^{2n+1}\underline{\underline{\kappa}}$, - which can be inserted into the conventional crystallographic terms $A(\underline{Q})$ and $B(\underline{Q})$ used to calculate structure factors (see Lipson and Cochran (1966); Johnson (1970)). Furthermore, the derivatives of the structure factors with respect to the tensor elements may be calculated analytically, resulting in a considerable saving in computational time over any method requiring a numerical calculation. Any atomic site symmetry can be treated readily by determining those elements of the tensors, $^{n}\underline{\underline{\kappa}}$, which are independent and not identically zero. Such elements can be

obtained from a consideration of the transformation matrices appropriate to the symmetry operators of the atomic site.

Weighed against these computational advantages are several features which may cause problems in interpretation. First, by virtue of the approximations involved in its derivation, the Edgeworth expansion can show markedly non-physical effects. These can arise from the fact that truncation of the temperature-factor expansion after only a few terms biasses the values of those factors which are retained from their 'true' values. In addition, it is not strictly permissible (although it is necessary) to truncate the Edgeworth expansion simply *because* the temperature-factor expansion has been truncated. This is because each $Q_m(\underline{r}_1)$ contains elements from tensors of different ranks (see Johnson (1970)). Two approximations have therefore to be made : the first in the truncation of the temperature-factor expansion and the second in the subsequent use of expression (2.3.1) to obtain the corresponding direct-space p.d.f.. It has been shown (Barton and Dennis (1952)) that the three-cumulant model (in which cumulant tensors are retained only up to third rank in expression (2.3.2)) cannot produce a completely non-negative p.d.f. - although the four-cumulant model can. A further difficulty may arise depending upon the resolution of the data collected. From expression (2.3.2) it is clear that the elements of the tensors could be *chosen* in such a way that the temperature factor diverges at finite wave vector. The possibility of obtaining elements with such values via the standard refinement techniques will increase in general if the data collected is of low resolution, ie, if it is concentrated relatively close to the origin of the reciprocal space. For points close to the origin, the contribution to $W_i(\underline{Q})$ from tensors with $n > 2$ will almost certainly be insignificant compared with the second-order contribution. However, the higher-order contribution will become dominant as the value of $\underline{Q}$ increases, so that effects on $W_i(\underline{Q})$ which are small and *apparently* well-behaved at low $\underline{Q}$ may become large and completely non-physical when extrapolated beyond the range of the measured data to high $\underline{Q}$. A third (usually less

important) difficulty sometimes becomes apparent when an attempt is made to visualise the effect of individual, higher-cumulant tensor elements on the form of the temperature factor (Johnson (1970)). This problem can be overcome to some extent by decomposition of the standard tensors into mutually orthogonal component tensors of increasing symmetry (Sirotin (1964); Thornley (unpublished)). The tensor coefficients in the orthogonal representation are linearly related to the tensor elements in the non-orthogonal representation. Although it is certainly possible to refine the coefficients of the orthogonal component tensors directly (see the next section) and hence obtain greater accuracy in their refined values, the method of cumulants then loses its generality and specific routines have to be written to calculate the temperature factor and the appropriate least-squares derivatives for each different site symmetry individually.

### 2.3.3 Computer Implementation

The crystallographic least-squares fitting program, ORFLS (Busing et al (1962)), has been modified so that cumulant parameters of orders three and four may be refined in the temperature-factor expansion for any site symmetry. Optionally, fourth- and sixth-order orthogonal-cumulant parameters may be refined for symmetries m3m and 4/mmm (those relevant to the perovskite structure). A program, EDGE, has also been written to calculate the Edgeworth expansion up to fourth order based on the formula of Johnson (1970) (his equations 4-7).

For the perovskite structure it can be shown that the only independent non-zero $n^{th}$-order cumulant parameters for $2 \leq n \leq 6$ are as follows. For the metal ions, M, on sitesymmetry m3m, these six :

$$n = 2 \quad u(M) = u^{11}(M) = u^{22}(M) = u^{33}(M)$$

$$n = 4 \quad \kappa^{1111}(M) = \kappa^{2222}(M) = \kappa^{3333}(M)$$

$$\kappa^{1122}(M) = \kappa^{2233}(M) = \kappa^{3311}(M)$$

$$n = 6 \quad \kappa^{111111}(M) = \kappa^{222222}(M) = \kappa^{333333}(M)$$

$$\kappa^{111122}(M) = \kappa^{111133}(M) = \kappa^{222211}(M)$$

$$= \kappa^{222233}(M) = \kappa^{333311}(M) = \kappa^{333322}(M)$$

$$\kappa^{112233}(M)$$

and for the X ion, on site symmetry 4/mmm, these twelve :

$$n = 2 \quad u^{11}(X) = u^{22}(X) \; ; \; u^{33}(X)$$

$$n = 4 \quad \kappa^{1111}(X) = \kappa^{2222}(X) \; ; \; \kappa^{3333}(X)$$

$$\kappa^{1122}(X) \; ; \; \kappa^{2233}(X) = \kappa^{3311}(X)$$

$$n = 6 \quad \kappa^{111111}(X) = \kappa^{222222}(X) \; ; \; \kappa^{333333}(X)$$

$$\kappa^{111122}(X) = \kappa^{222211}(X)$$

$$\kappa^{111133}(X) = \kappa^{222233}(X)$$

$$\kappa^{113333}(X) = \kappa^{223333}(X)$$

$$\kappa^{112233}(X)$$

The elements of the odd-rank tensors are all zero for these (and for any centrosymmetric) site symmetries.

In an attempt to illustrate and clarify the modifications made to the harmonic temperature factor resulting from the addition of individual higher-order orthogonal-cumulant terms, the maps of Figures 2.3.1(a) - (d) have been compiled. Having chosen site symmetry 4/mmm as more suitable for the example than m3m (purely because it has a greater number of independent non-zero parameters), the maps were constructed as follows. The fourth- and sixth-rank cumulant tensors, $^{4}\underline{\underline{\kappa}}(X)$ and $^{6}\underline{\underline{\kappa}}(X)$, were orthogonalised giving four and six component tensors respectively. The resulting set of fourth-rank tensors comprises two with tetragonal symmetry, and one each with cubic and isotropic symmetry; the corresponding set of sixth-rank tensors comprises three with tetragonal symmetry, two with cubic and one with isotropic symmetry. Coefficients of the orthogonal component tensors are related to the elements of the corresponding standard tensors (as given in expression (2.3.3)) via the relationships (Nelmes (private communication)) :

| Tensor Symmetry | Coefficient |
|---|---|
| n = 4 | |
| isotropic | $d^{O} = \frac{1}{5}\{(2d^{1111} + d^{3333}) + 2(2d^{1133} + d^{1122})\}$ |
| cubic | $d^{C} = \frac{1}{15}\{2(2d^{1111} + d^{3333}) - 6(2d^{1133} + d^{1122})\}$ |
| first-tetragonal | $d^{T1} = \frac{1}{3}\{d^{1111} - d^{3333}\}$ |
| second-tetragonal | $d^{T2} = \frac{1}{3}\{d^{1133} - d^{1122}\}$ |
| n = 6 | |
| isotropic | $f^{O} = \frac{1}{7}\{(2f^{111111} + f^{333333}) + 6(f^{111122} + f^{111133} + f^{113333} + f^{112233})\}$ |

first-cubic $$f^{C1} = \frac{2}{11}\left\{(2f^{111111}+f^{333333}) - 5(f^{111122}+f^{111133}+f^{113333})\right\}$$

second-cubic $$f^{C2} = \frac{2}{231}\left\{(2f^{111111}+f^{333333}) + 6(f^{111122}+f^{111133}+f^{113333}) - 99f^{112233}\right\}$$

first-tetragonal $$f^{T1} = \frac{1}{3}\left\{f^{111111} - f^{333333}\right\}$$

second-tetragonal $$f^{T2} = \frac{1}{6}\left\{f^{111122} + f^{111133} - 2f^{113333}\right\}$$

third-tetragonal $$f^{T3} = \frac{1}{2}\left\{f^{111122} - f^{111133}\right\}$$

A small ('infinitesimal') value was then assigned to each of these coefficients. Using expression (2.3.2) suitably modified for orthogonal tensors, the higher-order ($n > 2$) terms involving the individual component tensors were then added *separately* to the harmonic term and the resulting three-dimensional temperature factors calculated. Retaining the same (arbitrary) second-order term on its own, the corresponding harmonic temperature factor was also calculated. (By choosing the coefficients of the higher-order tensors to be very small, it can be assumed that resulting bias in the second-order terms is negligible for the purposes considered here.) The difference between each of the ten distinct anharmonic temperature factors so produced and the harmonic one can now be identified specifically with the addition of the corresponding anharmonic orthogonal-cumulant tensor to the harmonic model.

Difference temperature-factor maps are shown in Figures 2.3.1(a) - (d), by way of example, for the isotropic, cubic and

Figure 2.3.1 Difference maps illustrating the modifications to the harmonic, 4/mmm-symmetry temperature factor arising from the addition of individual, fourth-order, orthogonal-cumulant terms to the expansion. Maps (a)-(d) are obtained using the $d^{O}$, $d^{C}$, $d^{T1}$ and $d^{T2}$ terms respectively. The method of construction is fully described in the text. Only one section of the difference maps is shown; the axes labelled X* and Y* are perpendicular to the four-fold axis of the distribution and along the conventional major axes of the harmonic thermal ellipsoid (so that the planes containing the four-fold axis and either X* or Y* are mirror planes.) The sign in the bottom right-hand corner is that given to the coefficient of the fourth-order term. $W_a$ and $W_h$ are the anharmonic and harmonic temperature factors respectively.

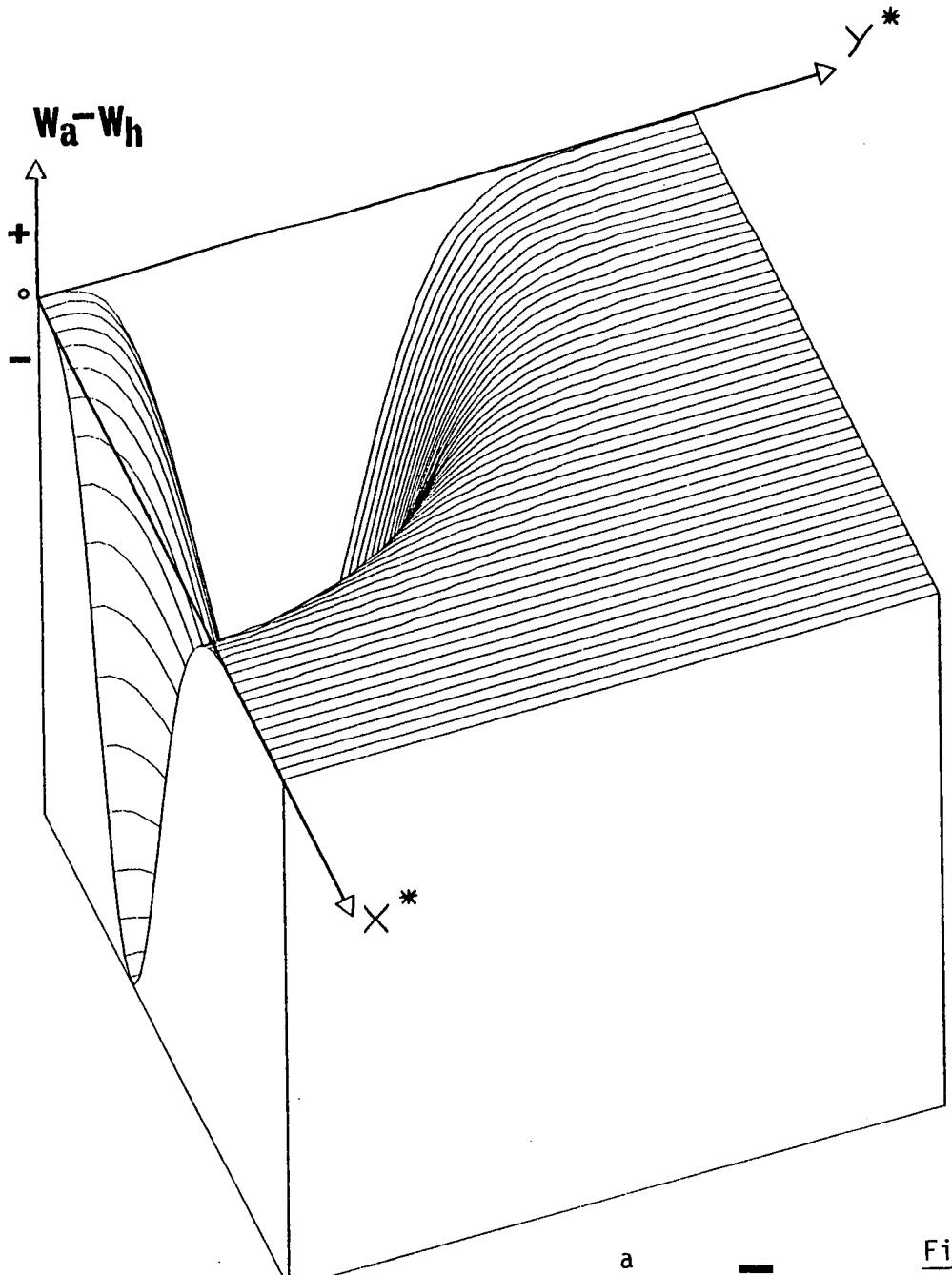


a

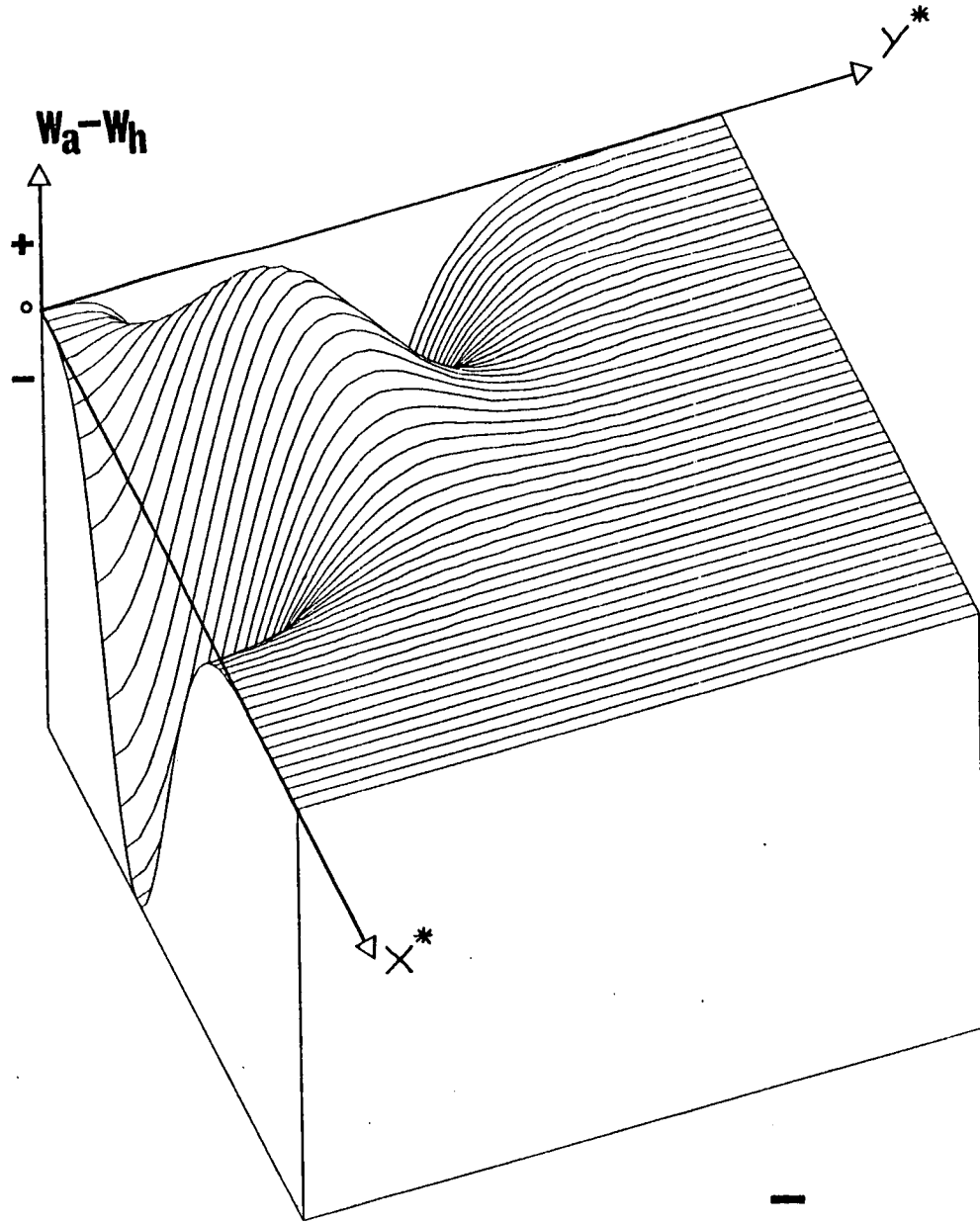


b

Figure 2.3.1

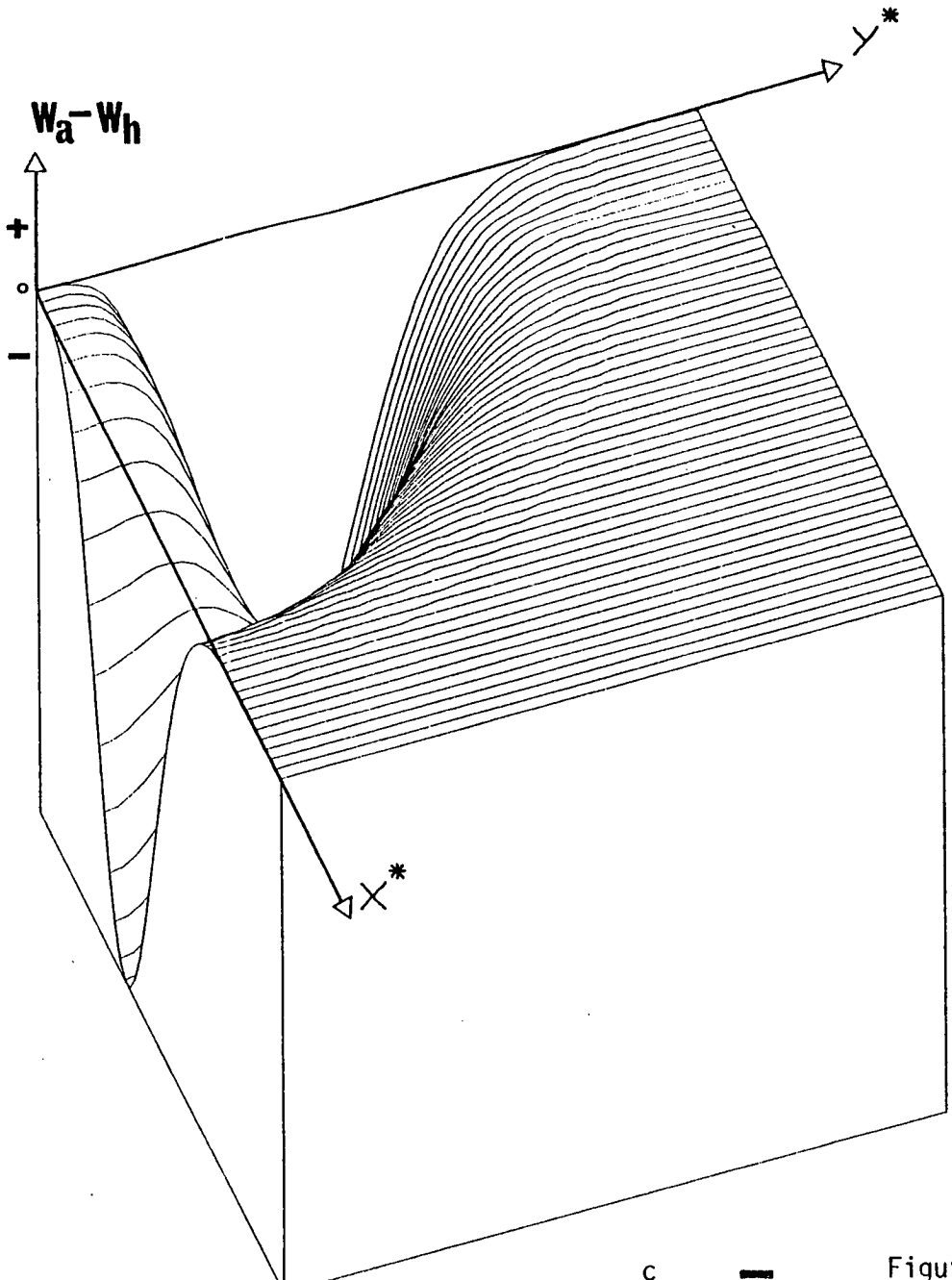


c −

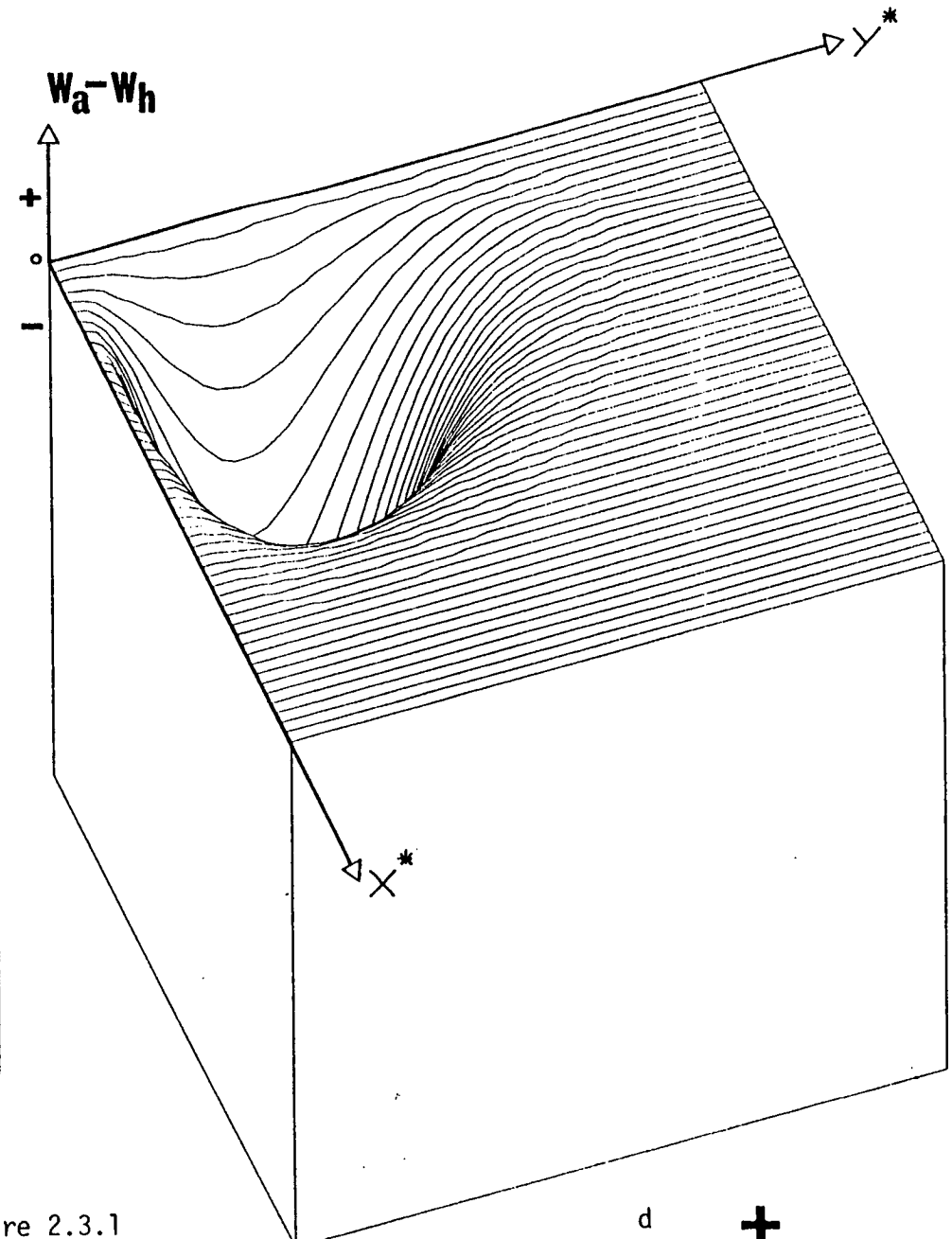


d +

Figure 2.3.1

first- and second-tetragonal fourth-rank tensors respectively; corresponding maps showing the modifications due to the addition of the sixth-rank component tensors are not reproduced here. The axes labelled X* and Y* in the figures are perpendicular to the unique (four-fold) axis and along the conventional major axes of the harmonic thermal ellipsoid. The sign of the fourth-order coefficient used in each case is also given; one of opposite sign would in some cases cause divergence of the temperature factor in the section considered here (for the reasons discussed in Section 3.2).

It is the intention of these maps only to give an indication of the *type* of deductions which might be possible from a refinement yielding significant higher-order cumulant parameters, and to provide a qualitative comparison with corresponding maps derived from an alternative anharmonic temperature-factor formalism described in the next section. From Figure 2.3.1(c) for instance, it may be tentatively concluded that refinement of a significant first-tetragonal fourth-cumulant parameter would not imply significant thermal anisotropy in the X* - Y* section, whereas refinement of a significant second-tetragonal parameter (Figure 2.3.1(d)) might well do. Caution must be exercised, however, in the interpretation of these maps; very small anharmonic parameters have been used in their construction. Relatively large anharmonic parameters will in general bias the second-order parameters so that the shape (though not the symmetry) of the extracted difference maps could change significantly from those of Figures 2.3.1(a) - (d). The magnitude of the difference p.d.f. would also be correspondingly greater. (No scale has been attached to the maps shown here because the anharmonic parameters were chosen so small as to be considered infinitesimal.)

## 2.4 FOURIER-INVARIANT TREATMENT OF ANHARMONIC THERMAL MOTION

### 2.4.1 Introduction

This method is based on the formalism developed by Kurki-Suonio and his co-workers (Kurki-Suonio (1977); Kurki-Suonio et al (1979)) and most of the notation and terminology used in this section is theirs.

It is assumed that the effective one-particle potential, $V(\underline{r})$, may be separated into the sum of two parts - $V_o(\underline{r})$, which has the form of a quadratic polynomial, and $\Delta V(\underline{r})$, which contains higher-order terms in $\underline{r}$ . While Kurki-Suonio et al (1979) speak of $V_o(\underline{r})$ as the 'basic harmonic approximation' there seems no obvious reason why $V_o(\underline{r})$ need necessarily be the same as the best-fitting harmonic approximation (see the discussion of Chapter 1.3), although in practice it will probably not differ greatly - see the results of the refinements in Chapter 4. The general, anharmonic atomic p.d.f. takes the form

$$P_i(\underline{r}) = \frac{1}{N} \exp\left\{\frac{-V_o(\underline{r}) - \Delta V(\underline{r})}{kT}\right\} \qquad \ldots (2.4.1)$$

where k and T are the Boltzmann constant and the absolute temperature respectively, and N is a normalisation constant.

Making a first-order approximation in the exponential and defining unit vectors in the directions of the principal axes of the harmonic p.d.f., the general p.d.f. can be written as

$$P_i(\underline{r}) = \frac{1}{N} \exp\left\{-\tfrac{1}{2} \sum_{j=1}^{3} B_j^2 r_j^2\right\}\left\{1 - \frac{\Delta V(\underline{r})}{kT}\right\} \qquad \ldots (2.4.2)$$

where $B_j^2$ is the reciprocal of the mean-square second-order vibrational amplitude along axis j and $\underline{r} = (r_1, r_2, r_3)$.

As pointed out by Kurki-Suonio (1977), $V(\underline{r})$ could in principle be expanded in terms of any complete set of functions, and some of the points relevant to the selection are discussed by him. One particularly appealing approach is revealed through an examination of the Fourier-invariance Theorem (F.I.T.) :

"If the ground state of a three-dimensional harmonic oscillator is given by $\psi_0 = \exp(-\frac{1}{2}\sum_{j=1}^{3} B_j^2 r_j^2)$ and an arbitrary n-phonon excited state by $\psi_n = f(B_1r_1, B_2r_2, B_3r_3)$, then $\int f(B_1r_1, B_2r_2, B_3r_3) \exp(2\pi i \underline{S} \cdot \underline{r})\, d^3r = i^n (2\pi)^{3/2}/B_1B_2B_3 \times f(b_1S_1, b_2S_2, b_3S_3)$ where $B_jb_j = 2\pi$ and $\underline{S} = \underline{Q}/2\pi$ is the scattering vector." ($\underline{S}$ has been used instead of $\underline{Q}$ here to facilitate comparison with the text of Kurki-Suonio et al (1979).)

From this, it can be seen that if $P_i(\underline{r})$ is written in the form $f(B_1r_1, B_2r_2, B_3r_3)$, then the corresponding temperature factor may be derived analytically. This form can be realised through a consideration of the stationary wave functions of a harmonic oscillator and can best proceed by an initial division of the problem into one of three separate cases : one in which the harmonic approximation to $P_i(\underline{r})$ has either isotropic, axial, or general (1) symmetry. The procedure in the axial symmetry case (it being relevant to 4/mmm site symmetry) will be outlined here by way of example. For full details concerning the derivation of the functions required in each of these three cases see Kurki-Suonio et al (1979).

First, taking full account of the site symmetry, the set of wave functions forming a basis is obtained. These functions are given, for the axial symmetry cases, by

$$\left\{H_{n_z}(B_3r_3)P_{n\,|m|}(B_1\rho)\Phi_{mp}(\emptyset)\exp(-\tfrac{1}{2}(B_1^2\rho^2 + B_3^2r_3^2))\right\} \quad \ldots (2.4.3)$$

where $H_{n_z}$ are the Hermite polynomials; $P_{n\,|m|}(x) = x^m L^m_{\frac{1}{2}(n-m)}(x^2)$, where L is the associated Laguerre polynomial; $\Phi_{mp}(\emptyset) = \cos m\emptyset$ or $\sin m\emptyset$ according as p = + or - ; and $(r_3, \rho, \emptyset)$ are the cylindrical

coordinates of $\underline{r}$. The indices ($n_z$, n, m, p) run as follows :

$$n_z = 0, 1, 2, \ldots\ ;$$

$$n = 0, 1, 2, \ldots\ ;$$

$$m = n, n-2, \ldots, -n\ ;$$

$$p = + \text{ or } -\ .$$

$n_z + n$ specifies the order of the anharmonicity (the degree of excitation).

By representing the potential as an expansion in terms of the basis wave functions and assuming the second-order terms to dominate the expansion, $P_i(\underline{r})$ can be written

$$P_i(\underline{r}) = \frac{B_1^2 B_3}{(2\pi)^{3/2} N} \exp(-\tfrac{1}{2}(B_1^2\rho^2 + B_3^2 r_3^2)) \left\{1 - \sum_{n_z} \sum_{n} \sum_{m} \sum_{p} b_{n_z nmp} H_{n_z}(B_3 r_3) P_{nm}(B_1 \rho) \Phi_{mp}(\emptyset)\right\} \quad \ldots (2.4.4)$$

where N, the normalisation constant, is a finite expansion depending only upon the coefficients $b_{n_z nmp}$ to be determined in the refinement and is defined by Kurki-Suonio et al (1979).

By the F.I.T., $W(\underline{S})$ is then given as

$$W(\underline{S}) = \frac{1}{N} \exp(-\tfrac{1}{2}(b_1^2\sigma^2 + b_3^2 S_3^2)) \left\{1 - \sum_{n_z} \sum_{n} \sum_{m} \sum_{p} i^{(n_z+n)} b_{n_z nmp} H_{n_z}(b_3 S_3) P_{nm}(b_1\sigma) \Phi_{mp}(\emptyset_S)\right\}$$

$$\ldots (2.4.5)$$

where $(S_3, \sigma, \emptyset_S)$ are the cylindrical coordinates of $\underline{S}$ and $i = \sqrt{-1}$. For any specific site symmetry the independent, non-zero functions in these expansions are obtained from a list of 'index-picking rules' constructed from a consideration of the site symmetry's constituent operators.

The steps in the derivation of $P_i(\underline{r})$ and $W_i(\underline{S})$ are similar for the other two cases in which the harmonic approximation to $P_i(\underline{r})$ has either isotropic or general symmetry.

### 2.4.2 Features of the Fourier-Invariant Treatment

As suggested by the name, the ease of Fourier transformation is a very clear advantage of this method. In spite of, and indeed because of, the mathematical approximations made in the derivation of expressions (2.4.2) and (2.4.4), it is true that the exact, analytic nature of the transformation is not compromised in any way. The generality of the space spanned by $P_i(\underline{r})$ is however modified (restricted) because of these approximations. Compared with the method of cumulants, the expressions involved for $W_i(\underline{S})$ tend to be rather unwieldy. Furthermore, separate computer routines have to be written to calculate $W_i(\underline{S})$ and its least-squares derivatives for each individual site symmetry. It will, nevertheless, be possible to achieve some condensation of the computer programming for site symmetries involving similar groups of operators. For the symmetries relevant to this study (m3m and 4/mmm), the exact mathematical forms (expression (2.4.5)) were used in the calculation of the temperature factors. Since a similar exact calculation for the necessary derivatives would involve very lengthy expressions indeed (because the normalisation constant, N, is a function of some of the variable parameters of $W_i(\underline{S})$), the approximation N = 1 was made in the computations. As noted later in this section, this is a possible source of convergence problems in the refinements, although the use of suitable damping factors applied to the parameter shifts might be expected to give satisfactory results if $N \sim 1$, ie, if the anharmonic terms are not too large.

### 2.4.3 Computer Implementation

Separate subroutines have been written, to be accessed from ORFLS (see Section 3.3), so that $W_i(\underline{S})$ and its derivatives may be calculated for m3m and 4/mmm site symmetries up to sixth order. Again, the odd-order terms are identically zero for these symmetries. A program, FOURREAL, has also been written to calculate the corresponding direct-space p.d.f.'s up to sixth order - the program is of course substantially the same as the routines written to calculate the temperature factors (compare expressions (2.4.4) and (2.4.5)).

The non-zero functions required in the calculation of $W_i(\underline{S})$ for the site symmetries m3m and 4/mmm can be obtained from the list of index-picking rules tabulated by Kurki-Suonio et al (1979). The corresponding parameters to be determined in the refinements are then as given below, using the notation of Kurki-Suonio et al for the orders $n > 2$. For the metal ions, M, on site symmetry m3m, these six :

$n = 2$ $\quad u(M) = u^{11}(M) = u^{22}(M) = u^{33}(M)$

$n = 4$ $\quad a_{40+}(M)$ ; $a_{44+}(M)$

$n = 6$ $\quad a_{60+}(M)$ ; $a_{64+}(M)$ ; $a_{66+}(M)$

and for the X ions, on site symmetry 4/mmm, these twelve :

$n = 2$ $\quad u^{11}(X) = u^{22}(X)$ ; $u^{33}(X)$

$n = 4$ $\quad b_{040+}(X)$ ; $b_{044+}(X)$ ; $b_{220+}(X)$ ; $b_{400+}(X)$

$n = 6$ $\quad b_{060+}(X)$ ; $b_{064+}(X)$ ; $b_{240+}(X)$

$\quad b_{244+}(X)$ ; $b_{420+}(X)$ ; $b_{600+}(X)$

Difference temperature-factor maps, appropriate to the 4/mmm site symmetry and illustrating the modifications to the harmonic temperature factor due to the addition of individual higher-order Fourier-invariant (F.I.) terms, were constructed in an entirely analogous way to those described in detail for cumulant terms in Section 3.3. These maps are reproduced in Figures 2.4.1(a) - (h) for the functions with indices ($n_z$, n, m, p) = (0, 4, 0, +), (0, 4, 4, +), (2, 2, 0, +), (0, 6, 0, +), (0, 6, 4, +), (2, 4, 0, +), (2, 4, 4, +) and (4, 2, 0, +) respectively; those with indices (4, 0, 0, +) and (6, 0, 0, +) have been omitted because they are identically zero in the plane of the reciprocal space considered here. It is noted that only those functions with m = 4 characterise the four-fold symmetry of the site : the others are isotropic about the unique axis. The choice of sign given to the coefficients, $b_{n_z nmp}$ , of the F.I. terms is stated on the maps - one of opposite sign would simply reverse the sign of the observed differences.

The note of caution as regards interpretation, voiced at the end of Section 3.3, is again relevant. However, it does seem, at least so far as fourth-order terms are concerned, that the gross features observed in the difference maps are substantially similar whether cumulant or F.I. anharmonic terms are used (compare Figures 2.3.1(a) - (d) with Figures 2.4.1 (a) - (c)) - bearing in mind any differences attributable only to the choice of sign of the F.I. coefficients. It might therefore be expected that the improvement in fit to observed data, resulting from the addition of fourth-order parameters to the harmonic temperature factor, will be about the same for either cumulant or F.I. parameters - at least for site symmetry 4/mmm. This observation is confirmed in the refinements of Chapter 4.

## 2.5 TEST REFINEMENTS

### 2.5.1 Introduction

In this section, the words 'real' and 'test' will be used to denote respectively situations which deal with the *actual* data

Figure 2.4.1 Difference maps illustrating the modifications to the harmonic, 4/mmm-symmetry temperature factor arising from the addition of individual F.I. terms to the expansion. Maps (a)-(h) are obtained using the $b_{040+}$, $b_{044+}$, $b_{220+}$, $b_{060+}$, $b_{064+}$, $b_{240+}$, $b_{244+}$ and $b_{420+}$ terms respectively. The method of construction is fully described in the text. Only one section of the difference maps is shown; the axes labelled X* and Y* are perpendicular to the four-fold axis of the distribution and along the conventional major axes of the harmonic thermal ellipsoid (so that the planes containing the four-fold axis and either X* or Y* are mirror planes). The sign in the bottom right-hand corner is that given to the coefficient of the anharmonic term. $W_a$ and $W_h$ are the anharmonic and harmonic temperature factors respectively.

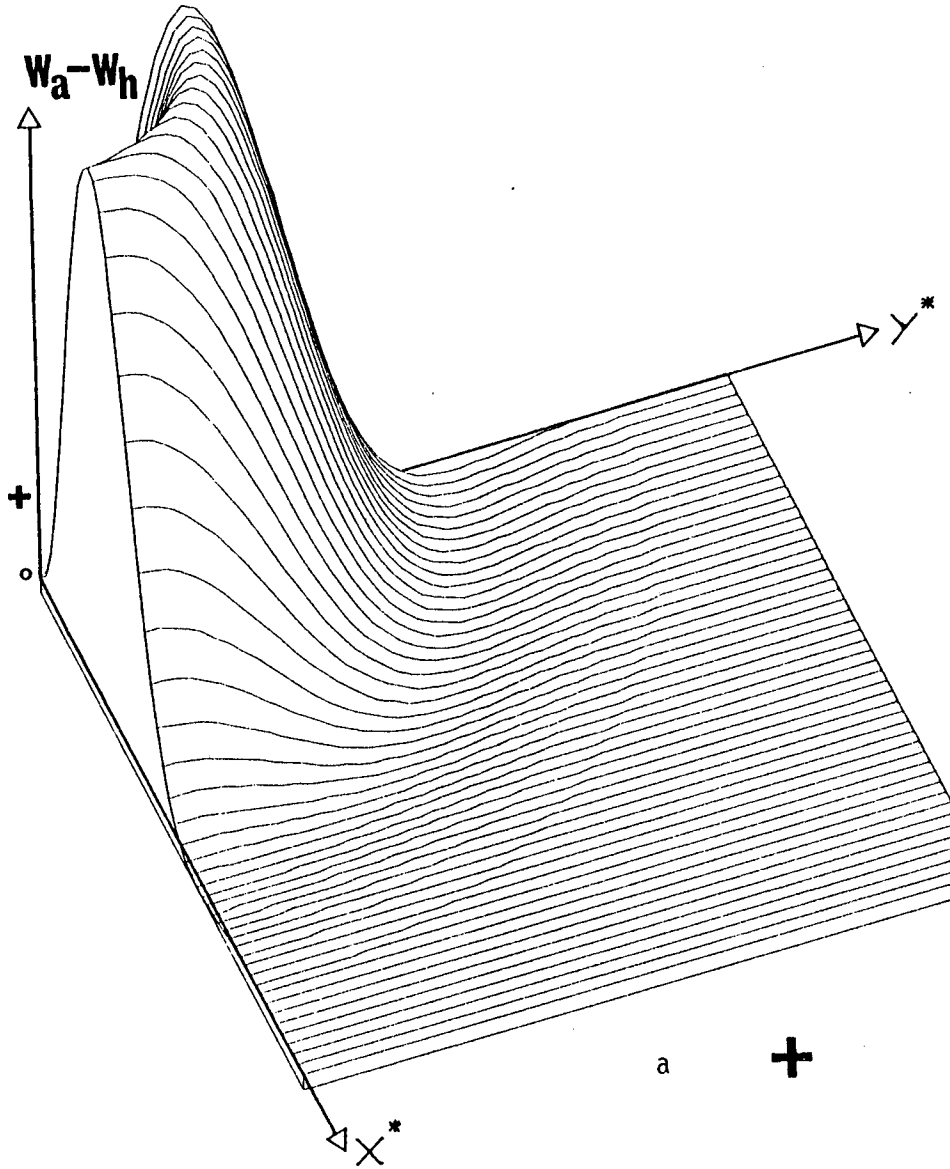


a

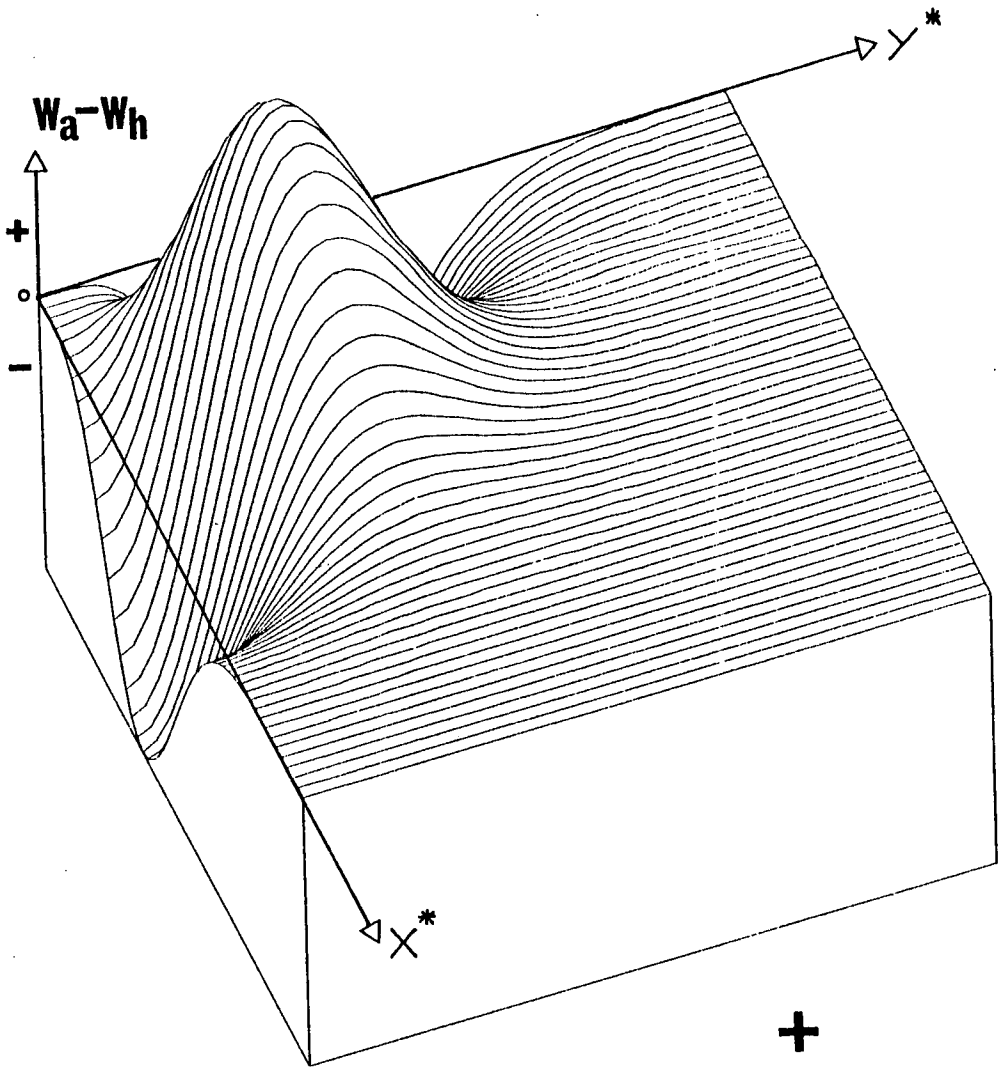


b

Figure 2.4.1

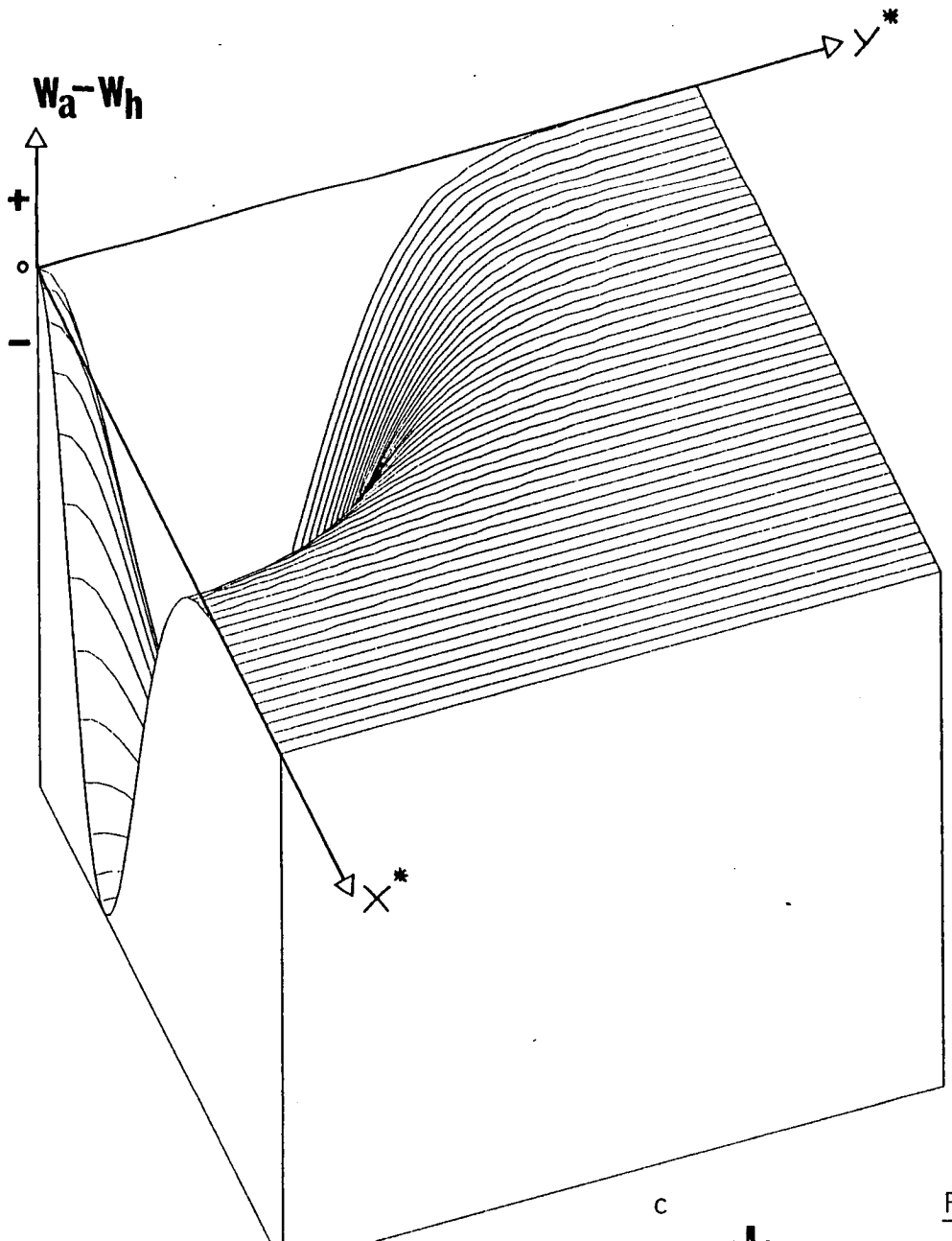


c

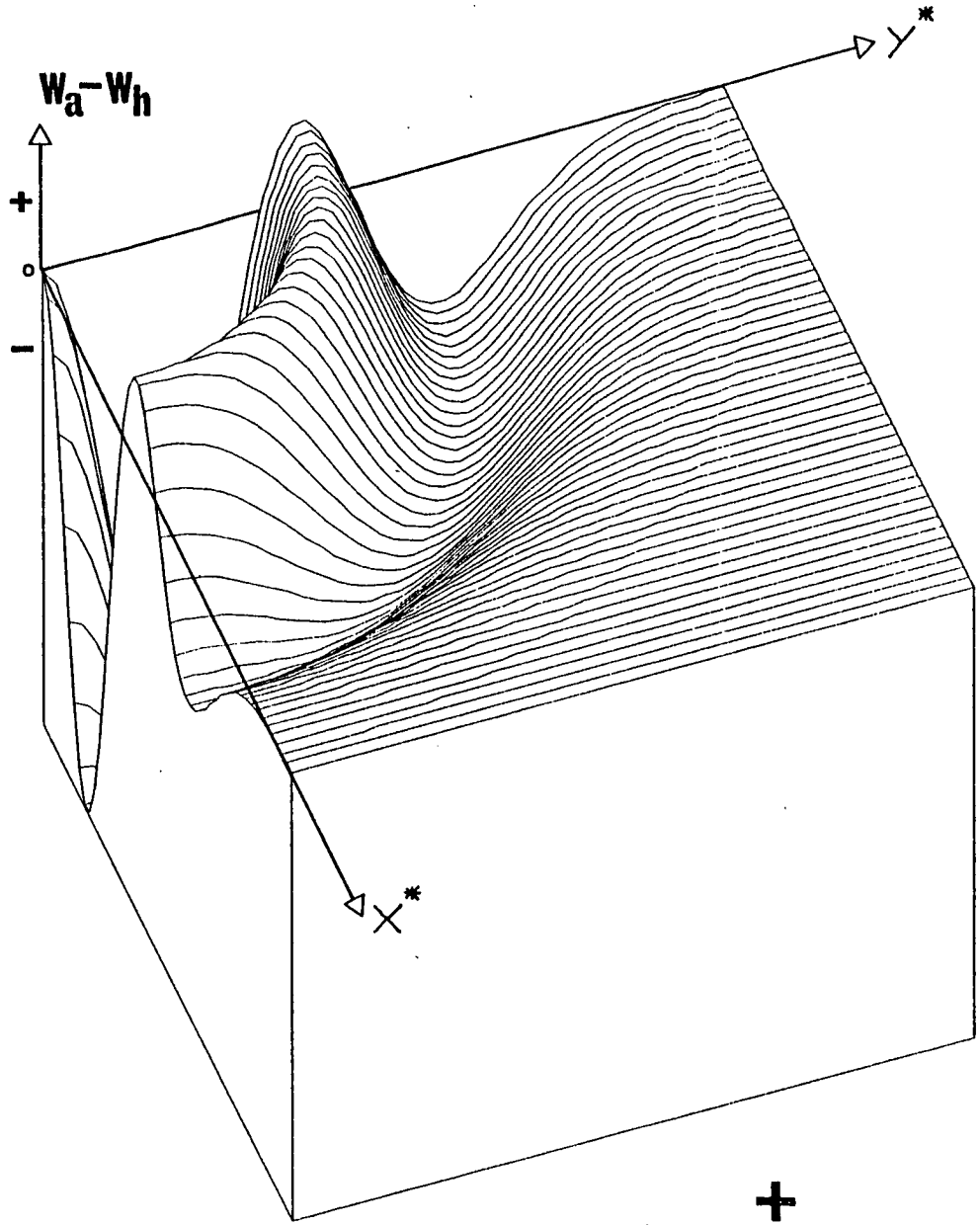


d

Figure 2.4.1

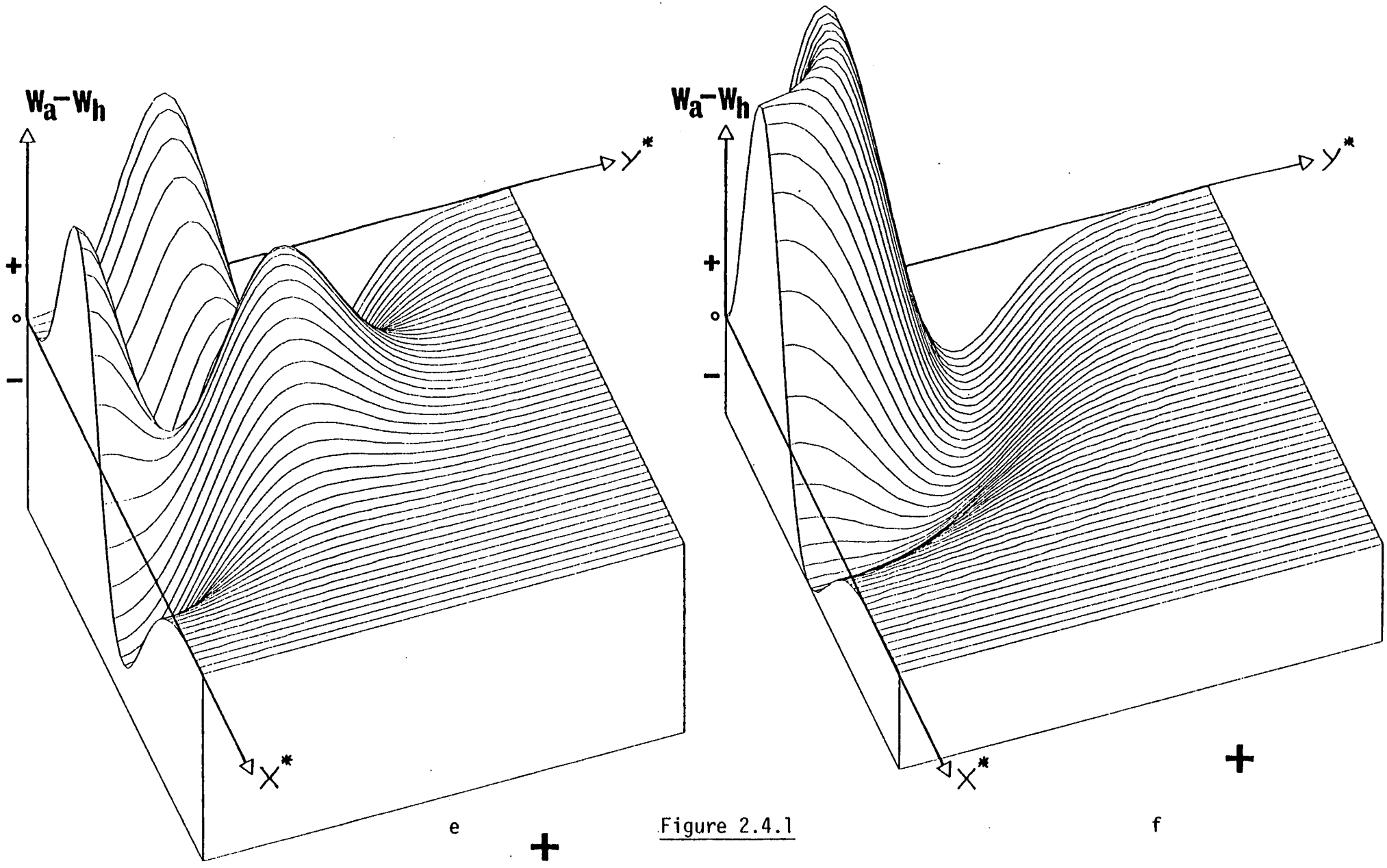


Figure 2.4.1

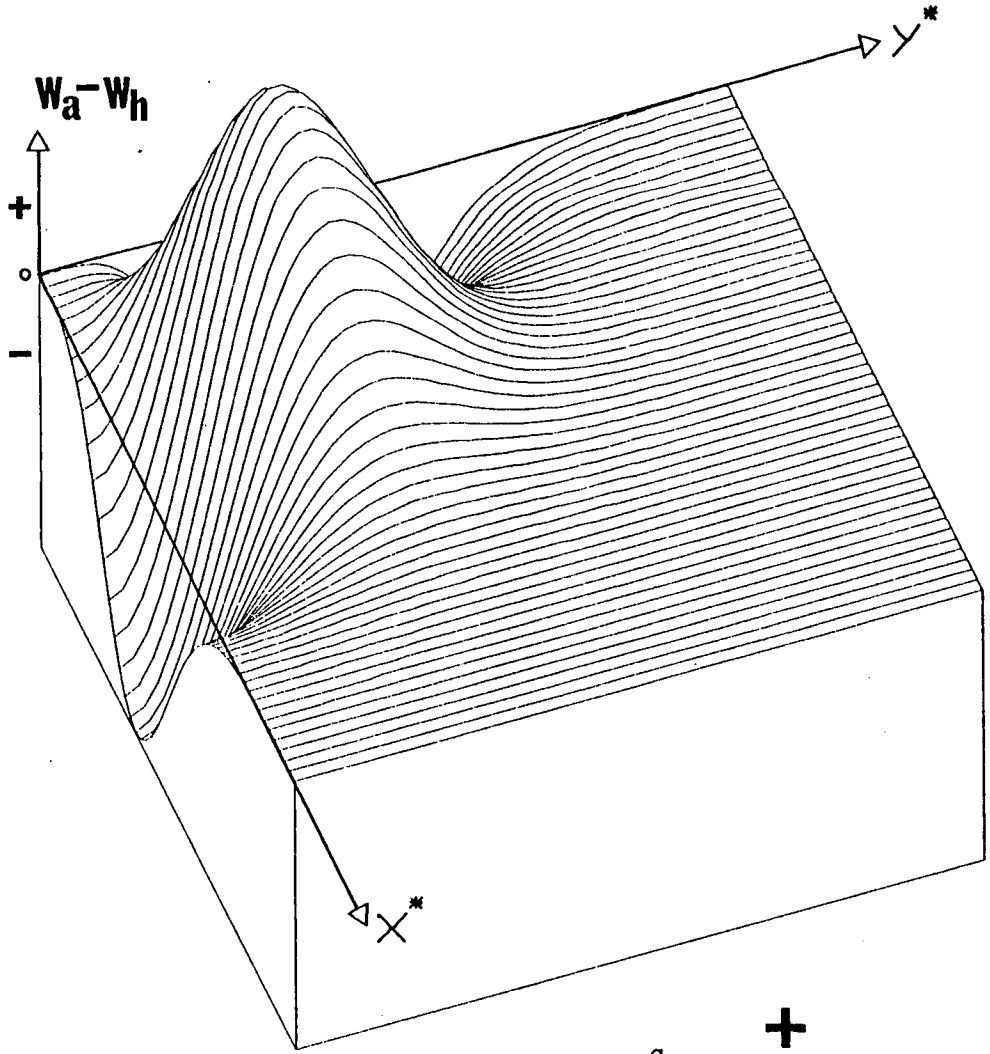


g

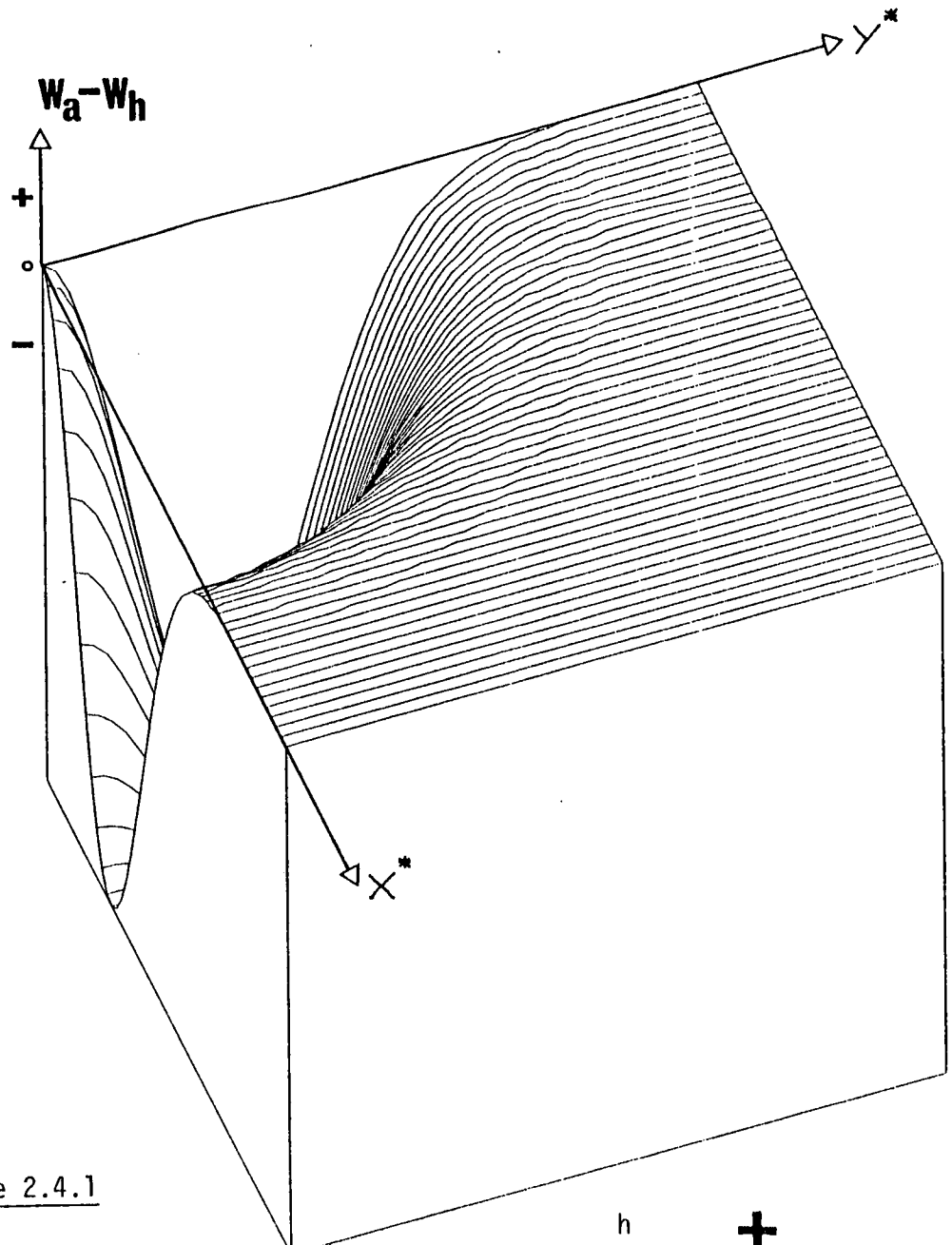


h

Figure 2.4.1

collection and its analysis (Chapter 4) and situations in which the data involved have been artificially *generated* using the methods to be described in Sections 5.2 and 5.3.

The object of carrying out the series of refinements on such test data was to obtain some estimate of the reliability and physical meaning of the anharmonic parameters obtained during the analysis of the real data : in other words, to determine the extent to which these parameters may be artefacts resulting from some systematic error in data collection/analysis.

With this aim in view, it was decided to carry out a fairly thorough investigation using as 'data', structure amplitudes generated from model crystals whose positional and thermal parameters were given precisely known values. To keep within manageable time schedules, it was decided to restrict the investigation to systems whose parameters were representative - as far as possible - of those of the real crystals studied (cubic perovskites) and to data sets of comparable size and accuracy to the ones actually collected. Ultimately, the parameters obtained from refinements using the data sets so produced can be used to reconstitute the test model structure. Objective comparison is then possible between what is *known* to exist and what may be *derived* with the tools available.

It is an inevitable consequence in a detailed analysis of this kind that some condensation of the terminology employed is both desirable and essential. For this reason, an attempt is made in the next two sections to develop a concise method of labelling the large number of test models used and the data sets obtained from them.

### 2.5.2 The Structure of the Test Model

The structure of the test model, illustrated in Figure 2.5.1(a), was based on the standard perovskite structure of Figure 1.4.1. The

Figure 2.5.1 The structure of the test models. One cubic unit cell is shown. The labelling of the axes is the same as that of Figure 1.4.1. Only one X ion is shown here; the others are located at the symmetry-related face-centre positions.

(a) The central component of the X-ion distribution, denoted by the large open diamond, has twice the occupancy of the 'satellites', denoted by the small open diamonds. $\delta$, the site separation, is the only variable parameter. This is the structure denoted $k = 1$ in the text.

(b) The X-ion distribution rotated by $45^{o}$ about the unique axis (the four-fold perpendicular to the cube face and passing through its centre). This is the structure denoted $k = 2$ in the text.

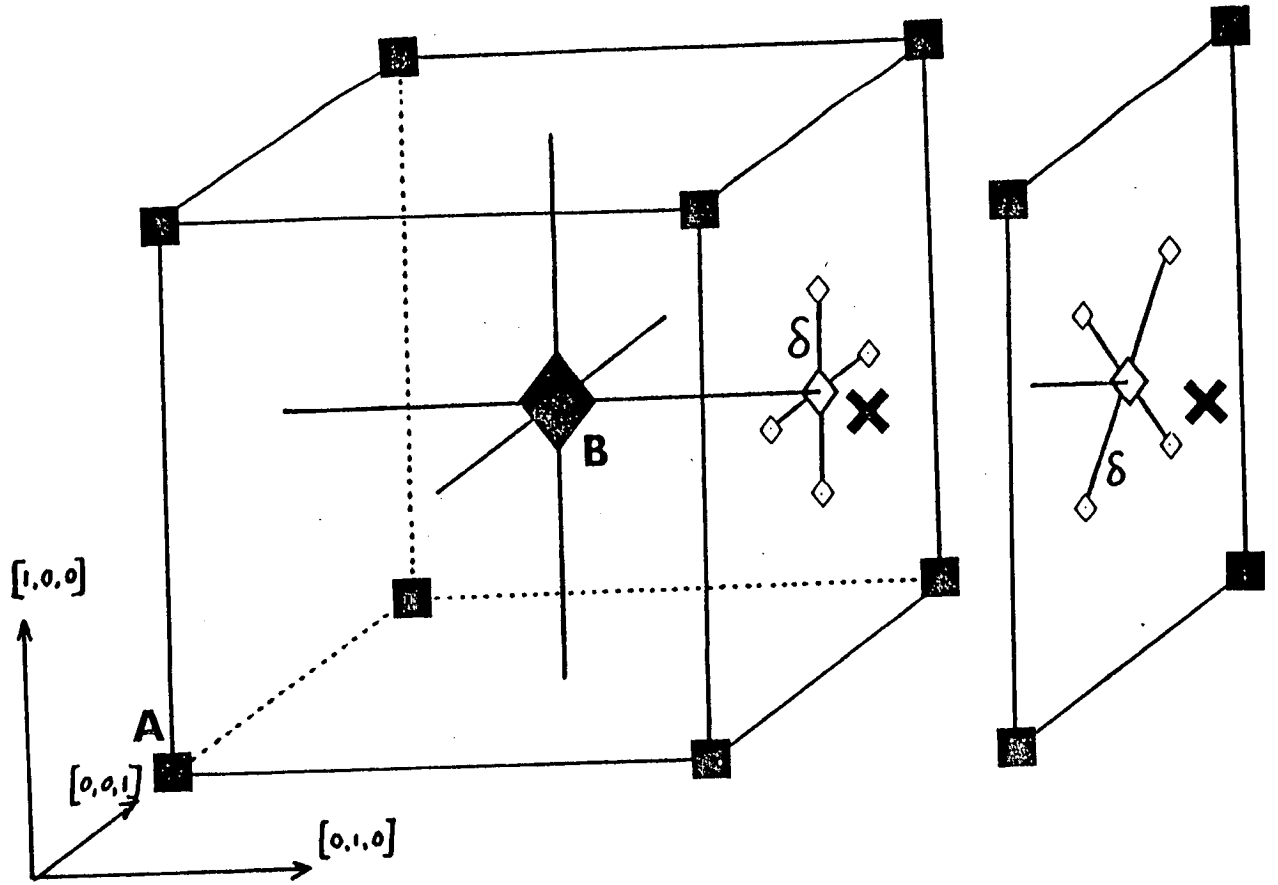


a b

Figure 2.5.1

cubic cell edge was assigned a dimension a = 4 $\mathring{A}$ and the ions A, B and X were placed as shown on site symmetries m3m, m3m and 4/mmm respectively. Since one tentative conclusion reached from initial refinements on the real perovskite data was that thermal anharmonicity is largely confined to the 'cations', X, the 'metal ions', A and B, were constrained to vibrate in harmonic potential wells.

The X-ion distribution was parameterised as shown in Figure 2.5.1(a) for the following reasons. First, because recent theoretical thinking (see Chapter 1.2) may be suggestive of some underlying, intrinsic disorder in cubic perovskites just above $T_c$. If such disorder is in fact present it might be expected, in a time-averaged situation, to display this type of intrinsic microstructure (see Chapter 1.4). However, so that the analysis would in no way appear to assume the correctness of this postulation, data sets were also generated using models with the same X-ion distribution rotated by $45^o$ about the four-fold axis, ie, taking the 'satellite' ions to the positions shown in Figure 2.5.1(b). Second, it is possible by varying $\delta$ (the local order parameter and the only variable parameter in the test models) to observe a smooth progression from a harmonic p.d.f. ($\delta = 0$) to one which is unambiguously disordered ($\delta \gg \sqrt{u(X)}$, u(X) being the m.s.a.'s assigned to the constituent parts of the X ion).

Irrespective of the value assigned to $\delta$, the central part of the X ion, located at the standard perovskite position, was given twice the occupancy of each of the 'satellites' (see Chapter 1.4 for 'justification'). The total scattering length was fixed at $b(X) = 0.6 \times 10^{-12}$cm. b(A) and b(B) were fixed at 0.75 and $0.45 \times 10^{-12}$cm respectively. Each ion (treating the X-ion satellites now as individual ions) was constrained to vibrate harmonically and isotropically with the following m.s.a.'s : $u(A) = 0.02$ $\mathring{A}^2$, $u(B) = 0.01$ $\mathring{A}^2$, and $u(X) = 0.01$ $\mathring{A}^2$. Extinction in the test crystal was assumed to be isotropic, secondary, Type I, with Lorentzian mosaic spread and therefore specified by a single parameter, g (see Becker and Coppens (1974)), which was assigned

a value 100. This gives a r.m.s. mosaic spread of 1' of arc and results in the most severely affected 'intensities' being attenuated by about 20%.

It is again emphasised that the microstructure of the test model has been chosen primarily for convenience in prescribing a controlled amount of anharmonicity to the thermal motion of the X ion. Specifically, it is not intended to serve as a proposed microstructure existing in any cubic perovskite crystal.

### 2.5.3 The Test Data

For convenience, the list of 146 independent reflections obtained during the refinement on $RbCaF_3$ at 205°K (see Chapter 4.3) was adopted. A set of structure amplitudes was then generated for each model, specified by the single parameter, $\delta$, and the orientation of the X-ion satellites. An incident wavelength $\lambda = 0.4$ Å was used. Because of the high $(\sin \theta_B/\lambda)_{max}$ resolution of the data collected and also because of the relatively high thermal amplitudes often obtaining, it was found in the real experiments that the accuracy of the measured intensities fell off rather markedly with increasing Bragg angle. To reproduce the effects of this in the test data and to take proper account of the effects due to random errors in the 'collection', each of the generated data sets was passed through a specially written program for modification. This program did the following :

First, each $F_{obs}$, the observed structure amplitude, was assigned a corresponding standard deviation, $\sigma(F_{obs})$, based on a given empirical relationship - either $\sigma_1(F_{obs}) = (1 + 30/F_{obs}) \times F_{obs}/100$ or $\sigma_2(F_{obs}) = (1 + 7/F_{obs} + 50/F_{obs}^2) F_{obs}/100$. The percentage accuracy assigned to each $F_{obs}$ was then as shown in Figure 2.5.2. It was found that these accuracies were broadly representative of those achieved in the real data collections. (The arbitrary scale factor applied to the generated $F_{obs}$ values was chosen so that the 'strong' reflections had $F_{obs} \approx 100$ and

Figure 2.5.2 The variation of accuracy, $(\sigma(F_{obs})/F_{obs})$ with $F_{obs}$, as applied to the data used in the test refinements. Graph 1 is the accuracy obtained using standard deviations calculated from $\sigma_1(F_{obs}) = (1 + 30/F_{obs})F_{obs}/100$; Graph 2 is that obtained from $\sigma_2(F_{obs}) = (1 + 7/F_{obs} + 50/F_{obs}^2)F_{obs}/100$.

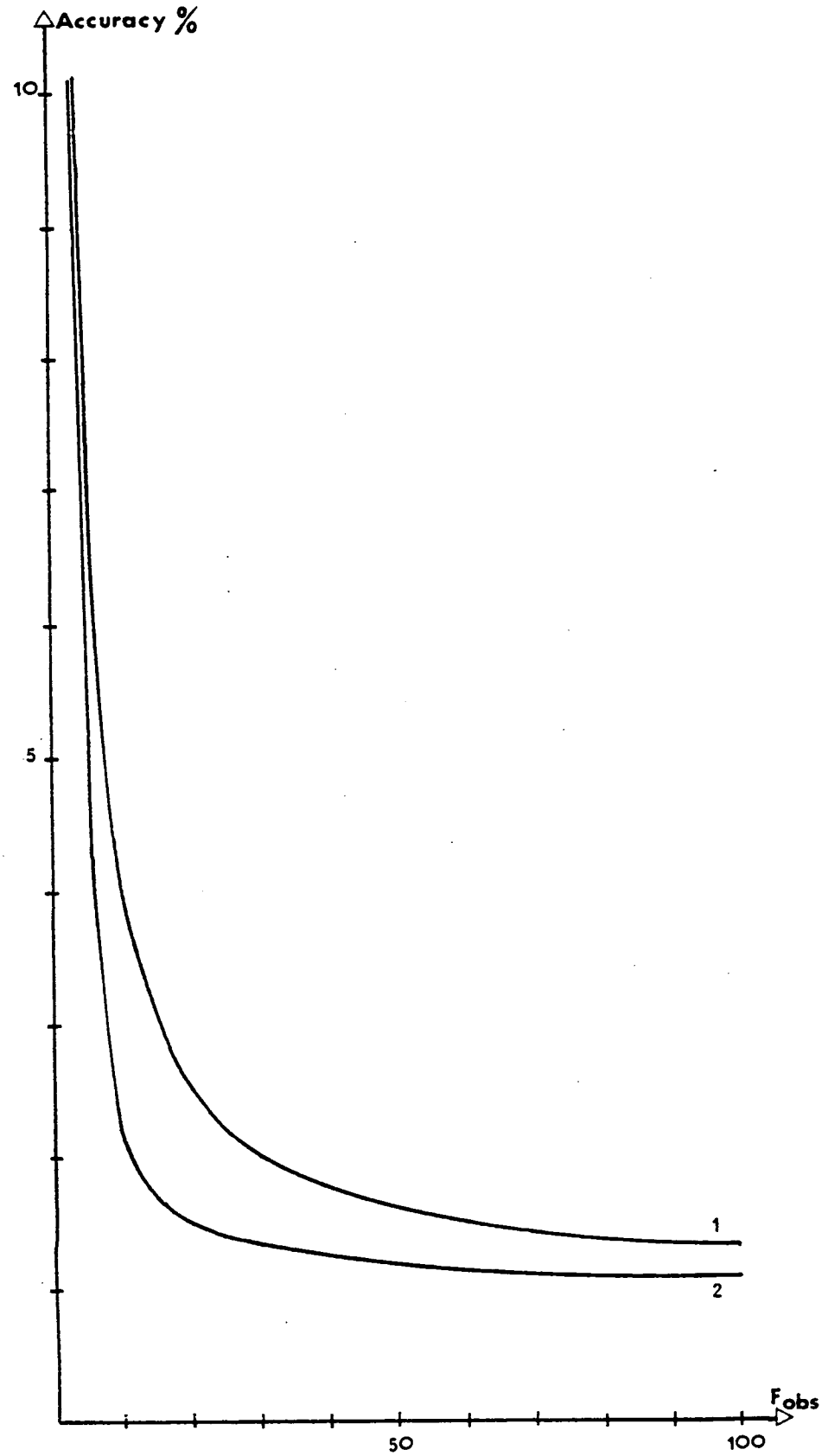


Figure 2.5.2

therefore $\sigma(F_{obs})/F_{obs} \approx 0.01$.)

In the second stage, the program employed a random number generator (see Appendix C) to modify each $F_{obs}$ by some small pseudo-random amount calculated using the flow chart of Figure 2.5.3. The modifications were constrained to be between $\pm 3\sigma(F_{obs})$ and chosen so that the spread in departures from the true $F_{obs}$'s, as generated by the test model, followed an approximately normal distribution, as it might reasonably be expected to do. Different initial integers used as input to the generator enabled different, but reproducible, modified data sets to be obtained. Three different sets of initial integers were used, giving three modified data sets denoted 1, 2 and 3 for each test model. It was found, taking the data set 1 statistics as an example, that 65% of the modified $F_{obs}$'s were less than $1\sigma(F_{obs})$ from the 'true' $F_{obs}$ with a further 27% less than $2\sigma(F_{obs})$ away. The other data sets gave similar statistics.

Each of the structure amplitude lists so produced can then be completely specified by four parameters and will, for the sake of conciseness and ease of reference, be denoted List(i,j,k,$\ell$). i may be either 1, 2 or 3 and serves as a label for different statistical fluctuations during the 'collection', i = 1 corresponding to data set 1 etc; j is the value assigned to $\delta$ in the test model and hence specifies the extent of the intrinsic X-ion disorder (the amount of anharmonicity); k specifies the orientation of the X-ion 'satellites', that is, the *structure* of the anharmonicity - 1 and 2 denoting the orientations of Figures 2.5.1(a) and (b) respectively; and $\ell$ = 1 or 2 specifies the empirical formula used to generate the $\sigma(F_{obs})$'s - either $\sigma_1(F_{obs})$ or $\sigma_2(F_{obs})$.

A short computer program has been written so that the actual real-space p.d.f. of the X ion can be calculated and mapped out directly from the model parameters. This allows a comparison to be made between the known distribution, as used to generate the unmodified structure amplitudes, and the distributions derived from

Figure 2.5.3 The flow chart used to calculate small pseudo-random modifications to the $F_{obs}$'s of the test data. The random vector $(N_1, N_2, N_3)$ is obtained from the generator (see Appendix C) by taking three successive random numbers $N_1$, $N_2$ and $N_3$. The range of possible values for each number has been chosen so that the spread in modifications to the $F_{obs}$'s is approximately Gaussian.

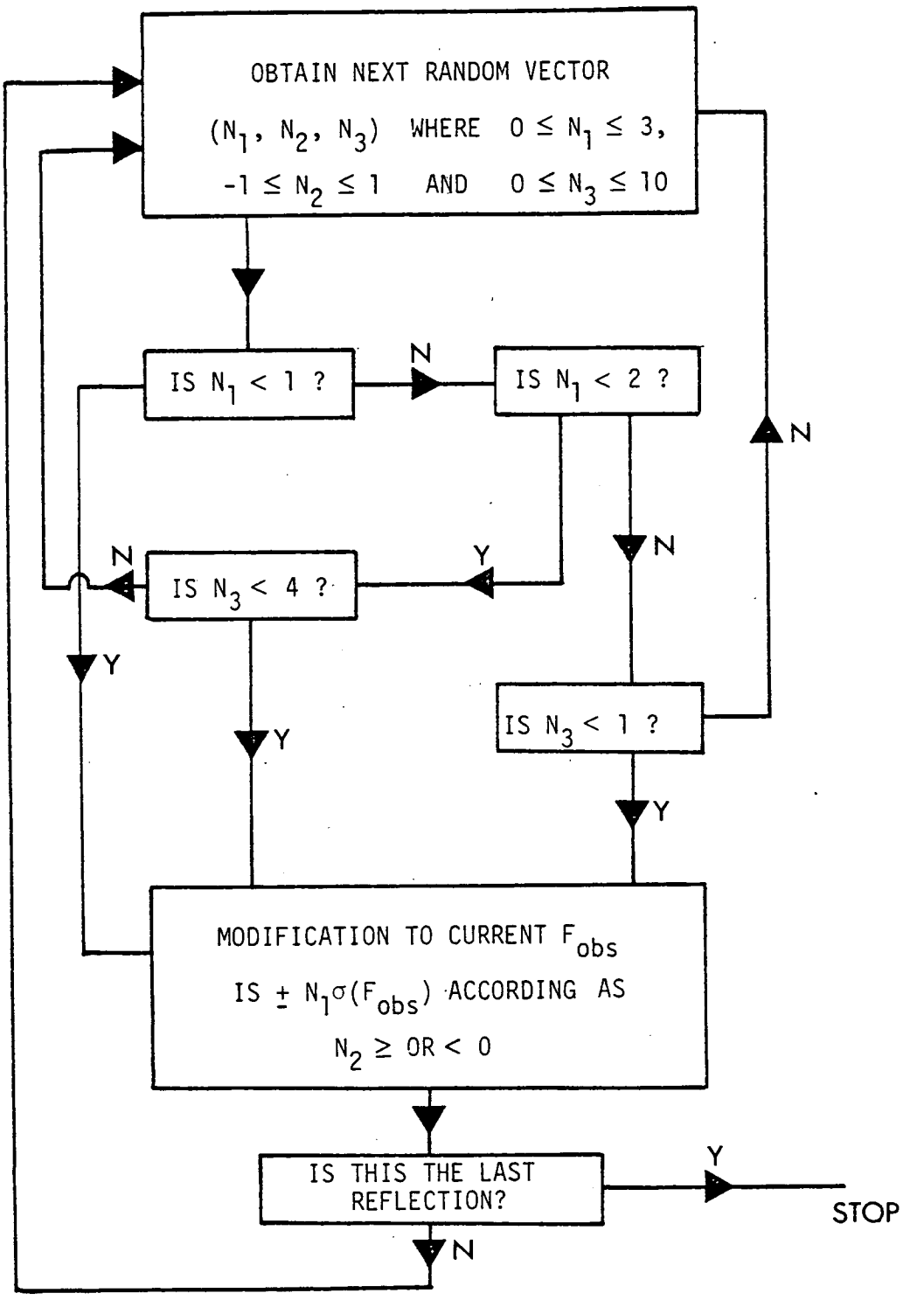
OBTAIN NEXT RANDOM VECTOR
$(N_1, N_2, N_3)$ WHERE $0 \leq N_1 \leq 3$,
$-1 \leq N_2 \leq 1$ AND $0 \leq N_3 \leq 10$
IS $N_1 < 1$ ?
N
IS $N_1 < 2$ ?
N
IS $N_3 < 4$ ?
N
Y
Y
N
IS $N_3 < 1$ ?
N
Y
Y
MODIFICATION TO CURRENT $F_{obs}$
IS $\pm N_1\sigma(F_{obs})$ ACCORDING AS
$N_2 \geq$ OR $< 0$
IS THIS THE LAST REFLECTION?
Y
STOP
N

Figure 2.5.3

the refined parameters of the temperature-factor expressions discussed in the earlier sections of this Chapter.

### 2.5.4 The Test Refinements

In each series of test refinements carried out on these generated data sets the parameters allowed to vary were (i) the overall scale parameter, Sc (see equation (3.7.1)), (ii) the extinction parameter, g, and (iii) the thermal parameters as specified. Neutron scattering lengths were fixed at their test-model values. Refinements were carried out by the method of least squares (Chapter 3.7) with the weight attached to each $F_{obs}$ being proportional to the inverse square of the corresponding $\sigma(F_{obs})$. The final data sets are labelled according to the convention established earlier : that is, according to the specific test model used (defined by j and k), and the specific modifications made (defined by i and $\ell$), in their production.

The notation employed later in this section is most easily illustrated by an example : for instance, the heading 'Refinements using List(i, 0.10 Å, k, $\ell$) i = 1, 2, 3, k = 1, 2, $\ell$ = 1, 2, means that the refinements specified in the text following the heading are carried out using each of the twelve data sets obtained by taking all combinations of i, k and $\ell$ with $\delta$ = 0.10 Å. The amount of intrinsic X-ion disorder is therefore fixed at $\delta$= 0.10 Å in the test models used to generate these particular data sets. By changing the values of i, k and $\ell$ individually, it is then possible to link specific differences in the refined parameter values with specific differences in the X-ion structure (the value of k) or the 'statistical' modifications made to the generated data sets (the values of i and $\ell$).

It would be extremely time-consuming, and would add little of value, to reproduce the results of every refinement in detail. In the example just quoted, twelve different data sets were used and five different refinement models tested for each - a total of sixty refinements. Therefore, although the results from each

of these refinements were fully considered, only a concise summary is given below of the general and unambiguous conclusions. For instance, condensed terminology such as 'statistical fluctuations in the data collection do not significantly bias parameter values' is used wherever possible to *imply* a more lengthy statement such as 'it was found that if j, k and $l$ are fixed, then the refined parameter values are not sensitive to changes in the value of i'. Continual, explicit reference to the parameters i, j, k and $l$ is therefore avoided.

(a) Refinements using List(i, 0, 1, $l$) i = 1, 2, 3, $l$ = 1, 2

The main points of interest extracted from refinements on these harmonic ($\delta$ = 0) data sets were as follows.

(i) Neither statistical fluctuations in the data collection nor reasonable changes in the weighting scheme significantly affect the refined parameter values : the value of any particular parameter obtained using any of the data sets was never more than two estimated standard deviations, as determined by the least-squares program, from its 'true' value. It is noted here that the six different data sets used in these refinements are derived from a *single* test model; the choice of i and $l$ simply specifies the modification of the 'true' data (which would be obtained in a completely ideal and error-free experiment) for effects due to the unavoidable inadequacies inherent in a real data collection.

(ii) The partial weights analysis (p.w.a.) - see Chapter 3.7 - is good : any fluctuations in the partial residuals over the Bragg range covered are non-systematic and can be entirely explained by random errors in the data collection (choice of i).

(iii) The addition of fourth-order anharmonic terms to any of the ionic temperature factors produces no significant improvement in fit to the data.

(b) Refinements using List (i, 0.05 Å, k, $\ell$) i = 1, 2, 3, k = 1, 2 $\ell$ = 1, 2

The conclusions summarised in paragraph (a), including (iii), remain true even in the face of the small X-ion anharmonicity.

(c) Refinements using List (i, 0.10 Å, k, $\ell$) i = 1, 2, 3, k = 1, 2 $\ell$ = 1, 2

It is still true that the refined parameter values are insensitive to either statistical fluctuations in the data collection or choice of weighting scheme. However, the addition of fourth-order terms, whether cumulant or F.I., to the X-ion temperature factor now results in a significantly better fit than that obtained using a purely harmonic model. As might be expected, the significance is greater when the more accurate ($\ell$ = 2) data is used ( $\xi$ = 4 compared with $\xi$ = 3 for the $\ell$ = 1 data - see Chapter 3.8 for a definition of $\xi$ ). The p.w.a., which shows some disturbing structure in the harmonic refinement, becomes much better (smoother as a function of Bragg angle) when the significant anharmonic terms are included. It is also noted that parameter correlation between the coefficients of the mutually orthogonal cumulant tensors is less than that between the elements of the non-orthogonal ones. Practically identical residuals (see equation (3.8.3)) are obtained using either the cumulant or the corresponding F.I. anharmonic descriptions. The refined anharmonic X-ion parameters are found to be extremely sensitive to the configuration of the 'satellites' (k = 1 or 2). In particular, the F.I. parameter $b_{044+}(X)$ is well determined and statistically very significant, as shown by an addditional refinement constraining it alone to be zero. The value of

$b_{044+}(X)$ is found to be negative or positive according as k = 1 or 2. The modification to the harmonic temperature factor resulting from the inclusion of this parameter in the anharmonic expansion is shown in Figure 2.4.1(b); the four-fold symmetry about the unique axis is clearly illustrated. It is sometimes found that refinements involving F.I. metal-ion anharmonic parameters tend to oscillate slightly. However, the use of damping coefficients of the order 0.7 - 0.8 applied to the parameter shifts, always results in satisfactory convergence. The fourth-order metal-ion parameters are again insignificant.

(d) Refinements using List (1, 0.15 Å, k, $\ell$) k = 1, 2, $\ell$ = 1, 2

From the results of the refinements using the $\delta < 0.15$ Å test data, there seemed little point in continuing to test the effect on the refined parameter values arising from random errors in the data collection : it is reasonable to assume that fluctuations of this nature will not be a major source of inaccuracy in the refined parameter values. For this reason only data sets with i = 1 are considered from now on in these test refinements.

The points to emerge from refinements carried out using the $\delta$ = 0.15 Å data sets confirm and reinforce those summarised in the previous paragraphs : if k = 1 then $b_{044+}(X)$ is negative; if k = 2 then $b_{044+}(X)$ is positive; the significance of the inclusion of fourth-order anharmonic terms in the X-ion temperature factor is greater for the more accurate ($\ell$ = 2) data set; and the thermal anharmonicity of the A and B ions is insignificant. However, effects due to the magnitude of the intrinsic, underlying disorder now begin to manifest themselves more clearly : even the inclusion of full fourth-order anharmonic thermal terms in the model does not result in an entirely satisfactory p.w.a. - although it is a substantial improvement over the very unsatisfactory one obtained from the harmonic refinement.

(e) Refinements using List (1, 0.2 Å, 1, $\ell$) $\ell$ = 1, 2

Since the configuration of the X-ion satellites has been shown

to give such unambiguous results with regard to the sign of $b_{044+}(X)$, it was decided to restrict the remaining refinements to the test configuration k = 1 (Figure 2.5.1(a)).

Again, the improvement in fit resulting from the inclusion of fourth-order anharmonic terms in the X-ion temperature factor is extremely significant ($\xi$ = 28 for the $\ell$ = 2 data); the further addition of metal-ion anharmonic terms is not. However, the fits (and the p.w.a.'s) have now become so poor that the refinement models themselves must be considered inadequate. Further refinements were therefore carried out using the more accurate ($\ell$ = 2) data with models incorporating anharmonic terms up to sixth order in the X-ion temperature factor. The results are very interesting. The improvement in fit using the cumulant formalism, over that obtained with the full fourth-order model, is slight ($\xi$ = 2); on the contrary, a very substantial reduction in the weighted residual is obtained when the F.I. formalism is used ($\xi$ = 19). Two of the sixth-order parameters, $b_{060+}(X)$ and $b_{064+}(X)$, are reasonably well determined - to 14% and 6% respectively - implying a correspondingly large degree of statistical significance. Even so, the p.w.a. is not completely satisfactory. It is nonetheless true that the reduction in the weighted sum of squares (equation (3.7.2)) from the harmonic fit value (6000) to the value obtained using the sixth-order F.I. model (400) is extremely large by any normal standards.

(f) Refinements using List (1, 0.3 Å, 1, 2)

This model structure was investigated for the sake of completeness, since the large value of $\delta$ (= 0.3 Å) means that the disorder within the X ion is *in principle* resolvable, ie, the p.d.f. is multi-peaked in an equilibrium situation. As expected, the resulting residuals are very large ($R$ = 0.21 and $R_W$ = 0.29) for the harmonic model. In spite of this, the p.w.a. for the model with up to sixth-order F.I. terms is not completely unacceptable and certainly much better than that obtained from the refinement using the sixth-order cumulant model. The model limitations are,

however, clearly highlighted by the unacceptably large values obtained for the residuals (R and $R_W$ = 0.08 and 0.09 respectively for the full sixth-order F.I. model).

### 2.5.5 Analysis of the Results of the Test Refinements

Some indication of the appropriateness of the different anharmonic thermal formalisms discussed earlier in the chapter can clearly be obtained from a consideration of such features as the fit (the value of the weighted residual) obtained from the refinements and the amount of structure in the p.w.a..

However, the criteria to be adopted in determining the suitability of the models used should certainly be more rigorous than these. In particular, care should be taken to ensure that each refined parameter is susceptible to a meaningful physical interpretation : in other words, if a particular variance analysis (for example the Ratio Test of Hamilton - see Chapter 3.8) shows that the addition of extra variable parameters to the refinement model gives a significantly better fit, then the information contained therein should manifest some feature of the system being modelled which is not accessible to the refinement model *without* the extra parameters. It may happen that the refined values of the additional parameters are, in themselves, of little interest to the analyst. For instance, although corrections for attenuation due to extinction are now commonplace in crystallography, the fact that extinction parameters can often be made to yield some estimate of the spread in mosaic block orientations is usually ignored; if such corrections give an improvement in fit then they are usually assumed to be valid and greater confidence is accordingly placed in the values of the other, more interesting parameters.

However, care must be taken when some interpretation of the refined parameters *is* required. Both Merisalo and Larsen (1977) and Sakata et al (1979) have reported results from diffraction analyses in which completely different sets of refined anharmonic potential parameters have given quantitatively similar and otherwise

acceptable fits to the data being tested. In the latter case, the specific functional form of the refinement model was different for each set of parameters; in the former, the model was the same for each set.

For the purpose of the present study it is therefore of interest and importance to critically compare the p.d.f.'s *derived* from the parameters of the test refinements with the *known* generating distribution. In the ideal case - that is, with a perfect model - the distributions would be the same. In practice, the shape of the derived p.d.f. will deviate from the true shape. The appropriateness of the anharmonic models must therefore be crucially dependent upon the size of such deviations and, just as important, upon their structure if any.

### 2.5.6 Comparison of the Known and Derived Test Model P.d.f.'s

Comparisons were restricted to the X-ion p.d.f.'s because harmonic thermal descriptions were always found to be adequate for the A and B ions. It was further decided to concentrate attention on those model systems with $\delta \geq 0.15$ Å; anharmonicity for those with $\delta < 0.15$ Å was small (see Sections 2.5.4(a) - (c)). Several different methods are available for the reconstitution of the p.d.f.'s from the refined thermal parameters and from these the following three were chosen.

#### (i) Fourier Method

The parameters from the cumulant-model refinements were used to generate complete three-dimensional structure-amplitude lists out to a resolution limit $(\sin \theta_B/\lambda)_{max} = 1.8$ Å$^{-1}$. This was the resolution of the 'real' data, ie, the data obtained during the experiment on $RbCaF_3$ at 205°K. Because of the high crystal symmetry, only 1/48 of the complete set has to be calculated. The p.d.f. was then obtained by a standard Fourier summation. It was found from a few initial trials that series termination effects (see Lipson and Cochran (1966)) were often disturbingly large.

For this reason, the lists were extended to a resolution of 2.2 $\mathring{A}^{-1}$, this choice affording a reasonable compromise between accuracy and speed of calculation. Difference syntheses were also calculated using unweighted coefficients ($F_A$ - $F_H$), so that any significant features in the p.d.f.'s obscured by termination ripples might be more apparent. ($F_A$ and $F_H$ are respectively the structure amplitudes generated from the models with and without anharmonic cumulant parameters.)

(ii) Edgeworth Expansion Method

The refined cumulant parameters, having been converted from the orthogonal status to the standard non-orthogonal, were also used to obtain p.d.f.'s via the Edgeworth expansion (expression (2.3.1)). Again difference maps were calculated using the best-fitting harmonic approximation as the reference. Normalisation of the anharmonic p.d.f. to the value obtained for the best-fitting harmonic approximation was checked by summation over the full three-dimensional distributions.

It is noted in passing that any observed differences between the p.d.f.'s generated using the methods (i) and (ii) must be attributable to the different approximations involved in the *use* of the refined parameters, since the parameter values themselves are the same in each case.

(iii) Fourier-invariants Method

The p.d.f.'s were obtained using expression (2.4.4) and difference maps from these by subtraction of the best-fitting harmonic distribution. From an examination of the work of Kurki-Suonio et al (1979), it is clear that particular attention must be paid to the proper normalisation of $P_i(\underline{r})$ so that the p.d.f.'s derived from different sets of parameters can be meaningfully compared. This potential problem does not arise in the work just quoted for two reasons : (a) due to parameter correlation problems, the second-order thermal parameters were kept fixed at

their refined harmonic-approximation values; and (b) only fourth-order thermal parameters were refined. The result of (a) is that the prefactor $B_1^2 B_3$ in expression (2.4.4) remains unchanged between their harmonic-model and anharmonic-model analyses. For reason (b), the part within curly brackets in expression (2.4.4) takes precisely the value N at $\underline{r} = \underline{0}$. (This must be so because, since $i^4 = 1$, the expansions in expressions (2.4.4) and (2.4.5) have the same value when $\underline{S} = \underline{r} = \underline{0}$.) If, however, the second-order thermal parameters are allowed to (and *do*) change between refinements, or if sixth-order terms are included, $P_i(\underline{0})$ will not be a constant in general. Restrictions on the generality of the temperature factor, such as those - (a) and (b) - imposed by Kurki-Suonio et al (1979), therefore lead to clearly identifiable restrictions on the extracted p.d.f.

Anharmonic and difference maps were calculated for the three test models, List (1, 0.15/0.20/0.30 Å, 1, 2) using each of these methods. Each p.d.f. was calculated at the points of a cubic grid. Spacings along the principal axes of the grid of 0.02 Å, 0.025 Å and 0.03 Å respectively for the $\delta$ = 0.15 Å, 0.20 Å and 0.30 Å models were found to be adequately small so that no detail was obscured.

An examination of the resulting X-ion maps showed that the interesting anharmonic features were predominantly confined to the section perpendicular to the unique four-fold axis and containing the A ions - not an unexpected observation considering the structure of the test models. Only the difference maps of this section are reproduced here for the $\delta$ = 0.15 Å and 0.20 Å models (Figures 2.5.4 and 2.5.5); for the $\delta$ = 0.3 Å model both p.d.f. and difference maps of this section are shown (Figure 2.5.6). The axes labelled X and Y are respectively those denoted [1, 0, 0] and [0, 1, 0] in Figure 1.4.3, ie, the conventional major axes of the

harmonic p.d.f.. The model used in the anharmonic refinement in each case is specified in the accompanying figure captions. For each series of maps, corresponding to the three different test models examined, the best-fitting harmonic p.d.f.was normalised so that the value $P(\underline{0}) = 10{,}000$; the p.d.f.'s derived from the anharmonic parameters via the methods (i), (ii) and (iii) above were then normalised in the ways already stated. The p.d.f.'s calculated from the *known* distributions were normalised by summation over the full three-dimensional grid; the arbitrary scaling constants were then adjusted so that the sum was equal to that obtained from a parallel summation over the harmonic distribution. In this way, the total density was maintained constant between each of the p.d.f.'s obtained for any given test model. It should be noted, however, that the density in any given *section* of the p.d.f. need not be a constant and, in general, will not be.

A clear qualitative comparison of the appropriateness of the methods used in the derivation of these p.d.f.'s can be obtained from an examination of the maps shown in Figures 2.5.4 - 6. For ease of reference, specific features of interest are detailed in the accompanying figure captions and need not be repeated here. It is clear though, that caution must be exercised in drawing conclusions from these maps : in particular , the different vertical scales should be noted.

To put the comparison of the anharmonic p.d.f.'s derived by the three different methods on a more quantitative basis, several specific features were measured for the known and each of the derived p.d.f.'s and the results tabulated in Table 2.5.1.

First, the height of the distribution at the mean position, 0, was obtained. Second, the distances along [1, 0, 0] to the points at which the p.d.f. drops to 0.5 and to 0.25 of its peak value were measured. And third, a measure of the *anisotropy* in the section arising from the underlying structured *anharmonicity* was obtained as the ratio of the p.d.f. values at equal distances from 0 along the [1, 0, 0] and [1, 1, 0] directions. These distances

Figure 2.5.4 Known and reconstituted X-ion difference p.d.f.'s obtained for the test model List (1, 0.15, 1, 2). The labelling of the axes (X and Y) is as established in Figure 1.4.3; the full A-X section may therefore be obtained by $90^{o}$ rotations about the four-fold axis. Each anharmonic p.d.f., $P_a$, is normalised to the value of the harmonic approximation p.d.f., $P_h$, which is assigned the (arbitrary) value 10,000 at 0. The r.m.s.a. in the harmonic approximation (which is isotropic about the four-fold axis) is indicated by the vertical line on the X-axis at 0.137 Å.

(a) The known difference p.d.f..

(b) The Fourier-invariant difference p.d.f., constructed using the methods of Section 5.6(iii) from the fourth-order parameters obtained for the model with fourth-order parameters on all ions.

(c) The Fourier-difference p.d.f., constructed using the methods of Section 5.6(i) from the structure amplitudes obtained for the model with fourth-order cumulant parameters on all ions.

(d) The Edgeworth-expansion difference p.d.f., constructed using the methods of Section 5.6(ii) from the fourth-order cumulant parameters obtained for the same model as that of (c).

The different vertical scales used in the maps should be noted before any objective comparisons are made. For instance, the magnitude of the known difference-distribution peaks along X and Y (see map (a)), is not reproduced in either of maps (b) and (c), although (b) provides a better approximation. The known difference distribution shows a large dip at 0 corresponding to a reduction of about 15% in the p.d.f. at that point compared with the value given by the harmonic-approximation p.d.f.; by comparison, the dip shown in map (c) corresponds to a difference of less than 2%.

Clearly, the distribution given by map (d) provides (at least subjectively) the worst agreement with the known distribution. It is recalled that maps (c) and (d) have been produced from the *same* refined parameters.

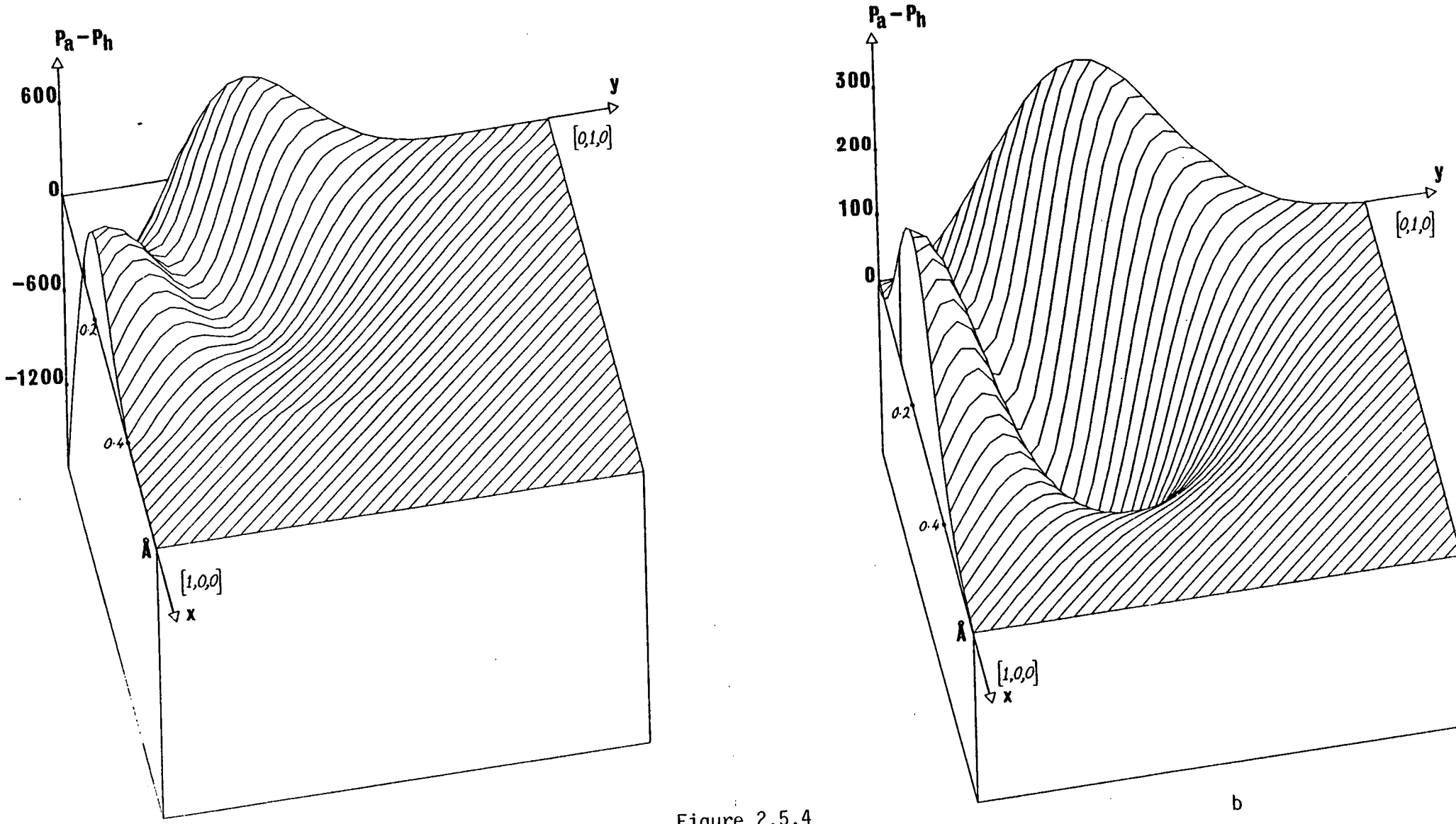
$P_a - P_h$
600
0
-600
-1200
y
[0,1,0]
0.2
0.4
Å
[1,0,0]
x
a
$P_a - P_h$
300
200
100
0
y
[0,1,0]
0.2
0.4
Å
[1,0,0]
x
b

Figure 2.5.4

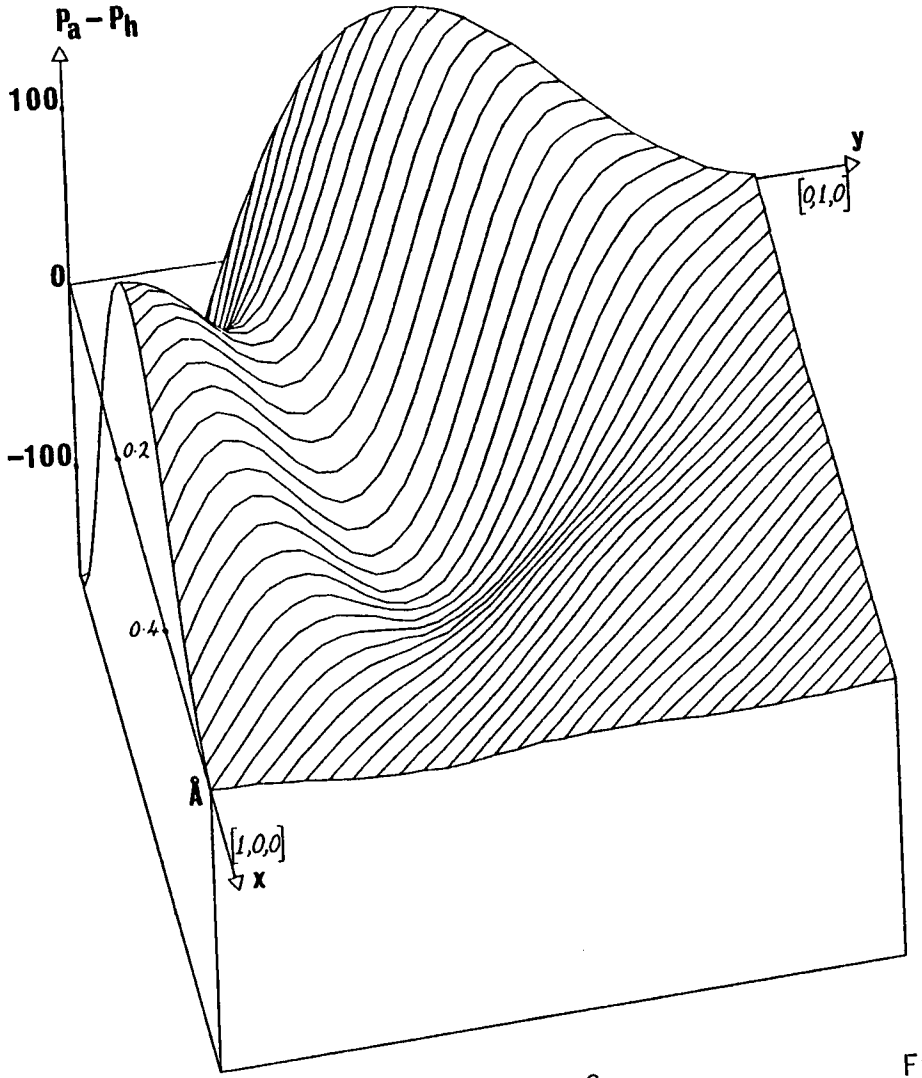


c

Figure 2.5.4

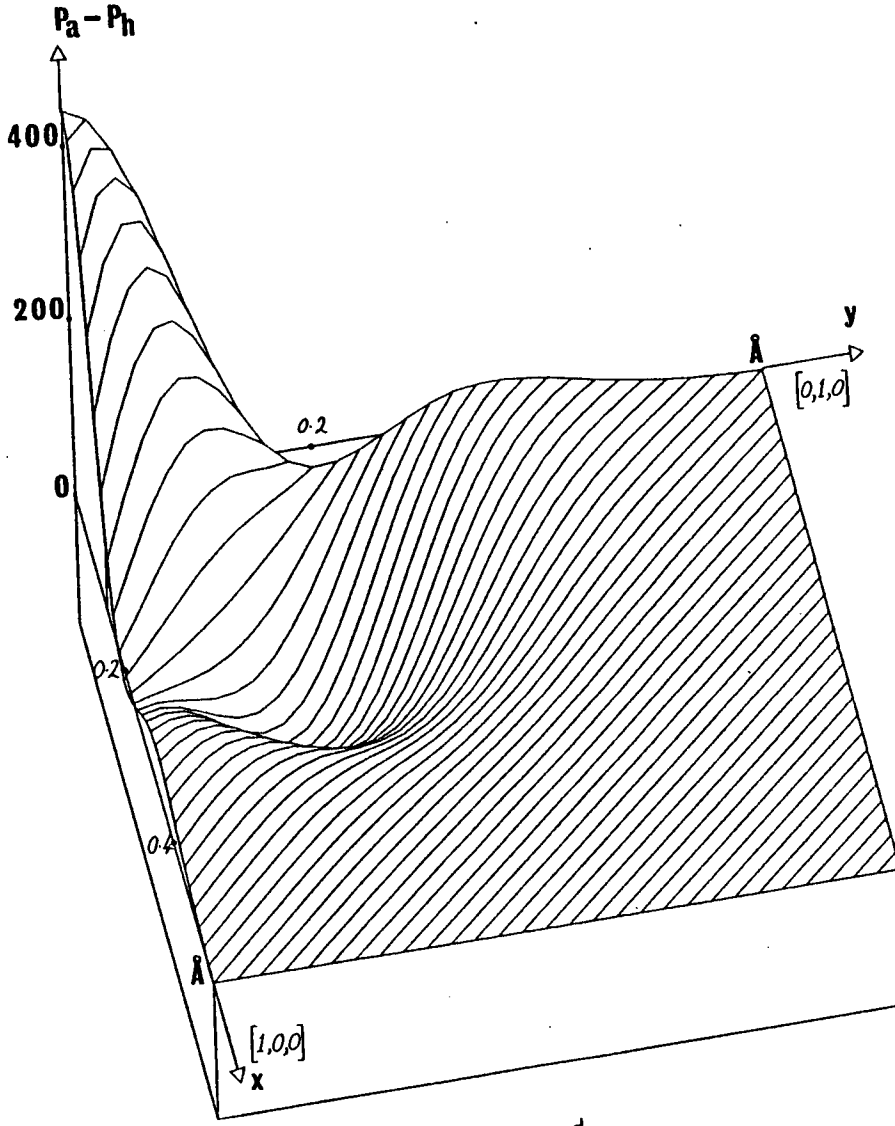


d

Figure 2.5.5 Known and reconstituted X-ion difference p.d.f.'s obtained for the test model List (1, 0.20, 1, 2). The labelling of the axes (X and Y) is as established in Figure 1.4.3; the full A-X section may therefore be obtained by $90^{o}$ rotations about the four-fold axis. Each anharmonic p.d.f., $P_a$, is normalised to the value of the harmonic-approximation p.d.f., $P_h$, which is assigned the (arbitrary) value 10,000 at 0. The r.m.s.a. in the harmonic approximation (which is isotropic about the four-fold axis) is indicated by the vertical line on the X-axis at 0.16 $\mathring{A}$.

(a) The known difference p.d.f..

(b) The Fourier-invariant difference p.d.f., constructed using the methods of Section 5.6 (iii) from the fourth- and sixth-order parameters obtained for the model with such parameters on all ions.

(c) The Fourier difference p.d.f., constructed using the methods of Section 5.6(i) from the structure amplitudes obtained for the model with fourth- and sixth-order cumulant parameters on all ions.

(d) The Edgeworth-expansion difference p.d.f., constructed using the methods of Section 5.6(ii) from the fourth-order cumulant parameters obtained for the same model as that of (c). The sixth-order parameters were not used in the construction because the program written to calculate the Edgeworth expansion is truncated at fourth order. However, as stated in the text (Section 5.4(e)), the sixth-order terms are only marginally significant and do not bias the lower-orders.

The different vertical scales used in these maps should again (see the caption to Figure 2.5.4) be noted. Subjectively (see the text for a more quantitative and objective comparison), the reconstituted difference distributions vary considerably in their agreement with the known distribution of map (a). Map (b) compares very favourably while map (d) certainly does not. Series termination ripples are very clearly shown in map (c).

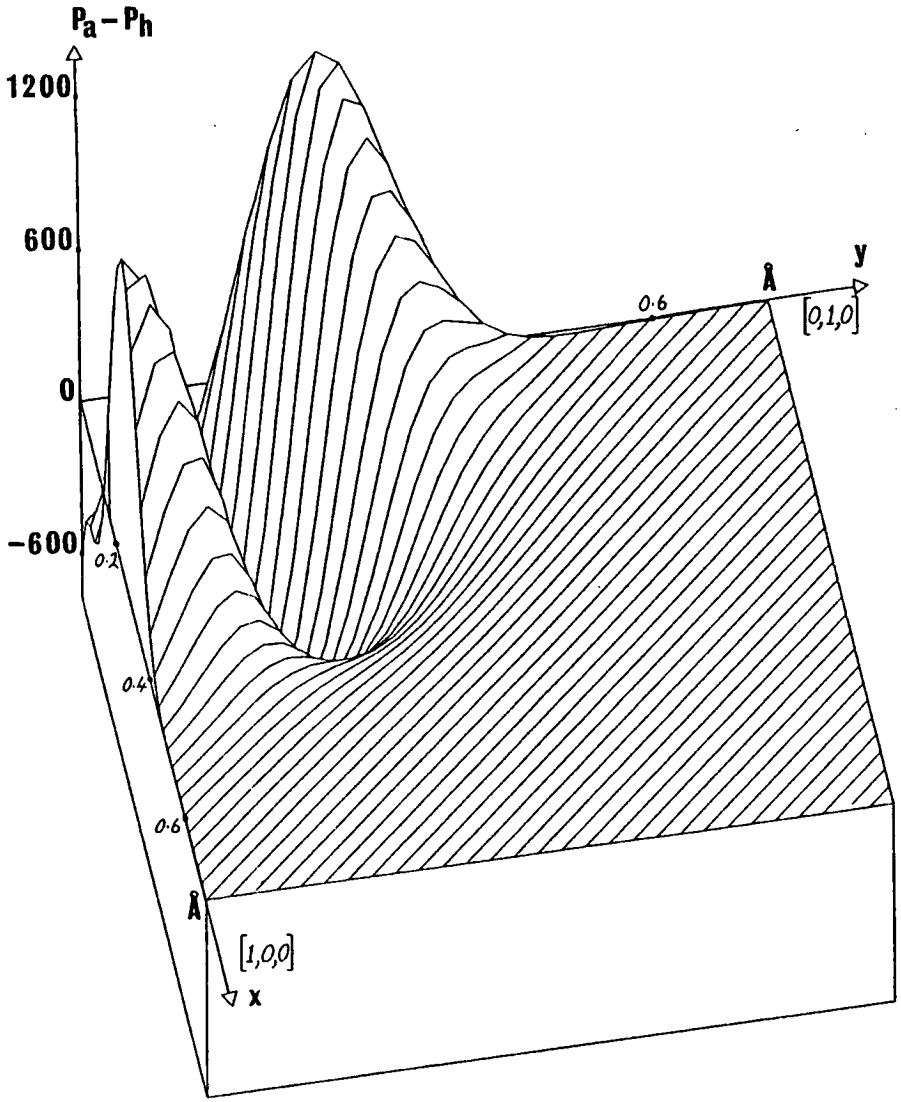


a

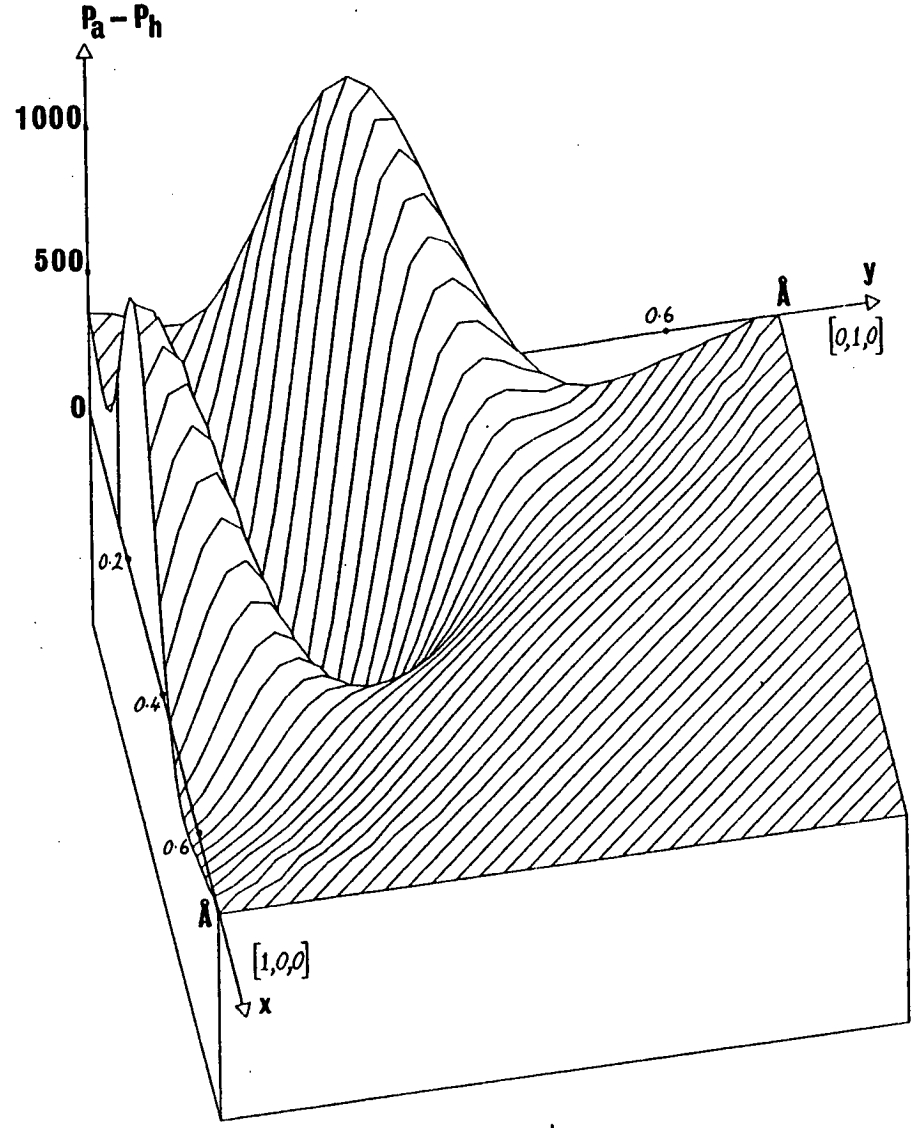


b

Figure 2.5.5

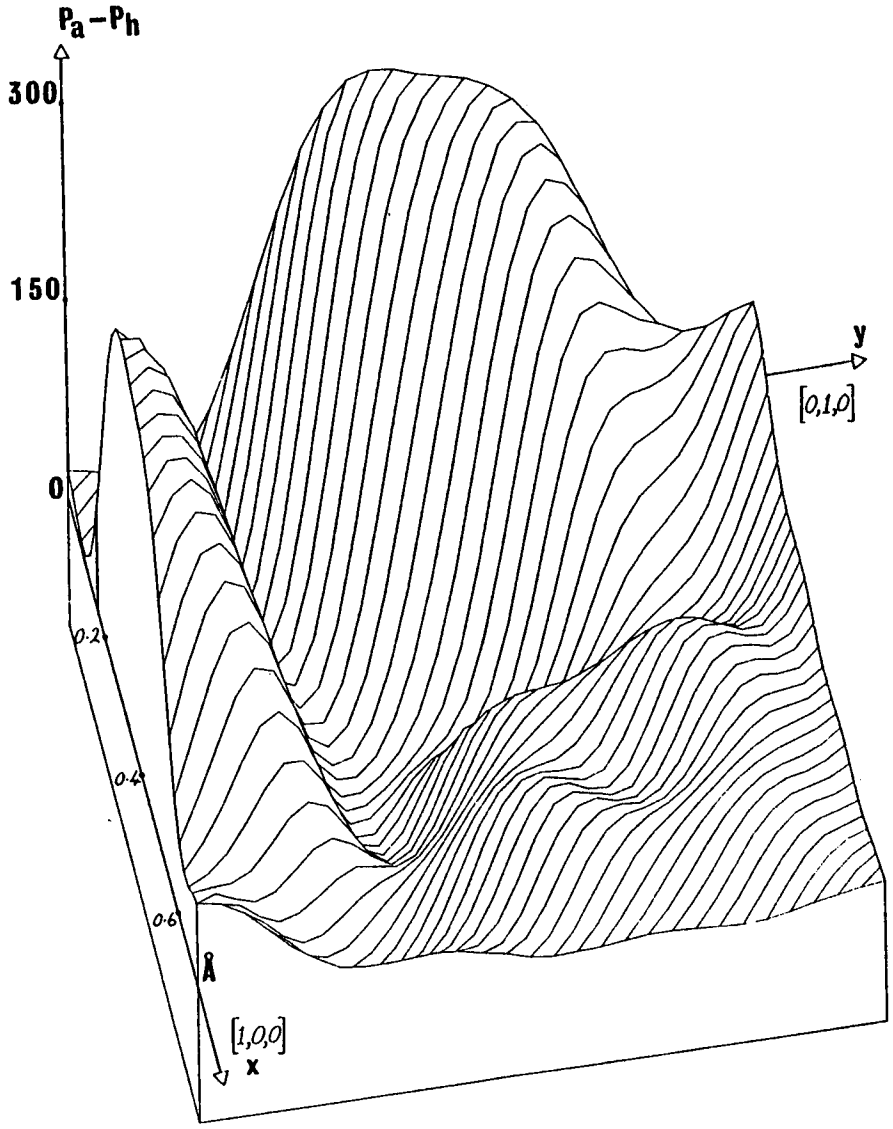


c

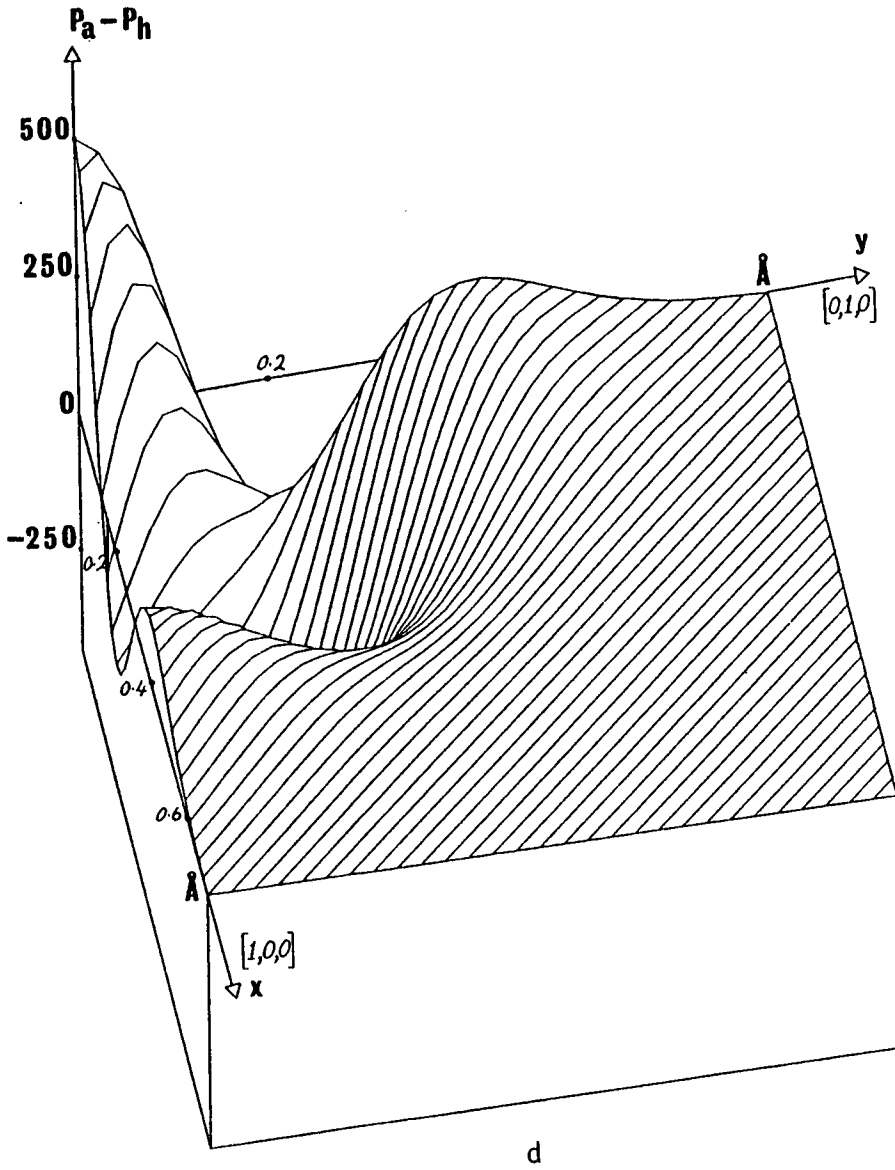


d

Figure 2.5.5

Figure 2.5.6 X-ion p.d.f.'s and difference p.d.f.'s obtained for the test model List (1, 0.30, 1, 2). The labelling of the axes (X and Y) is as established in Figure 1.4.3; the full A-X section may therefore be obtained by $90^{o}$ rotations about the four-fold axis. The anharmonic p.d.f.'s, $P_a$, are normalised to the value of the harmonic-approximation p.d.f., $P_h$, which is assigned the (arbitrary) value 10,000 at 0. The r.m.s.a. in the harmonic approximation (which is isotropic about the four-fold axis) is indicated by the vertical line on the X-axis at 0.2 Å.

(a) The known p.d.f..

(b) The Fourier-invariant p.d.f., constructed using the methods of Section 5.6(iii) from the fourth- and sixth-order parameters obtained for the model with such parameters on all ions.

(c) The known difference p.d.f..

(d) The Fourier-invariant difference p.d.f..

Known resolvable disorder has clearly not been reproduced in map (b). Comparison of maps (b) and (d) shows that what appears in the *difference* map to be a substantial modification to the harmonic-approximation p.d.f., may in fact produce an apparently small change in the *actual* p.d.f..

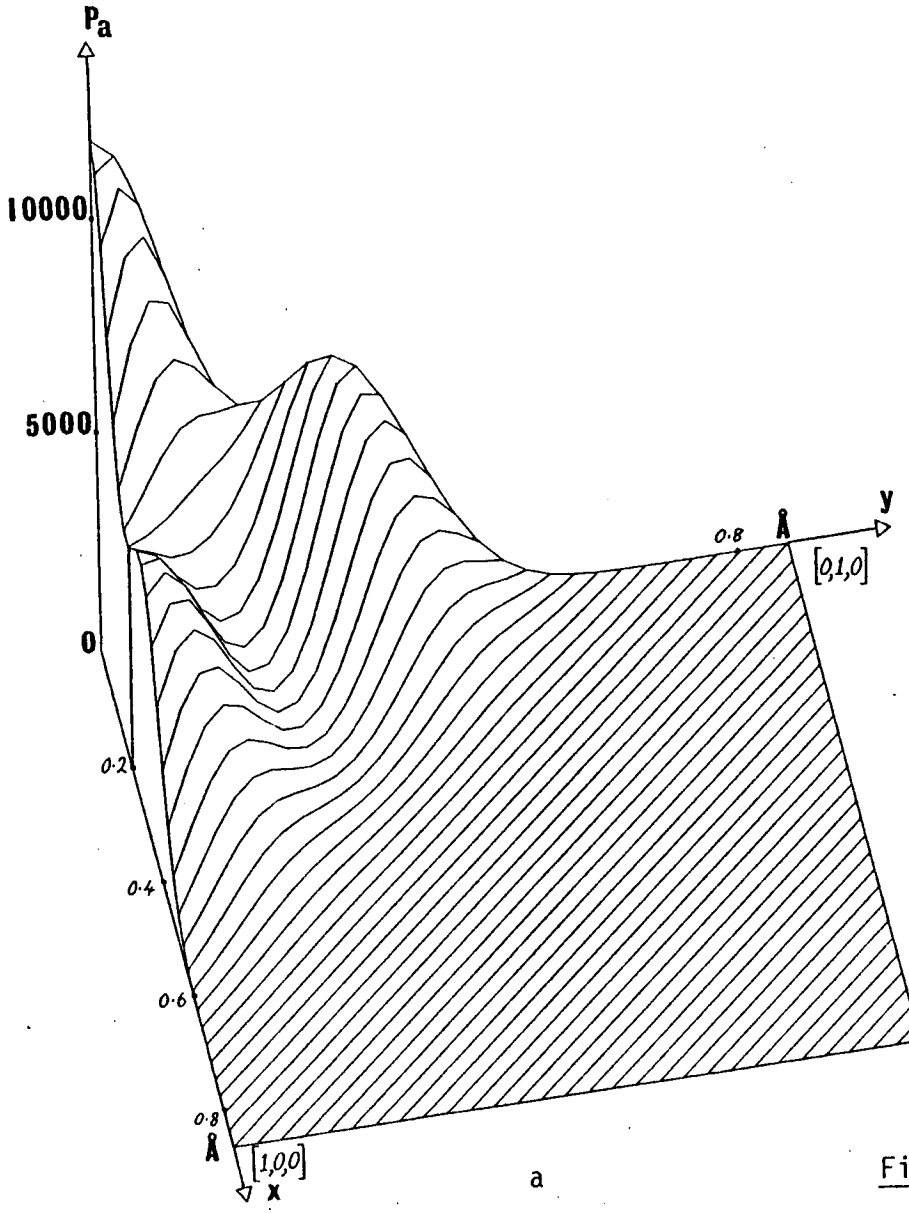


a

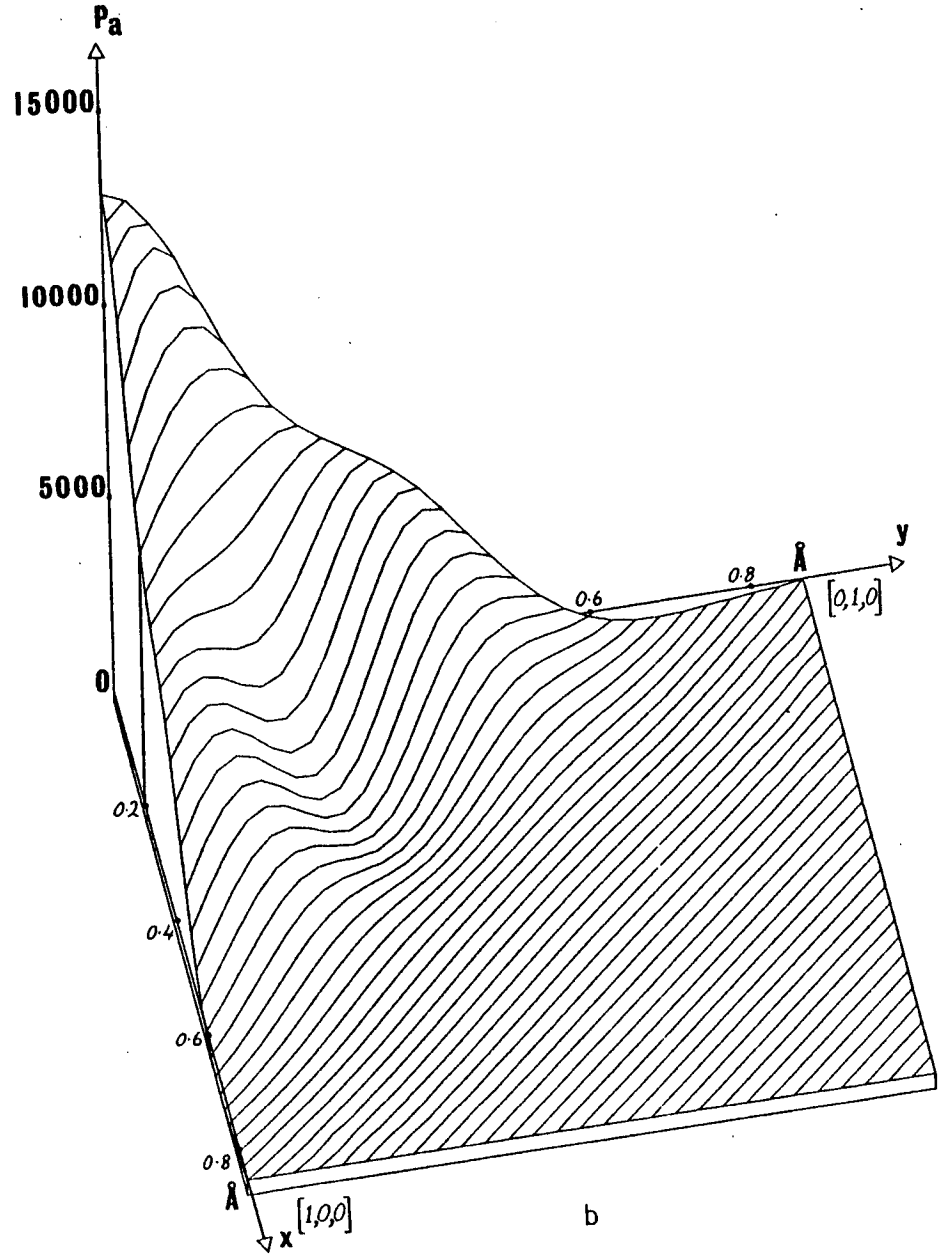


b

Figure 2.5.6

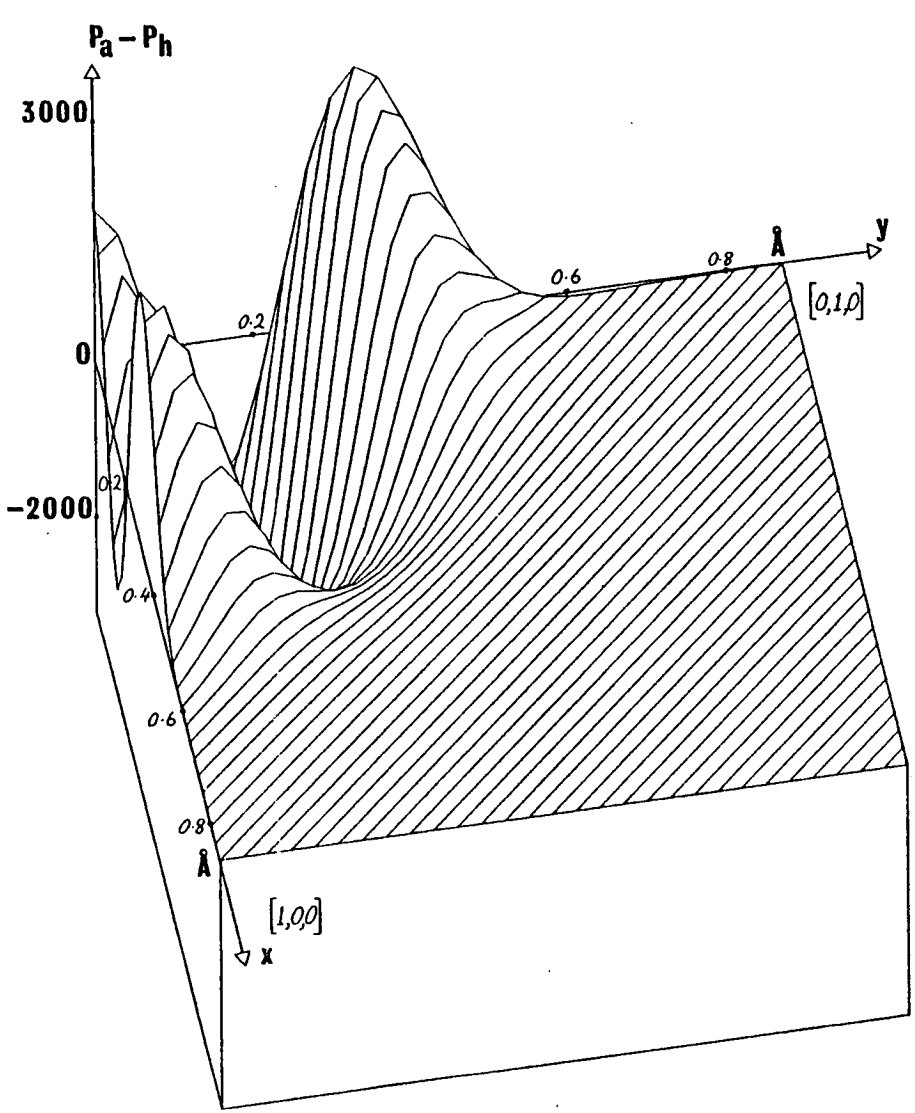


c

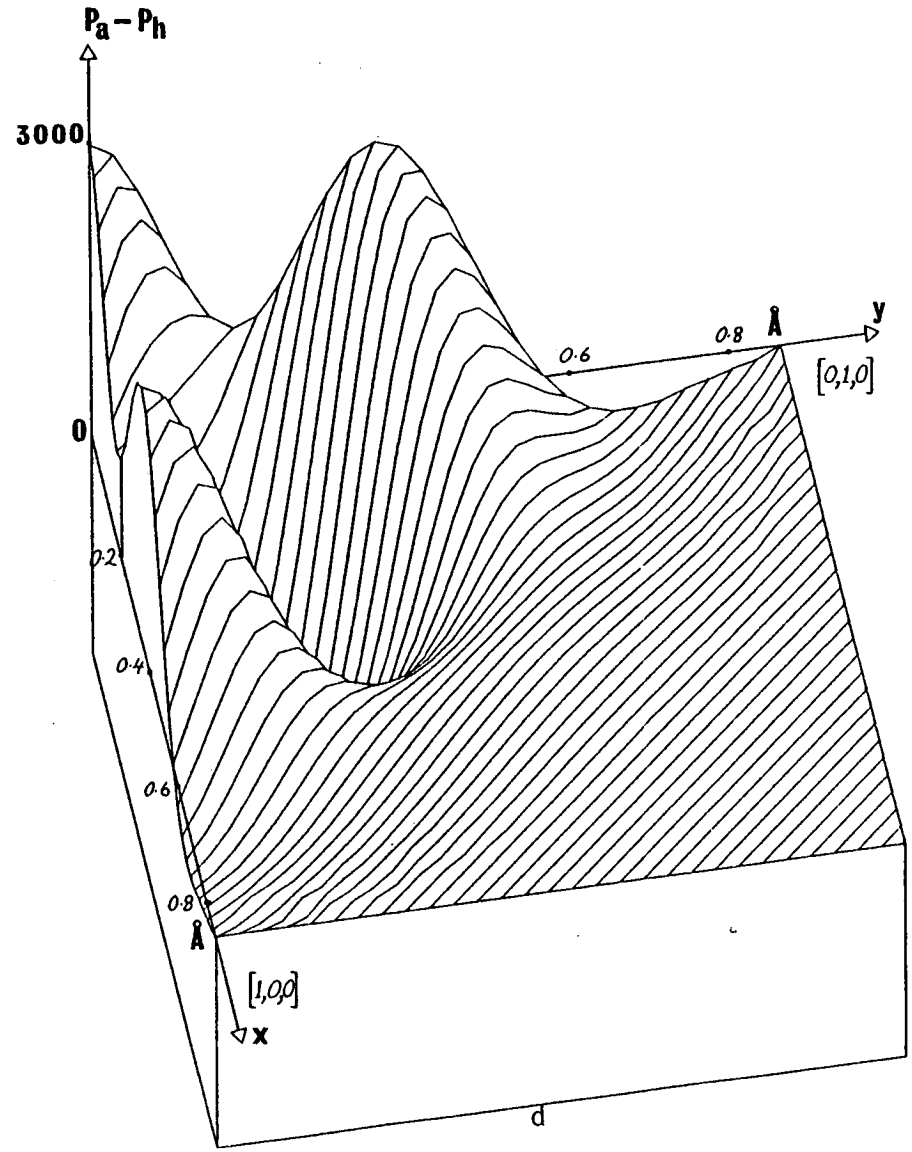


d

Figure 2.5.6

Table 2.5.1. Comparison of known X-ion p.d.f.'s with corresponding p.d.f.'s derived from refined F.I. and cumulant thermal parameters. The test distributions $\delta$ = 0.15Å/0.20Å/0.30Å are those labelled List (1, 0.15/0.20/0.30, 1, 2) in the text. The distributions Known, F.I., Fourier and Edgeworth refer respectively to the p.d.f.'s generated direct from the test model parameters, to those generated using the F.I. method (section 5.6(iii)), to those generated using the Fourier method (section 5.6 (i) ) and to those generated using the Edgeworth expansion method (Section 5.6 (ii) ). The columns list (i) the value of the p.d.f. at the centre of the distribution - $P(\underline{0})$ - when the harmonic-approximation p.d.f. is normalised to 10,000 at that point, (ii), the distance along the axis [1,0,0] of Figure 1.4.3 at which the value of the p.d.f. falls to $\frac{1}{2}P(\underline{0})$ - $X(\frac{1}{2}P(\underline{0}))$, (iii) the corresponding distance for $\frac{1}{4}P(\underline{0})$ - $X(\frac{1}{4}P(\underline{0}))$, and (iv) the ratio of the p.d.f. values at equal distances along [1,0,0] and [1,1,0] - Ratio. These distances are taken to be 0.2Å, 0.25Å and 0.3Å for the $\delta$ = 0.15Å, 0.2Å and 0.3Å test models respectively, and the integers specifying the ratio are the p.d.f. values divided by 100. The $\delta$ = 0.3Å model p.d.f.'s have not been reconstituted using the Fourier or Edgeworth-expansion methods because the corresponding fits in the refinements were so poor.

The meaning of the numbers can be clarified by an example. For instance, the p.d.f. reconstituted via the Fourier method, from the cumulant parameters refined using the $\delta$ = 0.2Å test data, is characterised as follows. The value of the distribution at its centre (10018) is greater than the known value at that point (9402). The distribution falls off rather more quickly than the known one, to 0.5 and 0.25 of $P(\underline{0})$ at distances 0.19Å and 0.27Å along [1,0,0] compared with 0.22Å and 0.31Å in the known distribution. The anisotropy in the A-X section, defined by P(0.25Å, 0,0) : P($\sqrt{0.25}$ Å, $\sqrt{0.25}$ Å, 0) is 3100 : 2800 - much less than that obtaining in the known distribution (4000 : 2100).

| Distribution | P (0) | X ($\frac{1}{2}$P(0) ) | X ($\frac{1}{4}$P(0) ) | Ratio |
|---|---|---|---|---|
| $\delta$ = 0.15Å | | | | |
| Known | 8419 | 0.19Å | 0.25Å | 38:33 |
| F.I. | 9992 | 0.16 | 0.24 | 36:33 |
| Fourier | 9839 | 0.16 | 0.24 | 36:35 |
| Edgeworth | 10451 | 0.16 | 0.23 | 33:32 |
| $\delta$ = 0.20Å | | | | |
| Known | 9402 | 0.22Å | 0.31Å | 40:21 |
| F.I. | 10350 | 0.20 | 0.31 | 38:22 |
| Fourier | 10018 | 0.19 | 0.27 | 31:28 |
| Edgeworth | 10511 | 0.17 | 0.25 | 26:24 |
| $\delta$ = 0.30Å | | | | |
| Known | 11841 | 0.28Å | 0.42Å | 60:10 |
| F.I. | 12970 | 0.22 | 0.42 | 53:10 |
| Fourier | - | - | - | - |
| Edgeworth | - | - | - | - |

were taken to be 0.2 Å, 0.25 Å and 0.3 Å respectively for the $\delta$ = 0.15 Å, 0.2 Å and 0.3 Å test models.

The results of these comparisons for each of the three test models were as follows.

(i) $\delta$ = 0.15 Å Model

The value of the known p.d.f. (as used in the test model), at the mean position, 0, is about 20% less than the corresponding value obtained from the harmonic approximation to it. Furthermore, none of the derived anharmonic p.d.f.'s is able to improve significantly upon this large disagreement - each gives a value about 20% high (see Table 2.5.1, Column 1). It also appears, perhaps as a corollary of the first observation, that the flattened shape of the p.d.f. near 0 cannot be reproduced satisfactorily : each derived p.d.f. is sharper than the known one, and by about the same amount for each. This can be seen from the fact that the distance from 0 to the position along X at which the p.d.f. falls to $\frac{1}{2}P(\underline{0})$ is significantly greater for the known distribution - see Table 2.5.1, Column 2. However, further from 0 along the X axis, the point at which the distribution drops to $\frac{1}{4}P(\underline{0})$ is reproduced reasonably well by each method. The specific area in which one method seems clearly to be preferred to the others is in the description of the anisotropy of the distribution. The parameters of the cumulant model, whether employed via the Edgeworth expansion method or via the Fourier Synthesis method, yield anharmonic p.d.f.'s which underestimate the anisotropy : in fact, using this *ad hoc* definition of anisotropy, the X-Y sections are nearly isotropic about the four-fold axis - see Table 2.5.1, Column 4. Although the F.I. p.d.f. does not show quite enough anisotropy, it is clear that in this respect it provides a more realistic description of the true distribution. It is interesting to point out that the weighted sum of squares obtained in the refinement yielding the cumulant parameters was actually slightly *lower* than that obtained with the F.I. model (249 and 260 respectively).

(ii) $\delta = 0.20$ Å Model

Again, the values of the derived anharmonic p.d.f.'s at 0 are higher than that of the known distribution. There is still a tendency to underestimate the distance along X at which the distribution height is 0.5 of its peak value (at 0), so that the flattening of the p.d.f. around 0 is not accurately reproduced by any of the methods. However, it can be seen that the p.d.f. derived from the F.I. parameters does provide a slightly better description than those derived from the cumulant parameters (see Table 2.5.1, Column 2). Further along the X-axis, it is found that the p.d.f. derived from the F.I. parameters matches the known distribution very closely. Turning to the question of anisotropy in the X-Y section, it is clear from the last column in Table 2.5.1 that the ratio obtained from the F.I. p.d.f. is in very good agreement with the true ratio; the ratios obtained from the cumulant p.d.f.'s certainly are not. The apparent superiority of the F.I. description might have been expected for this test model because the weighted sums of squares obtained from the F.I. - and cumulant - model refinements were 409 and 941 respectively.

(iii) $\delta = 0.3$ Å Model

The fit obtained with the anharmonic cumulant model was so poor that it was not considered worthwhile constructing the X-ion p.d.f. from the refined parameters. However, the maps obtained from the refined F.I. parameters were examined for significant features. From Table 2.5.1 it can be seen that the derived p.d.f. is again the sharper - as it has been for each of the test models investigated. In spite of this, some consolation can be extracted from the facts that the known and derived p.d.f.'s match well further from 0 and that there is a reasonable correspondence between the ratios specifying the anisotropy. Clearly, though, the resolvably disordered structure in the p.d.f. is not reproduced.

## 2.5.7 Conclusions

In attempting to summarise the findings from these test refinements, it must be borne in mind that strictly speaking, any conclusions reached *may* only be valid for the specific symmetry (4/mmm) examined. The proper validation of any general description of atomic thermal motion must be based on its proven suitability over a much greater range of conditions (different site symmetries, thermal amplitudes, etc) than time has permitted here. However, because the model systems have been *chosen* so as to reproduce specific features (and (perhaps?) postulated features) of cubic perovskite crystals, it is reasonable to contend that the conclusions reached will have some relevance in the analysis of these crystals.

The conclusions summarised below are based on input from a large number of test refinements some of which, as stated at the outset, have not been specifically identified in this chapter.

(i) In no cases are the refined values of the higher-order ($n > 2$) thermal parameters found to be significantly affected by reasonable modifications of the data such as might be attributable either to random fluctuations during the data collection, or even to specific trends in the accuracy of the measured intensities (the choice of weighting scheme).

(ii) Any *significant* improvement in fit resulting from the addition of anharmonic terms to the harmonic temperature factor is invariably accompanied by a flattening in the structure of the p.w.a. as a function of Bragg angle.

(iii) The use of mutually orthogonal cumulant tensors instead of the standard ones significantly reduces inter-parameter correlation. Correlation problems encountered when second- and higher-order F.I. metal-ion parameters are refined simultaneously may be due to some inadequacy in

the approximations made in the calculation of the corresponding least-squares derivatives (see Chapter 2.4.2).

(iv) From the results of ANOVA significance tests (see Chapter 3.8) it is generally true that anharmonic thermal parameters with refined accuracy less than about 20% are of marginal significance ($\xi \leqslant 2$).

(v) Harmonic models provide completely adequate descriptions of intrinsically disordered systems in which $\delta \leqslant \frac{1}{2}\sqrt{\sigma}$, $\delta$ being the site separation and $\sigma$ the m.s.a. of vibration. (It must be remembered that the occupancy of the X-ion 'satellites' was only half that of the central component, so that this conclusion only serves to draw attention to the fact that the harmonic treatment will 'work' even in the face of surprisingly large site separations.)

(vi) The derived anharmonic p.d.f.'s may include regions of negative (non-physical) density. However, such regions are always well removed from 0 and their values are never more than one or two percent of $P(\underline{0})$.

(vii) Comparison of Figures 2.5.6(a) and (b) shows clearly that disorder which is in principle resolvable may not be reproducible using the F.I. formalism. Such large anharmonicity also appears to be completely outside the regime of validity of the cumulant formalism.

(viii) No evidence of artefacts is found in the description of the ionic thermal motion; in particular, the metal-ion anharmonic parameters (constrained to be zero in the test models) are always found to be insignificant in the refinements.

(ix) An examination of the corresponding difference maps of Figures 2.5.4 - 6 and the contents of Table 2.5.1 shows that, in general, the anharmonic p.d.f.'s derived from the refined F.I. parameters are much more satisfactory than those derived from the corresponding cumulants. Furthermore, the relative superiority of the F.I. formalism appears to increase with increasing anharmonicity. If cumulants are to be used in the thermal description of an atom, then there are fairly clear indications that the construction of a Fourier map - using extrapolated data if necessary - may give a more realistic description than the Edgeworth map (compare especially Figures 2.5.5(c) and (d) with Figure 2.5.5(a)). It is recalled, however, that the generation of useful high $\underline{Q}$ data will depend upon the sign of the refined cumulant parameters being favourable. Otherwise, the temperature factor may diverge.

# CHAPTER 3 : METHODS OF STUDY

# CHAPTER 3 : METHODS OF STUDY

## 3.1 INTRODUCTION

It is the intention in this chapter to outline the features of the collection and analysis of single-crystal elastic-diffraction data which are common to all of the experimental studies described in Chapter 4. Unless specifically stated otherwise in that chapter, it may be assumed that the procedures involved in any aspect of the data collection, handling or refinement are as described here.

In a crystallographic structural study some incident beam of X-rays or neutrons is diffracted from arrays of atoms within the crystal. Taking into account the periodicity of the crystal lattice, the diffracted beams emerge from the crystal in well defined directions and their intensities can be measured using some suitable counter. After making corrections for various known geometrical factors, these measured intensities can be transformed into the corresponding $F_{obs}$'s (see Section 6). However, it is found that several additional corrections to the measured intensities will in general be required if the derived $F_{obs}$'s are to be close approximations to the true ones. For example, the importance of systematic errors due to absorption, extinction and thermal diffuse scattering (TDS), as well as random errors due to instabilities in the incident flux or counting chain, must all be considered and corrected for if possible. If a rigorous correction is not possible for any reason then the resulting existence of bias in the $F_{obs}$'s should be recognised and its possible effects on any conclusions estimated.

In the studies carried out here, the crystal structures are already known approximately, enabling a reasonably accurate list of structure amplitudes to be calculated *a priori*. The variable parameters of the model describing the structure can then be adjusted by the method of least-squares refinement until the agreement between the calculated and observed structure amplitudes

is optimised.

## 3.2 NEUTRONS AND X-RAYS

Since most of the technical details of neutron and X-ray beam production are well expounded in the literature, only those features which have a direct bearing on the present experimental study are recapped here.

The choice of whether to use an incident beam of neutrons or X-rays in any given diffraction experiment will depend, in general, upon a consideration of many aspects, several of which are highly correlated. However, because of the much higher running costs of neutron production machinery - reactors - compared with X-ray generators, the onus of justification falls heavily on those proposing to use neutron-diffraction methods.

A common feature of the spectra emitted from X-ray and neutron sources is that it is polychromatic and must be monochromated for the purposes of elastic-diffraction experiments. This is usually accomplished in the neutron case by Bragg diffraction of the 'white' beam from a crystal (often copper or beryllium) whose inter-planar spacing is well known; the diffracted beam is then a selected 'window' of the spectrum as shown in Figure 3.2.1. The white spectrum from an X-ray tube takes a more structured form (see Arndt and Willis (1966)), the wavelength of the prominent lines being characteristic of the metal target in the tube. In addition to the monochromating technique described above, a second, and more common method is available for X-rays in which a metal filter is used to attenuate the unwanted $K_\beta$ component.

In this study, neutron-diffraction methods were used in each of the principal experiments described in Chapter 4. The justification for using neutrons (instead of X-rays) was based on the following facts.

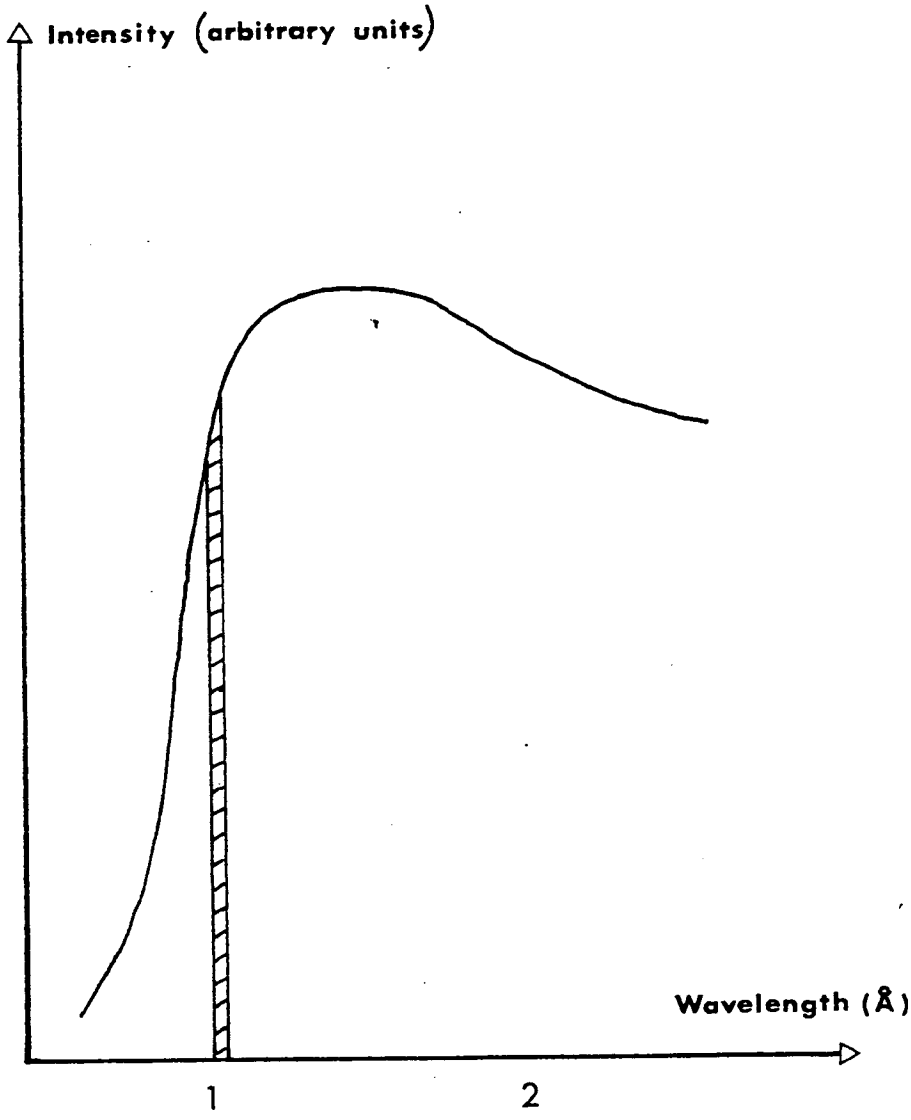


Figure 3.2.1 The wavelength spectrum from a reactor showing a typical 'window' selected by the monochromating crystal.

First, there are purely physical considerations associated with the different scattering mechanisms involved; X-rays are scattered from the electron cloud surrounding the nuclei, neutrons from the nuclei themselves. As a result, neutron scattering is nearly isotropic and does not depend upon atomic number in any systematic way. On the contrary, X-ray scattering is proportional to the number of atomic electrons at low Bragg angles and displays a marked fall-off with increasing angle of scatter. For these reasons, neutron-diffraction methods are often to be preferred when there are light atoms in the crystal in the presence of heavy ones which will dominate the scattering for X-rays.

A further consideration arises through the inverse relationship existing between attainable, reciprocal-space resolution and incident wavelength; the shortest commonly available X-ray wavelength ($\lambda \approx 0.56$ Å from a silver tube) is significantly longer than the ultra-short wavelengths now available from a 'hot' source at a modern, high-flux reactor ($\lambda \approx 0.4$ Å or less at the Institut Laue-Langevin, Grenoble (I.L.L.) - still with a usable flux). In principle, then, assuming that Bragg angles $\theta_B \approx 60^o$ can be reached with both X-ray and neutron diffractometers, the maximum attainable resolution $(\sin \theta_B/\lambda)_{max}$ is of the order 1.6 $Å^{-1}$ and 2.1 $Å^{-1}$ respectively.

Additional technical problems have to be overcome if the data have to be collected at non-ambient temperatures or pressures. In general, the much larger and heavier neutron diffractometers are more suitable for the mounting of ancilliary equipment such as cryostats, furnaces and pressure cells.

Weighed against these points are others favouring the use of X-ray techniques. The question of cost has been mentioned already. Availability of sources is a natural consequence. More important from a strictly physical point of view, is that the usable flux from an X-ray tube is very much greater than that which is obtainable from a reactor. This means that X-ray samples can be much smaller (and indeed have to be because of absorption within the crystal)

and that the counting times required to reach a given level of statistical accuracy in the measurements are usually relatively short. These can be important considerations if either the growth of a 'neutron-size' single crystal is difficult or if the crystal interacts with the atmosphere in any way after prolonged exposure.

All of the points summarised in this section are considered and enlarged upon by Arndt and Willis (1966).

## 3.3 THE DIFFRACTOMETERS

The diffractometers used in the data collection were the D8 and D9 four-circle machines at I.L.L.. Since they differ from each other in detail rather than overall features, only a general description is given here.

A schematic diagram of a standard four-circle diffractometer is illustrated in Figure 3.3.1, with the independent machine shafts, conventionally labelled $\theta$, $\omega$, $\chi$ and $\phi$, as shown. (This diagram is essentially a modified version of that used by Arndt and Willis (1966) - their Figure 15.) The crystal is mounted at position C, defined as the intersection of the four shafts, and can therefore be rotated to any specified orientation about that point. In the Normal Beam Equatorial Geometry (Arndt and Willis (1966)), the detector moves in the horizontal equatorial plane with the incident beam normal to the crystal oscillation axis, $\omega$.

Before starting any experiment, a check should be made that the uniform cross-section of the incident beam is large enough to clothe the crystal completely. The point C, as determined optically using a suitably placed telescope, should be in the middle of the beam (within a small acceptable error) for any of the possible crystal orientations taken up during the measurements. This can be checked by placing a small Cd point on the crystal-mounting head at C and photographing the incident beam with the machine axes in several extreme positions.

Figure 3.3.1 Independent shafts of a conventional four-circle diffractometer, based on the diagram used by Arndt and Willis (1966) (their Figure 15): the $\omega$ and $\theta$ (table and detector) shafts rotate about a common (fixed) vertical axis; the $\phi$ shaft is mounted on the $\chi$-circle; and the $\chi$ shaft is perpendicular to the plane of the $\chi$-circle and through its centre. The crystal sample is mounted at C, the intersection of the shafts.

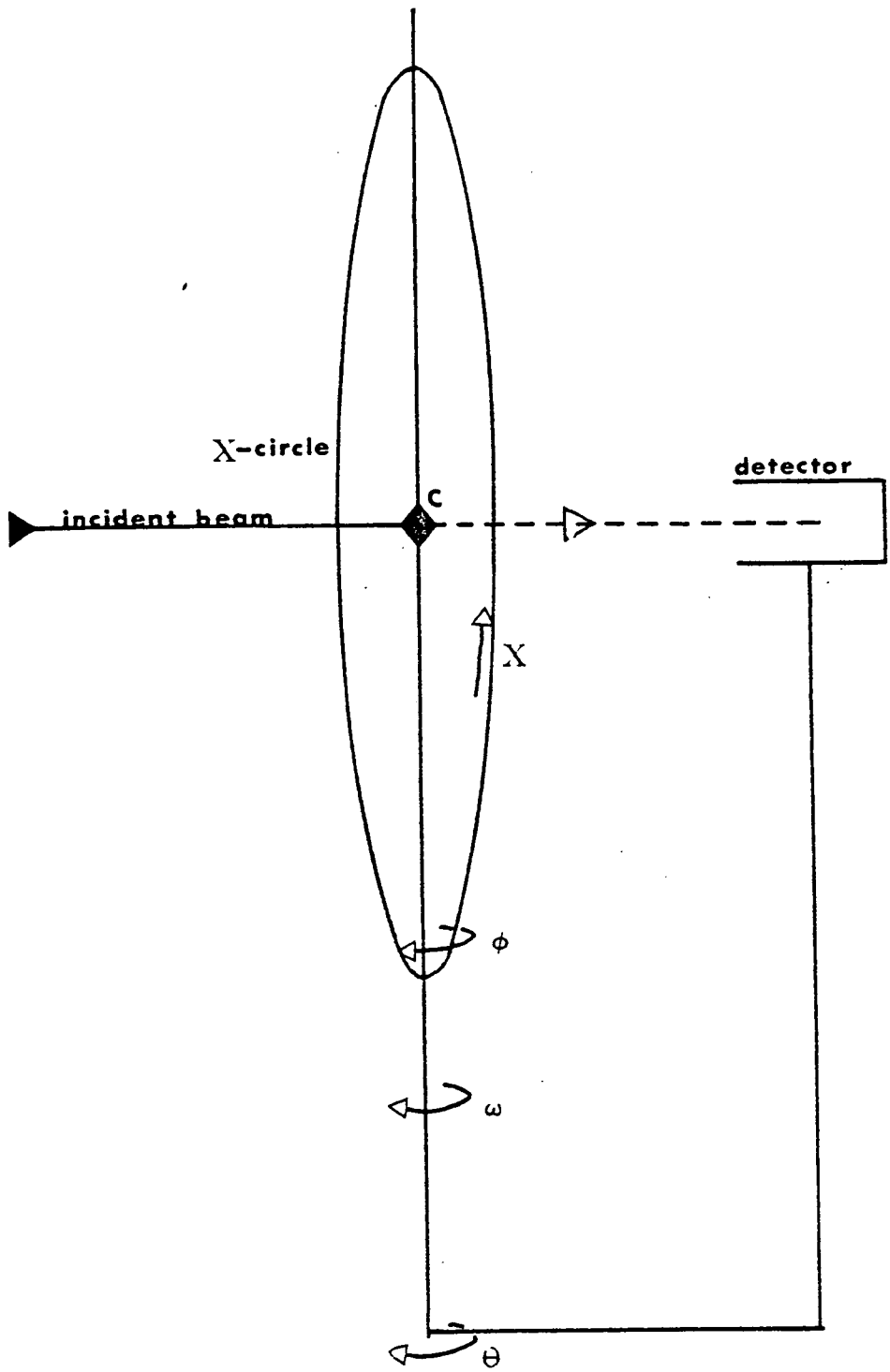


Figure 3.3.1

Cryostats and furnaces, when used, are fixed to the χ-circle (see Figure 3.3.1) and their temperature stability monitored via their thermocouple output on a chart recorder. For the purposes of the experiments described in Chapter 4 it was not necessary to calibrate the temperature devices accurately. In each case, the temperature was set to a value a prescribed number of degree relative to some well defined critical point (in practice a few degrees above $T_c$). The temperature controls were found to be stable within about $\frac{1}{2}^{o}$.

A low-efficiency monitor is placed in the incident beam so that the crystal may be exposed to a predetermined quantity of radiation during each measurement; small random fluctuations in reactor power output are therefore inconsequential to the running of the experiment. Detection of the diffracted beam is by means of an enriched $BF_3$ counter. Diffractometer control during an experiment is carried out by an on-line computer working from a sequence of input parameters : the attention of the experimentalist is therefore largely of a supervisory nature.

## 3.4 GENERAL ASPECTS OF CRYSTAL AND EXPERIMENTAL PREPARATION

The production of single crystals of high purity and optical isotropy,which are suitable for use in neutron-diffraction experiments,is a time-consuming and often difficult specialist task. For this reason, the crystals used in these experiments were obtained from the sources acknowledged in the introduction to each experiment (Chapter 4). Because neutron beam time is so expensive, strict time limits are set for the completion of each experiment. This means that careful sample preparation and preliminary analysis are essential if the best possible use is to be made of the allocated time. Usually, some compromise between conflicting ideals will have to be made in the preparatory work.

The size and shape to which the crystal will be cut is an important decision and will depend upon a variety of considerations. An exact constraint is the cross-sectional size of the uniform

incident beam, which in turn depends upon the geometry of the beam collimation : the size of the crystal must not be so great that in some possible orientation it is not irradiated uniformly. Quantitatively, for experiments using the D9 diffractometer, this imposes an upper limit of about 6mm for the largest crystal dimension. (A crystal cut to the shape of a cube with side 4mm would therefore be too large since its cube diagonal dimension is nearly 7mm. If, however, the *actual* orientations taken up in the experiment are a subset of the *possible* orientations, it may be feasible to use such a crystal.) Scattering power scales approximately with crystal volume so that if very weak reflections are anticipated it will be desirable to use as large a crystal as possible. On the other hand, if extinction (see Appendix A) is expected to be severe, a large crystal will make for a more difficult and unreliable correction. From the point of view of making an absorption correction, the crystal should ideally be spherical so that the mean path length of the beam through it is the same for all orientations (reflections). No correction is then required. However, physical grinding has the disadvantage that strain may thereby be induced in the crystal.

The (cubic) crystals used in the experiments of this study were usually cleaved along principal lattice planes to a cuboid shape with approximately equal sides. The bounding surfaces were then easily characterised for the purposes of making the path-length calculations sometimes necessary for the corrections involved in the data processing (Section 6).

After cleaving, the crystals were examined for signs of strain or high impurity content. Indications of these can be obtained respectively by rotating the crystal under a polarising microscope and observing the degree of uniformity of the transmitted light, and by noting the amount of side-scattered light from a low-power laser beam in transmission through the crystal. X-ray back-scattering photographs were then taken as a check that the cleavage planes were in fact those anticipated. The photographs were also examined for evidence of poorly defined or split spots. Finally, if possible,

preliminary elastic-scattering measurements were made using diffractometers at A.E.R.E., Harwell, with a view to ensuring that the crystal was not twinned and to obtaining some estimate of the atomic thermal parameters and the severity of extinction. As a result, reflections could be grouped according to predicted relative intensities, thus optimising the data collection as outlined in the next section.

## 3.5 DATA COLLECTION

The orientation of the crystal axes with respect to some specified diffractometer axes must be known accurately if the reflections are to be well centred in the detector aperture. In practice, the transformation (UB-) matrix giving the desired relationship is found by indexing a group of reasonably strong reflections on the basis of the known crystal cell parameters. A recursion centering program is then used to scan through each reflection, varying the independent diffractometer shafts in turn until the measured angular setting of the profile remains unchanged from the previous cycle of scans. The UB-matrix is then refined from the list of angular settings by the method of least-squares (see Section 7). The reflections chosen for this purpose should preferably have diffraction vectors well separated (orthogonal or nearly so) in the reciprocal space. The software of some diffractometers allows for a periodic check of the centering of a few control reflections; where it does not, and depending upon the timescale of the experiment, some manual check of the orientation stability should be made periodically.

Choice of standard reflection(s) is fairly arbitrary except that the reflection should be strong enough for its intensity to be measured readily to at least one percent accuracy and, if there are two or more, they should be well separated in the reciprocal space. The frequency of measurement should be as high as reasonably practical. It was, however, soon realised that long measurement times were often required if very high-angle reflections were to be measured to an acceptable accuracy. The computer software on the D8 and D9 diffractometers was not of sufficient sophistication to enable the

specification of shorter counting times for the standard reflections, so that on some occasions the time between their measurement was of necessity several hours. (On the other hand, this is not so worrying as it appears at first because short-term fluctuations, which are the ones most likely to avoid detection, will not affect the measured intensity of very weak reflections so significantly.)

The $\omega$:2$\theta$, background-peak-background mode of collection was employed in which the table and detector ($\omega$ and $\theta$) shafts rotate about a common vertical axis, the stepping interval of the former being half that of the latter. Although the optimum $\omega$:x$\theta$ ratio (in the sense that the diffracted beam passes through the centre of the detector aperture) is a function of Bragg angle, it was always found that setting x=2 was adequate, even in the low-angle region where $x_{optimum} \ll 2$.

In the case of the very high-resolution experiments on the D9 diffractometer, time did not permit the collection of an entire data set of independent reflections (with at least one additional symmetry equivalent for each) out to the desired angular limit. However, from refinements carried out on a lower-resolution, but complete, perovskite data set, it was clear that the refined model parameter values were not sensitive to a reduction in the data set achieved by deleting a random selection of reflections. The accuracy of the refined parameter values decreases of course. Bearing in mind the experimental objectives, it was clearly desirable to sacrifice a small amount of parameter accuracy for the collection of high-resolution data. For this reason, in the experiments carried out on the D9 diffractometer, a random number was assigned to each independent reflection by the method outlined in Appendix C, and only those reflections whose associated number fell within a given range were measured. The specified range could be modified easily depending upon changes in the experimental conditions without affecting the random nature of the choice of reflections.

Because the number of reflections to be measured in these experiments was relatively small (in crystallographic terms),

the reflections were often input individually by paper tape instead of using one of the more sophisticated hkl zig-zag generation schemes available. Thus it was possible to group together reflections with comparable predicted intensities and measure them at the same rate.

The machine 'dead-time' must also be taken into account. This is the time during which the machine shafts are in motion and no counting is being done, and is long enough to cause concern, especially on D9. The number of steps in each scan was therefore determined by the conflicting needs to reduce dead-time and to make the integration under the reflection peak profile valid. Usually about 35 steps in the total scan including background afforded the best compromise.

The reflection profiles and full documentation were stored directly on to either discs or magnetic tape.

## 3.6 DATA PROCESSING

The data collected on the D8 and D9 diffractometers are background corrected in the routine processing by scanning each peak profile, designating peak and background areas on the basis of trends in the recorded counts, and making a linear subtraction. A check is then made that the background areas are large enough to be statistically accurate and that they show no systematic structure. Reflections failing to meet those requirements are marked in the output and their profiles can be further examined by the user.

An estimated standard deviation, based on the counting statistics, is then assigned to each integrated intensity and a correction made for the reduction in the true intensity due to the Lorentz Effect (Arndt and Willis (1966)). When this has been done, each data set can be checked for signs of either long-term drift or erratic variation in the standard reflection intensities. If any such variation is considered significant, an empirical fit can be made to these intensities and the resulting function applied as a correcting factor to the entire data set.

Absorption effects are usually found to be negligible in neutron elastic-scattering experiments, particularly if the samples are of reasonable shape as here. A quick calculation of a few sample transmission factors (with exaggerated path-length differences for safety) confirms this to be so for each of the crystals studied. However, effects due to TDS are sometimes found to be very significant, especially at high Bragg angles, and a correction was made to each data set using the method outlined in Appendix B.

At this point, the agreement between the corrected intensities of symmetry-equivalent reflections was examined. If it appeared that the agreement was reasonable (that is, if the differences in intensity were compatible with the accuracy of the measurements), the equivalents were averaged and converted to give a set of non-equivalent structure amplitudes (see Lipson and Cochran (1966)). The assigned standard deviations were taken to be the larger of the counting statistics error and the r.m.s. deviation of the set of equivalent reflections. If the agreement was considered to be unacceptably poor, no averaging was done. Extinction effects are sometimes found to be significantly anisotropic (Rossmanith (1977)) and observed differences in the intensities of equivalent reflections can arise from them. Path-length effects (see Appendix A) can cause similar problems if the extinction is severe - whether it is anisotropic or not. Corrections for extinction are, however, made using parameters obtained in the refinements.

Finally, constraints were often placed on the accuracy of the $F_{obs}$'s. Since the weight assigned to each during the refinements is proportional to the inverse square of the corresponding $\sigma(F_{obs})$ (see the next section), it is often found that the refinement is heavily biassed towards fitting the strong, statistically well determined reflections. For this reason, a limiting accuracy (usually about 1%) was assigned for each $F_{obs}$ whose measured accuracy exceeded this value. Those $F_{obs}$'s with accuracy less than some specified lower limit were often discarded, although in practice this was not found to significantly affect the refined parameter values.

## 3.7 REFINEMENT METHOD

For the simple cubic structures considered in this study, the structure amplitudes were calculated using the formula

$$F_{calc}(\underline{Q}) = Sc \cdot E(\underline{Q}) \left| \sum_i b_i \cos(\underline{Q} \cdot \underline{r}_o)_i W_i(\underline{Q}) \right| \qquad \ldots (3.7.1)$$

where Sc is the overall scaling factor and $E(\underline{Q})$ is the extinction correction factor defined in Appendix A. The functional forms used for $W_i(\underline{Q})$ are fully discussed in Chapter 2.

The refinements were carried out by the full-matrix least-squares method using computer programs based on ORFLS (Busing et al (1962)). Modifications to incorporate the general anisotropic extinction correction of Becker and Coppens (1974 , 1975) and anharmonic temperature-factor calculations are described in Appendix A and Chapter 2 respectively.

The theory of the least-squares method is covered in many standard texts (for example, Lipson and Cochran (1966)) and only a brief summary of the details relevant to crystallography in general and the present study in particular is given here.

The object of the method is to achieve a minimisation of the quantity

$$\sum w\Delta^2 = \sum_i w_i \left( |F_{obs}| - |F_{calc}| \right)_i^2 \qquad \ldots (3.7.2)$$

by a suitable, controlled variation of the model parameters used to compute the $F_{calc}$'s. The summation is over the independent structure amplitudes and $w_i$ is the weight to be assigned to the $i^{th}$ $F_{obs}$. $\sum w\Delta^2$ is commonly called the Weighted Sum of Squares. Incorrect choice of values for the $w_i$'s will make the estimation

of the accuracy of the derived model parameter values uncertain, and as has been pointed out by Cruickshank et al (1961), the formula used to estimate the parameter standard deviations is in fact *invalid* unless the weighting scheme is reasonable. In spite of this, the refined parameter values themselves are often found to be rather insensitive to the choice of even drastically different weighting schemes (see Chapter 4.2 in particular). Cruickshank et al (1961) have advocated the use of the empirical weighting scheme $w_i = 1/(a + |F_{obs}| + c\,|F_{obs}|^2)_i$ where a and c are about $2F_{obs}^{min}$ and $2/F_{obs}^{max}$ respectively. However, other schemes have given 'better' results in some cases (Truter et al (1960)). In the refinements of Chapter 4, the weights are based on the counting statistics - $w_i = 1/\sigma_i^2(F_{obs})$ - often with some specified upper and lower limits on the percentage accuracy of any $F_{obs}$ (see Section 6).

It is common practice, towards the end of a refinement, to partition the weighted sum of squares (expression (3.7.2)) into component sums over small intervals of $|F_{obs}|$ or position in reciprocal space, $\underline{Q}$. A check is then made that there are no systematic variations of unacceptable proportions with either of these variables (or indeed with *any* variable which might be supposed to have a bearing on the assigned standard deviations). This check is called a partial weights analysis. (The words 'partial weights analysis' will often be used in this thesis to mean the spectrum of partial weighted residuals as a function of some variable (usually $\theta_B$).) Of course, the observation of any such systematic trend need not *necessarily* be an indictment of the weighting scheme itself; the use of an entirely inappropriate structure model could result in similar features. Clearly, then, care must be taken to identify correctly the cause of any disturbing trends in the partial weights analysis.

The correlation matrix, $\underline{\underline{\lambda}}$, is calculated at the end of each refinement from the elements of the design matrix. Although, in principle, each variable parameter may be determined if $\lambda_{ij} \neq 1$ for all $i \neq j$, difficulties may arise if any of the values is close to

unity. It may then be worth reconstituting the functional form of the structure model in such a way that the correlation between the new parameters is reduced. For instance, decomposition of the standard cumulant tensors into orthogonal component tensors (see Chapter 2.3.2) is shown to lead to a significant reduction in interparameter correlation (see conclusion (iii) of Chapter 2.5.7). Correlation coefficients will be relatively large in general between parameters describing physical characteristics of any given atom and will tend to be smaller between parameters describing characteristics of different atoms.

The least-squares refinement program also allows a modification to the standard calculation of structure-amplitude derivatives so that it is possible to constrain any parameter to have a fixed relationship with any others. This is particularly useful when some statistical measure of the significance of the inclusion of additional parameters in the model is desired, and full use has been made of the facility in the present study (see the next section for a discussion of the statistical considerations and Chapter 4 for examples obtained from the refinements).

Finally, provision was made for the use of a damping or 'fudge' factor. This is a number (typically $\sim 0.7$) by which each calculated parameter shift is multiplied at the end of each cycle of the refinement. Otherwise, and often for no very apparent reason, the refinement may tend to oscillate or even diverge about a position in the parameter space close to the minimum sought.

## 3.8 STATISTICAL TESTS

In the refinements of each of the crystal structures to follow (Chapter 4), it is of crucial importance to be able to state as objectively as possible, the merit of adopting one model as opposed to some other. For this reason, the statistical basis of the tests carried out to determine such merit is examined in some detail.

Usually one structure model will contain more variable parameters than another and will fit the observed data better; in fact, it has been pointed out by Hamilton (1965) that if the parameters of the smaller set constitute a subset of the larger, then the model with the larger set of parameters can always be made to give at least as good a fit to the data. This is intuitively obvious - as is the realisation that a position must eventually be reached at which the addition of any further parameters to the model will not contribute to a better understanding of the true crystal structure. That is to say, the accuracy of such parameters will be very small, so that the extra structural information which may be extracted therefrom will be slight and incompatible with the extra time and effort required to obtain it. The problem then is to construct some test which will have as wide a range of applicability as possible and which will provide a suitable indicator of the worth of adopting the model with the extra parameters.

The general problem has been extensively studied in statistics. First, it is necessary to define the hypothesis to be tested : that is, some statement about the population whose truth is to be tested in the light of the observed sample taken from it. *Assuming* the hypothesis to be true, the test is then a determination of whether or not the result obtained from a given sample could reasonably have been expected. In other words, the possibility to be explored is that the (non-perfect) final fit of a model to the observed data is a reasonable consequence of purely statistical fluctuations within the observed data. If the hypothesis were true, then the fit would be expected to become better with an increased number of observations, whereas it would not in general if the hypothesis were incorrect.

In any test of this nature, with a finite sample of data, it is necessary to partition the sample space (that is, the set of all possible observations) into two regions; if the actual observations fall into one - the critical region - the hypothesis is rejected, and if they fall into the other - the acceptance region - the hypothesis is accepted. These two regions of the sample space may

be delineated if the probability distribution of the observations under the hypothesis is known and if some decision is made as to a suitable significance level for the test. The significance level, $\alpha_s$, gives the probability of rejecting the hypothesis when in actual fact it is true, and is commonly taken in statistics to be 0.05 or 0.01. The level chosen in any test is of course arbitrary to some extent and clearly depends upon the 'cost' of reaching an ill-judged conclusion about the hypothesis.

The extension of the methods of hypothesis testing to the problem in hand (as outlined at the beginning of this section) is through the statistical process of analysis of variance (ANOVA) (Kobayashi (1978)). The weighted sums of squares, $\sum w\Delta^2$, are obtained for the models with and without constraints (restrictions) and are denoted $G_Q$ and $G_0$ respectively, adopting the notation of Hamilton (1965). The hypothesis to be tested is that the constrained model, with the fewer number of parameters, affords an acceptable description of the real system as characterised by the set of observations. It can be shown that if n is the number of independent observations, m and m-b are the number of parameters used in the unconstrained and constrained models respectively, and the hypothesis *is* true then

$$F = \frac{G_Q - G_0}{G_0} \quad \frac{(n - m)}{b} \qquad \ldots (3.8.1)$$

has the F-distribution for b and n-m degrees of freedom. The hypothesis is therefore rejected if the value of F obtained from expression (3.8.1) is greater than the point on the F-distribution, for b and n-m degrees of freedom, which cuts off 100 $\alpha_s$% of the distribution tail. Hamilton (1965) then goes on to show that the ratio F may be manipulated and recast as a ratio of conventional weighted residuals $R = R_Q/R_0$ whose significant points are obtained as

$$R_{b,n-m,\alpha_s} = \left\{ \frac{b}{n-m} F_{b,n-m,\alpha_s} + 1 \right\}^{\frac{1}{2}} \quad \ldots (3.8.2)$$

The weighted and unweighted residuals, $R_w$ and R, are defined by

$$R_w = \left\{ \sum w\Delta^2 / \, wF^2_{obs} \right\}^{\frac{1}{2}} ; \quad R = \left\{ \sum \Delta^2 / \, F^2_{obs} \right\}^{\frac{1}{2}} \quad \ldots (3.8.3)$$

The ratio $R$ above may be obtained from either the weighted or unweighted residuals; however, in this study, the weighted residuals will always be used for the purposes of ANOVA tests. This method therefore provides a ready statistical measure of the significance of the additional b parameters used in the unconstrained model.

The problems of non-linearity in the hypothesis being tested are discussed by Hamilton (1965). Although the effects are often difficult to assess accurately, it appears that they are probably not too serious in the types of problem normally encountered in crystallography. It is also true that the statistical information extracted using ANOVA methods is to be preferred to any judgement based on the parameter standard deviations as estimated from the least-squares refinement (Hamilton (1965)). In this way, Merisalo and Järvinen (1978) have used ratio-test methods in prescribing an accuracy to refined parameters. The errors were taken to be the parameter shifts required, from the refined values, in order to produce a significantly ($\alpha_s$ = 0.25) worse fit to their data.

Unfortunately, the relationship between statistical and physical or chemical significance is seldom clear from the results of least-squares refinement of crystal structures. The basis of the difficulty lies in the fact that in many cases there is some uncertainty about the validity of the structure model being used; for example, when extinction and TDS corrections are non-negligible. Even a small adjustment in the weighting scheme can sometimes manifest itself in noticeable changes in the derived levels of statistical

significance (see Chapter 2.5.4). It is contended then that some effort be made to ensure that the significance levels obtained from any ratio test are not dependent upon the *unfounded* acceptance of any particular set of corrections made to the data. For instance, if the corrections due to TDS might be in error by ten percent (not unreasonable in some cases - see Chapter 4.2), the dependence of the refined R-factors upon changes of this order to these corrections should be examined.

In an attempt to work towards a plausible criterion for the assertion of *physical* significance, Pawley (1971) suggests that the ratio

$$\xi = (R - 1)/(R_{b,n-m,0.01} - 1) \qquad \ldots (3.8.4)$$

be calculated. $\xi$ has been given the evocative title of 'the (Pawley) factor of scepticism' (Thornley et al (1976)). The values obtained for $\xi$ from the results of a variety of constrained and unconstrained refinements, using data obtained for different materials, are shown to fall predominantly in the range 1 - 10. A tentative conclusion, based on the results of complementary experiments on the same materials and theoretical considerations, is that a value for $\xi$ towards the lower end of this range might not be indicative of actual physical significance. Values of $\xi$ are commonly quoted where appropriate in this thesis as a ready measure of the *comparative* significance of the addition of different sets of parameters to a given model. Care must, however, be taken to avoid the attachment of too much meaning to individual, absolute values of $\xi$ - the test is entirely empirical.

Of course, if the validity of the model were assured then the concepts of statistical and physical significance would be interchangeable : the fact that such validity cannot in general be assumed means that caution must be exercised when stating conclusions based on these significance tests. For instance, many examples are

found in the analyses of Chapter 4 in which the addition of a set of parameters to a basic refinement model is 'statistically significant' at a level $\alpha_s < 0.001$. That is, the possibility that the additional parameters are *not* statistically significant is less than 1 part in 1000. Such levels would often be treated with some scepticism by a statistician - which is why significance levels $\alpha_s = 0.05$ or 0.01 have become the 'standard' criteria in statistical work. This is not to say that figures $\alpha_s < 0.001$ (or any other level) are in themselves disputable; they are obtained using well-founded statistical principles. Rather, the implication is that the additional parameters *may* compensate to some extent for inaccuracies in the corrections for extrinsic effects such as TDS, extinction and absorption; the indispensibility of the additional parameters, *implied* by terminology such as '1 part in 1000', may therefore be somewhat exaggerated.

# CHAPTER 4 : EXPERIMENTAL WORK

# CHAPTER 4 : EXPERIMENTAL WORK

## 4.1 INTRODUCTION

Sections 2-7 of this chapter contain accounts of each of the six experiments and the processing and refinements carried out on the data obtained. Each section is divided into three subsections as follows.

1. An account is given of those specific features of the experiment and data processing not already included in the general descriptions of Chapter 3.

2. A summary is first given - part (a) - of the results obtained from the 'control' refinements, defined as those using $F_{obs}$'s properly corrected for TDS, $\sigma(F_{obs})$'s as derived from the counting statistics, and coherent neutron scattering lengths as quoted by Bacon (1975). Absorption within the bulk crystal is negligible in each case as shown in Chapter 3.6 and corrections were therefore not made. Overall scale and extinction correction parameters were always included in the refinements along with thermal parameters as specified.

   A description is then given - part (b) - of further refinements which were carried out using data and/or conditions modified in some way from those obtaining in the 'control' refinements. These refinements were considered necessary because of the specific nature of the conclusions it was hoped to extract from the refined model parameters : it was essential to eliminate extrinsic effects as a possible cause of confusion and misinterpretation. In other words, modifications to phenomena supposedly independent of the method of parameterisation of the ionic thermal motion must not have a significant bearing upon the qualitative nature of any conclusions extracted from the refined thermal parameters.

The effects which might come into this category are those due to extinction, TDS, choice of weighting scheme, assignment of coherent neutron scattering lengths and so on. Of these, extinction is refined along with the other parameters and therefore cannot be considered as a truly extrinsic effect - although the refined extinction parameters would not be expected to change significantly between refinements using different thermal models. *Ad hoc* modifications to the others are however possible, and were made as described in each section.

Details of refined parameter values, residuals and significance levels are given in the appropriate tables.

3. A general discussion is given of the results obtained in the refinements described in Subsection 2 with particular emphasis placed on the derived descriptions of the ionic thermal p.d.f.'s.

Section 8 then goes on to give a general overview and to compare and contrast the results obtained and the conclusions derived for the series of crystals as a whole.

## 4.2 THE $CsPbCl_3$ EXPERIMENT

### 4.2.1 Experimental Details

The sample used in the experiment was a cuboid of approximate dimensions 5.5 x 4.0 x 3.0 mm cut from a crystal grown by Dr P M Dryburgh, University of Edinburgh. It was opaque with a greenish tinge and was found to cleave easily along the principal crystal planes. When examined under crossed polars it appeared to be reasonably strain-free (optically isotropic) and X-ray back-scattering photographs showed no evidence of poorly defined spots.

The experiment was performed on the D9 diffractometer at I.L.L. with the (2,0,0) planes of the Cu monochromator being used to give an incident wavelength of 0.656 Å. During the experiment, the crystal was enclosed in a furnace maintained at 325°K, 5° above the cubic → tetragonal phase transition. The cell constant used was the one quoted by Harada et al (1976), namely $a = 5.605$ Å. Coupled $\omega:2\theta$ scans were made of nearly all of the independent reflections in the first five reciprocal lattice layers out to a maximum Bragg angle of 50° ($(\sin\theta_B/\lambda)_{max} = 1.2$ Å$^{-1}$), beyond which no measureable peaks were observed. This gave a total of 230 reflections whose measured accuracy, in general, fell off markedly with increase of Bragg angle. Time did not permit the measurement of a symmetry-related reflection for each of the independent reflections. Instead, a sample of 38 was chosen at random and a symmetry-equivalent reflection measured for comparison. It was found that the agreement in integrated intensity was, except in a very few cases, within three standard deviations (for the weaker reflections) and within 5% (for the strong, statistically well determined reflections). It seemed, then, that variation in absorption with crystal orientation could be assumed to be small. This was in fact confirmed in a subsequent lower-resolution experiment in which at least two equivalents were measured for all reflections.

Because only one measurement was made for most of the reflections , the resulting data set cannot be considered ideal. However, it was felt that the agreement between those equivalents which were measured, together with the subsequent good fits in the refinements, justified acceptance of the data.

The standard reflections were found to agree within acceptable limits and so no adjustment for long-term variation in the counting chain stability was required. TDS contributions were calculated using the method described in Appendix B; the circular receiving aperture actually used in the experiment was replaced, for the purposes of the computer program, by a square one

of the same area. The elastic constants, derived from the dispersion curves of Fujii et al (1974), were as follows : $C_{11} = 3 \times 10^{11}$, $C_{44} = 0.76 \times 10^{11}$ and $C_{12} = 2.1 \times 10^{11}$ dyne/cm$^2$. These values give correction factors of up to $\alpha \sim 1$ for reflections at the highest Bragg angles - that is, modifications to the observed structure amplitudes of up to about 30%. It was estimated that the values obtained for the elastic constants could well be in error by about 10% because of inaccuracies inherent in the reading of the dispersion curves. A lower limit $\sigma(F_{obs})/F_{obs} \geq 0.02$ was applied and 20 reflections with $\sigma(F_{obs})/F_{obs} \geq 0.50$ were omitted from the refinements leaving 210 independent measurements. (The refinements were not found to be sensitive to changes in these specified limits.)

Since preliminary refinements showed extinction to be small, an approximation to the Becker and Coppens (1974) treatment of secondary extinction was used - see Appendix A - in which it was assumed that the mean path length through the crystal was the same for all reflections. The extinction was assumed to be isotropic, Type I, with Lorentzian mosaic spread.

### 4.2.2 The Refinements

#### (a) The Control Refinements

The thermal parameters obtained from the refinement using a purely harmonic model (see Table 4.2.1) are larger than those obtained by Harada et al (1976) with lower-resolution data. (Their values should be divided by $8\pi^2$ to convert them to m.s.a.'s in Å$^2$.) This is probably at least partly due to their failure to make a TDS correction. An examination of the p.w.a., however, shows the distribution of partial weighted residuals to have a marked structure both as a function of $|F_{obs}|$ and as a function of Bragg angle : a very large peak in the spectrum (see Figure 4.2.1) is observed corresponding to observations made around $\theta_B \approx 20^o$ - the middle of the range in $F_{obs}$ values.

Table 4.2.1 The refined parameters of $CsPbCl_3$ at $325^{o}K$. Model I contains harmonic thermal parameters on all ions. Models II, III, IV and V contain, in addition to the parameters of Model I, fourth-order F.I. parameters on the Cs, Pb and Cl ions and on all ions respectively. Models VI and VII contain, in addition to the parameters of Model V, sixth-order F.I. parameters on the Cl ions and on all ions respectively. In addition, the scale (arbitrary) and extinction parameters, Sc and g, were always refined. The extinction parameter is as defined by Becker and Coppens (1974) for isotropic Type I secondary extinction with a Lorentzian mosaic spread. Estimated standard deviations (from the least-squares refinement) are given in parentheses; where none is given, the parameter was fixed during refinement. R, $R_w$ and $\Sigma w\Delta^2$ are defined in the text. $\Sigma w\Delta^2$ is the weighted sum of squares obtained in the corresponding refinement using cumulant parameters instead of F.I. parameters.

| Model | I | II | III | IV | V | VI | VII |
|---|---|---|---|---|---|---|---|
| Sc | 8.3(1) | 8.3(1) | 8.6(2) | 8.3(1) | 8.7(1) | 8.7(1) | 8.5(1) |
| Caesium | | | | | | | |
| $bx10^{12}$cm | 0.55 | 0.55 | 0.55 | 0.55 | 0.55 | 0.55 | 0.55 |
| u ($Å^2$) | 0.082(1) | 0.081(1) | 0.083(1) | 0.077(1) | 0.079(1) | 0.079(1) | 0.079(1) |
| $a_{40+}$ | | -0.01(1) | | | -0.004(7) | -0.004(6) | -0.004(7) |
| $a_{44+}$ | | -0.016(5) | | | -0.008(2) | -0.007(2) | -0.006(2) |
| $a_{60+}$ | | | | | | | 0.00(1) |
| $a_{64+}$ | | | | | | | 0.001(1) |
| $a_{66+}$ | | | | | | | -0.0002(2) |
| Lead | | | | | | | |
| $bx10^{12}$cm | 0.94 | 0.94 | 0.94 | 0.94 | 0.94 | 0.94 | 0.94 |
| u ($Å^2$) | 0.0249(4) | 0.0249(4) | 0.0147(4) | 0.0250(4) | 0.0224(3) | 0.0229(4) | 0.0229(4) |
| $a_{40+}$ | | | -0.24(1) | | -0.054(5) | -0.043(5) | -0.05(1) |
| $a_{44+}$ | | | -0.01(1) | | -0.003(2) | -0.002(2) | -0.02(1) |
| $a_{60+}$ | | | | | | | -0.01(1) |
| $a_{64+}$ | | | | | | | -0.007(3) |
| $a_{66+}$ | | | | | | | -0.0010(4) |
| Chlorine | | | | | | | |
| $bx10^{12}$cm | 0.96 | 0.96 | 0.96 | 0.96 | 0.96 | 0.96 | 0.96 |
| $u^{11}$($Å^2$) | 0.194(1) | 0.194(1) | 0.196(1) | 0.199(1) | 0.201(1) | 0.201(1) | 0.200(1) |
| $u^{33}$($Å^2$) | 0.0233(3) | 0.0233(5) | 0.025(1) | 0.0238(3) | 0.0258(5) | 0.0253(5) | 0.0258(5) |
| $b_{040+}$ | | | | 0.050(3) | 0.047(3) | 0.052(3) | 0.053(3) |
| $b_{044+}$ | | | | -0.011(1) | -0.010(1) | -0.011(1) | -0.011(1) |
| $b_{220+}$ | | | | 0.002(2) | 0.003(2) | 0.001(2) | -0.001(2) |
| $b_{400+}$ | | | | -0.0006(4) | -0.0004(4) | -0.0005(8) | 0.001(1) |
| $b_{060+}$ | | | | | | 0.008(3) | 0.008(3) |
| $b_{064+}$ | | | | | | -0.0022(4) | -0.0023(4) |
| $b_{240+}$ | | | | | | 0.001(1) | 0.001(1) |
| $b_{244+}$ | | | | | | 0.0004(4) | 0.0005(4) |
| $b_{420+}$ | | | | | | 0.0004(3) | 0.0005(4) |
| $b_{600+}$ | | | | | | 0.0000(1) | -0.0001(1) |
| $gx10^{-4}$ | 0.17(5) | 0.16(4) | 0.23(6) | 0.21(3) | 0.29(3) | 0.28(3) | 0.25(3) |
| R | 0.060 | 0.060 | 0.054 | 0.043 | 0.037 | 0.035 | 0.034 |
| $R_w$ | 0.074 | 0.073 | 0.072 | 0.040 | 0.036 | 0.032 | 0.031 |
| $\Sigma w\Delta^2$ | 1274 | 1219 | 1188 | 369 | 306 | 234 | 217 |
| $^c\Sigma w\Delta^2$ | 1274 | 1227 | 1187 | 505 | 415 | 353 | 328 |

| Model | I | II | III | IV | V | VI | VII |
|---|---|---|---|---|---|---|---|
| N.P. | 6 | 8 | 8 | 10 | 14 | 20 | 26 |
| F.I. | | | | | | | |
| $\Sigma w\Delta^2$ | 1274 | 1219 | 1188 | 369 | 306 | 234 | 217 |
| $\alpha_s$ | | $0.005_I$ | $0.001_I$ | $0.001_I$ | $0.001_{IV}$ | $0.001_V$ | $0.05_{VI}$ |
| $\xi$ | | 1 | 2 | 27 | 3 | 3 | 1 |
| cumulant | | | | | | | |
| $\Sigma w\Delta^2$ | 1274 | 1227 | 1187 | 505 | 415 | 353 | 328 |
| $\alpha_s$ | | $0.005_I$ | $0.001_I$ | $0.001_I$ | $0.001_{IV}$ | $0.001_V$ | $0.05_{VI}$ |
| $\xi$ | | 1 | 2 | 19 | 3 | 2 | 1 |

| Parameter | $a_{44+}$(Cs) | $a_{40+}$(Pb) | $b_{040+}$(Cl) | $b_{044+}$(Cl) | $b_{060+}$(Cl) | $b_{064+}$(Cl) |
|---|---|---|---|---|---|---|
| $\xi$ | $1_I$ | $2_I$ | $18_I$ | $14_I$ | $4_V$ | $6_V$ |

Table 4.2.2 The significance levels derived from the fits of Table 4.2.1. The models with N.P. variable parameters and fits specified by $\Sigma w\Delta^2$ and $\Sigma w\Delta^2$ are as defined in Table 4.2.1. $\alpha_s$ and $\xi$ are defined in the text. The meaning of the value for $\alpha_s$ and its subscript can best be made clear by an example : $0.001_{IV}$ for Model V means that the improvement in fit given by this model, compared with the fit of Model IV, is statistically significant at the level $\alpha_s \leq 0.001$. The corresponding value for $\xi$ is stated on the next line in each case. The bottom two rows give the most significant of the anharmonic F.I. parameters. The subscript on the $\xi$ value indicates the model against which the improvement in fit due to the addition of the individual parameter is tested.

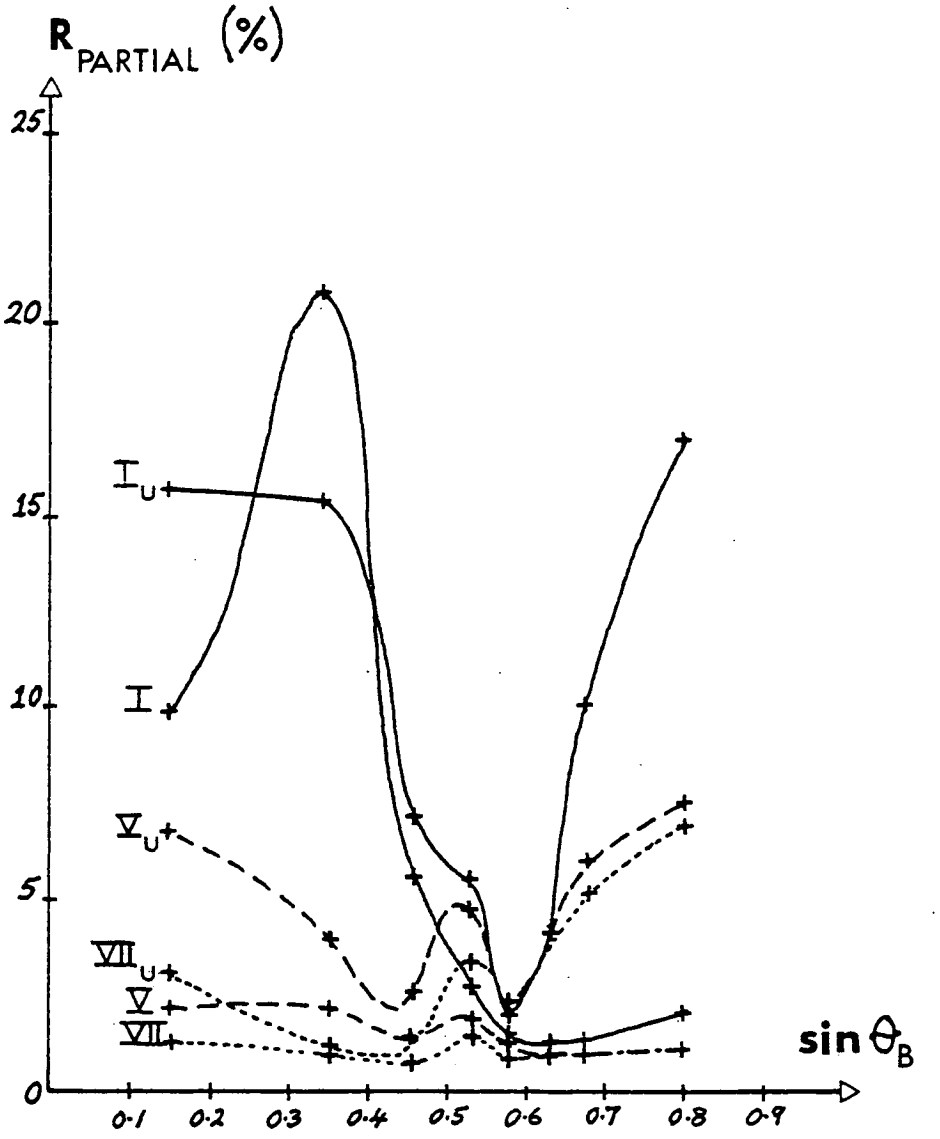


Figure 4.2.1 The partial weighted residuals obtained from the refinements of the $CsPbCl_3$ (325°K) data. The contributions to $R_{partial}$ were averaged over small intervals of $\theta_B$ and gave the values marked by crosses. The lines are guides to the eye. The graphs labelled I, V and VII were obtained with the 'control' data using Models I, V and VII defined in Table 4.2.1. Those labelled $I_u$, $V_u$ and $VII_u$ were obtained in the same way using the data with *unit* weights applied to each observation.

In addition, the overall weighted residual, $R_w$, is 0.074 - rather higher than might be expected on the basis of the accuracies achieved in the data collection. It appears, then, that either the harmonic model is not a plausible one or that the counting-statistics weighting scheme is inappropriate.

The addition of either F.I. or cumulant fourth-order parameters to each of the metal-ion temperature factors in turn gives similar, relatively small (in the sense of $\xi$) reductions in $\sum w\Delta^2$ from the value obtained in the harmonic refinement - see Tables 4.2.1 and 4.2.2 for a summary of the fits and significance levels obtained in these refinements. From separate refinements it can be shown that practically all of the improvements in fit can be attributed to the addition of the $a_{44+}$ (Cs) and $a_{40+}$ (Pb) parameters. (In cases where the addition of F.I. and cumulant parameters give comparable improvements in fit only the individual significance of the F.I. parameters will be investigated in this way.) It is noted in the passing that the inclusion of the $a_{40+}$ (Pb) parameter in the model results in the Pb second-order thermal parameter falling to just over one half of its harmonic-approximation value (see Table 4.2.1 Models I and III) although the appropriate correlation coefficient is only 0.75.

The corresponding reduction in $\sum w\Delta^2$ arising from the addition of fourth-order Cl-ion thermal parameters to the harmonic model is found to be massive for both the cumulant and F.I. treatments and larger (significantly so) for the F.I. model ($\xi$ = 27 compared with 19 - see Table 4.2.2). Nearly all of this improvement is due to the $b_{040+}$ (Cl) and $b_{044+}$ (Cl) parameters ($\xi$ = 18 and 14 for the addition of each individually); added separately to the harmonic model, the $b_{220+}$ (Cl) and $b_{400+}$ (Cl) parameters hardly reduce $\sum w\Delta^2$ at all.

As can be seen from Table 4.2.1, the addition of up to fourth-order and up to sixth-order terms to the temperature factors of all ions produces further, but relatively small, improvements to the fit obtained with fourth-order terms on the Cl ion alone.

Even so, it is worth pointing out that two of the sixth-order parameters, $b_{060+}$ (Cl) and $b_{064+}$ (Cl), can be added with some justification to the model with fourth-order parameters on all ions ($\xi$ = 4 and 6 respectively).

It is interesting to examine the way that the p.w.a. evolves from the totally unacceptable spectrum derived from the harmonic fit. The corresponding p.w.a.'s for the full fourth-order and full sixth-order models have been added to Figure 4.2.1. The improvement in the structure of the partial residuals as a function of Bragg angle is clearly very satisfactory.

(b) The Non-standard Refinements

Refinements were first carried out using the data uncorrected for TDS. Although the second-order thermal parameters are found to decrease significantly from the values obtained with the corrected data, as expected (and in fact to become very close to the values quoted by Harada et al (1976)), the higher-order parameters are remarkably insensitive. The resulting fits are also slightly poorer than the corresponding ones obtained with the corrected data which gives confidence that the TDS corrections are at least reasonable.

The correctness of the counting-statistics weighting scheme is largely justified by the observed flatness of the anharmonic p.w.a. graphs of Figure 4.2.1. As a check for unforeseen features, however, selected refinements were carried out using the data with unit weights applied to each $F_{obs}$. The corresponding p.w.a. graphs have been added to those already shown in Figure 4.2.1. It can be seen that the refinement of higher-order terms need not, *in itself*, lead to a dramatic flattening of the p.w.a. spectrum. Despite the obvious (and expected) unsuitability of these weights, it is found that the refined parameter values do not change significantly from those obtained in the refinements using the 'control' data.

From the form of the structure-amplitude expression (equation (3.7.1)), it is clearly impossible to refine the scale parameter and each of the scattering lengths simultaneously. For this reason, b (Cl) was fixed at the value quoted by Bacon (1975) and refinements carried out allowing the others to vary. It was found that b (Cs) tends to increase by about 4% from the quoted value, but that neither the refined values of the other parameters nor the significance levels associated with the addition of specific anharmonic thermal parameters change significantly.

### 4.2.3 Discussion

From the results of the previous section it can be stated with reasonable certainty that any inherent inaccuracy (of foreseeable proportions) in the TDS corrections, the weighting scheme, or the assignment of neutron scattering lengths, is unlikely to affect the value or significance of the refined anharmonic thermal parameters. Furthermore, on the basis of a comparison of the weighted residuals obtained in the 'control' and the 'non-standard' refinements, it seems clear that reasonable choices have been made in the control data processing and refinement for all of these. The value of b(Cs) does show a consistent tendency to increase slightly from the value quoted by Bacon (1975) when it is refined with the other parameters; however, it is difficult to assess the significance of this increase and in any case the effect on the values of the other parameters is negligible. b (Cs) is therefore not highly correlated with any other individual model parameter.

For these reasons, the parameter values as set out in Table 4.2.1 and the significance levels as summarised in Table 4.2.2 are taken to be accurate, and are used with confidence in the derivation of the ionic p.d.f.'s to follow. (It must of course be remembered that the refinement *models* cannot be treated with equal confidence - see Chapter 2.5.)

One interesting feature to emerge from a comparison of the results of the harmonic refinements using the TDS-and non-TDS-corrected data is that the difference between the refined values of u (Cs) is only about 2%; the corresponding difference for $u^{11}$ (Cl) is comparable. On the other hand, the differences for u (Pb) and $u^{33}$ (Cl) are each about 12%. It is further observed that u (Pb) $\approx$ $u^{33}$ (Cl) (see Table 4.2.1 Model I). Similar features are found to arise in the experimental results for the other perovskites investigated (see the following sections).

Bearing in mind the general conclusions reached with regard to the comparative suitability of the cumulant and F.I. thermal treatments (Chapter 2.5.7 especially conclusion (ix)) and the fits and significance levels obtained from the control refinements, it seems entirely justifiable, in the derivation of the ionic p.d.f.'s, to confine attention primarily to the F.I. models. The corresponding cumulant models will only be considered explicitly if they give results either in sharp qualitative disagreement or in very close agreement.

The F.I. and cumulant models for the Cs ion give results in good agreement with each other. The $a_{40+}$ and $d^{O}$ fourth-order terms, characterising isotropic thermal anharmonicity about the m3m site, are completely insignificant when added singly to the harmonic model. (The expression '$a_{40+}$ fourth-order term' is used throughout to mean that term within the temperature-factor expansion of which $a_{40+}$ is the coefficient.) Such anharmonicity as does exist, then, although of highly marginal significance, appears to be structured and characterised adequately by a single cubic-symmetry term - either $a_{44+}$ or $d^{C}$. These conclusions are qualitatively confirmed even in the presence of full fourth-order anharmonic terms on the Pb and Cl ions (compare the Cs-ion thermal parameters of Models II and V in Table 4.2.1.) This result seems very clear, but the marginal significance of the anharmonicity is at variance with the results of Sakata et al (1978, 1979) who find Cs to be in a 'very strong anharmonic potential'.

The lead-ion anharmonicity is more open to question. Although the addition of F.I. and cumulant fourth-order terms to the harmonic model give identical (if small) improvements in fit which can be traced almost exclusively to the effects of the isotropic $a_{40+}$ and $d^0$ terms respectively, the resulting bias in the second-order parameter is very different in each case. u (Pb) is found to decrease very significantly when fourth-order F.I. parameters are refined simultaneously and to increase when the corresponding cumulant parameters are refined. However, in the presence of anharmonic terms on the other ions, the refined value of u (Pb) reverts close to its harmonic-approximation value with an accompanying decrease in the size of the anharmonic parameters (compare Models III and V of Table 4.2.1). It is tempting to relate this behaviour to an attempt by the anharmonic terms to compensate for effects arising from the non-inclusion of anharmonic terms on the other ions. (The instability of the Pb-ion thermal parameters is also reminiscent of the observations reported by Merisalo and Larsen (1977) concerning their refined potential parameters.) In any case, the addition of fourth-order terms to the Pb-ion temperature factor, despite causing such drastic modifications to the second-order parameter, does not result in a very significant improvement in fit. This conclusion substantiates the findings of Sakata et al (1978, 1979).

For the reasons just given, it was not considered worthwhile constructing the direct-space p.d.f.'s for either the Cs or Pb ions.

It is clear from an inspection of Tables 4.2.1 and 4.2.2 that the improvement in fit resulting from the addition of anharmonic F.I. or cumulant terms to the Cl ions is very large indeed. Accordingly, the Cl-ion p.d.f. was calculated from the refined parameters of Model VI. (The extra metal-ion parameters refined in Model VII do not improve the fit further or modify the Cl parameters significantly.) Several points emerge :

(i) A small ripple can be seen in the anharmonic p.d.f. map (not shown here) such that some regions have a negative value. However, these negative regions always have values less than ¼% of the peak height at the mean ionic position, 0 (the 4/mmm site), and are always at least 1 Å from it. It is therefore thought unlikely that they will affect the detail of the p.d.f. appreciably. The p.d.f. map is not shown here because, in spite of its extremely *significant* anharmonicity, its shape does not *look* very non-Gaussian.

(ii) The thermal anisotropy in the plane perpendicular to the unique axis and containing the 4/mmm site (the Cs-Cl plane) is fairly small but increases with distance from the centre causing the p.d.f. to bulge out in the directions [1,0,0] and [0,1,0] of Figure 1.4.3. This observation is in agreement with the results obtained by Harada et al (1976) using difference-Fourier methods. Put on a quantitative scale, the differences between the p.d.f. values along [1,0,0] and along the face-diagonal direction [1,1,0] are 5%, 25% and 90% at 0.5 Å, 0.7 Å and 1.0 Å from 0.

(iii) There is no evidence of resolvable disorder; that is, the p.d.f. is single-peaked.

(iv) An examination of the difference map, obtained by subtracting the Model I p.d.f. from the Model VI p.d.f., shows in a clearer way how the harmonic approximation to the p.d.f. is modified by the anharmonic terms. A quarter of the Cs-Cl section is shown in Figure 4.2.2. It must be remembered, in the interpretation of the map, that the best-fitting harmonic distribution has been normalised to 10,000 at 0, so that the apparently large peaks and troughs, when viewed in that light, become less dramatic. For instance, the negative value of the map at 0 means that the probability of the Cl ion being located at that position is about 10%

Figure 4.2.2 The $Cl$-ion difference p.d.f. for $CsPbCl_3$ at $325^{o}K$ obtained by subtraction of $P_{Model\ I}(\underline{r}) - P_h$ - from $P_{Model\ VI}(\underline{r}) - P_a$. The labelling of the axes (X and Y) is as established in Figure 1.4.3; the full A-X section may therefore be obtained by $90^{o}$ rotations about the four-fold axis. $P_a$ is normalised to $P_h$ which is assigned the value 10,000 at 0. The r.m.s.a. of $P_h$ (which is isotropic about the four-fold axis) is indicated by the vertical line on the X-axis at 0.44 $\mathring{A}$. As an aid to interpretation, the quantity $(P_a - P_h)/P_a$ is expressed as a percentage at a number of starred locations on the map.

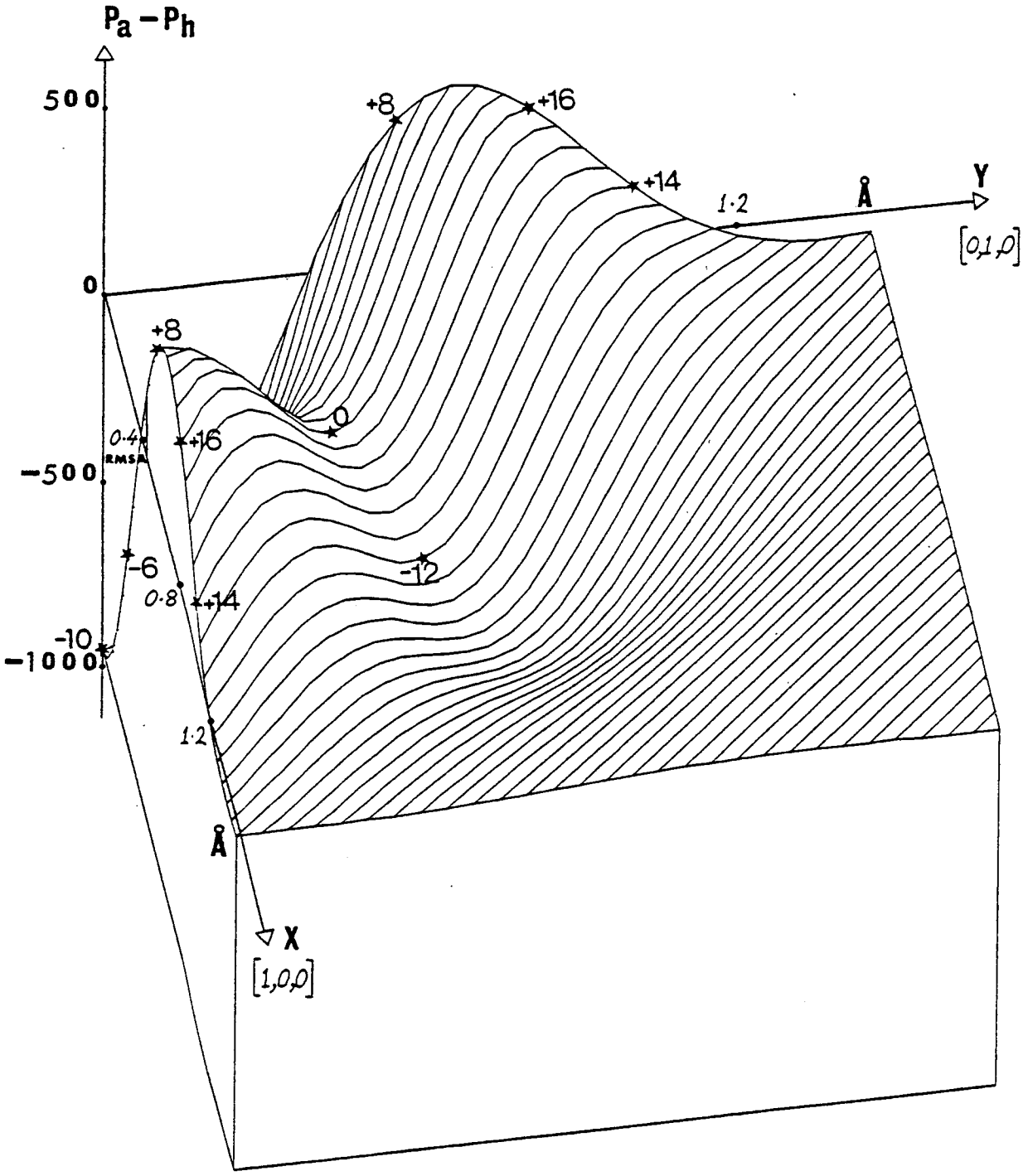
Pa − Ph
500
0
−500
−1000
+8
+16
+14
1·2
Å
Y
[0,1,0]
+8
0
0·4
RMSÅ
+16
-6
0·8
+14
-10
-12
1·2
Å
X
[1,0,0]

Figure 4.2.2

less than the harmonic approximation p.d.f. would predict. As an aid to interpretation, the quantity $(P_{\text{Model VI}}(\underline{r}) - P_{\text{Model I}}(\underline{r}))/P_{\text{Model VI}}(\underline{r})$ is expressed as a percentage on the map at a number of locations. From these figures it is clear that, in qualitative terms, the probability density has been removed from around O and deposited further along the principal axes (X and Y) of the diagram. The density is largely unchanged along the face-diagonal direction. (The calculated difference of -12% marked on the map along this direction can be seen to correspond to a distance of about four r.m.s.a.'s from O so that the density at this point is negligible anyway.)

From the observations of this section and the results obtained from the test refinements of Chapter 2.5, several conclusions may be advanced as regards the extent and character of thermal anharmonicity in cubic $CsPbCl_3$ at $T_c + 5^o$. First, there is no good reason to propose any very significant level of anharmonicity on either of the metal ions. This is a particularly interesting conclusion for the Cs ion in the face of its exceptionally large thermal amplitude. Second, the anharmonicity on the Cl ions is extremely large. The very size of the effect on the fit precludes any reasonable interpretation in terms of systematic errors in data collection or analysis. Third, the Cl-ion p.d.f. bulges out perpendicular to the unique axis and along the directions of the principal crystal axes, $\langle 1,0,0 \rangle$. There is, however, no indication of resolvable disorder.

## 4.3 THE $RbCaF_3$ EXPERIMENT AT $T_c + 10^o$

### 4.3.1 Experimental Details

The $RbCaF_3$ specimen, provided by Dr M Rousseau, Le Mans, was cut to the shape of a cuboid of sides 4.5 x 4.5 x 3.0 mm. A considerable amount of side scatter from an incident low-power laser beam was observed, indicating the likely presence of impurities, although the crystal was optically isotropic under

crossed polars. Some evidence of split spots in an X-ray back-scattering photograph prompted a preliminary experiment at A.E.R.E. (Harwell) on a two-circle diffractometer. This experiment confirmed the crystal to be split by about $0.5^{o}$ around a $\langle 1,1,0 \rangle$ direction. However, a consideration of the diffraction geometry showed that the effects on the measurements arising from this splitting could be minimised by a careful choice of the equivalents to be measured, and that the size of the receiving aperture required to accommodate the beam would not be unmanageably large.

Data were collected on the D9 diffractometer at I.L.L. with an incident wavelength $\lambda$ = 0.528 Å, using Hf filters to reduce the $\lambda/2$ contamination. The crystal was enclosed in a cryostat whose temperature was maintained at $205^{o}$K, $10^{o}$ above the cubic $\rightarrow$tetragonal phase transition temperature, $T_c$. ($T_c$ was found by monitoring the scattered intensity at $\frac{1}{2}(3,1,1)$ of the cubic phase against temperature - see Figure 4.3.1.) The cell constant used was obtained from the work of Ridou et al (1977) - a = 4.445 Å. Using the $\omega$:$2\theta$ scan method, two symmetry-equivalent reflections were measured for a randomly selected sample of about 40% of the available independent reflections out to $\theta_B = 60^{o}$. This gave a resolution $(\sin\theta_B/\lambda)_{max}$ = 1.7 $Å^{-1}$. Some of these reflections were too weak to be measured to an acceptable accuracy in a realistic time and were discarded.

Preliminary refinements showed extinction to be negligibly small; that is, the inclusion of any extinction parameter in the refinement models resulted in no significant improvement in the fit. In fact, in some cases, a slightly *negative* (physically impossible) extinction was refined. For these reasons, extinction parameters were not included in the refinements described in the next section.

Equivalent reflection intensities were averaged leaving 146 independent measurements. TDS correction factors were then calculated as outlined in Appendix B, using the approximation

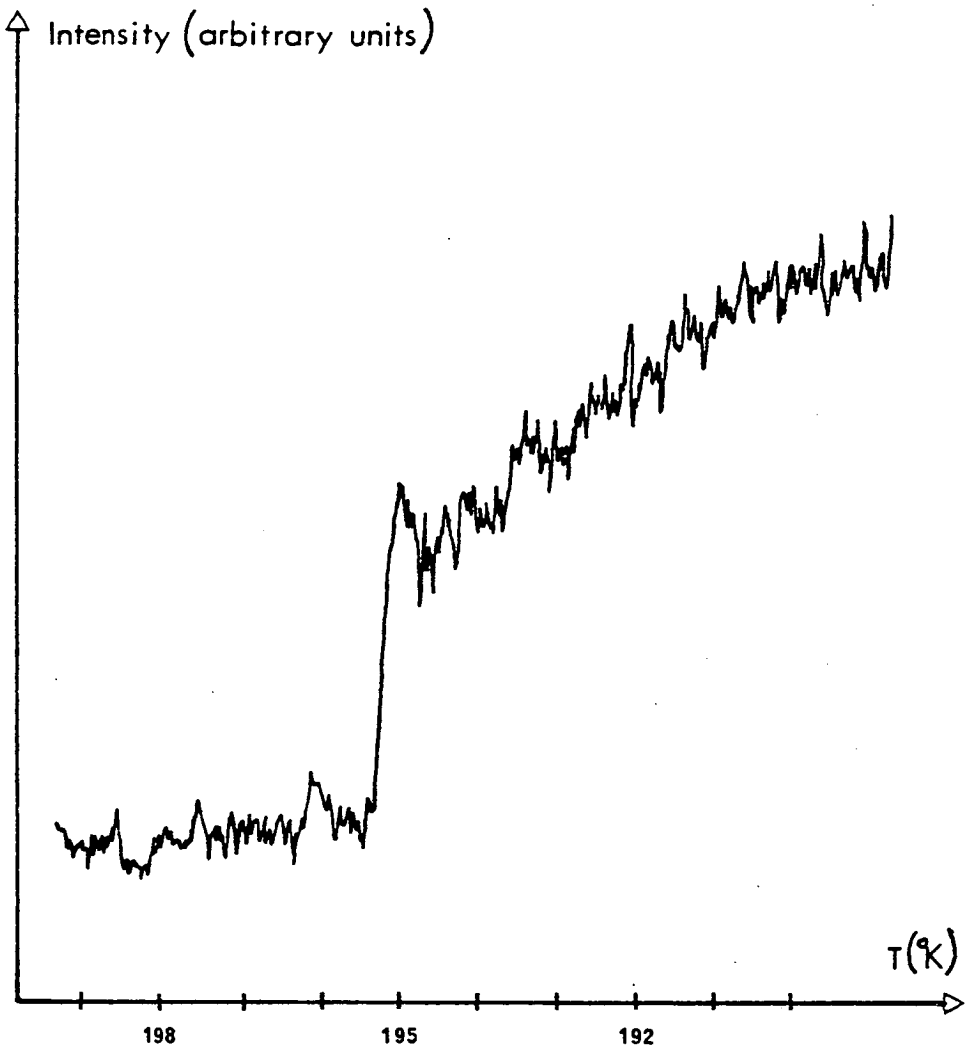


Figure 4.3.1 The intensity of scattering observed at the $\frac{1}{2}(3,1,1)$ point of the cubic phase in $RbCaF_3$ near the cubic → tetragonal phase transition temperature. The temperature scale is accurate to within $\pm 1^{o}$.

described therein in the definition of the circular receiving aperture. Elastic constants were calculated from the work of Rousseau et al (1977)* and were found to result in the derivation of extremely large correction factors ($\alpha \sim 2$ for the reflections at the high-angle limit).

A maximum accuracy of 1.5% was finally assigned to the $F_{obs}$ values.

### 4.3.2 The Refinements

#### (a) The Control Refinements

The residual R = 0.027, obtained from the harmonic-model refinement, is of the order to be expected on the basis of the accuracy achieved in the data collection. The refined thermal parameters (see Table 4.3.1) are found to be in good agreement with the values quoted by Bulou et al (1979). Again, as in the corresponding harmonic refinement using the $CsPbCl_3$ data (Section 2.2), the p.w.a. shows a marked, but not so systematic structure with Bragg angle. The reason for this is clear from an examination of the final lists of $F_{obs}$ and $F_{calc}$ values : of the total $\sum w\Delta^2 = 631$, over 200 is contributed by six outliers to the fit - an unreasonably large proportion. It is also found that, in general, the $F_{calc}$ of very high-angle reflections underestimates the observed structure amplitude. In the light of these observations, the individual reflection profiles were scrutinised for any evidence to support the downweighting or deletion of any reflections. None was found.

It was discovered immediately that any attempt to refine fourth-order F.I. parameters on either the Rb or Ca ions causes the refinement to diverge, even if damping factors are used. This is surprising in view of the fact that no evidence of high parameter correlation is obtained from the correlation matrices. Moreover, when the refinements are repeated allowing b(Rb) and b(Ca) to vary, the convergence is good and the refined values of

* The elastic constants used were :
$c_{11} = 0.23$, $c_{44} = 0.04$ and $c_{12} = 0.02 \times 10^{12}$ dyne/cm$^2$

Table 4.3.1 The refined parameters of $RbCaF_3$ at $205^oK$. Model I contains harmonic thermal parameters on all ions. Models II, III, IV and V contain, in addition to the parameters of Model I, fourth-order F.I. parameters on the Rb, Ca and F ions and on all ions respectively. In addition, the arbitrary scale parameter, Sc, was always refined. Convergence of the refinements using Models II, III and V was conditional upon the simultaneous refinement of the metal-ion scattering lengths. Extinction within the crystal was neglected. Estimated standard deviations (from the least-squares refinement) are given in parentheses; where none is given, the parameter was fixed during refinement. R, $R_w$ and $\Sigma w\Delta^2$ are defined in the text. $^c\Sigma w\Delta^2$ is the weighted sum of squares obtained in the corresponding refinement using cumulant parameters instead of F.I. parameters. $^{cc}\Sigma w\Delta^2$ is the value obtained using cumulant parameters with the metal-ion scattering lengths fixed at the values used in the Model I refinement.

| Model | I | II | III | IV | V |
|---|---|---|---|---|---|
| Sc | 214(1) | 214(3) | 218(2) | 216(1) | 210(2) |
| **Rubidium** | | | | | |
| $b \times 10^{12}$ cm | 0.71 | 0.70(1) | 0.70(1) | 0.71 | 0.73(1) |
| u ($Å^2$) | 0.0182(1) | 0.0186(3) | 0.0182(2) | 0.0182(2) | 0.0182(2) |
| $a_{40+}$ | | 0.013(5) | | | -0.002(4) |
| $a_{44+}$ | | -0.007(2) | | | -0.001(2) |
| **Calcium** | | | | | |
| $b \times 10^{12}$ cm | 0.47 | 0.47(1) | 0.47(1) | 0.47 | 0.50(2) |
| u ($Å^2$) | 0.0077(1) | 0.0076(1) | 0.0073(3) | 0.0080(1) | 0.0076(4) |
| $a_{40+}$ | | | -0.03(2) | | -0.03(2) |
| $a_{44+}$ | | | -0.023(4) | | -0.006(5) |
| **Fluorine** | | | | | |
| $b \times 10^{12}$ cm | 0.56 | 0.56 | 0.56 | 0.56 | 0.56 |
| $u^{11}$ ($Å^2$) | 0.0431(5) | 0.0431(5) | 0.0431(5) | 0.0439(4) | 0.0431(5) |
| $u^{33}$ ($Å^2$) | 0.0076(2) | 0.0076(2) | 0.0085(2) | 0.0068(1) | 0.0072(4) |
| $b_{040+}$ | | | | 0.036(4) | 0.037(5) |
| $b_{044+}$ | | | | -0.006(1) | -0.007(1) |
| $b_{220+}$ | | | | 0.002(2) | -0.001(2) |
| $b_{400+}$ | | | | -0.0033(4) | -0.002(1) |
| g | 0 | 0 | 0 | 0 | 0 |
| R | 0.027 | 0.027 | 0.024 | 0.021 | 0.019 |
| $R_w$ | 0.041 | 0.038 | 0.035 | 0.027 | 0.025 |
| $\Sigma w\Delta^2$ | 631 | 565 | 466 | 271 | 234 |
| $^{c}\Sigma w\Delta^2$ | 631 | 568 | 463 | 292 | 264 |
| $^{cc}\Sigma w\Delta^2$ | | 576 | 477 | | 281 |

| Model | I | II | III | IV | V |
|---|---|---|---|---|---|
| N.P. | 5 | 9 | 9 | 9 | 15 |
| F.I. | | | | | |
| $\Sigma w\Delta^2$ | 631 | 565 | 466 | 271 | 234 |
| $\alpha_s$ | | $0.005_I$ | $0.001_I$ | $0.001_I$ | * |
| $\xi$ | | 1 | 3 | 11 | * |
| cumulant | | | | | |
| $c\Sigma w\Delta^2$ | 631 | 568 | 463 | 292 | 264 |
| $\alpha_s$ | | $0.005_I$ | $0.001_I$ | $0.001_I$ | * |
| $\xi$ | | 1 | 3 | 10 | * |
| Parameter | $a_{44+}$(Rb) | $a_{44+}$(Ca) | $b_{040+}$(F) | $b_{044+}$(F) | $b_{400+}$(F) |
| $\xi$ | $1_I$ | $6_I$ | $8_I$ | $3_I$ | $6_I$ |

Table 4.3.2 The significance levels derived from the fits of Table 4.3.1. This table has been constructed in an entirely analogous way to Table 4.2.2; the reader is referred to the caption of that table for an explanation of the notation used. The symbol '*' indicates that the refined values of the metal-ion scattering lengths were not consistent with those refined using the other models. The derivation of significance levels is therefore inappropriate.

the scattering lengths are not significantly different from those held fixed initially (see Table 4.3.1). The corresponding refinements with cumulant parameters converge normally, whether the scattering lengths are refined or not, giving very similar fits to those obtained in the refinements using F.I. parameters.

Refinement of a model with fourth-order parameters on only the fluorine ions results in a substantial reduction in the value of $\sum w\Delta^2$ from the value obtained with the harmonic model. The reduction is greater, and more significant, than that obtained when fourth-order parameters are refined on either of the metal ions individually. A very much improved p.w.a. is also produced, the contribution from the outliers referred to above being only slightly higher than average. Refinements of models with fourth-order terms in the temperature factor of every ion and further models with up to sixth-order terms, continue to give small improvements in fit. However, convergence of the refinements with F.I. metal-ion parameters always depends upon the simultaneous refinement of b(Rb) and b(Ca). It is found in these cases that the refined values of the scattering lengths differ significantly from those quoted by Bacon (1975) (see for example Table 4.3.1, Model V).

(b) The Non-Standard Refinements

Because the TDS correction factors are very large indeed (in some extreme high-angle cases reducing the measured intensity by over 60%) it is desirable to give some consideration to the dependence of the refined parameter values upon the exact corrections used. Refinements were therefore carried out for several models using the data completely uncorrected for TDS contributions. The thermal parameters obtained using the harmonic model are found to decrease by large amounts, as expected, from the corresponding values obtained with the corrected data. However, it is disturbing to note that the weighted residual actually *improves* by a small but significant amount. On the other hand, the weighted

residual obtained using the model with fourth-order F.I. terms on the F ions alone is slightly poorer than that obtained from the corresponding refinement using the corrected data. In none of the refinements were the values of the fourth-order thermal parameters found to be sensitive to the TDS corrections made.

### 4.3.3 Discussion

It is disturbing that the fourth-order F.I. refinements using Models II, III, and V in Table 4.3.1 only converge if b(Rb) and b(Ca) are refined simultaneously with the other parameters. The reason for this is not obvious - especially in view of the facts (i) that when they *are* refined their values do not change significantly (except in the case of Model V where both appear to increase slightly) and (ii) that the corresponding refinements using cumulant parameters converge normally. For the cumulant refinements using Models II, III and V the value of $\sum w\Delta^2$ is given in Table 4.3.1 for the separate cases in which b(Rb) and b(Ca) were and were not refined. From a comparison of each set of values ($\overset{c}{\sum} w\Delta^2$ and $\overset{cc}{\sum} w\Delta^2$) it can be seen that most of the reduction in $\sum w\Delta^2$ from the harmonic model value does *not* result from the simultaneous refinement of the scattering lengths. However, the significance levels of Tables 4.3.2 are based on the number of parameters actually refined, including scattering lengths. The probable result of this will be to slightly reduce the derived significance levels associated with the addition of metal-ion anharmonic terms compared with the levels which would be obtained were it possible to keep these scattering lengths fixed. (This change arises from the different degrees of freedom, b and n-m, used in the ANOVA significance tests (Chapter 3.8).)

The TDS correction factors are very large and therefore the cause of some concern. It might be worthwhile to attempt a more exact correction than has been possible here, although any resulting modifications to the anharmonic thermal parameters would probably be small - bearing in mind their relative insensitivity to whether a correction is made or not. The values

quoted in Table 4.3.1 for the second-order thermal parameters, however, may be subject to some additional (although again probably small) systematic error. While it is true that the harmonic-model refinement gives a lower $\sum w\Delta^2$ value with the *uncorrected* data, this may be as much an indictment of the model as of the TDS correction.

A check was not made on the validity of the weighting scheme. From the results of the test refinements (Chapter 2.5) and the refinements carried out using the $CsPbCl_3$ data (Section 2.2), any slight inaccuracy in the weights is thought to be an unlikely source of error in the refined parameter values. In addition, an examination of the p.w.a.'s of Models IV and V reveals no systematic trends of any significance.

For the above reasons, the parameters of Table 4.3.1 are assumed to provide accurate descriptions of the thermal motion obtaining in the crystal (within any limitations imposed by model inadequacies, as discussed in Chapter 2.5); it is expected, with some justification, that any non-Gaussian structure in the derived ionic p.d.f.'s will not be significantly biassed by the slight uncertainty surrounding the values of the second-order parameters.

Attention is first drawn to the near equivalence of the refined harmonic-model values of u(Ca) and $u^{33}$(F) (see Table 4.3.1 Column 1). This equivalence is observed to hold even when the parameter values themselves change significantly as a result of using the data uncorrected for TDS.

The anharmonic descriptions provided by the F.I. and cumulant models for the Rb ion are in good agreement with each other (see Table 4.3.1 Model II). The anharmonicity is small - although its significance is not entirely negligible - and predominantly characterised by the fourth-order cubic-symmetry terms with coefficients $a_{44+}$ and $d^c$. It is found, however (Model V), that the value and significance of the Rb fourth-order terms becomes more open to question in the presence of fourth-order terms on all of the ions.

The thermal description of the Ca ion (Model III) is very similar to that of the Rb ion except that the anharmonicity is apparently much greater and considerably more significant (see Table 4.3.2). Again it is characterised predominantly by the cubic-symmetry terms, and in fact the significance of $a_{44+}$(Ca) ($\xi$ = 6) could be advanced - see Chapter 3.8 - as evidence of physically significant anharmonicity, were it not for the observation that in the presence of anharmonic terms on the other ions (Model V) the value of $a_{44+}$ (Ca) becomes small and ill-determined.

From Tables 4.3.1 and 4.3.2 it can be seen that the improvement in fit, resulting from the addition of fourth-order terms to the F ions alone, is large and of comparable size for both the F.I. and cumulant treatments. It is also clear that the F-ion anharmonic parameters are the only ones to maintain their integrity in the presence of anharmonic terms on the other ions (compare the results for Models IV and V). Table 4.3.2 shows that the most significant of these parameters are $b_{040+}$ and $b_{400+}$ ($\xi$ = 8 and 6 respectively for their individual addition to the harmonic temperature factor). The functions corresponding to both of these parameters are isotropic about the four-fold axis.

In the light of the marginal significance of the Rb-ion anharmonic parameters, and their corresponding ill-determinacy, the construction of the p.d.f. from the parameters of Model II was not thought worthwhile. It would also seem inappropriate, for the reasons given above, to derive much significance from a Ca-ion p.d.f. based on the parameters of Model III. Only the F-ion p.d.f. - from the F.I. parameters of Model IV - was therefore constructed. An examination of this p.d.f. (not shown here) shows the following features.

The regions of negative density always have values less than 0.5% of the peak height at the mean position, 0, and are well removed from it, so that their effect on the gross features of the distribution can be assumed to be negligible. Slight bulges in the p.d.f. can be observed along the directions [1,0,0] and [0,1,0]

of Figure 1.4.3. The thermal anisotropy in the Rb-F plane (defined previously as the difference of the p.d.f. at equal distances from 0 along [1,0,0] and [1,1,0] is 2%, 25% and 70% at distances 0.3 Å, 0.4 Å and 0.5 Å respectively. Although the anisotropic bulging of the F-ion p.d.f. is not large, its significance is probably non-negligible ($\xi$ = 3 for the addition of $b_{044+}(F)$ to the parameters of the harmonic model which is isotropic in the Rb-F section). In any case, whether the bulging is or is not significant, the present results would appear to be qualitatively incompatible with the dynamical model proposed recently by Rousseau (1977, 1979). His model would also suggest a time-averaged bulging in the Rb-F section, but along the *face diagonal* directions of the cubic unit cell as shown in Figure 2.5.1(b). Such a microstructure would, as demonstrated unambiguously in the test refinements of Chapter 2.5.4, result in the refined value of $b_{044+}$ being *positive*.

Subtracting the Model I p.d.f. from that of Model IV, the difference p.d.f., of which the Rb-F section is shown in Figure 4.3.2, is obtained. The points marked on the map show the quantities $(P_{\text{Model IV}}(\underline{r}) - P_{\text{Model I}}(\underline{r}))/P_{\text{Model IV}}(\underline{r})$. From the map, it is clear that the effect of the anharmonic terms is to concentrate density into the Rb-F section - note that the difference density is predominantly of positive sign. There must therefore be a corresponding depletion of density elsewhere in the distribution. The peak in the difference distribution occurring at the harmonic r.m.s.a. is mainly due to the $b_{040+}$ parameter. The relatively small value obtained for $b_{044+}$ results in only very slight evidence of four-fold symmetry about the unique axis.

## 4.4 THE $KMnF_3$ EXPERIMENT AT $T_c + 10^o$

### 4.4.1 Experimental Details

The single-crystal $KMnF_3$ specimen, obtained from Dr J Storey of the Clarendon Laboratory, Oxford, was melt-grown and showed no signs of strain birefringence. It was slightly pink in colour and

Figure 4.3.2 The F-ion difference p.d.f. for $RbCaF_3$ at $205^oK$ obtained by subtraction of $P_{Model\ I}(\underline{r}) - P_h$ - from $P_{Model\ IV}(\underline{r}) - P_a$. The labelling of the axes (X and Y) is as established in Figure 1.4.3; the full A-X section may therefore be obtained by $90^o$ rotations about the four-fold axis. $P_a$ is normalised to $P_h$ which is assigned the value 10,000 at 0. The r.m.s.a. of $P_h$ (which is isotropic about the four-fold axis) is indicated by the vertical line on the X-axis at 0.21 Å. As an aid to interpretation, the quantity $(P_a - P_h)/P_a$ is expressed as a percentage at a number of starred locations on the map.

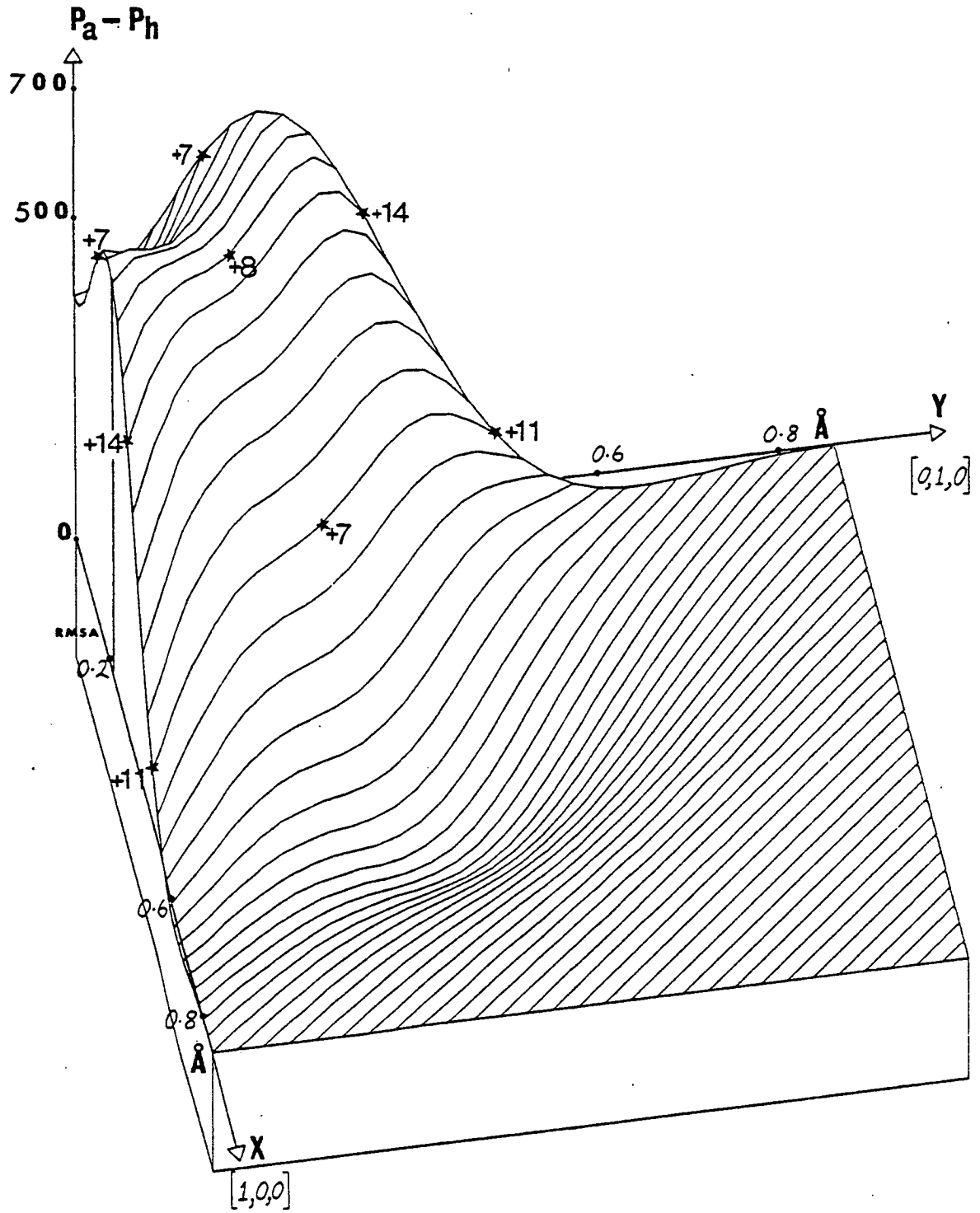


Figure 4.3.2

was found to cleave rather less easily than $RbCaF_3$ along its principal planes. Nonetheless, a reasonable 'cube' of side approximately 4 mm was obtained.

The experiment was carried out on the D9 diffractometer at I.L.L. with an incident wavelength $\lambda = 0.4245$ Å. From a knowledge of the pre-determined machine resolution curves at various wavelengths it was decided that this choice would leave enough background between reflection profiles for an accurate correction to be made, whilst maximising the attainable resolution. Hf filters were used to reduce higher-order wavelength contamination. Using a small crystal from the same batch, the cryostat was calibrated by observing the abrupt change in scattered intensity with temperature at the superlattice point $\frac{1}{2}(3,1,1)$ of the cubic phase. A very small amount of reproducible hysteresis was observed so that $T_c$ was subject to an error of about $1^o$ on the temperature control scale. The experiment was carried out at $T_c + 10^o$ (probably $\sim 197^oK$). Using a cell constant $a = 4.190$ Å (Rousseau et al (1974)), two symmetry-equivalent reflections were measured for about 40% of the independent reflections out to a $\theta_B$ - limit of $60^o$, giving over 200 independent measurements with a resolution $(\sin\theta_B/\lambda)_{max} = 2$ Å$^{-1}$. At the highest Bragg angles it was found beneficial, from the point of view of obtaining smooth background, to tape extra Cd sheeting to the diffractometer $\chi$-circle.

TDS contributions were calculated with the circular aperture used in the experiment being approximated by a square one of the same area (see Appendix B). The values adopted for the elastic constants were those of Aleksandrov et al (1966)* and resulted in correction factors, $\alpha$, of up to 0.5 at the $\theta_B$ limit. Even the most severely affected measured intensities were therefore reduced by only about 30%.

From preliminary refinements using the harmonic model it was clear that extinction, although not severe, was certainly non-negligible. The various extinction models summarised in

* The elastic constants used were :
$c_{11} = 1.15$, $c_{44} = 0.4$ and $c_{12} = 0.27 \times 10^{12}$ dyne/cm$^2$

Appendix A were therefore tested in turn by carrying out refinements using the harmonic thermal model together with the appropriate extinction parameter(s). From these refinements it was clear first, that the Type 1 Lorentzian mosaic spread model gives a significantly better fit than any other isotropic model and second, that the further improvement in fit obtained as a result of adopting an anisotropic correction was completely insignificant. For this reason, the isotropic Type 1 model with Lorentzian mosaic spread was used throughout the refinements described in the next section. It was therefore implicitly assumed that the relative suitabilities of the extinction models were not dependent upon the particular thermal models being tested.

### 4.4.2 The Refinements

#### (a) The Control Refinements

The weighted residual $R_w$ = 0.034, obtained from the harmonic-model refinement, is reasonable considering the accuracy of the data collected. However, an inspection of the p.w.a. reveals that the fit to the low-angle reflections is very poor. For example, the partial weighted residual for the 24 reflections with $\sin\theta_B \leq 0.2$ is nearly 0.090. Bearing in mind that the harmonic model gives a not entirely unsatisfactory fit to the $RbCaF_3$ data (Section 3.2) and that the thermal anharmonicity in $KMnF_3$ is not expected to be significantly greater than that obtaining in $RbCaF_3$ (see the general discussion of Chapter 1.4), it was thought improbable that any inadequacies inherent in the harmonic model itself would manifest themselves in this way. Nor would any inaccuracy in either TDS corrections (small anyway for $KMnF_3$ and especially so for low-angle reflections) or extinction corrections (less than about 10% to the $F^2_{calc}$ of even the most severely affected reflections - well within the regime of validity of the methods used) be expected to present problems. Accordingly, a further refinement, still using the harmonic thermal model, was carried out allowing b(K) and b(Mn) to refine along with the other parameters. The results of interest were as follows :

(i) The refined value of b(Mn) was found to change by about 5% from the value quoted by Bacon (1975) ($-0.39 \rightarrow -0.37 \times 10^{-12}$cm). Mn has many isotopes with widely different scattering lengths so that difficulty might have been anticipated in the assignment of a mean value. The refined value is actually in better agreement with the one quoted by Bacon (1974).

(ii) The refined values of some of the other parameters, including b(K), changed by small *but significant* amounts from the values refined keeping the scattering lengths fixed at the values quoted by Bacon (1975).

(iii) The improvement in fit achieved by refining the two scattering lengths ($\Sigma w\Delta^2 = 1465 \longrightarrow 1275$) is statistically significant at a level $\alpha_s \leq 0.001$.

(iv) The p.w.a., although still not completely smooth as a function of Bragg angle, is very much improved.

For these reasons it was decided to carry out the anharmonic thermal model refinements allowing b(K) and b(Mn) to refine with the other parameters.

(b) The Non-Standard Refinements

A summary of the refined F.I. parameters and the significance levels obtained from the Ratio Test calculations (Chapter 3.8) is given in Tables 4.4.1 and 4.4.2 respectively. The broad measure of agreement between the fits obtained from corresponding refinements using the cumulant and F.I. thermal treatments is again apparent. It is also clear that the only anharmonic thermal parameters with any noteworthy degree of significance are the fourth-order ones on the F ions : the metal-ion anharmonicity is negligible by comparison. It is considerably reassuring that the refined values for the coherent scattering lengths of the metal ions are found to be consistent between all of the refinements.

Table 4.4.1 The refined parameters of $KMnF_3$ at 197°K. Model I contains harmonic thermal parameters on all ions. Models II, III, IV and V contain, in addition to the parameters of Model I, fourth-order F.I. parameters on the K, Mn and F ions and on all ions respectively. In addition, the arbitrary scale parameter, Sc, the extinction parameter, g, and the metal-ion scattering lengths, b(K) and b(Mn), were always refined. The extinction parameter is as defined by Becker and Coppens (1974) for isotropic Type I secondary extinction with a Lorentzian mosaic spread. Estimated standard deviations (from the least-squares refinement) are given in parentheses; where none is given, the parameter was fixed during refinement. R, $R_w$ and $\Sigma w\Delta^2$ are as defined in the text. $\overset{c}{\Sigma} w\Delta^2$ is the weighted sum of squares obtained in the corresponding refinement using cumulant parameters instead of F.I. parameters.

| Model | I | II | III | IV | V |
|---|---|---|---|---|---|
| Sc | 16.4(1) | 16.4(1) | 16.4(1) | 16.3(1) | 16.3(2) |
| **Potassium** | | | | | |
| $b \times 10^{12}$ cm | 0.369(3) | 0.369(3) | 0.369(3) | 0.369(3) | 0.369(3) |
| u ($\AA^2$) | 0.0132(1) | 0.0134(2) | 0.0132(2) | 0.0132(2) | 0.0134(3) |
| $a_{40+}$ | | 0.00(1) | | | 0.013(8) |
| $a_{44+}$ | | -0.005(3) | | | -0.004(3) |
| **Manganese** | | | | | |
| $b \times 10^{12}$ cm | -0.375(3) | -0.375(3) | -0.375(3) | -0.381(3) | -0.38(1) |
| u ($\AA^2$) | 0.0044(1) | 0.0044(1) | 0.0047(3) | 0.0046(1) | 0.0047(3) |
| $a_{40+}$ | | | 0.02(2) | | 0.01(2) |
| $a_{44+}$ | | | -0.008(7) | | 0.01(1) |
| **Fluorine** | | | | | |
| $b \times 10^{12}$ cm | 0.56 | 0.56 | 0.56 | 0.56 | 0.56 |
| $u^{11}$ ($\AA^2$) | 0.0312(2) | 0.0312(2) | 0.0312(2) | 0.0320(3) | 0.0320(3) |
| $u^{33}$ ($\AA^2$) | 0.0050(1) | 0.0050(1) | 0.0050(1) | 0.0048(2) | 0.0046(4) |
| $b_{040+}$ | | | | 0.021(2) | 0.022(3) |
| $b_{044+}$ | | | | -0.0027(6) | -0.0026(7) |
| $b_{220+}$ | | | | 0.000(2) | 0.000(2) |
| $b_{400+}$ | | | | -0.0006(6) | -0.001(1) |
| g x $10^{-4}$ | 0.11(1) | 0.11(1) | 0.11(1) | 0.11(1) | 0.11(1) |
| R | 0.054 | 0.054 | 0.054 | 0.051 | 0.051 |
| $R_w$ | 0.032 | 0.031 | 0.032 | 0.029 | 0.029 |
| $\Sigma w\Delta^2$ | 1275 | 1266 | 1270 | 1074 | 1061 |
| $^c\Sigma w\Delta^2$ | 1275 | 1265 | 1270 | 1077 | 1065 |

| Model | I | II | III | IV | V |
|---|---|---|---|---|---|
| N.P. | 8 | 10 | 10 | 12 | 16 |
| F.I. | | | | | |
| $\Sigma w\Delta^2$ | 1275 | 1266 | 1270 | 1074 | 1061 |
| $\alpha_s$ | | $0.5_I$ | $0.5_I$ | $0.001_I$ | $1_{IV}$ |
| $\xi$ | | 0 | 0 | 3 | 0 |
| cumulant | | | | | |
| $^c\Sigma w\Delta^2$ | 1275 | 1265 | 1270 | 1077 | 1065 |
| $\alpha_s$ | | $0.5_I$ | $0.5_I$ | $0.001_I$ | $1_{IV}$ |
| $\xi$ | | 0 | 0 | 3 | 0 |

| Parameter | $b_{040+}(F)$ |
|---|---|
| $\xi$ | $3_I$ |

Table 4.4.2 The significance levels derived from the fits of Table 4.4.1. The table has been constructed in an entirely analogous way to Table 4.2.2; the reader is referred to the caption of that table for an explanation of the notation used.

### 4.4.3 Discussion

The reasonable p.w.a.'s, the consistency of the refined scattering lengths, and the smallness of the corrections required both for TDS and extinction, give confidence that the parameters set out in Table 4.4.1 constitute accurate descriptions of the $KMnF_3$ structure at $T_c + 10^o$ (within, as usual, any inherent limitations of the F.I. thermal formalism). From the harmonic parameters (Model I), it can be seen that $KMnF_3$ follows, to a fair approximation, the trend established earlier for $CsPbCl_3$ and $RbCaF_3$ : $u(Mn) \approx u^{33}(F)$. It is also noted that the thermal m.s.a.'s are about 30% lower than those found in $RbCaF_3$ at a similar temperature (Table 4.3.1).

The refinements have also demonstrated convincingly the need to establish the correctness of the scattering lengths used and, if possible, to refine them as a check with the other parameters. As noted previously, the complete correlation between Sc and the set of scattering lengths means that at least one scattering length (or Sc) must remain fixed in any given refinement so that only the *ratio* between the scattering lengths can be obtained in general. However, in this case, both b(F) (fixed) and b(K) (refined) remain unchanged from the values quoted by Bacon (1975) and are assumed to be accurate (with justification since b(K) could have changed). The departure from the quoted value by b(Mn) is therefore *implicitly* significant.

The construction of anharmonic p.d.f.'s for the K and Mn ions, based on the refined parameters of Models II and III respectively, was not carried out; only the F-ion p.d.f., based on the parameters of Model IV, was produced.

An examination of the F-ion p.d.f. (not shown here) shows that the values of the negative regions are extremely small and can therefore be ignored. The thermal anisotropy in the K-F plane is also small except at distances far from the mean ionic position, O, where the value of the p.d.f. itself is small. For example,

following the definition established in Sections 2.3 and 3.3, the anisotropy at distances 0.25 Å, 0.35 Å and 0.45 Å from O is 0%, 15% and 55%.

The K-F section of the difference map, obtained by subtraction of $P_{\text{Model I}}(\underline{r})$ from $P_{\text{Model IV}}(\underline{r})$, is shown in Figure 4.4.1. Clearly, the F-ion anharmonicity is predominantly isotropic about the four-fold axis. (Comparison of the relative sizes of the refined $b_{040+}(F)$ and $b_{044+}(F)$ in Table 4.4.1) shows that this must be the case.)

## 4.5 THE $SrTiO_3$ EXPERIMENT

### 4.5.1 Experimental Details

The flux-grown single-crystal specimen, provided by Dr H J Scheel, I.B.M., Zürich, was cut to an approximately cuboidal shape with sides 3.2 mm, 3.0 mm and 2.8 mm. The crystal had a yellow tinge and was found to show marked strain birefringence under crossed polars. However, only one inclusion, contributing no more than an estimated few percent of the birefringence, was identified (Scheel (private communication)). Any remaining strain was thought to be the result of damage caused to the crystal surface when it was cut. Accordingly, about 100 μm was etched off the surface using concentrated phosphoric acid at 553°K. The crystal was then found to be uniformly black under the crossed polars with only a little stray light emanating from some residual surface pitting.

The measurements were made on the D9 diffractometer at I.L.L. using the (3,1,1) planes of the Cu monochromator to give a wavelength $\lambda = 0.3976$ Å. Scans along the principal directions of the reciprocal lattice showed that this choice of wavelength left just enough background between peak profiles to enable accurate background measurements to be made.

Using another crystal from the same batch, the cryostat to be used in the experiment was calibrated by monitoring scattered

Figure 4.4.1 The F-ion difference p.d.f. for $KMnF_3$ at $197^oK$ obtained by subtraction of $P_{Model\ I}(\underline{r}) - P_h$ - from $P_{Model\ IV}(\underline{r}) - P_a$. The labelling of the axes (X and Y) is as established in Figure 1.4.3; the full A-X section may therefore be obtained by $90^o$ rotations about the four-fold axis. $P_a$ is normalised to $P_h$ which is assigned the value 10,000 at O. The r.m.s.a. of $P_h$ (which is isotropic about the four-fold axis) is indicated by the vertical line on the X-axis at 0.18 Å. As an aid to interpretation, the quantity $(P_a - P_h)/P_a$ is expressed as a percentage at a number of starred locations on the map.

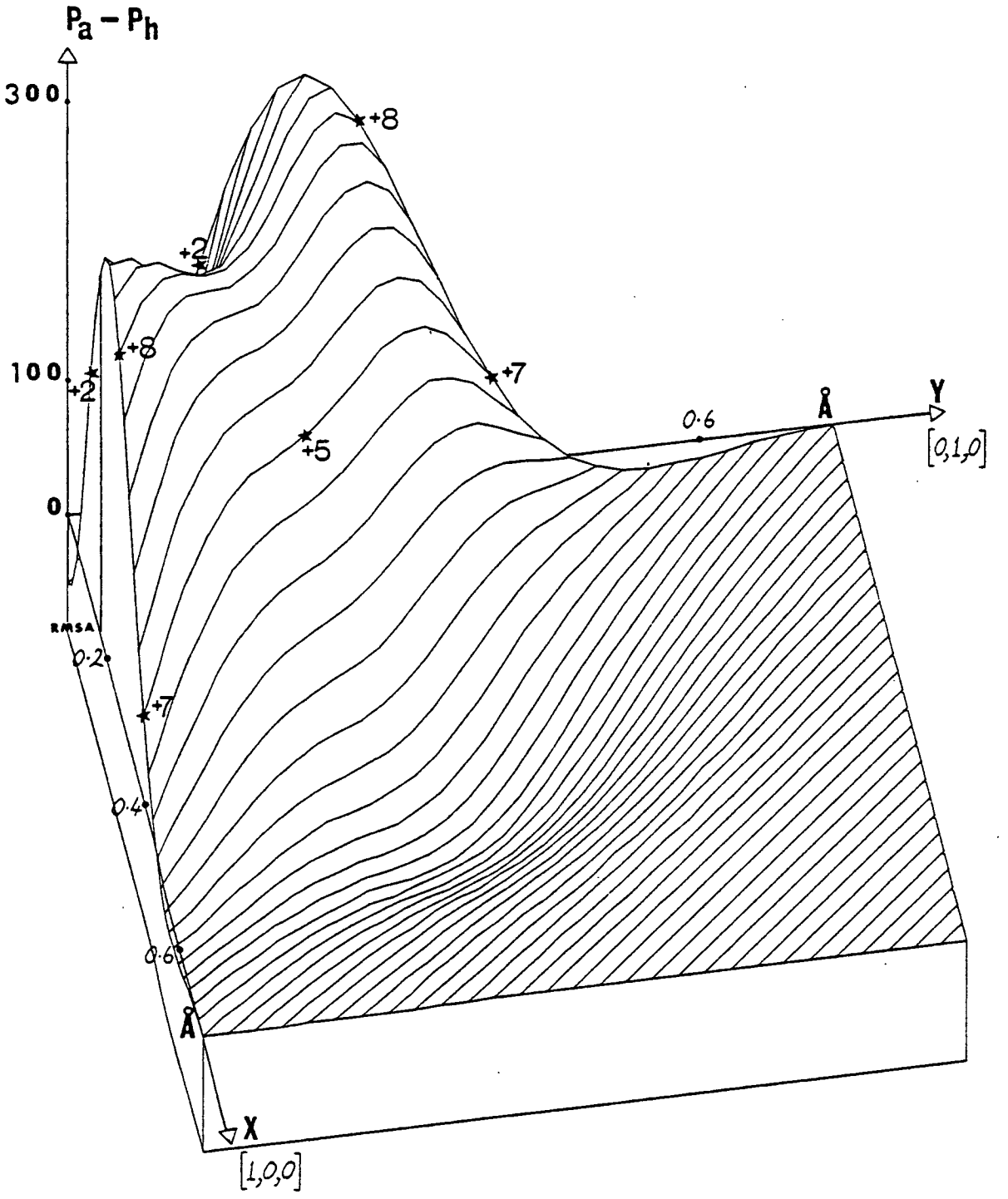


Figure 4.4.1

intensity against temperature near $T_c$ at the (2,0,0) point of the cubic phase. A very large change in intensity was observed at about 107°K and the measurements were made 5°K above this. The cell constant used was a = 3.905 Å (Heidemann and Wettengel (1973)). At least two symmetry-equivalent reflections were then measured for about 40% of the total number of independent reflections out to $\theta_B = 60^\circ$. This gave nearly 240 independent measurements with a resolution $(\sin\theta_B/\lambda)_{max} = 2.1$ Å$^{-1}$.

Two features of interest were observed during the data collection itself : first, symmetry-equivalent reflections with a large $l$ index scattered up to 60% more intensity than those with small $l$ index; and second, the difference in intensity between the strong reflections and the weak ones was much less than that expected on the basis of calculated thermal parameters (Stirling (1972)).

TDS corrections, calculated using the elastic constants of Bell and Rupprecht (1963)*, were small : even those reflections at the angular limit required less than 10% correction to their measured intensity.

### 4.5.2 The Refinements

#### (a) The Control Refinements

From the observations noted in the previous section, it was clear that effects due to extinction are very large and anisotropic. The first problem was then to decide which of the extinction models available is best able to cope, and indeed to decide whether *any* of them can cope satisfactorily. An additional problem was anticipated in the choice of value to be assigned to b(Ti). (Ti is similar to Mn in that it has a variety of isotopes and published values for its mean scattering length.) However, since these two problems were not expected to be highly correlated, it was decided in the first instance to set b(Ti) = $-0.33 \times 10^{-12}$ cm and to find the most satisfactory extinction model.

* The elastic constants used were :
$c_{11} = 3.3$, $c_{44} = 1.3$ and $c_{12} = 1.0 \times 10^{12}$ dyne/cm$^2$

Refinements were therefore carried out using purely harmonic thermal parameters and different extinction models as summarised in Appendix A. The results of these refinements are shown in Table 4.5.1. From them, it is clear that the choice of extinction model will be a matter of considerable importance; not only do the weighted residuals vary by large amounts depending upon the model used but also the refined values of the scale and thermal parameters. It seems sensible to disregard Type II extinction (Model I of Table 4.5.1 - see Becker and Coppens (1974, 1975)) as a realistic model. The residual is the highest obtained for any of the models and the value of the refined Sr-ion m.s.a. is very different from the corresponding values obtained when the other extinction models are used. These values are, between themselves, reasonably consistent. Perhaps the most surprising observation is the very much poorer fit obtained using the Gaussian mosaic distribution (Model II) compared with the Lorentzian (Model V) $-\sum w\Delta^2$ = 4095 and 1077 respectively. It has been pointed out in the past (Rossmanith (1977) and references therein) that a Lorentzian distribution is usually found to offer a more realistic description but it is nonetheless remarkable that the observed difference is of this magnitude. The use of an anisotropic correction (Model V) instead of an isotropic one (Model III) has considerable statistical justification. However, it is found that the inclusion of a primary extinction correction in the most general model available (Model IV) - refining Types I and II simultaneously - gives rise to correlation problems and in fact leads to a worse fit than that obtained with the Type I secondary extinction correction alone.

From all of these considerations it is reasonable to conclude that the model best suited to describe the extinction effects (at least, the best suited of those considered here) is the anisotropic one based on Type I secondary extinction with the crystal mosaic blocks oriented as a three-dimensional Lorentzian distribution. However, returning to the note of caution expressed earlier in the section, can it be said that this model copes in a *satisfactory* way? To answer this, it is helpful to examine the p.w.a. as a function of Bragg angle. When this is done, it is clear that

Table 4.5.1 The refined harmonic parameters of $SrTiO_3$ at $112^oK$ obtained using different extinction models as defined by Becker and Coppens (1974, 1975). The arbitrary scale constant, Sc, was always refined along with the harmonic thermal parameters. The additional parameters contained in each model are as follows.

Model I contains the parameters specifying anisotropic Type II secondary extinction. g(1) - g(6) are the parameters g(1,1), g(2,2), g(3,3), g(1,2), g(1,3), g(2,3) x $10^{-8}$ defining the mean particle size tensor. The negative value of g(3,3) is non-physical.

Model II contains the parameters specifying anisotropic Type I secondary extinction with Gaussian mosaic spread. g(1) - g(6) are the parameters g(1,1) - g(2,3) x $10^8$ defining the mosaic spread tensor.

Model III contains the parameter specifying isotropic Type I secondary extinction with Lorentzian mosaic spread. g(1) is the parameter g x $10^{-4}$ defining the mosaic spread tensor.

Model IV contains the parameters specifying anisotropic general extinction with Lorentzian mosaic spread. g(1) - g(6) are the parameters g(1,1) - g(2,3) x $10^8$ defining the mosaic spread tensor and g(7) is the parameter $r/\lambda$ x $10^4$ where r is the mean radius of the mosaic blocks (in cm).

Model V contains the parameters specifying anisotropic Type I secondary extinction with Lorentzian mosaic spread. g(1) - g(6) are the parameters g(1,1) - g(2,3) x $10^8$ defining the mosaic spread tensor.

Estimated standard deviations (from the least-squares refinement) are given in parentheses; where none is given, the parameter was fixed during refinement. R, $R_w$ and $\Sigma w\Delta^2$ are defined in the text.

| Model | I | II | III | IV | V |
|---|---|---|---|---|---|
| Sc | 9.3(2) | 8.4(1) | 10.5(2) | 9.2(1) | 10.3(1) |
| Strontium | | | | | |
| $bx10^{12}$cm | 0.69 | 0.69 | 0.69 | 0.69 | 0.69 |
| u ($Å^2$) | 0.0019(1) | 0.0027(1) | 0.0027(1) | 0.0025(1) | 0.0026(1) |
| Titanium | | | | | |
| $bx10^{12}$cm | -0.33 | -0.33 | -0.33 | -0.33 | -0.33 |
| u ($Å^2$) | 0.0013(1) | 0.0015(1) | 0.0021(1) | 0.0016(1) | 0.0020(1) |
| Oxygen | | | | | |
| $bx10^{12}$cm | 0.58 | 0.58 | 0.58 | 0.58 | 0.58 |
| $u^{11}$($Å^2$) | 0.0046(1) | 0.0059(1) | 0.0056(1) | 0.0053(1) | 0.0056(1) |
| $u^{33}$($Å^2$) | 0.0014(1) | 0.0024(1) | 0.0023(1) | 0.0021(1) | 0.0023(1) |
| g(1) | 0.0020(3) | 0.20(5) | 22(1) | 0.04(1) | 0.010(2) |
| g(2) | 0.0015(3) | 0.08(4) | | 0.03(1) | 0.010(2) |
| g(3) | -0.001(4) | 0.044(3) | | 0.007(2) | 0.0022(2) |
| g(4) | 0.0000(1) | -0.04(3) | | -0.01(1) | -0.001(1) |
| g(5) | 0.003(1) | 0.01(1) | | 0.000(2) | 0.0006(3) |
| g(6) | -0.003(1) | 0.00(1) | | 0.002(2) | 0.0017(3) |
| g(7) | | | | 75(6) | |
| R | 0.058 | 0.055 | 0.034 | 0.036 | 0.032 |
| $R_w$ | 0.066 | 0.060 | 0.039 | 0.034 | 0.031 |
| $\Sigma w\Delta^2$ | 4908 | 4095 | 1746 | 1306 | 1077 |

the low-angle reflections are by far the most poorly fitted in general. The partial residual is about 0.090 for those reflections with $\sin \theta_B \leq 0.3$ and about 0.020 for all of the others. This cannot be considered acceptable and it appears that the extinction model is being pushed beyond its regime of validity. This conclusion is hardly surprising considering that the calculated corrections to the most severely affected reflection intensities are about 98%. However, to gauge the extent to which the highly structured p.w.a. *may* result from an incorrect choice of b(Ti), further refinements were carried out allowing b(Ti) to refine simultaneously with the other parameters. The results are summarised in part (b).

(b) The Non-Standard Refinements

Adopting the extinction model deemed to be the most satisfactory (Model V of Table 4.5.1), a harmonic-model refinement was carried out allowing b(Sr) and b(Ti) to refine simultaneously with the other parameters. The following observations were made. First, the value of b(Sr) does not change significantly from the value quoted by Bacon (1975) whilst that of b(Ti) decreases from -0.33 $\rightarrow$ -0.37 $\times 10^{-12}$ cm. Second, although the reduction in the weighted sum of squares from the value obtained keeping the scattering lengths fixed (1077$\longrightarrow$944) is not large, it is accompanied by significant changes in the refined parameter values. And finally, the fit to the troublesome low-angle reflections is improved, that to the others remaining about the same as before. It is still true, nevertheless, that the low-angle reflections are still the most poorly fitted.

For this last reason in particular, it was decided that although the extinction-model inadequacy is perhaps *exaggerated* by the use of an incorrect value for b(Ti), the model is intrinsically unable to describe the drastic extinction obtaining in this crystal. Accordingly, the remaining refinements were carried out using the data set obtained by deleting from the full list those reflections with $h^2 + k^2 + \ell^2 < 40$. The refined parameters listed in

Table 4.5.2 and the significance levels summarised in Table 4.5.3 are those obtained using this reduced data set. In each of the refinements, b(Sr) and b(Ti) were refined simultaneously with the other model parameters and their values were found to be consistent between the different models. It was however found that the simultaneous refinement of Sr-ion second- and higher-order F.I. parameters in Model II was impossible because of very high correlation.

### 4.5.3 Discussion

The refined harmonic thermal parameters are found to be in reasonable agreement with the lattice dynamical calculations of Stirling (1972) - especially with his Model 5. From an examination of Table 4.5.3, it is clear that the significance of any of the anharmonic thermal parameters is marginal.

Although the extinction correction factors are exceedingly large, considerable effort has been made to ensure that the model used is satisfactory over the range of extinction obtaining in the final data set. By diagonalising the mosaic spread tensor, g(i,j), obtained from the refinements of Table 4.5.2, it can be shown that the r.m.s. mosaic orientations along the 'principal' axes of the distribution, are quantified by the dimensions (0.44, 0.40, 0.20) seconds of arc. Clearly these figures should be treated as order of magnitude estimates only. For example, taking the mosaic spread tensor obtained in Model V of Table 4.5.1 (ie, with the unabridged data set), the corresponding dimensions are about 30% lower. From these figures it would be fair to describe the crystal as highly 'perfect'. There is, however, no apparent reason from either the p.w.a.'s, the refined values of the thermal parameters, or the consistency of the refined scattering lengths, to doubt that the extinction corrections made are reasonable. The deletion of the very low-angle reflections would not be expected to alter the main conclusion drawn : that there is no very significant anharmonicity associated with the thermal motion of any of the ions in $SrTiO_3$ at $T_c + 5^o$.

Table 4.5.2 The refined parameters of $SrTiO_3$ at $112^oK$. Model I contains harmonic thermal parameters on all ions. Models II, III, IV and V contain, in addition to the parameters of Model I, fourth-order F.I. parameters on the Sr, Ti and O ions and on all ions respectively. In addition, the arbitrary scale parameter, Sc, the extinction parameters, g(i,j), and the metal-ion scattering lengths, b(Sr) and b(Ti), were always refined. The extinction parameters are as defined by Becker and Coppens (1974, 1975) for anisotropic Type I secondary extinction with a Lorentzian mosaic spread. Estimated standard deviations (from the least-squares refinement) are given in parentheses; where none is given, the parameter was fixed during refinement. R, $R_w$ and $\Sigma w\Delta^2$ are defined in the text. $^c\Sigma w\Delta^2$ is the weighted sum of squares obtained in the corresponding refinement using cumulant parameters instead of F.I. parameters.

| Model | I | II | III | IV | V |
|---|---|---|---|---|---|
| Sc | 9.6(2) | * | 9.6(2) | 9.4(3) | 9.5(3) |
| **Strontium** | | | | | |
| $bx10^{12}$cm | 0.687(5) | | 0.688(5) | 0.70(2) | 0.7(2) |
| u ($Å^2$) | 0.00248(7) | | 0.00248(7) | 0.00243(7) | 0.002(1) |
| $a_{40+}$ | | | | | -0.1(1) |
| $a_{44+}$ | | | | | -0.04(3) |
| **Titanium** | | | | | |
| $bx10^{12}$cm | -0.35(1) | | -0.35(1) | -0.36(1) | -0.36(4) |
| u ($Å^2$) | 0.0021(1) | | 0.0020(8) | 0.0022(1) | 0.0023(5) |
| $a_{40+}$ | | | 0.0(1) | | 0.0(1) |
| $a_{44+}$ | | | 0.00(2) | | -0.01(2) |
| **Oxygen** | | | | | |
| $bx10^{12}$cm | 0.58 | | 0.58 | 0.58 | 0.58 |
| $u^{11}$ ($Å^2$) | 0.00557(6) | | 0.00556(6) | 0.0058(1) | 0.0057(1) |
| $u^{33}$ ($Å^2$) | 0.0022(1) | | 0.0022(1) | 0.0025(2) | 0.0026(2) |
| $b_{040+}$ | | | | 0.00(1) | -0.01(1) |
| $b_{044+}$ | | | | -0.003(2) | -0.004(2) |
| $b_{220+}$ | | | | -0.016(6) | -0.018(6) |
| $b_{400+}$ | | | | 0.001(1) | 0.001(1) |
| $g(1,1)x10^{8}$ | 0.016(3) | | 0.016(3) | 0.018(4) | 0.016(4) |
| g(2,2) | 0.016(3) | | 0.016(3) | 0.018(4) | 0.016(4) |
| g(3,3) | 0.0039(6) | | 0.0039(6) | 0.004(1) | 0.004(1) |
| g(1,2) | -0.003(1) | | -0.003(1) | -0.004(2) | -0.003(2) |
| g(1,3) | 0.001(1) | | 0.001(1) | 0.001(1) | 0.001(1) |
| g(2,3) | 0.002(1) | | 0.002(1) | 0.002(1) | 0.002(1) |
| R | 0.030 | | 0.030 | 0.030 | 0.030 |
| $R_w$ | 0.027 | | 0.027 | 0.027 | 0.026 |
| $\Sigma w\Delta^2$ | 641 | | 641 | 616 | 589 |
| $^{c}\Sigma w\Delta^2$ | 641 | 626 | 640 | 616 | 588 |

| Model | I | II | III | IV | V |
|---|---|---|---|---|---|
| N.P. | 13 | 15 | 15 | 17 | 21 |
| F.I. | | | | | |
| $\Sigma w\Delta^2$ | 641 | * | 641 | 616 | 589 |
| $\alpha_s$ | | * | $1_I$ | $0.01_I$ | $0.05_{IV}$ |
| $\xi$ | | * | 0 | 1 | 1 |
| cumulant | | | | | |
| $\overset{c}{\Sigma w\Delta^2}$ | 641 | 626 | 640 | 616 | 588 |
| $\alpha_s$ | | $0.05_I$ | $1_I$ | $0.01_I$ | $0.05_{IV}$ |
| $\xi$ | | 1 | 0 | 1 | 1 |

---

| Parameter | - |
|---|---|
| $\xi$ | - |

Table 4.5.3 The significance levels derived from the fits of Table 4.5.2. The table has been constructed in an entirely analogous way to Table 4.2.2; the reader is referred to the caption of that table for an explanation of the notation used. The symbol '*' indicates that convergence could not be obtained with the model.

## 4.6 THE $RbCaF_3$ EXPERIMENT AT ROOM TEMPERATURE

### 4.6.1 Experimental Details

The crystal used in this experiment was the same one as used in the experiment at $T_c + 10^o$ (see Section 3.1 for details). Experimental conditions were also largely as described in that section except that the cryostat was removed and the measurements made at room temperature, $100^o$ above $T_c$. The lattice constant was taken from the work of Ridou et al (1977) - a = 4.454 Å. Two symmetry-equivalent reflections were measured for nearly 25% of the available independent reflections out to an angular limit $\theta_B = 60^o$, giving a resolution $(\sin\theta_B/\lambda)_{max} = 1.7$ Å$^{-1}$.

As found in Section 3.1, extinction in the crystal is negligible at this wavelength ( $\lambda = 0.528$ Å) so that the symmetry-equivalent reflection intensities were averaged leaving 98 independent measurements. TDS corrections were found to be extremely large,* as expected, giving correction factors $\alpha \sim 3$ for those reflections at the highest Q values. The structure amplitudes of these reflections were thus reduced to about 50% of their 'observed' values.

A maximum accuracy of 1.5% was assigned to the resulting $F_{obs}$'s.

### 4.6.2 The Refinements

#### (a) The Control Refinements

The refinement of a purely harmonic model yields thermal parameters larger than those obtained by Bulou et al (1979) from powder-diffraction data. For u(Rb) and $u^{11}$(F) the difference is only about 4% but it is larger for u(Ca) and $u^{33}$(F) - about 10% and 14% respectively. The p.w.a. found here is slightly structured but not unacceptable.

* The elastic constants used were :
$c_{11} = 0.23$, $c_{44} = 0.04$ and $c_{12} = 0.02 \times 10^{12}$ dyne/cm$^2$

Similar convergence problems to those mentioned in the refinements using the $T_c$ + 10° data (Section 3.2) were discovered when an attempt was made to refine fourth-order F.I. parameters on either of the metal ions; however, suitable parameter shift damping did give convergence of the refinement with Ca-ion anharmonic terms. No convergence problems were encountered in the corresponding refinements using anharmonic cumulant models. Nor was any evidence found of exceptionally high parameter correlation. A summary of the refined F.I. parameters and the fits and significance levels obtained is given in Tables 4.6.1 and 4.6.2. Addition of fourth-order F.I. parameters to the F-ion temperature factor alone results (see Model IV of Table 4.6.2) in a significant improvement to the fit obtained using a purely harmonic model. The p.w.a. is now much improved and shows hardly any structure with angle. The corresponding refinement using the cumulant model gives a better (although not very significantly so) fit.

Refinement of fourth-order parameters on all ions and sixth-order F-ion parameters continues to give improvements in the fit. However, the improvements are of marginal significance and are not considered further.

(b) The Non-Standard Refinements

Particular care must be taken for two main reasons when attempting to draw conclusions from the parameters obtained in the control refinements. In the first instance, the data set is the smallest of those used in this study. Although the ratio between the number of observations and the maximum number of variable parameters ( 6.5 : 1) would still normally be considered acceptable (Johnson (1970)) there remains some doubt as to whether the selection of such a small sample (25%) of the independent reflections is entirely justified. Second, the TDS corrections are the largest calculated for any of the data sets and are extremely large in absolute terms.

Table 4.6.1 The refined parameters of $RbCaF_3$ at room temperature. Model I contains harmonic thermal parameters on all ions. Models II, III, IV and V contain, in addition to the parameters of Model I, fourth-order F.I. parameters on the Rb, Ca and F ions and on all ions respectively. In addition, the arbitrary scale parameter, Sc, was always refined. Convergence of the Models II and V was conditional upon the simultaneous refinement of the metal-ion scattering lengths. Extinction within the crystal was neglected. Estimated standard deviations (from the least-squares refinement) are given in parentheses; where none is given, the parameter was fixed during refinement. R, $R_w$ and $\Sigma w\Delta^2$ are defined in the text. $\overset{c}{\Sigma} w\Delta^2$ is the weighted sum of squares obtained in the corresponding refinement using cumulant parameters instead of F.I. parameters.

| Model | I | II | III | IV | V |
|---|---|---|---|---|---|
| Sc | 22.6(1) | 23.0(2) | 23.1(2) | 23.2(1) | 23.2(2) |
| Rubidium | | | | | |
| $bx10^{12}$cm | 0.71 | 0.68(1) | 0.71 | 0.71 | 0.69(1) |
| u ($Å^2$) | 0.0246(1) | 0.0247(2) | 0.0252(1) | 0.0252(1) | 0.0248(1) |
| $a_{40+}$ | | 0.012(4) | | | 0.003(3) |
| $a_{44+}$ | | -0.006(1) | | | -0.002(1) |
| Calcium | | | | | |
| $bx10^{12}$cm | 0.47 | 0.45(1) | 0.47 | 0.47 | 0.46(1) |
| u ($Å^2$) | 0.0101(1) | 0.0098(1) | 0.0094(1) | 0.0106(1) | 0.0101(2) |
| $a_{40+}$ | | | -0.033(5) | | -0.01(1) |
| $a_{44+}$ | | | -0.009(3) | | 0.000(4) |
| Fluorine | | | | | |
| $bx10^{12}$cm | 0.56 | 0.56 | 0.56 | 0.56 | 0.56 |
| $u^{11}$($Å^2$) | 0.0479(4) | 0.0488(4) | 0.0481(3) | 0.0474(3) | 0.0482(3) |
| $u^{33}$($Å^2$) | 0.0099(2) | 0.0101(2) | 0.0106(2) | 0.0092(1) | 0.0097(3) |
| $b_{040+}$ | | | | 0.004(4) | 0.009(4) |
| $b_{044+}$ | | | | -0.004(1) | -0.004(1) |
| $b_{220+}$ | | | | 0.004(2) | 0.001(2) |
| $b_{400+}$ | | | | -0.0028(3) | -0.0018(5) |
| g | 0 | 0 | 0 | 0 | 0 |
| R | 0.024 | 0.020 | 0.020 | 0.019 | 0.015 |
| $R_w$ | 0.028 | 0.025 | 0.025 | 0.021 | 0.017 |
| $\Sigma w\Delta^2$ | 216 | 162 | 161 | 117 | 81 |
| $^c\Sigma w\Delta^2$ | 216 | 162 | 158 | 100 | 80 |

| Model | I | II | III | IV | V |
|---|---|---|---|---|---|
| N.P. | 5 | 9 | 7 | 9 | 15 |
| F.I. | | | | | |
| $\Sigma w\Delta^2$ | 216 | 162 | 161 | 117 | 81 |
| $\alpha_s$ | | $0.001_I$ | $0.001_I$ | $0.001_I$ | $0.001_{IV}$ |
| $\xi$ | | 2 | 4 | 5 | 2 |
| cumulant | | | | | |
| $^c\Sigma w\Delta^2$ | 216 | 162 | 158 | 100 | 80 |
| $\alpha_s$ | | $0.001_I$ | $0.001_I$ | $0.001_I$ | $0.005_{IV}$ |
| $\xi$ | | 2 | 4 | 7 | 1 |
| Parameter | $a_{44+}$(Rb) | $a_{40+}$(Ca) | $a_{44+}$(Ca) | $b_{044+}$(F) | $b_{400+}$(F) |
| $\xi$ | $2_I$ | $2_I$ | $4_I$ | $2_I$ | $6_I$ |

Table 4.6.2 The significance levels derived from the fits of Table 4.6.1. The table has been constructed in an entirely analogous way to Table 4.2.2; the reader is referred to the caption of that table for an explanation of the notation used.

Accordingly, the validity of the already restricted data set was tested by further reducing it and carrying out a series of duplicate refinements. As expected, the *accuracy* of the refined parameters systematically decreases as the number of independent reflections is reduced. However, it is noted that their *values* do not change significantly. In the light of these observations, it is assumed that the number of independent reflections measured in the experiment is sufficiently large to justify the use of the data set.

Unfortunately, the tests carried out to check the validity of the TDS corrections did not yield such unambiguous results. For each of the F.I. models listed in Table 4.6.1, a refinement was carried out using the data set without correction for TDS. It was found in each case that a significantly lower $\sum w\Delta^2$ value was obtained with the uncorrected data. (It is recalled that a similar feature was found in the corresponding harmonic refinements using the $T_c + 10^o$ data (Section 3.2) although better fits were obtained in that case for the anharmonic models using the corrected data.) The harmonic-model thermal parameters refined using the uncorrected data are found to be much smaller, as expected, than those obtained using the corrected data. - by up to about 60% for u(Ca) and $u^{33}$(F) - and to be in far worse agreement with values quoted by Bulou et al (1979). The observations then to be reconciled are (i) that the use of the non-TDS-corrected data always produces the better fits irrespective of the thermal model being refined, and (ii) that the use of the TDS-corrected data provides refined parameters in better agreement with those quoted in the literature. From the point of view of a study of the anharmonic effects it was reassuring, however (if surprising), that the values of the refined F.I. parameters are not sensitive to whether the TDS corrections are made or not, and further, that the significance of each parameter is about the same using either corrected or uncorrected data sets.

It was noted that b(Rb) and b(Ca) tend to become slightly smaller than the values quoted by Bacon (1975) when they are

refined with the other parameters (see Models II and V of Table 4.6.1). From separate refinements it was, however, seen that the refined values of the other parameters were not sensitive to these small changes.

### 4.6.3 Discussion

Clearly the uncertainty surrounding the validity of the TDS corrections is disturbing, and any conclusions must be drawn with this in mind. Little confidence can therefore be attached to the exact values extracted for the second-order thermal parameters, although as said they are in fair agreement with those obtained by Bulou et al (1979).

In spite of this uncertainty, some features of interest do appear irrespective of whether a correction is made or not. First, it is found that $u(Ca) \approx u^{33}(F)$ when the harmonic model is refined. Second, although a significant improvement in fit is obtained when fourth-order thermal parameters are included in the metal-ion temperature factors (Models II and III of Table 4.6.2), these parameters become ill-determined in the presence of fourth-order parameters on the F-ions (Model V). This means that the derived significance of $a_{44+}(Ca)$ especially ($\alpha = 4$) must be treated with some scepticism. There is, however, no reason to doubt the integrity of the refined F.I. anharmonic F-ion parameters. Of these parameters by far the most significant (see Table 4.6.2) is $b_{400+}(F)$. It is interesting to note that the function within the temperature-factor expansion corresponding to this parameter (see equation (2.4.5)) is identically zero in the Rb-F plane. The effect of $b_{400+}(F)$ on the F-ion p.d.f. may therefore be considered to be primarily along the direction of the unique axis.

The F-ion p.d.f. has been constructed using the F.I. parameters of Model IV. An examination of the p.d.f. shows that it bulges out slightly in the same directions as the F-ion p.d.f. derived from the refined parameters using the $T_c + 10^o$ data. The size of the thermal anisotropy in the Rb-F plane is small; adopting the definition of Section 2.3, it is quantified by the values 3%, 7% and 40% at

distances 0.35 Å, 0.45 Å and 0.55 Å from the mean position, 0. Again, as in the case of the observed bulging at $T_c + 10^o$ (see the comments of Section 3.3) these results seem qualitatively incompatible with the predictions of Rousseau (1977, 1979).

The nature of the modifications to the harmonic p.d.f. due to the refined anharmonic parameters of Model IV can be seen more clearly by an examination of the difference map obtained by subtracting $P_{\text{Model I}}(\underline{r})$ from $P_{\text{Model IV}}(\underline{r})$. The Rb-F section is shown in Figure 4.6.1. From this, it appears that the density around 0 is slightly greater than that predicted by the harmonic model. (It must be remembered that the p.d.f. need not be normalised in any particular section.). As stated above, the most significant, although still small, modifications to the harmonic-approximation p.d.f. do not affect the probability density in the plane considered in Figure 4.6.1.

## 4.7 THE $KMnF_3$ EXPERIMENT AT ROOM TEMPERATURE

### 4.7.1 Experimental Details

The sample, obtained from the same batch as the one used in the experiment at $T_c + 10^o$ (Section 4.1), was cleaved to a cube of side approximately 3 mm. The experiment was carried out on the D8 diffractometer at I.L.L. using an incident wavelength $\lambda = 0.7235$ Å. This gave a resolution $(\sin\theta_B/\lambda)_{max} = 1.1$ Å$^{-1}$.

Two symmetry-equivalent reflections were collected for a complete set of independent reflections with a third equivalent being measured for a further 25. Because the wavelength used in this experiment was longer than that used in the experiment at $T_c + 10^o$, extinction effects were expected to be correspondingly larger. For this reason, the intensities of symmetry-equivalent reflections were not averaged in case there were significant path-length differences between them. The isotropic, Type I extinction model with Lorentzian mosaic distribution was used in all of the

Figure 4.6.1 The F-ion difference p.d.f. for $RbCaF_3$ at room temperature obtained by subtraction of $P_{Model\ I}(\underline{r})$ - $P_h$ - from $P_{Model\ IV}(\underline{r})$ - $P_a$. The labelling of the axes (X and Y) is as established in Figure 1.4.3; the full A-X section may therefore be obtained by $90^o$ rotations about the four-fold axis. $P_a$ is normalised to $P_h$ which is assigned the value 10,000 at 0. The r.m.s.a. of $P_h$ (which is isotropic about the four-fold axis) is indicated by the vertical line on the X-axis at 0.22 Å. As an aid to interpretation, the quantity $(P_a - P_h)/P_a$ is expressed as a percentage at a number of starred locations on the map.

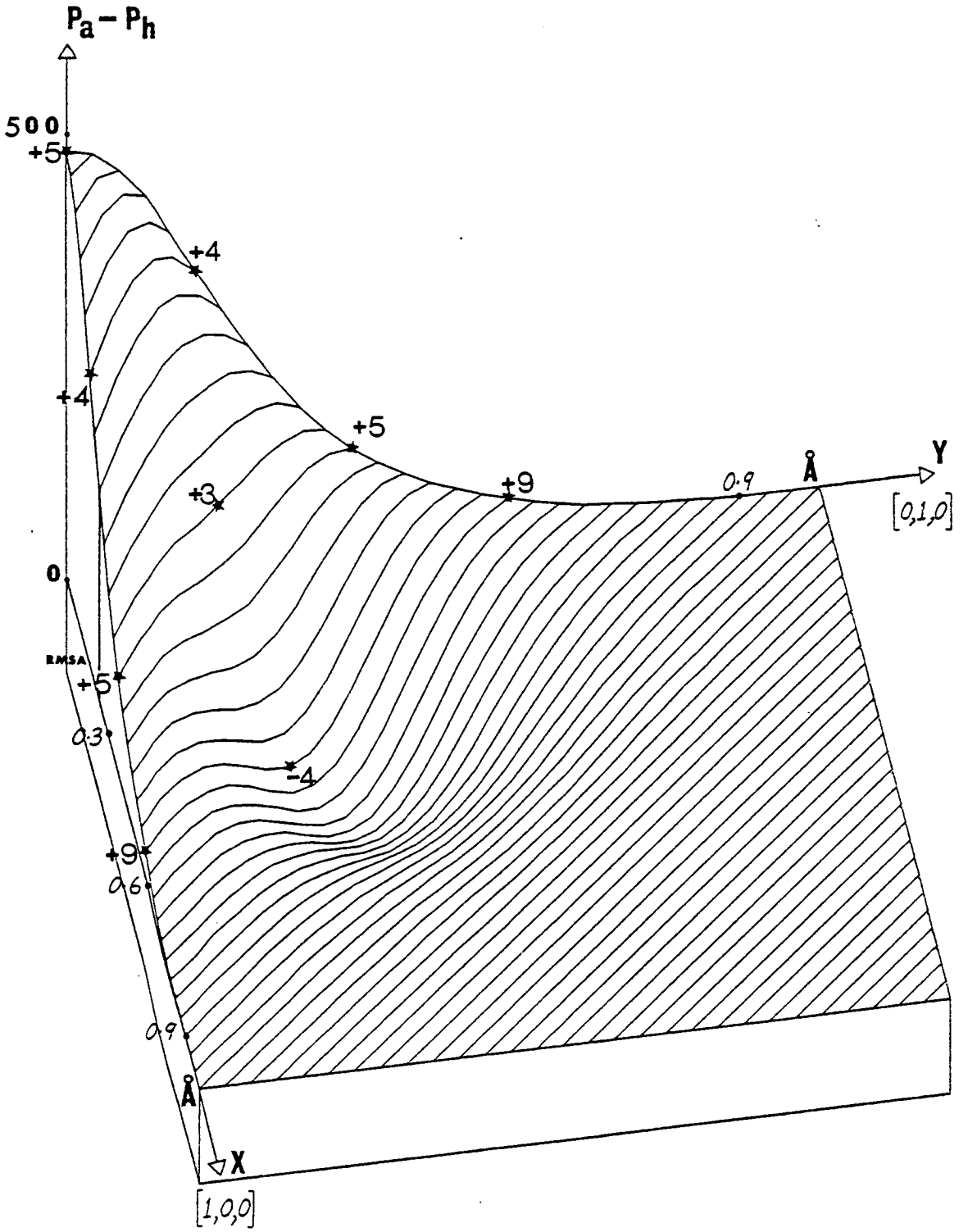


Figure 4.6.1

refinements. (It was found from refinements carried out using the data obtained at $T_c + 10^o$ that the extinction was not significantly anisotropic.) TDS corrections were then made as described in Appendix B.*

4.7.2 The Refinements

(a) The Control Refinements

Because the value of b(Mn) was previously found to deviate from the value quoted by Bacon (1975), and because this was found to significantly bias the refined parameter values (see Section 4.2), it was decided to allow both b(K) and b(Mn) to refine simultaneously with the other parameters in each refinement. These refinements are therefore described in part (b).

(b) The Non-Standard Refinements

The refined model parametersand the derived significance levels are given in Tables 4.7.1 and 4.7.2 respectively. Again only the F.I. parameters have been listed explicitly; corresponding models using cumulant parameters always produce practically identical fits.

The weighted residual $R_w = 0.026$, obtained from the harmonic-model refinement is reasonable, given the accuracy achieved in the data collection. An examination of the p.w.a. shows a rather uneven distribution with Bragg angle although there are no systematic trends. It is also noted that the refined value of b(Mn) is significantly smaller than that obtained from the refinements using the $T_c + 10^o$ data set.

The addition of fourth-order F.I. parameters to each of the constituent ions in turn results in reductions to $\Sigma w\Delta^2$ ranging from very substantial (for the Mn ion - see Model III) to negligible (for the K ion - see Model II). Disturbing inconsistency is found in the refined values obtained for b(Mn); those obtained for b(K) are consistent and compatible with the values refined using the $T_c + 10^o$ data set. Refinement of fourth-order F.I. parameters on

* The elastic constants used were :
$c_{11} = 1.15$, $c_{44} = 0.4$ and $c_{12} = 0.27 \times 10^{12}$ dyne/cm$^2$

Table 4.7.1 The refined parameters of $KMnF_3$ at room temperature. Model I contains harmonic thermal parameters on all ions. Models II, III, IV and V contain, in addition to the parameters of Model I, fourth-order F.I. parameters on the K, Mn and F ions and on all ions respectively. In addition, the arbitrary scale parameter, Sc, the extinction parameter, g, and the metal-ion scattering lengths, b(K) and b(Mn), were always refined. The extinction parameter is as defined by Becker and Coppens (1974) for isotropic Type I secondary extinction with a Lorentzian mosaic spread. Estimated standard deviations (from the least-squares refinement) are given in parentheses; where none is given, the parameter was fixed during refinement. R, $R_w$ and $\Sigma w\Delta^2$ are as defined in the text. $\overset{c}{\Sigma} w\Delta^2$ is the weighted sum of squares obtained in the corresponding refinement using cumulant parameters instead of F.I. parameters.

| Model | I | II | III | IV | V |
|---|---|---|---|---|---|
| Sc | 80(1) | 81(1) | 81(1) | 77(1) | 70(1) |
| **Potassium** | | | | | |
| $bx10^{12}$cm | 0.368(2) | 0.37(1) | 0.375(2) | 0.368(5) | 0.369(3) |
| u ($\AA^2$) | 0.0227(3) | 0.0218(7) | 0.0234(3) | 0.0217(4) | 0.0233(3) |
| $a_{40+}$ | | -0.02(1) | | | 0.05(1) |
| $a_{44+}$ | | 0.000(3) | | | 0.000(1) |
| **Manganese** | | | | | |
| $bx10^{12}$cm | -0.354(3) | -0.351(3) | -0.341(5) | -0.368(3) | -0.376(3) |
| u ($\AA^2$) | 0.0096(1) | 0.0095(1) | 0.0130(4) | 0.0095(2) | 0.0142(3) |
| $a_{40+}$ | | | 0.08(1) | | 0.11(1) |
| $a_{44+}$ | | | 0.003(4) | | 0.014(4) |
| **Fluorine** | | | | | |
| $bx10^{12}$cm | 0.56 | 0.56 | 0.56 | 0.56 | 0.56 |
| $u^{11}$($\AA^2$) | 0.0384(2) | 0.0386(2) | 0.0383(2) | 0.0387(3) | 0.0387(2) |
| $u^{33}$($\AA^2$) | 0.0115(2) | 0.0116(2) | 0.0115(2) | 0.0130(5) | 0.0143(3) |
| $b_{040+}$ | | | | 0.012(3) | 0.029(3) |
| $b_{044+}$ | | | | -0.001(1) | 0.000(1) |
| $b_{220+}$ | | | | -0.004(2) | -0.012(2) |
| $b_{400+}$ | | | | 0.003(1) | 0.0055(5) |
| g x $10^{-4}$ | 0.39(2) | 0.40(2) | 0.39(2) | 0.33(2) | 0.23(1) |
| R | 0.031 | 0.032 | 0.028 | 0.029 | 0.021 |
| $R_w$ | 0.026 | 0.025 | 0.023 | 0.024 | 0.017 |
| $\Sigma w\Delta^2$ | 730 | 718 | 597 | 634 | 333 |
| $^c\Sigma w\Delta^2$ | 730 | 718 | 587 | 632 | 330 |

| Model | I | II | III | IV | V |
|---|---|---|---|---|---|
| N.P. | 8 | 10 | 10 | 12 | 16 |
| F.I. | | | | | |
| $\Sigma w\Delta^2$ | 730 | 718 | 597 | 634 | 333 |
| $\alpha_s$ | | $0.1_I$ | $0.001_I$ | $0.001_I$ | $0.001_{IV}$ |
| $\xi$ | | 1 | 7 | 2 | 15 |
| cumulant | | | | | |
| $^c\Sigma w\Delta^2$ | 730 | 718 | 587 | 632 | 330 |
| $\alpha_s$ | | $0.1_I$ | $0.001_I$ | $0.001_I$ | $0.001_{IV}$ |
| $\xi$ | | 1 | 7 | 2 | 15 |

| Parameter | $a_{40+}$(Mn) | $b_{040+}$(F) | $b_{400+}$(F) |
|---|---|---|---|
| $\xi$ | $6_I$ | $2_I$ | $2_I$ |

Table 4.7.2 The significance levels derived from the fits of Table 4.7.1. The table has been constructed in an entirely analogous way to Table 4.2.2; the reader is referred to the caption of that table for an explanation of the notation used.

each ion simultaneously (Model V) reduces $\sum w\Delta^2$ significantly from the values obtained when these parameters are added to the individual ions. The values obtained for the anharmonic thermal parameters are also found to be sensitive to the presence of such parameters on the other ions (compare the values of Model V with those of Models II, III and IV). The refined value of b(Mn) using Model V is in good agreement with those obtained previously (Section 4.2) and the corresponding p.w.a. is very satisfactory.

It is worth noting that the refined value of the overall scale parameter, Sc, changes from about 80 to about 70 between the harmonic and the most general fourth-order refinements. This change is compensated for to some extent by the change in the extinction parameter. For example, the most highly extinguished reflection, (1,1,1), has its true intensity reduced by 72% according to the harmonic-refinement value of E(1,1,1), compared with 67% according to the Model V value. Clearly, this compensation does not adequately account for the observed difference in the scale-parameter values. The difference must therefore be taken up in the refined values of the other parameters, in particular b(Mn) which changes by about 6% between Models I and V.

### 4.7.3 Discussion

The TDS corrections are small enough to be discounted as a source of significant error in the refined parameters. Extinction, although quite severe (see the example of the previous section), seems to be treated adequately by the model used : no particularly poorly fitted low-angle reflections were found. The most disturbing feature is the range of refined values obtained for b(Mn), although it is of some comfort that the best-fitting model (Model V) gives scattering lengths in good agreement with those refined in Section 4.2.

It seems reasonable then to consider that the refined parameters of Model V yield a plausible description (within any limitations inherent in the F.I. formalism - see Chapter 2.5) of the crystal

structure at room temperature. Caution is required, however, in prescribing significance levels based on the residuals obtained using Models II, III and IV where the refined values of b(Mn) are probably, on the evidence of Model V and the refined values of Table 4.4.1, too small.

The thermal parameters extracted from the harmonic refinement again demonstrate the near equivalence in value of u(B) and $u^{33}(X)$. From Models II and V, it is clear that the thermal anharmonicity of the K ion is small and isotropic; the cubic-symmetry parameter, $a_{44+}(K)$, is zero to a high degree of accuracy. The authenticity of the refined Mn-ion anharmonicity is somewhat shadowed by the uncertainty surrounding the value of b(Mn). In spite of this, comparing the parameters of Models III and V, it does seem that the anharmonic thermal parameters, particularly $a_{40+}$, are rather insensitive to significantly large changes in the other parameters. From Table 4.7.2 it can be seen that this anharmonicity is predominantly isotropic, like that of the K ion, and very significant ($\xi = 6$ for $a_{40+}(Mn)$). Comparison of Models IV and V shows that the refined accuracy (and most probably the significance) of the F-ion anharmonic parameters is influenced by the simultaneous refinement of the metal-ion anharmonic parameters. The significance of the individual parameters is therefore probably higher than the values quoted in Table 4.7.2, which are based on the addition of the F-ion anharmonic parameters to the harmonic model and take no account of correlated metal-ion anharmonicity. It is quite clear, however, that $b_{044+}(F)$, the parameter characterising any anisotropy about the four-fold axis, is the least significant of the F-ion anharmonic parameters.

The K- and Mn-ion p.d.f.'s have not been reproduced here, in the case of the former because deviations from harmonicity are negligible, and in the case of the latter because the deviations are principally isotropic about the mean position, 0. The sign of $a_{40+}(Mn)$ means that the p.d.f. is flattened around the centre of the distribution. The difference p.d.f., obtained by subtraction of $P_{Model\ I}(\underline{r})$ from $P_{Model\ V}(\underline{r})$, would then take the form of a shell of positive

density surrounding a region of negative density around O. Using the refined F.I. parameters of Model V, the F-ion p.d.f. has been calculated and is found to show the following features.

The values of the p.d.f. in regions of negative density are so small as to be insignificant. Because the refined value of $b_{044+}(F)$ is zero, there is no anisotropy about the unique axis. Subtracting $P_{\text{Model I}}(\underline{r})$ from $P_{\text{Model V}}(\underline{r})$, the difference p.d.f. is obtained, of which the K-F section is shown in Figure 4.7.1. The most obvious feature shown by the map is the very considerable flattening of the p.d.f. (as evidenced by the large dip in the difference p.d.f.) around the mean position, O, reducing the value of the p.d.f. from the harmonic-approximation value at that point by over 10%. Further from O, beyond the r.m.s.a. of the harmonic approximation, the effects arising from inclusion of anharmonic terms in the model are very small.

## 4.8 INTERPRETATION OF THE RESULTS

It is clear from the results of the test refinements (Chapter 2.5) that even the F.I. formalism by no means offers a completely satisfactory description of anharmonic p.d.f.'s (compare for example the difference p.d.f.'s of Figures 2.5.6(c) and (d)). However, it does seem in general that any discrepancies between the real and derived distributions are due primarily to the fact that the formalism cannot satisfactorily handle the *magnitude* of the anharmonicity rather than its *structure*. For this reason, features such as the degree of anisotropy arising from intrinsic, underlying anharmonicity are reproduced reasonably well (see the last column of Table 2.5.1), whereas the amount of anharmonicity itself tends to be underestimated (see the first example of the paragraph). These facts must be borne in mind in attempting to interpret the p.d.f.'s derived in the preceding sections of this chapter.

It must also be remembered that detailed analysis has been restricted primarily to the thermal motion of the X ions in the A-X plane. The reasons for this are three-fold : first, the motions

Figure 4.7.1 The F-ion difference p.d.f. for $KMnF_3$ at room temperature obtained by subtraction of $P_{\text{Model I}}(\underline{r}) - P_h$ - from . $P_{\text{Model V}}(\underline{r}) - P_a$. The labelling of the axes (X and Y) is as established in Figure 1.4.3; the full A-X section may therefore be obtained by $90^{\circ}$ rotations about the four-fold axis. $P_a$ is normalised to $P_h$ which is assigned the value 10,000 at 0. The r.m.s.a. of $P_h$ (which is isotropic about the four-fold axis) is indicated by the vertical line on the X-axis at 0.20 Å. As an aid to interpretation, the quantity $(P_a - P_h)/P_a$ is expressed as a percentage at a number of starred locations on the map.

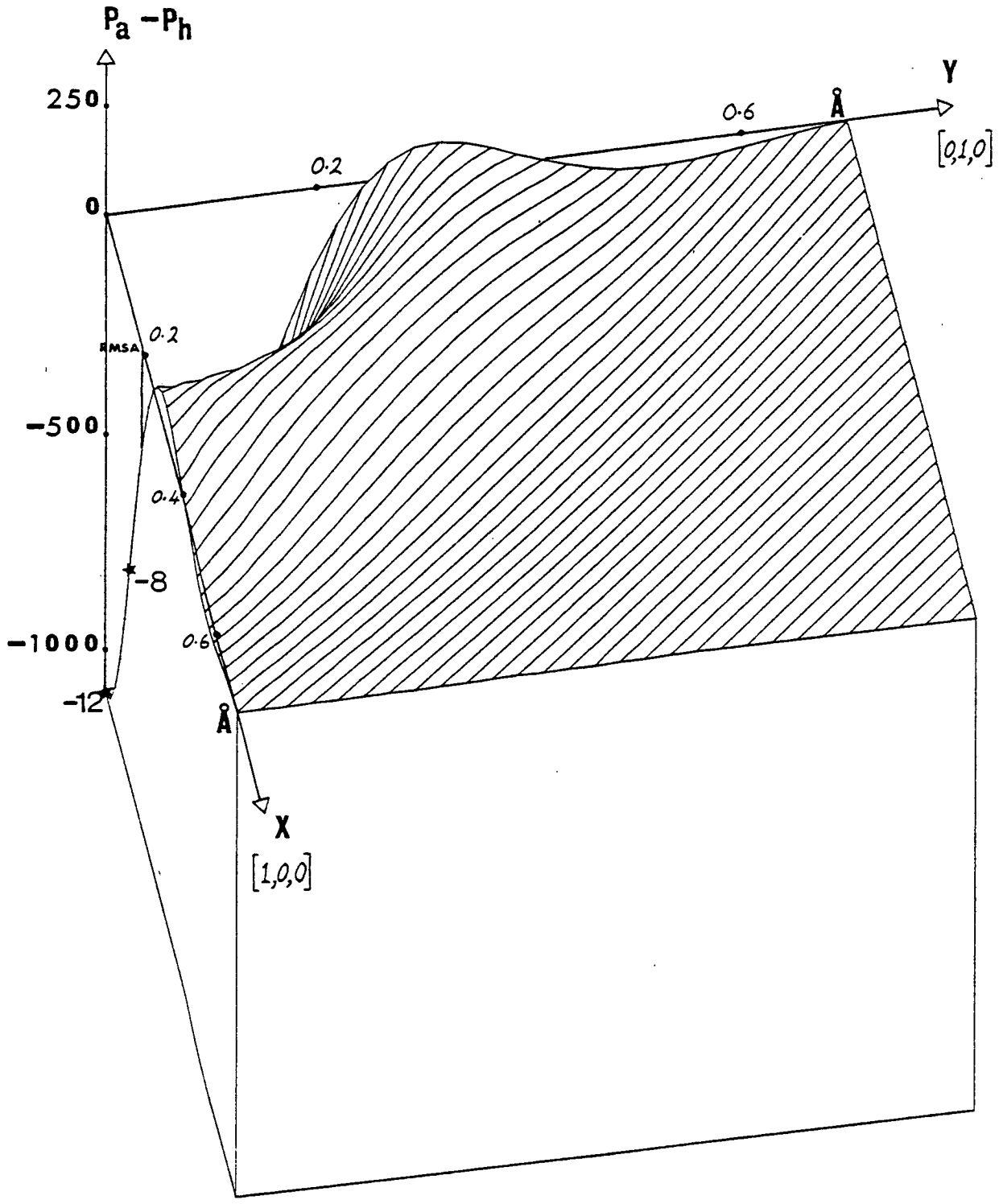


Figure 4.7.1

of the metal ions have been shown to be describable to a good approximation in terms of purely harmonic potentials (the motion of the Mn ion in $KMnF_3$ at room temperature is the only unambiguous exception found here); second, time has not permitted fully adequate testing of the anharmonic thermal formalisms so that any derived conclusions regarding motion of the X ions out of the A-X planes would be rather tentative at present; and finally, the interesting anharmonic thermal motion in these perovskites is expected to be predominantly associated with the X ions in the A-X planes.

An examination of the refined harmonic thermal parameters obtained for each of the crystals shows that in general $u(B) \approx u^{33}(X)$. The same feature can be seen in the parameters obtained by Sakata et al (1979) for cubic $CsPbCl_3$ over a range of temperatures above $T_c$. For $KMnF_3$ the agreement is no more than qualitative, the two parameters differing from each other by 13% and 18% at $T_c + 10^o$ and at room temperature respectively. However, for the other crystals, and in particular $RbCaF_3$ at both temperatures investigated, the equivalence in value is quite remarkable. This may be evidence of a 'hard' interaction along the B-X direction and could well be connected with the anomalous behaviour sometimes exhibited by the B-ion thermal parameters - especially the Ca ion in $RbCaF_3$ (compare Models III and V in both Tables 4.3.1 and 4.6.1).

As far as trends in the thermal anharmonicity in the series $CsPbCl_3 \rightarrow RbCaF_3 \rightarrow KMnF_3 \rightarrow SrTiO_3$ (a few degrees above $T_c$) are concerned, some of the results seem quite clear. In particular, the degree of anharmonicity associated with the thermal motion of the X ion decreases significantly along the series. This conclusion may be unambiguously extracted from a consideration of several features.

(i) A comparison may be made of the reductions in $\sum w\Delta^2$ associated with the addition of X-ion fourth-order F.I. parameters to the harmonic model. These reductions are $3.45 \longrightarrow 1$, $2.33 \longrightarrow 1$,

1.18⟶1, and 1.04⟶1 for the Cl, F, F and O ions respectively in the above crystal series.

(ii) An examination and comparison of the difference maps of Figures 4.2.2, 4.3.2 and 4.4.1 - the corresponding map for $SrTiO_3$ is not shown because the anharmonic parameters are so insignificant - reveals the modifications made to the harmonic p.d.f. due to addition of F.I. parameters. These modifications are largest for the Cl ion in $CsPbCl_3$, the difference between the anharmonic and harmonic densities ranging from about -10% to +16%. The corresponding values for $RbCaF_3$ and $KMnF_3$ are about +4% to +14% and 0% to +8% respectively. From comparisons with the results of the test refinements it would not be unreasonable to expect the magnitude of the *actual* difference p.d.f.'s to be greater than those derived here from the F.I. model parameters - perhaps by as much as a factor of two (compare the differences between the test p.d.f.'s of Figures 2.5.4(a) and (b) and between 2.5.5(a) and (b)). This observation would not, however, significantly affect the *relative* sizes of the anharmonicities specified by the numbers above.

A clear qualitative comparison of the amount of anharmonic structure (that is, structure of a lower symmetry to that accessible using a harmonic temperature factor) in the A-X plane of the X-ion p.d.f.'s can be obtained from Figures 4.2.2, 4.3.2 and 4.4.1. The twin peaks for $CsPbCl_3$ begin to merge for $RbCaF_3$ and to practically disappear for $KMnF_3$. The different vertical scales should be noted in any comparison, especially those associated with the maps for $RbCaF_3$ and $KMnF_3$. In the light of the unambiguous results obtained in the test refinements (see the last column of Table 2.5.1), it can be stated with reasonable certainty that these features are *at least* qualitatively authentic.

In each of these crystals just above $T_c$ it can therefore be asserted that the thermal motion of the X ion is preferentially along the directions [1,0,0] and [0,1,0] established in Figure 1.4.3, that the degree of this preference is greatest for the Cl ion in $CsPbCl_3$ and that it decreases along the series $CsPbCl_3$ ... $SrTiO_3$,

becoming negligible for $SrTiO_3$.

Several features of interest may also be extracted from an examination of the refined thermal parameters obtained for the same crystal at different temperatures.

In the case of $RbCaF_3$, the improvement in fit, both at $T_c + 10^o$ and at room temperature, arising from the addition of F-ion anharmonic terms to the harmonic thermal model, is comparable. Further, the significance associated with the addition of the parameters $b_{044+}$, $b_{220+}$ and $b_{400+}$ individually is about the same at both temperatures ($\xi \approx 3$, 0 and 6 respectively - see Tables 4.3.2 and 4.6.2). The main difference lies in the value and significance of $b_{040+}$. At $T_c + 10^o$ it can be seen from Figure 4.3.2 that the large positive refined value for this parameter results in a predominantly isotropic bulge in the difference p.d.f. around the unique axis. On the contrary at room temperature $b_{040+}$ is relatively small so that this feature is missing - see Figure 4.6.1. The amount of structure in the Rb-F plane of the F-ion p.d.f., characterised by $b_{044+}$, is small and similar at both temperatures. On cooling towards $T_c$, it therefore appears that the F-ion p.d.f. becomes slightly flatter around its mean position than the harmonic approximation to it. At room temperature there is no significant flattening.

It is usually expected that the thermal m.s.a.'s obtaining in a crystal scale approximately with absolute temperature, ie, $\langle u \rangle^{\frac{1}{2}} \sim \beta T^{\frac{1}{2}}$. However, using the $RbCaF_3$ harmonic parameters of Tables 4.3.1 and 4.6.1, it is found that the ratio $u_{293^oK}/u_{205^oK}$ is 1.35, 1.31, 1.11 and 1.30 for the Rb, Ca, $F^{11}$ and $F^{33}$ ions respectively, while the ratio of the temperatures is 1.43. Although the scaling between u's and T's is not exact for any of the ions, it is nonetheless clear that the ratio obtained for $F^{11}$ is anomalous. For this reason, an attempt was made to fit the ratios by assuming that in addition to the expected thermal scaling, a critical component, $\Delta$, with dimensions of length, exists such that $\langle u^{11} \rangle^{\frac{1}{2}}_{observed} = \langle u^{11} \rangle^{\frac{1}{2}}_{intrinsic} + \Delta$. $\Delta$ takes a finite value as $T_c$ is approached from above and is zero at sufficiently high

temperatures above $T_c$. It is further assumed that $u^{11}_{intrinsic}$ scales with temperature as the average of the scaling factors of the other three independent m.s.a.'s which do not have an additional critical component. Using the refined $RbCaF_3$ harmonic m.s.a.'s of Tables 4.3.1 and 4.6.1, a value $\Delta = 0.018$ Å is then extracted.

It is emphasised that this is an empirical result and specifically that $\Delta$ is not to be identified with $\delta$, the local order parameter obtaining in a cluster-model system. $\Delta$ merely gives an estimation of the linear extent of the $F^{11}$ motion which is incompatible with the thermal scaling law obeyed by the other m.s.a.'s.

The temperature dependence of the anharmonicity in $KMnF_3$ appears to display a markedly different form from that observed in $RbCaF_3$. Thermal anharmonicity is very significant at room temperature and is peculiar in that it constitutes the only example, of those considered here, in which the effects are not predominantly associated with the thermal motion of the cation. An examination of the functions in the temperature-factor expansion associated with $a_{40+}(Mn)$ and $b_{400+}(F)$, together with a consideration of the large positive values refined for these parameters using the room-temperature data, clearly indicates a hardening of the Mn- and F-ion potentials along the Mn-F direction. In other words, significant values of the ionic p.d.f.'s do not extend so far along this direction from the mean positions as predicted using the harmonic thermal model. The corresponding parameters obtained using the $T_c + 10^o$ data set show that this hardening of the potentials becomes insignificant as $T_c$ is approached. From Figures 4.4.1 and 4.7.1, it is clear that the F-ion p.d.f. is flatter than harmonic around the mean position at both temperatures and that there is no very significant anisotropy about the unique axis.

Carrying out an empirical analysis similar to that already described for $RbCaF_3$, a value $\Delta = 0.04$ Å is obtained. However, the corresponding ratios of the m.s.a.'s for K, Mn and $F^{33}$ are not so consistent between themselves as those obtained for $RbCaF_3$, so that less confidence can be placed in the derived

value of $\Delta$. (If, for instance, the thermal scaling of $u^{11}(F)_{intrinsic}$ is taken to be the same as that of u(K), a value $\Delta = 0.03$ Å is derived.)

The number of independent observations made by Sakata et al (1979) for $CsPbCl_3$ at a range of temperatures above $T_c$ is unfortunately not large enough to justify refinement of a full anharmonic model. As pointed out by these authors, the relatively low resolution of their data may also be insufficient for the refinement of accurate anharmonic parameters. However, a value $\Delta = 0.1$ Å can be extracted from their refined harmonic thermal parameters at $325^oK$ and $623^oK$.

As stated in Chapter 1.2 only a demonstration of the existence of two-timescale dynamics can provide unqualified support for the formation of clusters. To the extent that the techniques used in this study cannot *in principle* provide such a demonstration, it is clear that the results of this chapter cannot be interpreted completely unambiguously. Although no evidence of resolvable disorder has been found in any of the ions, the p.d.f.'s of several, in particular some of the cations, have shown significantly anharmonic features. The question therefore addressed is : what is the most likely explanation of the derived modifications to the harmonic p.d.f.'s?

Clearly there are several possibilities :

(i) The ions are not disordered in any way. The refined anharmonic parameters merely indicate a 'flattening' or 'hardening' of the potentials compared with the best-fitting harmonic distribution, such as might be predicted by an anharmonic phonon theory.

(ii) There is actual disorder, possibly arising from an underlying cluster structure, but it is unresolvable so that the equilibrium p.d.f.'s are single-peaked.

(iii) There is disorder, which in principle is resolvable, but the models used are inadequate to reproduce it.

(iv) The refined anharmonic parameters are artefacts.

The latter two proposals may be discarded as highly unlikely in the light of the results obtained in the test refinements of Chapter 2.5. Although it is true that actual resolvable disorder would probably not be reproduced anyway, even using the F.I. formalism (see Figures 2.5.6(a) - (d)), it is clear from the refinements of Chapter 2.5.4(f) that the weighted residuals obtained in the harmonic-model refinements of the real perovskite data sets (always significantly less than 0.10) are incompatible with resolvably disordered structures.

Proposals (i) and (ii) cannot be distinguished on the basis of these results alone. In principle, bearing in mind that the F.I. formalism tends to underestimate the magnitude of the anharmonic contributions considerably, and making the unlikely assumption that the idealised cluster-model structure adopted in Chapters 1.2 and 1.4 is entirely appropriate, it would be possible to extract an upper bound for $\delta$ from each of the derived X-ion p.d.f.'s. This has not been done here. Nor has any attempt been made to interpret more fully the significance of the values derived for $\Delta$; the anomalous scaling with temperature is however of interest in itself. As pointed out by Bruce et al (1979) and confirmed by the results of the test refinements of Chapter 2.5.4(b), the derived value of $\delta = 0.008$ Å obtaining in $SrTiO_3$ at a few degrees above $T_c$ (an order of magnitude less than the refined r.m.s.a.) will be entirely masked by harmonic fluctuations. The insignificant anharmonicity found here for $SrTiO_3$ is therefore at least compatible with a $\delta$ of this order.

It may be said then that although the equilibrium ionic p.d.f.'s existing in the perovskites studied here are qualitatively as reproduced in this chapter, the underlying dynamics giving rise to them cannot be unambiguously identified in an analysis of this type.

It is, however, worth giving some consideration to the form that the temperature dependence of the anharmonic thermal parameters might be *expected* to take. This was done, earlier in the section, for the harmonic m.s.a.'s in $RbCaF_3$ and $KMnF_3$, and although anomalous behaviour was found (so that values could be derived for $\Delta$), it was clear that the m.s.a.'s did scale (if only approximately) with temperature. For higher-order parameters, it is expected - at least for systems *not* complicated by the occurrence of a phase transition - that a similar, but more rapidly increasing, dependence upon temperature exists (see, for example, Willis (1969)). It would then be natural to link any obvious departure from this general trend, on approaching $T_c$, to the onset of criticality. From a consideration of the ionic displacements made in these perovskites (see Figure 1.4.2), it is reasonable to expect that the temperature dependence of the metal-ion anharmonic parameters - even close to $T_c$- will behave qualitatively according to the above ' phase-transitionless' trend. (The B-ion sublattice, in particular, remains essentially rigid on passing through $T_c$.) The cation anharmonic parameters, however, might well be expected to show anomalous enhancement as $T \rightarrow T_c$.

When the $RbCaF_3$ and $KMnF_3$ anharmonic parameters are examined in the light of these observations, some interesting features are found. In the case of $RbCaF_3$ (Model V at both temperatures), the metal-ion anharmonic parameters are very small and poorly determined; any attempt to establish a general trend in their temperature dependence would therefore be inconclusive. The F-ion anharmonic parameters, on the other hand, show what appears to be a marked dependence upon temperature, and one which indicates a significant enhancement of anharmonicity as $T_c$ is approached. In the case of $KMnF_3$, the values of the significant metal-ion anharmonic parameters (Model V at both temperatures) certainly increase, qualitatively as expected, with temperature - $a_{40+}$ (Mn) by an order of magnitude. The temperature dependence of the F-ion anharmonic parameters is less clear because these parameters are significantly biassed at room temperature by

the presence of similar parameters on the Mn ion (compare Models IV and V). In any case, whether the parameters of Model IV or V are used as the basis for comparison, it is clear that the significant F-ion anharmonic parameters do not (in general) decrease with temperature in the dramatic way found for those of the metal ions. In fact, the parameters of Model IV indicate an enhancement in anharmonicity as $T \rightarrow T_c^+$, qualitatively similar to that found for the F ion in $RbCaF_3$.

Direct evidence is therefore provided that the thermal anharmonicity of the cations in $RbCaF_3$ and $KMnF_3$ becomes anomalously enhanced as $T \rightarrow T_c^+$. No such evidence is found for the anions. Given the characteristic ionic displacement pattern at $T_c$, it is clear that the results presented here provide qualitative support for those theories of structural phase transitions in which the existence of pre-cursor non-linearity above $T_c$ plays a central role.

# CHAPTER 5 : CONCLUSIONS

## CHAPTER 5 : CONCLUSIONS

This final chapter contains a brief summary of the main conclusions reached regarding the collection and analysis of high-resolution neutron elastic-diffraction data. In a study such as this it is important, although sometimes not straight forward, to estimate the regime of validity of the conclusions reached; some may be perfectly general, others rather restricted in their applicability.

Given sufficient time, collection of the data itself was not found to present any particular problems other than those associated with ensuring long-term stability in the temperature control devices, counting chain and sample orientation. The measurement of a randomly selected subset of the total number of independent reflections always gives satisfactory results. (It was, however, found that the deletion of a *non-random* subset of the data, such as, for example, those reflections with one odd index, will not in general yield unbiassed model parameters.) Because the crystals studied here have small unit cells (linear dimensions of about 4-5 Å) and highly symmetric structures, the total number of independent reflections to be collected is relatively small. Considering that the data-collection time for some of these experiments was nearly four weeks, it is therefore clear that the collection of such high-resolution neutron data is likely to be impractical except for simple systems such as these. Nor would X-ray diffraction techniques provide a satisfactory alternative, being subject as they are to severe limitations arising from the fall-off in scattering power at high $\underline{Q}$ and the non-availability of wavelengths less than about 0.56 Å.

The proper treatments of TDS and thermal anharmonicity are two of the most immediately identifiable problems encountered in the analysis of high-resolution data.

It is already well established that the derivation of accurate harmonic thermal parameters is dependent upon reasonable corrections being made for TDS; this has certainly been confirmed. However, it has been found that higher-order F.I. parameters are almost

completely insensitive to whether corrections are made or not - irrespective of the size of the corrections themselves. On the contrary, the form of the cumulant-formalism temperature factor (expression (2.3.2)) ensures that the refined values of the anharmonic parameters *will* be (usually only slightly) biassed if a correction is not made.* The possible limitations in analysis arising from inaccurate TDS calculations are not at their most apparent in a study such as has been carried out here; the focus of attention has been on parameters which, as found consistently in the refinements, are relatively insensitive to TDS corrections. However, it is worth pointing out that, in the case of the $RbCaF_3$ room-temperature data set, the correction factors applied to the measured intensities increased from about 50% at a resolution $\sin\theta_B/\lambda = 1$ Å$^{-1}$ to about 75% at 1.5 Å$^{-1}$. Bearing in mind the disturbing results obtained from the refinements in Chapter 4.6.2(b), it is clear that the further development of high-resolution diffraction techniques should be accompanied by an investigation of the likely inaccuracies in the calculation of very large TDS contributions.

Most of the specific conclusions regarding the refinement of terms describing thermal anharmonicity have already been summarised in Chapter 2.5.7 and will not be repeated here. It is clear from these conclusions that some qualitatively authentic information about the time-averaged motion of atoms in a crystal *can* be extracted from the anharmonic thermal parameters obtained via refinements using elastic-diffraction data. That such a statement can be made has not been generally accepted in the past - see the discussion by Merisalo and Larsen (1977).

Although a definite preference has been established favouring the use of the F.I. formalism as opposed to the cumulant formalism, it is nonetheless true that the derived atomic p.d.f.'s are at best in only qualitative agreement with those actually obtaining in the real system. The extent of this agreement is also found to decrease (more markedly when cumulants are used) as the magnitude of the thermal anharmonicity increases. This is not surprising in view

---

* In the experiments, the detector apertures were always sufficiently large that anisotropy in the TDS corrections was small. If the required corrections had been *markedly* anisotropic, it is possible that the refined values of the *anharmonic* parameters might have been significantly biassed by inaccuracy in (or omission of) these

of the fact that the higher-order p.d.f.'s obtained using either formalism are essentially *perturbations* of a dominant second-order distribution (note the forms of $P_i(\underline{r})$ as given in expressions (2.3.1) and (2.4.4)).

One of the most immediately obvious inadequacies of the present analysis has been its restriction to systems of high symmetry; the anharmonic descriptions of the ionic thermal motion have consequently required a relatively small number of additional parameters. This number was often further reduced in practice by the specific nature of the anharmonicity : many cases were found in which the perovskite-ion anharmonicity was characterised just as well by two of the four independent fourth-order parameters as by the complete set. In cases such as these, constrained refinements can then be carried out and more accurate estimates obtained for those parameters known to be significant. Although the techniques of constrained refinement and significance testing may in general be expected to yield valuable information, additional problems can still be anticipated in the application of these anharmonic formalisms to the thermal analysis of atoms occupying positions of lower site symmetry. For example, the fourth-order temperature factor appropriate to the monoclinic, 2/m symmetry, contains nine independent anharmonic parameters. If the anharmonic motion of an atom occupying such a site is not predominantly characterised by any small subset of these twelve parameters, it is possible to envisage the existence of substantial refined anharmonicity without the accompanying procurement of any very significant, well determined anharmonic thermal parameters. The derivation of the corresponding atomic p.d.f. would then become unreliable.

Unfortunately, the problem which was often found to prevent convergence of refinements containing m3m symmetry F.I. parameters has not been resolved. The approximation made in the calculation of the least-squares derivatives (Chapter 2.4.2) would be expected to become less satisfactory as the size of the anharmonic parameters increases; it is therefore surprising that the problem persists

even when the anharmonic parameters are very small (Model II of Table 4.6.1) - and even more surprising that acceptable convergence is obtained with relatively very large anharmonic parameters (Model III of Table 4.2.1). It is also difficult to see how the approximation made could apparently become more reasonable when scattering lengths are refined simultaneously.* The problem is probably not then connected with this approximation. Further investigation is clearly required before the situation can be resolved. It would seem, however, that high correlation between the thermal parameters of different orders (as obtained by Kurki-Suonio et al (1979)) must be at least partly responsible for these effects - although there is no direct evidence of this from the elements of the correlation matrices. The simultaneous refinement of scattering lengths must therefore act to break this correlation.

Whether or not the possibility of including anharmonic terms in a refinement model should be investigated, is clearly rather subjective and will depend upon a consideration of the nature and accuracy of the conclusions sought. The additional time and effort required to program and refine anharmonic terms is non-negligible and must also be borne in mind. Several definite statements may be made with regard to the latter.

(i) The additional computer programming required so that F.I. anharmonic parameters may be refined in the atomic temperature factors is considerably greater than that required to include the corresponding cumulant parameters. Separate routines must in general be written for each site symmetry individually, and the functions involved in the calculation of the temperature factors and the necessary least-squares derivatives become increasingly tedious as the order of the anharmonicity increases and the site symmetry decreases.

---

* The scattering lengths used in this work are, apart from b(Ca), in good agreement with those recently tabulated by Koester (1977). Although b(Ca) differs significantly, its refined value is consistent throughout the present analysis, ie, it is insensitive to the particular thermal model and data set being examined. The value refined here is also in good agreement with that of Bacon (1975). For these reasons, the scattering lengths adopted are taken to be reliable; the possibility of significant bias in the refined thermal parameters, arising from the use of inaccurate scattering lengths, is therefore considered to be very small.

(ii) The difference in the computer running time required for anharmonic F.I. refinements and the corresponding cumulant refinements is considerable. Although difficult to generalise on the basis of the limited number of site symmetries investigated here, it would appear that the difference will be of the order 20%. The increase in running time over that required for a harmonic-model refinement is entirely dependent upon the number of anharmonic parameters to be refined; it is, however, clear that increases by factors of 2-4 will not be uncommon.

(iii) The derivation of atomic p.d.f.'s from the refined F.I. thermal parameters can be accomplished using essentially the same programming required to calculate the anharmonic temperature factors. The construction of a program to calculate the Edgeworth expansion (expression (2.3.1)) is also straightforward.

From these observations, it is clear that the relative superiority of the F.I. formalism is obtained at a price. For this reason, if only an estimate of the magnitude of the intrinsic anharmonicity is required, with no direct-space information, it may be more convenient to use the cumulant formalism - especially if the anharmonicity is small.

Input from many more refinements involving anharmonic thermal parameters will certainly be required before the full scope and potential yield of the methods described in this thesis can be identified. Experiments should preferably be confined to systems of high symmetry and in particular to those expected to display some characterisable anharmonic structure in their thermal motion - such as was tentatively proposed at the outset for the crystals studied here. Where possible,the plausibility of the results should be estimated by comparison with other experimental evidence. From the point of view of comparison with known thermal characteristics, information provided by further test refinements could again prove useful; care should be taken, however, to ensure that test data is generated in such a way that no spurious effects can bias the

refined parameter values.

Up to this point in the chapter, discussion of the cumulant and F.I. formalisms has been focused primarily on the relative merits of each. It is clear that the regime of validity of both formalisms falls considerably short of systems displaying resolvable atomic disorder. Returning now to the objectives set out in Chapter 1.1, the question then arises : can disordered models cope satisfactorily with that part of the anharmonic thermal spectrum extending from resolvably disordered structures to that part in which the anharmonic formalisms discussed in this thesis provide realistic descriptions? In other words, is the entire spectrum from harmonic to resolvably disordered structures susceptible to analysis by elastic-diffraction methods? Clearly, if the answer to this question is the affirmative, then one would expect the existence of a region of overlap in which both distinct types of model provide acceptable descriptions. From the conclusions already reached regarding the regimes of validity of the cumulant and F.I. formalisms, intrinsically disordered models would then have to cope with p.d.f.'s whose true equilibrium structure displays no evidence of resolvable peaks. Such a capacity has probably not yet been established.

Some of the potential interpretative pitfalls have been highlighted recently by Nelmes (1979). Concentrating attention on the family of hydrogen-bonded ferroelectrics isomorphous with $KH_2PO_4$, he shows that the simple (and commonly accepted) concept of proton disorder above $T_c$ is not unambiguously established by structural work to date. Specifically, he argues that refinement of a disordered model, even when its parameters yield a *resolvably* disordered p.d.f., does not in itself provide unqualified support for the actual *existence* of disorder, and that such an outcome may be a natural consequence of limitations in the generality of the refinement model. The situation described in Chapter 2.5.6, regarding the inability of the F.I. model to reproduce known disorder, is in many ways similar although it occurs in a different part of the anharmonic spectrum.

More work will have to be done, probably on test systems displaying a controlled amount of intrinsic disorder, before any general approach to the diffraction analysis of real systems like $KH_2PO_4$ can be formulated. It will be essential to compare very closely the results obtained using anharmonic (but single-site) models, such as those considered in this thesis, with results obtained using disordered models. Until this is done, the *true* time-averaged nature of such strongly anharmonic distributions will remain inaccessible to elastic-diffraction techniques.

## APPENDIX A

## EXTINCTION CORRECTION

Extinction is the phenomenon of attenuation, due to Bragg reflection, of the primary beam in its passage through the crystal. If it is severe, it can lead to a marked decrease in the observed scattered intensity. Two types are distinguishable : primary extinction, which is the result of multiply scattered beams in a perfect mosaic block, and secondary extinction, which is the result of scattering from similarly oriented mosaic blocks throughout the crystal volume.

The procedure adopted for the calculation of extinction corrections was based on the program LINEX74 (a modified version of ORFLS (Busing et al (1962)) ) which incorporates the formalism of Becker and Coppens (1974 , 1975). The range of validity of this formalism is much greater than that due to Zachariasen (1967), which becomes unreliable for corrections to intensities greater than about 25%. Considerable flexibility in the choice of extinction model is available. The various options are as follows :

(i) The extinction may be either isotropic or anisotropic. In general, five additional parameters are required in the latter case.

(ii) The extinction may be either secondary Type I, secondary Type II (Zachariasen (1967)) or general. Type I extinction refers to attenuation arising from the range of orientations of the mosaic blocks; Type II to attenuation arising from the size of the perfect blocks (see Becker and Coppens (1974 , 1975) for details). The general model contains parameters describing extinction arising from a combination of Types I and II effects; a component of the resulting correction factor can then be identified specifically with primary extinction.

(iii) The orientation of the mosaic blocks producing the Type I extinction effects can be described by a three-dimensional distribution function of either Gaussian or Lorentzian shape. The mean orientation of the blocks corresponds to the centre of the (symmetric) distribution and the relative number of blocks oriented at some slightly different angle is given by the value of the function at that point.

LINEX74 allows for a further choice between the 'Coppens-Hamilton' and 'Thornley-Nelmes' methods of the way in which the mosaic spread parameter(s) appropriate to Type I extinction is calculated (Coppens and Hamilton (1970); Thornley and Nelmes (1974)). However, the method due to Coppens and Hamilton has been shown to be incorrect in all situations (Nelmes (1979a)) and has not been considered in the present study.

If anisotropic extinction is to be refined, it is necessary to specify two unit vectors for each reflection (relative to the crystal axes when the crystal is in the Bragg reflection orientation). The first is the normal to the diffraction plane and the second is the direction of the primary beam. The corresponding mean path length through the crystal, $\bar{T}$, is also required whether the extinction is anisotropic or not. In view of the number of refinements to be carried out using each data set, it was decided to write a separate program to produce a file containing this information instead of using a routine in the main least-squares program to generate it during each refinement. The vectors are easily obtained from a consideration of the standard diffractometer settings. The $\bar{T}$'s are obtained by using a dummy linear absorption coefficient, $\mu$, in the program ABSCOR (Stewart (1972)) and calculating $\bar{T}_i = 1/\mu \ \ln(1/A_i)$ where $A_i$ is the transmission factor of the $i^{th}$ reflection output by the program. Using this information, together with the refined parameter(s) specifying the nature and magnitude of the extinction (see Becker and Coppens (1974, 1975)) the correction factors $E(\underline{Q})$ are obtained for each reflection. These are then used in the calculation of the structure amplitudes (equation (3.7.1)).

Clearly, several approximations are possible other than the one obviously made in assuming that *any* extinction can be described as truly isotropic. For instance, if the sample used is of nearly equi-dimensional shape (say a 'reasonable' cube), path-length differences will not be large. If the extinction is small, it may then be permissible to assign a 'mean' path length to each reflection, and hence eliminate the considerable computing time required for the exact $\overline{T}$ calculations using ABSCOR. Unfortunately, an alternative, more protracted method of calculating extinction corrections is often required simply to establish the validity of using an approximate method.

APPENDIX B

## THERMAL DIFFUSE SCATTERING CORRECTION

The anisotropic TDS correction employed was that of Merisalo and Kurittu (1978), using the program SXTDS1 (Kurittu and Merisalo (1977)). Their treatment assumes the second- and higher-order phonon scattering to be allowed for in the linear background subtraction and the dispersive effects in the acoustic modes to be small. The authors show that the three-dimensional numerical integration often required in such calculations can be reduced to a two-dimensional one and that further simplifications can be made if the scans are symmetric (as they always are in the cases considered here).

Although SXTDS1 is written specifically for calculations involving rectangular receiving apertures, it was clear from a number of trials that circular apertures can sometimes be accommodated within acceptable errors. For instance, the substitution of square apertures of area equal to the circular ones often used in the experiments of Chapter 4 will induce errors less than those in the counting statistics. Bearing in mind the inaccuracies often inherent in the derivation of suitable elastic constants (see for example Chapter 4.2.1), it is believed that the errors resulting from this approximation are not unacceptable.

The Bragg intensity, $I_B$, is given from the measured intensity, $I_M$, by $I_B = I_M/(1 + \alpha)$ where

$$\alpha = 2k_B T \sum_{lm} \tau_l \tau_m \sum_i^2 n_i \iint_{A_i} \frac{\left[\lambda^{-1}(\hat{q})\right]_{lm}}{q^2} \, dA_i$$

In this expression $k_B$ is the Boltzmann constant,
$T$ is the absolute temperature,
$\tau_i$ is the $i^{th}$ component of the reciprocal lattice vector,

$\underline{q}$ is the phonon wavevector,

$\hat{\underline{q}} = \underline{q}/|\underline{q}|$ ,

$\underline{\underline{\lambda}}$ is the dynamical matrix,

and $n_i$ are the normal distances from the reciprocal lattice point to the surfaces, $A_i$, over which the integration is carried out.

See Merisalo and Kurittu (1978) for definitions of the surfaces, $A_i$, and the labelling of the axes to which the vector components are referred.

## APPENDIX C

## RANDOM NUMBER GENERATION

Lists of (pseudo-) random numbers were obtained by the linear congruential method using the recurrence relation

$$Z_i = aZ_{i-1} + c \quad \text{(modulus m)}$$

(see Kobayashi (1978)) where a, c, m and $Z_0$ are the starting (random) integers. Each $Z_i$ lies in the range $0 \rightarrow m$ and can be converted to lie in any other specified range by straightforward division. Statistical tests were included in the generating program as a check on the randomness of the output.

## APPENDIX D1

The observed structure amplitudes and errors for $CsPbCl_3$ at 325°K as used in the refinement of the parameters in Table 4.2.1.

| h | k | l | $F_{obs}$ | $\sigma(F_{obs})$ | h | k | l | $F_{obs}$ | $\sigma(F_{obs})$ |
|---|---|---|---|---|---|---|---|---|---|
| 0 | 6 | 0 | 20.17 | 0.40 | 5 | 4 | 4 | 5.77 | 0.12 |
| 0 | 8 | 0 | 12.12 | 0.24 | 5 | 5 | 0 | 6.76 | 0.13 |
| 0 | 10 | 0 | 6.83 | 0.13 | 5 | 5 | 1 | 5.58 | 0.12 |
| 1 | 0 | 0 | 18.17 | 0.36 | 5 | 5 | 2 | 6.89 | 0.14 |
| 1 | 1 | 0 | 8.66 | 0.17 | 5 | 5 | 3 | 6.19 | 0.25 |
| 1 | 1 | 1 | 28.40 | 0.57 | 5 | 5 | 4 | 5.89 | 0.12 |
| 1 | 12 | 0 | 3.85 | 0.30 | 5 | 7 | 0 | 4.75 | 0.10 |
| 2 | 0 | 0 | 43.78 | 0.88 | 6 | 1 | 0 | 15.33 | 0.37 |
| 2 | 1 | 0 | 19.62 | 0.68 | 6 | 1 | 1 | 17.30 | 0.34 |
| 2 | 1 | 1 | 14.89 | 0.30 | 6 | 2 | 0 | 15.70 | 0.42 |
| 2 | 2 | 0 | 39.71 | 0.79 | 6 | 2 | 1 | 12.02 | 0.24 |
| 2 | 2 | 1 | 18.53 | 0.37 | 6 | 2 | 2 | 12.17 | 0.34 |
| 2 | 2 | 2 | 33.87 | 0.68 | 6 | 3 | 0 | 9.48 | 0.19 |
| 2 | 12 | 0 | 3.09 | 0.28 | 6 | 3 | 1 | 11.30 | 0.22 |
| 3 | 0 | 0 | 5.31 | 0.11 | 6 | 3 | 2 | 7.94 | 0.16 |
| 3 | 1 | 0 | 5.83 | 0.12 | 6 | 3 | 3 | 8.40 | 0.17 |
| 3 | 1 | 1 | 12.64 | 0.26 | 6 | 4 | 0 | 8.86 | 0.18 |
| 3 | 2 | 0 | 7.52 | 0.15 | 6 | 4 | 1 | 7.76 | 0.16 |
| 3 | 2 | 1 | 10.89 | 0.22 | 6 | 4 | 2 | 7.33 | 0.15 |
| 3 | 2 | 2 | 8.53 | 0.17 | 6 | 4 | 3 | 5.72 | 0.12 |
| 3 | 3 | 0 | 6.71 | 0.14 | 6 | 4 | 4 | 5.15 | 0.12 |
| 3 | 3 | 1 | 2.19 | 0.07 | 6 | 5 | 0 | 5.68 | 0.11 |
| 3 | 3 | 2 | 9.67 | 0.19 | 6 | 5 | 1 | 6.58 | 0.13 |
| 3 | 3 | 3 | 4.81 | 0.10 | 6 | 5 | 2 | 5.25 | 0.11 |
| 4 | 0 | 0 | 31.70 | 0.63 | 6 | 5 | 3 | 5.66 | 0.12 |
| 4 | 1 | 0 | 18.60 | 0.56 | 6 | 5 | 4 | 4.20 | 0.14 |
| 4 | 1 | 1 | 20.84 | 0.42 | 6 | 6 | 0 | 5.70 | 0.12 |
| 4 | 2 | 0 | 25.55 | 0.84 | 6 | 6 | 1 | 5.00 | 0.12 |
| 4 | 2 | 1 | 16.02 | 0.32 | 6 | 6 | 2 | 4.87 | 0.13 |
| 4 | 2 | 2 | 19.72 | 0.40 | 6 | 6 | 3 | 3.99 | 0.15 |
| 4 | 2 | 5 | 5.87 | 0.11 | 6 | 6 | 4 | 3.55 | 0.24 |
| 4 | 3 | 0 | 10.21 | 0.20 | 7 | 0 | 0 | 0.89 | 0.29 |
| 4 | 3 | 1 | 15.12 | 0.30 | 7 | 1 | 0 | 1.36 | 0.26 |
| 4 | 3 | 2 | 9.25 | 0.18 | 7 | 2 | 0 | 1.07 | 0.49 |
| 4 | 3 | 3 | 11.68 | 0.23 | 7 | 2 | 1 | 3.05 | 0.12 |
| 4 | 4 | 0 | 15.09 | 0.30 | 7 | 2 | 2 | 2.55 | 0.17 |
| 4 | 4 | 1 | 11.08 | 0.22 | 7 | 3 | 0 | 3.73 | 0.15 |
| 4 | 4 | 2 | 11.84 | 0.24 | 7 | 3 | 1 | 3.12 | 0.13 |
| 4 | 4 | 3 | 7.66 | 0.15 | 7 | 3 | 2 | 4.80 | 0.13 |
| 4 | 4 | 4 | 7.37 | 0.15 | 7 | 4 | 0 | 3.96 | 0.13 |
| 5 | 0 | 0 | 1.50 | 0.10 | 7 | 4 | 1 | 4.88 | 0.12 |
| 5 | 1 | 0 | 3.26 | 0.07 | 7 | 4 | 2 | 4.54 | 0.15 |
| 5 | 1 | 1 | 2.09 | 0.09 | 7 | 4 | 3 | 5.00 | 0.28 |
| 5 | 2 | 0 | 1.64 | 0.11 | 7 | 4 | 4 | 4.29 | 0.13 |
| 5 | 2 | 1 | 6.15 | 0.13 | 7 | 5 | 1 | 4.20 | 0.14 |
| 5 | 2 | 2 | 3.49 | 0.17 | 7 | 5 | 2 | 5.01 | 0.13 |
| 5 | 3 | 0 | 5.94 | 0.11 | 7 | 5 | 3 | 4.08 | 0.15 |
| 5 | 3 | 1 | 3.83 | 0.09 | 7 | 5 | 4 | 4.02 | 0.16 |
| 5 | 3 | 2 | 7.28 | 0.14 | 7 | 6 | 0 | 4.49 | 0.15 |
| 5 | 3 | 3 | 6.47 | 0.13 | 7 | 6 | 1 | 4.22 | 0.19 |
| 5 | 4 | 0 | 5.64 | 0.11 | 7 | 6 | 2 | 3.46 | 0.24 |
| 5 | 4 | 1 | 8.42 | 0.17 | 7 | 6 | 3 | 3.51 | 0.19 |
| 5 | 4 | 3 | 7.78 | 0.16 | | | | | |

| h | k | l | $F_{obs}$ | $\sigma(F_{obs})$ | h | k | l | $F_{obs}$ | $\sigma(F_{obs})$ |
|---|---|---|---|---|---|---|---|---|---|
| 7 | 6 | 4 | 3.16 | 0.25 | 9 | 6 | 0 | 2.58 | 0.23 |
| 7 | 7 | 0 | 3.53 | 0.21 | 9 | 6 | 2 | 2.39 | 0.33 |
| 7 | 7 | 1 | 3.26 | 0.37 | 9 | 6 | 3 | 2.55 | 0.30 |
| 7 | 7 | 2 | 3.20 | 0.20 | 9 | 7 | 0 | 2.02 | 0.52 |
| 7 | 7 | 4 | 2.54 | 0.34 | 9 | 7 | 1 | 1.64 | 0.27 |
| 8 | 1 | 0 | 10.43 | 0.21 | 9 | 7 | 2 | 2.60 | 0.37 |
| 8 | 1 | 1 | 10.46 | 0.21 | 9 | 7 | 3 | 2.37 | 0.52 |
| 8 | 2 | 0 | 9.50 | 0.19 | 9 | 8 | 0 | 1.60 | 0.50 |
| 8 | 2 | 1 | 8.31 | 0.17 | 9 | 8 | 1 | 2.29 | 0.41 |
| 8 | 2 | 2 | 7.47 | 0.15 | 9 | 8 | 3 | 1.95 | 0.44 |
| 8 | 3 | 0 | 6.86 | 0.13 | 9 | 9 | 2 | 2.18 | 0.57 |
| 8 | 3 | 1 | 6.83 | 0.13 | 9 | 9 | 3 | 1.25 | 0.35 |
| 8 | 3 | 2 | 5.60 | 0.14 | 10 | 1 | 0 | 6.48 | 0.21 |
| 8 | 3 | 3 | 5.01 | 0.10 | 10 | 1 | 1 | 6.07 | 0.14 |
| 8 | 4 | 0 | 5.54 | 0.13 | 10 | 2 | 0 | 5.77 | 0.14 |
| 8 | 4 | 1 | 5.24 | 0.13 | 10 | 2 | 1 | 4.99 | 0.11 |
| 8 | 4 | 2 | 4.63 | 0.18 | 10 | 2 | 2 | 4.54 | 0.18 |
| 8 | 4 | 3 | 3.96 | 0.16 | 10 | 3 | 0 | 4.26 | 0.19 |
| 8 | 4 | 4 | 3.29 | 0.18 | 10 | 3 | 1 | 4.10 | 0.22 |
| 8 | 5 | 0 | 4.71 | 0.16 | 10 | 3 | 2 | 3.40 | 0.26 |
| 8 | 5 | 1 | 4.48 | 0.20 | 10 | 3 | 3 | 3.13 | 0.20 |
| 8 | 5 | 2 | 3.62 | 0.22 | 10 | 4 | 0 | 3.09 | 0.22 |
| 8 | 5 | 3 | 3.13 | 0.21 | 10 | 4 | 1 | 2.56 | 0.33 |
| 8 | 5 | 4 | 3.03 | 0.26 | 10 | 4 | 2 | 2.22 | 0.32 |
| 8 | 6 | 0 | 3.41 | 0.21 | 10 | 4 | 3 | 2.24 | 0.47 |
| 8 | 6 | 1 | 3.06 | 0.31 | 10 | 4 | 4 | 1.78 | 0.50 |
| 8 | 6 | 2 | 3.35 | 0.26 | 10 | 5 | 0 | 2.98 | 0.31 |
| 8 | 6 | 3 | 2.88 | 0.28 | 10 | 5 | 1 | 2.73 | 0.41 |
| 8 | 6 | 4 | 2.80 | 0.23 | 10 | 5 | 2 | 2.74 | 0.38 |
| 8 | 7 | 0 | 2.52 | 0.31 | 10 | 5 | 3 | 1.84 | 0.34 |
| 8 | 7 | 1 | 3.66 | 0.26 | 10 | 6 | 0 | 2.04 | 0.39 |
| 8 | 7 | 2 | 2.33 | 0.29 | 10 | 6 | 3 | 1.67 | 0.57 |
| 8 | 7 | 3 | 1.72 | 0.40 | 10 | 6 | 4 | 1.50 | 0.53 |
| 8 | 8 | 1 | 2.08 | 0.43 | 10 | 7 | 1 | 1.70 | 0.70 |
| 8 | 8 | 2 | 2.25 | 0.45 | 10 | 7 | 2 | 2.20 | 0.50 |
| 9 | 0 | 0 | 1.53 | 0.57 | 10 | 7 | 3 | 1.35 | 0.55 |
| 9 | 2 | 0 | 1.64 | 0.46 | 11 | 2 | 0 | 2.00 | 0.48 |
| 9 | 2 | 1 | 2.06 | 0.44 | 11 | 4 | 1 | 1.75 | 0.30 |
| 9 | 2 | 2 | 1.95 | 0.24 | 11 | 4 | 2 | 1.91 | 0.62 |
| 9 | 3 | 0 | 2.13 | 0.26 | 11 | 5 | 1 | 1.74 | 0.49 |
| 9 | 3 | 1 | 2.50 | 0.34 | 11 | 5 | 2 | 2.05 | 0.65 |
| 9 | 3 | 2 | 3.03 | 0.26 | 11 | 6 | 2 | 1.73 | 0.65 |
| 9 | 3 | 3 | 2.29 | 0.30 | 11 | 7 | 2 | 2.01 | 0.52 |
| 9 | 4 | 0 | 2.71 | 0.31 | 11 | 8 | 2 | 1.66 | 0.69 |
| 9 | 4 | 1 | 2.68 | 0.24 | 12 | 0 | 0 | 3.71 | 0.27 |
| 9 | 4 | 2 | 3.20 | 0.28 | 12 | 2 | 1 | 3.51 | 0.35 |
| 9 | 4 | 3 | 2.82 | 0.29 | 12 | 2 | 2 | 2.10 | 0.44 |
| 9 | 4 | 4 | 3.16 | 0.36 | 12 | 3 | 1 | 1.48 | 0.56 |
| 9 | 5 | 0 | 2.90 | 0.24 | 12 | 4 | 1 | 1.85 | 0.54 |
| 9 | 5 | 1 | 2.76 | 0.23 | 12 | 5 | 0 | 1.68 | 0.67 |
| 9 | 5 | 2 | 2.70 | 0.34 | 12 | 5 | 1 | 2.48 | 0.44 |
| 9 | 5 | 3 | 2.79 | 0.32 | 12 | 6 | 2 | 2.43 | 0.45 |
| 9 | 5 | 4 | 2.50 | 0.25 | | | | | |

## APPENDIX D2

The observed structure amplitudes and errors for $RbCaF_3$ at $205^{o}K$ as used in the refinement of the parameters in Table 4.3.1.

| h | k | l | $F_{obs}$ | $\sigma(F_{obs})$ | h | k | l | $F_{obs}$ | $\sigma(F_{obs})$ |
|---|---|---|---|---|---|---|---|---|---|
| 1 | 0 | 0 | 12.62 | 0.19 | 7 | 7 | 2 | 10.57 | 0.39 |
| 1 | 1 | 1 | 74.51 | 1.12 | 7 | 7 | 4 | 10.48 | 0.35 |
| 2 | 1 | 1 | 23.92 | 0.43 | 7 | 7 | 6 | 8.97 | 0.34 |
| 2 | 2 | 0 | 101.72 | 1.53 | 8 | 1 | 0 | 15.88 | 0.24 |
| 2 | 2 | 2 | 93.31 | 1.40 | 8 | 2 | 0 | 34.71 | 0.52 |
| 3 | 1 | 1 | 58.47 | 0.88 | 8 | 2 | 1 | 15.03 | 0.23 |
| 3 | 3 | 0 | 20.41 | 0.31 | 8 | 2 | 2 | 32.03 | 0.48 |
| 3 | 3 | 1 | 45.04 | 0.68 | 8 | 3 | 0 | 13.20 | 0.20 |
| 3 | 3 | 2 | 22.27 | 0.33 | 8 | 3 | 2 | 11.49 | 0.35 |
| 3 | 3 | 3 | 33.97 | 0.51 | 8 | 3 | 3 | 22.84 | 0.34 |
| 4 | 2 | 0 | 76.82 | 1.13 | 8 | 4 | 0 | 26.58 | 0.43 |
| 4 | 2 | 1 | 14.94 | 0.22 | 8 | 4 | 1 | 12.10 | 0.34 |
| 4 | 2 | 2 | 72.24 | 1.08 | 8 | 4 | 3 | 9.01 | 0.52 |
| 4 | 3 | 3 | 26.64 | 0.40 | 8 | 4 | 4 | 19.15 | 0.29 |
| 4 | 4 | 0 | 59.76 | 0.90 | 8 | 5 | 0 | 7.57 | 0.36 |
| 4 | 4 | 1 | 14.73 | 0.22 | 8 | 5 | 2 | 7.06 | 0.39 |
| 4 | 4 | 2 | 54.86 | 0.82 | 8 | 5 | 3 | 17.18 | 0.26 |
| 4 | 4 | 4 | 42.07 | 0.63 | 8 | 6 | 0 | 18.13 | 0.27 |
| 5 | 1 | 0 | 16.36 | 0.25 | 8 | 6 | 1 | 8.86 | 0.49 |
| 5 | 1 | 1 | 36.49 | 0.55 | 8 | 6 | 3 | 6.73 | 0.23 |
| 5 | 3 | 0 | 16.48 | 0.25 | 8 | 6 | 6 | 9.15 | 0.22 |
| 5 | 3 | 1 | 26.15 | 0.39 | 8 | 7 | 5 | 9.42 | 0.14 |
| 5 | 3 | 2 | 17.77 | 0.27 | 8 | 8 | 0 | 11.52 | 0.50 |
| 5 | 3 | 3 | 18.51 | 0.28 | 8 | 8 | 1 | 5.76 | 0.39 |
| 5 | 4 | 1 | 22.06 | 0.33 | 8 | 8 | 4 | 8.75 | 0.56 |
| 5 | 5 | 0 | 15.17 | 0.43 | 8 | 8 | 8 | 4.59 | 0.61 |
| 5 | 5 | 1 | 14.38 | 0.21 | 9 | 1 | 1 | 9.31 | 0.30 |
| 5 | 5 | 4 | 16.26 | 0.26 | 9 | 2 | 2 | 1.86 | 1.80 |
| 5 | 5 | 5 | 2.69 | 1.16 | 9 | 3 | 1 | 3.64 | 0.43 |
| 6 | 1 | 0 | 16.69 | 0.68 | 9 | 4 | 3 | 8.73 | 0.30 |
| 6 | 1 | 1 | 36.64 | 0.55 | 9 | 5 | 4 | 8.99 | 0.27 |
| 6 | 2 | 1 | 16.03 | 0.29 | 9 | 6 | 1 | 9.39 | 0.14 |
| 6 | 3 | 0 | 11.28 | 0.17 | 9 | 6 | 3 | 9.00 | 0.19 |
| 6 | 3 | 2 | 11.58 | 0.44 | 9 | 6 | 5 | 8.05 | 0.34 |
| 6 | 3 | 3 | 26.77 | 0.52 | 10 | 0 | 0 | 25.04 | 0.52 |
| 6 | 4 | 0 | 41.18 | 0.62 | 10 | 1 | 0 | 14.50 | 0.24 |
| 6 | 4 | 2 | 37.42 | 0.56 | 10 | 1 | 1 | 23.40 | 0.35 |
| 6 | 5 | 5 | 16.43 | 0.25 | 10 | 2 | 1 | 13.15 | 0.20 |
| 6 | 6 | 1 | 10.79 | 0.16 | 10 | 2 | 2 | 21.02 | 0.32 |
| 6 | 6 | 4 | 19.25 | 0.29 | 10 | 3 | 0 | 11.70 | 0.32 |
| 7 | 1 | 0 | 11.25 | 0.17 | 10 | 3 | 1 | 19.67 | 0.30 |
| 7 | 1 | 1 | 19.28 | 0.29 | 10 | 3 | 2 | 10.41 | 0.36 |
| 7 | 2 | 1 | 11.85 | 0.30 | 10 | 3 | 3 | 16.67 | 0.25 |
| 7 | 3 | 1 | 13.69 | 0.20 | 10 | 4 | 0 | 17.43 | 0.34 |
| 7 | 3 | 2 | 13.11 | 0.65 | 10 | 4 | 1 | 9.98 | 0.15 |
| 7 | 4 | 3 | 14.35 | 0.21 | 10 | 4 | 3 | 8.24 | 0.12 |
| 7 | 5 | 1 | 5.72 | 0.33 | 10 | 5 | 0 | 8.06 | 0.18 |
| 7 | 5 | 2 | 11.98 | 0.31 | 10 | 5 | 2 | 7.05 | 0.29 |
| 7 | 5 | 4 | 12.49 | 0.19 | 10 | 5 | 3 | 12.09 | 0.37 |
| 7 | 6 | 3 | 13.96 | 0.21 | 10 | 5 | 5 | 9.33 | 0.17 |
| 7 | 6 | 5 | 11.67 | 0.42 | 10 | 6 | 0 | 11.60 | 0.20 |

| h | k | l | $F_{obs}$ | $\sigma(F_{obs})$ | h | k | l | $F_{obs}$ | $\sigma(F_{obs})$ |
|---|---|---|---|---|---|---|---|---|---|
| 10 | 6 | 6 | 6.65 | 0.25 | 12 | 5 | 1 | 9.35 | 0.25 |
| 10 | 7 | 2 | 4.69 | 0.34 | 12 | 5 | 2 | 6.24 | 0.14 |
| 10 | 7 | 7 | 5.13 | 0.15 | 12 | 5 | 3 | 8.17 | 0.12 |
| 10 | 8 | 0 | 7.82 | 0.38 | 12 | 6 | 0 | 7.57 | 0.18 |
| 10 | 8 | 2 | 7.33 | 0.40 | 12 | 6 | 1 | 5.13 | 0.43 |
| 10 | 8 | 4 | 5.99 | 0.34 | 12 | 6 | 4 | 5.79 | 0.15 |
| 10 | 8 | 6 | 4.35 | 0.27 | 12 | 6 | 6 | 4.46 | 0.32 |
| 10 | 9 | 1 | 5.57 | 0.38 | 12 | 7 | 1 | 6.37 | 0.10 |
| 10 | 9 | 3 | 5.58 | 0.34 | 12 | 7 | 3 | 5.61 | 0.14 |
| 10 | 10 | 0 | 5.54 | 0.40 | 14 | 0 | 0 | 10.41 | 0.42 |
| 10 | 10 | 2 | 5.46 | 0.28 | 14 | 1 | 0 | 8.70 | 0.34 |
| 11 | 6 | 3 | 5.50 | 0.14 | 14 | 1 | 1 | 10.46 | 0.38 |
| 12 | 1 | 0 | 11.60 | 0.17 | 14 | 2 | 0 | 9.50 | 0.34 |
| 12 | 1 | 1 | 15.91 | 0.24 | 14 | 2 | 1 | 8.60 | 0.13 |
| 12 | 2 | 1 | 10.62 | 0.25 | 14 | 2 | 2 | 9.25 | 0.22 |
| 12 | 3 | 0 | 9.77 | 0.15 | 14 | 3 | 0 | 7.61 | 0.39 |
| 12 | 3 | 1 | 13.07 | 0.23 | 14 | 3 | 1 | 8.23 | 0.19 |
| 12 | 3 | 2 | 8.57 | 0.46 | 14 | 3 | 2 | 7.42 | 0.21 |
| 12 | 3 | 3 | 11.18 | 0.26 | 14 | 3 | 3 | 7.42 | 0.39 |
| 12 | 4 | 1 | 8.12 | 0.34 | 14 | 4 | 0 | 7.79 | 0.12 |
| 12 | 4 | 3 | 6.69 | 0.18 | 14 | 4 | 1 | 6.24 | 0.09 |
| 12 | 5 | 0 | 6.49 | 0.10 | 14 | 4 | 2 | 7.39 | 0.18 |

## APPENDIX D3

The observed structure amplitudes and errors for $KMnF_3$ at $197^{o}K$ as used in the refinement of the parameters in Table 4.4.1.

| h | k | l | $F_{obs}$ | $\sigma(F_{obs})$ | h | k | l | $F_{obs}$ | $\sigma(F_{obs})$ |
|---|---|---|---|---|---|---|---|---|---|
| 0 | 1 | 0 | 6.85 | 0.09 | 2 | 11 | 0 | 16.26 | 0.27 |
| 0 | 2 | 0 | 46.02 | 0.46 | 2 | 11 | 1 | 12.76 | 0.19 |
| 0 | 3 | 0 | 12.48 | 0.12 | 2 | 11 | 2 | 14.32 | 0.39 |
| 0 | 4 | 0 | 35.43 | 0.35 | 2 | 13 | 0 | 12.72 | 0.23 |
| 0 | 5 | 0 | 19.40 | 0.20 | 2 | 13 | 1 | 11.08 | 0.28 |
| 0 | 6 | 0 | 22.07 | 0.22 | 2 | 13 | 2 | 11.69 | 0.26 |
| 0 | 7 | 0 | 22.59 | 0.25 | 2 | 15 | 0 | 8.54 | 0.35 |
| 0 | 8 | 0 | 13.10 | 0.16 | 2 | 15 | 0 | 8.31 | 0.33 |
| 0 | 10 | 0 | 6.40 | 0.29 | 2 | 15 | 1 | 7.74 | 0.56 |
| 0 | 11 | 0 | 17.92 | 0.22 | 2 | 15 | 2 | 8.04 | 0.39 |
| 0 | 13 | 0 | 13.60 | 0.29 | 3 | 0 | 0 | 12.65 | 0.13 |
| 0 | 13 | 11 | 3.63 | 1.68 | 3 | 0 | 0 | 12.82 | 0.13 |
| 0 | 15 | 0 | 9.57 | 0.40 | 3 | 0 | 3 | 17.76 | 0.18 |
| 1 | 0 | 0 | 6.79 | 0.07 | 3 | 1 | 0 | 18.14 | 0.18 |
| 1 | 0 | 0 | 6.82 | 0.07 | 3 | 1 | 1 | 58.25 | 0.58 |
| 1 | 1 | 0 | 18.53 | 0.19 | 3 | 1 | 3 | 52.48 | 0.53 |
| 1 | 1 | 1 | 60.56 | 0.61 | 3 | 2 | 0 | 11.72 | 0.12 |
| 1 | 1 | 3 | 57.95 | 0.58 | 3 | 2 | 2 | 10.83 | 0.11 |
| 1 | 1 | 7 | 33.93 | 0.34 | 3 | 3 | 0 | 17.28 | 0.17 |
| 1 | 2 | 0 | 6.70 | 0.08 | 3 | 3 | 0 | 17.72 | 0.18 |
| 1 | 3 | 1 | 59.51 | 0.60 | 3 | 3 | 1 | 52.29 | 0.52 |
| 1 | 5 | 0 | 17.79 | 0.18 | 3 | 4 | 0 | 9.36 | 0.09 |
| 1 | 7 | 0 | 17.74 | 0.19 | 3 | 4 | 2 | 9.57 | 0.11 |
| 1 | 7 | 1 | 34.21 | 0.34 | 3 | 4 | 3 | 9.00 | 0.15 |
| 1 | 9 | 0 | 15.52 | 0.15 | 3 | 5 | 0 | 17.00 | 0.18 |
| 1 | 9 | 1 | 23.98 | 0.34 | 3 | 6 | 2 | 6.10 | 0.18 |
| 1 | 11 | 0 | 13.83 | 0.21 | 3 | 7 | 0 | 14.58 | 0.25 |
| 1 | 11 | 1 | 17.04 | 0.22 | 3 | 7 | 3 | 24.34 | 0.27 |
| 1 | 13 | 0 | 10.54 | 0.31 | 3 | 9 | 1 | 20.95 | 0.43 |
| 1 | 13 | 1 | 12.97 | 0.25 | 3 | 9 | 2 | 11.82 | 0.16 |
| 1 | 15 | 0 | 9.28 | 0.25 | 3 | 11 | 0 | 11.62 | 0.22 |
| 1 | 15 | 1 | 9.93 | 0.41 | 3 | 11 | 1 | 14.86 | 0.34 |
| 2 | -2 | 2 | 38.66 | 0.39 | 3 | 11 | 2 | 10.29 | 0.26 |
| 2 | 0 | 0 | 44.16 | 0.44 | 3 | 11 | 3 | 12.56 | 0.28 |
| 2 | 0 | 0 | 44.87 | 0.45 | 3 | 13 | 0 | 8.97 | 0.43 |
| 2 | 0 | 0 | 44.00 | 0.44 | 3 | 13 | 2 | 9.02 | 0.26 |
| 2 | 1 | 0 | 6.61 | 0.07 | 3 | 13 | 3 | 8.92 | 0.27 |
| 2 | 1 | 2 | 6.72 | 0.08 | 3 | 15 | 1 | 7.60 | 0.64 |
| 2 | 2 | 1 | 6.12 | 0.06 | 4 | -4 | 4 | 12.13 | 0.17 |
| 2 | 2 | 2 | 37.88 | 0.38 | 4 | 0 | 0 | 34.82 | 0.35 |
| 2 | 3 | 0 | 11.55 | 0.12 | 4 | 0 | 0 | 35.34 | 0.35 |
| 2 | 3 | 2 | 11.05 | 0.13 | 4 | 0 | 4 | 22.38 | 0.25 |
| 2 | 5 | 0 | 18.26 | 0.18 | 4 | 1 | 4 | 4.99 | 0.25 |
| 2 | 5 | 1 | 15.64 | 0.16 | 4 | 2 | 4 | 19.47 | 0.20 |
| 2 | 5 | 1 | 15.21 | 0.16 | 4 | 3 | 0 | 9.08 | 0.10 |
| 2 | 6 | 0 | 19.15 | 0.25 | 4 | 3 | 2 | 9.57 | 0.24 |
| 2 | 6 | 1 | 3.61 | 0.16 | 4 | 3 | 3 | 8.91 | 0.12 |
| 2 | 6 | 2 | 16.86 | 0.25 | 4 | 3 | 4 | 8.11 | 0.12 |
| 2 | 7 | 0 | 21.76 | 0.21 | 4 | 4 | 0 | 21.93 | 0.22 |
| 2 | 7 | 1 | 15.87 | 0.20 | 4 | 4 | 1 | 5.34 | 0.18 |
| 2 | 7 | 2 | 18.86 | 0.30 | 4 | 4 | 2 | 19.32 | 0.20 |
| 2 | 8 | 0 | 9.71 | 0.20 | 4 | 4 | 3 | 8.17 | 0.19 |
| 2 | 8 | 0 | 9.36 | 0.16 | 4 | 4 | 4 | 11.94 | 0.15 |
| 2 | 8 | 2 | 8.78 | 0.20 | 4 | 5 | 1 | 9.70 | 0.21 |
| 2 | 9 | 0 | 20.36 | 0.45 | 4 | 5 | 2 | 14.12 | 0.35 |
| 2 | 9 | 2 | 17.91 | 0.49 | 4 | 6 | 0 | 12.92 | 0.23 |

| h | k | l | $F_{obs}$ | $\sigma(F_{obs})$ | h | k | l | $F_{obs}$ | $\sigma(F_{obs})$ |
|---|---|---|---|---|---|---|---|---|---|
| 4 | 6 | 2 | 10.10 | 0.28 | 6 | 2 | 0 | 13.89 | 0.19 |
| 4 | 6 | 3 | 6.97 | 0.19 | 6 | 2 | 1 | 3.76 | 0.31 |
| 4 | 7 | 0 | 17.01 | 0.30 | 6 | 2 | 2 | 16.88 | 0.17 |
| 4 | 7 | 1 | 10.22 | 0.17 | 6 | 3 | 1 | 0.78 | 1.59 |
| 4 | 7 | 2 | 16.04 | 0.29 | 6 | 3 | 2 | 5.93 | 0.29 |
| 4 | 7 | 3 | 10.26 | 0.15 | 6 | 3 | 3 | 2.36 | 1.00 |
| 4 | 7 | 4 | 12.78 | 0.29 | 6 | 3 | 6 | 6.66 | 0.25 |
| 4 | 8 | 2 | 4.51 | 0.99 | 6 | 4 | 0 | 13.22 | 0.15 |
| 4 | 9 | 1 | 10.49 | 0.26 | 6 | 4 | 2 | 9.86 | 0.21 |
| 4 | 9 | 2 | 15.75 | 0.25 | 6 | 4 | 2 | 10.10 | 0.19 |
| 4 | 9 | 3 | 9.58 | 0.20 | 6 | 4 | 3 | 7.04 | 0.23 |
| 4 | 11 | 0 | 12.92 | 0.22 | 6 | 5 | 1 | 5.39 | 0.43 |
| 4 | 11 | 1 | 9.24 | 0.24 | 6 | 5 | 4 | 8.49 | 0.38 |
| 4 | 11 | 2 | 11.75 | 0.24 | 6 | 6 | 0 | 6.37 | 0.19 |
| 4 | 11 | 3 | 7.35 | 0.24 | 6 | 6 | 3 | 6.97 | 0.59 |
| 4 | 11 | 4 | 9.94 | 0.33 | 6 | 7 | 0 | 12.30 | 0.32 |
| 4 | 13 | 0 | 9.35 | 0.38 | 6 | 7 | 1 | 6.49 | 0.33 |
| 4 | 13 | 1 | 6.72 | 0.54 | 6 | 8 | 5 | 7.39 | 0.43 |
| 4 | 13 | 4 | 7.00 | 0.35 | 6 | 9 | 0 | 10.82 | 0.23 |
| 5 | -5 | 5 | 20.36 | 0.28 | 6 | 9 | 2 | 10.82 | 0.20 |
| 5 | 0 | 0 | 19.54 | 0.20 | 6 | 9 | 4 | 9.13 | 0.25 |
| 5 | 0 | 0 | 19.35 | 0.19 | 6 | 11 | 0 | 9.14 | 0.23 |
| 5 | 0 | 5 | 14.24 | 0.27 | 6 | 11 | 1 | 5.52 | 0.52 |
| 5 | 1 | 0 | 17.85 | 0.18 | 6 | 11 | 2 | 8.54 | 0.31 |
| 5 | 1 | 0 | 17.84 | 0.18 | 6 | 11 | 4 | 7.64 | 0.31 |
| 5 | 1 | 1 | 46.52 | 0.47 | 7 | -7 | 7 | 7.49 | 0.28 |
| 5 | 1 | 5 | 31.19 | 0.31 | 7 | 0 | 0 | 22.87 | 0.23 |
| 5 | 2 | 0 | 18.17 | 0.18 | 7 | 0 | 0 | 22.45 | 0.23 |
| 5 | 2 | 1 | 15.80 | 0.16 | 7 | 0 | 0 | 22.51 | 0.23 |
| 5 | 2 | 5 | 12.68 | 0.15 | 7 | 1 | 0 | 17.24 | 0.18 |
| 5 | 3 | 0 | 16.61 | 0.17 | 7 | 1 | 0 | 17.51 | 0.18 |
| 5 | 3 | 0 | 16.86 | 0.17 | 7 | 1 | 1 | 34.24 | 0.34 |
| 5 | 4 | 1 | 9.42 | 0.17 | 7 | 1 | 7 | 15.62 | 0.28 |
| 5 | 4 | 2 | 13.96 | 0.15 | 7 | 2 | 0 | 21.49 | 0.21 |
| 5 | 4 | 5 | 8.92 | 0.18 | 7 | 2 | 1 | 15.52 | 0.16 |
| 5 | 5 | 0 | 14.54 | 0.16 | 7 | 2 | 2 | 18.95 | 0.19 |
| 5 | 5 | 1 | 31.11 | 0.31 | 7 | 2 | 7 | 8.90 | 0.39 |
| 5 | 5 | 2 | 12.94 | 0.22 | 7 | 3 | 0 | 14.54 | 0.15 |
| 5 | 5 | 4 | 8.84 | 0.15 | 7 | 3 | 3 | 24.39 | 0.24 |
| 5 | 5 | 5 | 20.19 | 0.31 | 7 | 4 | 0 | 16.96 | 0.16 |
| 5 | 6 | 1 | 4.72 | 0.29 | 7 | 4 | 1 | 10.62 | 0.26 |
| 5 | 6 | 4 | 9.32 | 0.21 | 7 | 4 | 2 | 15.33 | 0.16 |
| 5 | 7 | 2 | 10.30 | 0.24 | 7 | 4 | 3 | 10.95 | 0.21 |
| 5 | 7 | 3 | 18.30 | 0.53 | 7 | 4 | 4 | 12.93 | 0.27 |
| 5 | 8 | 0 | 6.26 | 0.29 | 7 | 5 | 2 | 10.70 | 0.44 |
| 5 | 8 | 4 | 7.56 | 0.24 | 7 | 5 | 3 | 18.95 | 0.19 |
| 5 | 9 | 0 | 10.86 | 0.18 | 7 | 6 | 0 | 12.67 | 0.36 |
| 5 | 9 | 3 | 12.77 | 0.21 | 7 | 6 | 1 | 7.21 | 0.30 |
| 5 | 11 | 0 | 8.53 | 0.32 | 7 | 6 | 3 | 4.02 | 1.00 |
| 5 | 11 | 2 | 8.46 | 0.34 | 7 | 6 | 5 | 5.05 | 0.58 |
| 5 | 11 | 3 | 10.00 | 0.34 | 7 | 7 | 1 | 15.42 | 0.37 |
| 5 | 11 | 5 | 7.24 | 0.57 | 7 | 7 | 2 | 9.43 | 0.47 |
| 5 | 13 | 1 | 7.65 | 0.33 | 7 | 7 | 4 | 5.87 | 0.49 |
| 6 | 0 | 0 | 21.91 | 0.22 | 7 | 7 | 7 | 7.89 | 0.34 |
| 6 | 0 | 0 | 22.00 | 0.22 | 7 | 8 | 0 | 7.26 | 0.29 |
| 6 | 0 | 6 | 6.55 | 0.28 | 7 | 9 | 1 | 10.65 | 0.53 |

| h | k | l | $F_{obs}$ | $\sigma(F_{obs})$ | h | k | l | $F_{obs}$ | $\sigma(F_{obs})$ |
|---|---|---|---|---|---|---|---|---|---|
| 7 | 9 | 3 | 9.26 | 0.66 | 9 | 9 | 3 | 6.21 | 0.77 |
| 7 | 10 | 0 | 5.42 | 0.66 | 9 | 9 | 4 | 4.99 | 0.66 |
| 7 | 11 | 0 | 5.53 | 0.42 | 9 | 9 | 9 | 3.99 | 1.00 |
| 8 | 0 | 0 | 13.04 | 0.15 | 10 | 0 | 0 | 6.57 | 0.59 |
| 8 | 0 | 0 | 12.69 | 0.40 | 10 | 0 | 0 | 7.05 | 0.43 |
| 8 | 2 | 0 | 9.39 | 0.24 | 10 | 2 | 0 | 5.25 | 0.57 |
| 8 | 2 | 0 | 9.55 | 0.17 | 10 | 2 | 2 | 3.94 | 0.64 |
| 8 | 2 | 2 | 8.89 | 0.20 | 10 | 3 | 0 | 2.43 | 1.37 |
| 8 | 4 | 2 | 5.17 | 0.51 | 10 | 3 | 3 | 0.98 | 3.64 |
| 8 | 4 | 2 | 6.44 | 0.64 | 10 | 4 | 2 | 2.85 | 1.09 |
| 8 | 4 | 3 | 4.64 | 0.45 | 10 | 5 | 2 | 4.64 | 0.57 |
| 8 | 5 | 0 | 6.41 | 0.57 | 10 | 5 | 4 | 5.63 | 0.58 |
| 8 | 5 | 4 | 7.29 | 0.48 | 10 | 6 | 1 | 3.29 | 1.30 |
| 8 | 6 | 3 | 6.35 | 0.60 | 10 | 6 | 4 | 0.78 | 4.48 |
| 8 | 6 | 4 | 0.19 | 22.66 | 10 | 6 | 5 | 5.82 | 0.71 |
| 8 | 6 | 5 | 7.36 | 0.55 | 10 | 6 | 6 | 3.72 | 1.00 |
| 8 | 7 | 0 | 7.89 | 0.59 | 10 | 7 | 0 | 6.35 | 0.67 |
| 8 | 7 | 1 | 2.30 | 1.57 | 10 | 7 | 4 | 5.20 | 0.55 |
| 8 | 7 | 3 | 3.02 | 0.91 | 10 | 7 | 6 | 4.38 | 0.96 |
| 8 | 7 | 6 | 6.68 | 0.79 | 10 | 7 | 7 | 0.96 | 7.56 |
| 8 | 8 | 3 | 5.54 | 0.74 | 10 | 8 | 2 | 2.89 | 1.16 |
| 8 | 8 | 4 | 3.20 | 0.93 | 10 | 8 | 5 | 5.08 | 1.08 |
| 8 | 8 | 7 | 6.58 | 1.16 | 10 | 8 | 6 | 3.38 | 1.06 |
| 8 | 9 | 0 | 7.51 | 0.32 | 10 | 9 | 1 | 2.16 | 3.75 |
| 8 | 9 | 2 | 7.46 | 0.30 | 10 | 9 | 4 | 6.06 | 1.15 |
| 9 | 0 | 0 | 21.68 | 0.25 | 10 | 9 | 8 | 1.21 | 4.39 |
| 9 | 1 | 0 | 15.94 | 0.16 | 10 | 9 | 9 | 2.58 | 2.51 |
| 9 | 1 | 0 | 15.83 | 0.42 | 10 | 10 | 4 | 3.34 | 0.82 |
| 9 | 1 | 1 | 24.21 | 0.24 | 10 | 10 | 5 | 4.17 | 1.08 |
| 9 | 1 | 1 | 24.27 | 0.24 | 10 | 10 | 6 | 1.58 | 1.56 |
| 9 | 1 | 9 | 7.49 | 0.33 | 10 | 10 | 7 | 2.34 | 4.08 |
| 9 | 2 | 0 | 19.97 | 0.25 | 11 | 0 | 0 | 17.75 | 0.32 |
| 9 | 2 | 2 | 18.38 | 0.19 | 11 | 0 | 0 | 17.65 | 0.21 |
| 9 | 3 | 1 | 20.04 | 0.24 | 11 | 1 | 0 | 13.56 | 0.43 |
| 9 | 3 | 2 | 11.77 | 0.19 | 11 | 1 | 0 | 13.35 | 0.35 |
| 9 | 4 | 1 | 10.22 | 0.33 | 11 | 1 | 1 | 17.52 | 0.37 |
| 9 | 4 | 2 | 15.23 | 0.24 | 11 | 1 | 1 | 18.27 | 0.28 |
| 9 | 4 | 3 | 10.30 | 0.16 | 11 | 2 | 0 | 16.95 | 0.23 |
| 9 | 5 | 0 | 10.75 | 0.22 | 11 | 2 | 1 | 12.52 | 0.19 |
| 9 | 5 | 2 | 9.53 | 0.27 | 11 | 2 | 2 | 15.07 | 0.32 |
| 9 | 5 | 3 | 12.99 | 0.39 | 11 | 3 | 0 | 11.70 | 0.50 |
| 9 | 6 | 0 | 11.42 | 0.20 | 11 | 3 | 1 | 14.85 | 0.38 |
| 9 | 6 | 2 | 11.02 | 0.23 | 11 | 3 | 2 | 10.32 | 0.49 |
| 9 | 6 | 3 | 6.22 | 0.70 | 11 | 3 | 3 | 12.67 | 0.48 |
| 9 | 6 | 4 | 9.42 | 0.23 | 11 | 4 | 0 | 13.27 | 0.28 |
| 9 | 6 | 5 | 3.98 | 1.00 | 11 | 4 | 1 | 9.43 | 0.26 |
| 9 | 6 | 6 | 6.76 | 0.72 | 11 | 4 | 2 | 12.31 | 0.38 |
| 9 | 7 | 1 | 11.71 | 0.45 | 11 | 4 | 3 | 8.86 | 0.49 |
| 9 | 7 | 2 | 6.57 | 0.44 | 11 | 4 | 4 | 10.06 | 0.28 |
| 9 | 7 | 3 | 9.64 | 0.53 | 11 | 5 | 0 | 9.74 | 0.58 |
| 9 | 8 | 0 | 7.49 | 0.39 | 11 | 5 | 2 | 8.74 | 0.38 |
| 9 | 8 | 2 | 8.05 | 0.78 | 11 | 5 | 3 | 10.10 | 0.42 |
| 9 | 8 | 3 | 3.23 | 1.20 | 11 | 5 | 4 | 6.07 | 0.62 |
| 9 | 8 | 6 | 7.00 | 0.64 | 11 | 5 | 5 | 7.19 | 0.44 |
| 9 | 8 | 8 | 3.54 | 2.17 | 11 | 6 | 0 | 9.67 | 0.36 |
| 9 | 9 | 1 | 7.88 | 0.57 | 11 | 6 | 1 | 7.06 | 0.73 |

| h | k | l | $F_{obs}$ | $\sigma(F_{obs})$ | h | k | l | $F_{obs}$ | $\sigma(F_{obs})$ |
|---|---|---|---|---|---|---|---|---|---|
| 11 | 6 | 2 | 8.29 | 0.34 | 13 | 5 | 2 | 6.87 | 0.95 |
| 11 | 6 | 4 | 7.13 | 0.76 | 13 | 5 | 4 | 5.37 | 1.23 |
| 11 | 7 | 0 | 7.20 | 0.76 | 13 | 6 | 0 | 6.84 | 0.76 |
| 11 | 7 | 2 | 5.92 | 0.92 | 13 | 6 | 2 | 6.15 | 0.73 |
| 11 | 7 | 4 | 4.44 | 0.69 | 13 | 7 | 0 | 3.84 | 1.58 |
| 11 | 8 | 0 | 5.80 | 0.43 | 13 | 7 | 2 | 2.27 | 3.49 |
| 11 | 8 | 2 | 4.65 | 0.31 | 13 | 7 | 3 | 2.75 | 2.02 |
| 11 | 8 | 3 | 4.33 | 1.27 | 13 | 8 | 3 | 5.81 | 1.25 |
| 11 | 8 | 4 | 5.06 | 1.07 | 13 | 8 | 5 | 3.49 | 3.19 |
| 11 | 8 | 5 | 2.52 | 1.80 | 13 | 8 | 7 | 4.47 | 1.47 |
| 11 | 9 | 6 | 4.79 | 1.48 | 13 | 9 | 1 | 4.47 | 1.41 |
| 11 | 9 | 7 | 5.37 | 1.11 | 13 | 11 | 0 | 3.68 | 2.23 |
| 11 | 9 | 9 | 3.05 | 3.64 | 14 | 0 | 0 | 2.87 | 1.88 |
| 11 | 10 | 3 | 5.15 | 1.33 | 14 | 0 | 0 | 3.22 | 1.36 |
| 11 | 10 | 8 | 2.00 | 3.38 | 14 | 3 | 1 | 0.99 | 6.83 |
| 11 | 11 | 4 | 2.70 | 2.87 | 14 | 3 | 2 | 1.41 | 2.76 |
| 12 | 0 | 0 | 1.53 | 1.57 | 14 | 4 | 2 | 1.19 | 3.56 |
| 12 | 0 | 0 | 3.99 | 1.40 | 14 | 6 | 0 | 1.15 | 2.76 |
| 12 | 1 | 0 | 3.86 | 1.05 | 14 | 6 | 1 | 2.45 | 0.79 |
| 12 | 2 | 1 | 0.54 | 5.18 | 14 | 6 | 2 | 1.90 | 1.60 |
| 12 | 3 | 0 | 1.46 | 1.64 | 14 | 6 | 6 | 2.61 | 1.79 |
| 12 | 4 | 0 | 1.41 | 2.60 | 14 | 7 | 4 | 4.39 | 0.87 |
| 12 | 4 | 4 | 1.93 | 1.55 | 14 | 8 | 1 | 4.68 | 1.19 |
| 12 | 5 | 4 | 2.90 | 1.72 | 14 | 8 | 2 | 2.85 | 1.93 |
| 12 | 6 | 2 | 0.63 | 8.80 | 14 | 8 | 5 | 2.44 | 4.05 |
| 12 | 6 | 4 | 0.89 | 3.62 | 14 | 9 | 0 | 3.63 | 1.23 |
| 12 | 6 | 5 | 1.07 | 4.44 | 14 | 9 | 2 | 3.22 | 2.08 |
| 12 | 6 | 6 | 3.06 | 1.00 | 15 | 0 | 0 | 8.61 | 0.35 |
| 12 | 7 | 2 | 2.54 | 1.10 | 15 | 0 | 0 | 8.95 | 0.68 |
| 12 | 7 | 4 | 1.73 | 2.05 | 15 | 1 | 0 | 7.91 | 0.83 |
| 12 | 7 | 7 | 3.67 | 2.09 | 15 | 1 | 0 | 9.03 | 0.44 |
| 12 | 9 | 0 | 3.01 | 2.11 | 15 | 1 | 1 | 8.21 | 0.72 |
| 12 | 9 | 3 | 2.71 | 2.86 | 15 | 1 | 1 | 9.56 | 0.44 |
| 12 | 9 | 5 | 4.17 | 2.13 | 15 | 2 | 0 | 7.94 | 0.41 |
| 12 | 9 | 7 | 0.89 | 9.94 | 15 | 2 | 1 | 7.69 | 0.94 |
| 12 | 10 | 1 | 5.10 | 1.44 | 15 | 2 | 2 | 8.44 | 0.53 |
| 12 | 10 | 3 | 6.29 | 1.13 | 15 | 3 | 0 | 7.28 | 0.88 |
| 12 | 11 | 2 | 1.10 | 4.73 | 15 | 3 | 1 | 8.53 | 0.63 |
| 12 | 11 | 5 | 1.53 | 5.44 | 15 | 3 | 2 | 6.34 | 0.85 |
| 12 | 12 | 1 | 2.21 | 2.03 | 15 | 3 | 3 | 4.49 | 1.36 |
| 13 | 0 | 0 | 13.45 | 0.29 | 15 | 4 | 0 | 6.10 | 0.78 |
| 13 | 0 | 0 | 13.03 | 0.63 | 15 | 4 | 1 | 4.69 | 1.29 |
| 13 | 1 | 0 | 9.26 | 0.70 | 15 | 4 | 2 | 5.66 | 0.72 |
| 13 | 1 | 0 | 10.81 | 0.28 | 15 | 4 | 3 | 7.53 | 0.92 |
| 13 | 1 | 1 | 12.68 | 0.22 | 15 | 4 | 4 | 7.09 | 1.10 |
| 13 | 1 | 1 | 12.35 | 0.69 | 15 | 5 | 4 | 6.09 | 1.37 |
| 13 | 2 | 0 | 12.58 | 0.56 | 15 | 6 | 1 | 4.77 | 2.02 |
| 13 | 2 | 0 | 12.14 | 0.36 | 15 | 6 | 4 | 4.97 | 1.49 |
| 13 | 2 | 1 | 10.68 | 0.29 | 15 | 7 | 4 | 4.94 | 0.91 |
| 13 | 2 | 2 | 11.65 | 0.32 | 15 | 8 | 1 | 8.49 | 1.54 |
| 13 | 3 | 0 | 8.80 | 0.35 | 16 | 5 | 0 | 2.40 | 1.99 |
| 13 | 3 | 2 | 8.70 | 0.36 | 16 | 5 | 2 | 0.96 | 4.03 |
| 13 | 3 | 3 | 9.69 | 0.52 | 17 | 0 | 0 | 3.53 | 2.18 |
| 13 | 4 | 0 | 9.72 | 0.38 | 17 | 0 | 0 | 5.90 | 1.05 |
| 13 | 4 | 1 | 8.28 | 0.65 | 17 | 1 | 0 | 4.38 | 1.31 |
| 13 | 4 | 4 | 7.63 | 0.61 | 17 | 1 | 1 | 4.26 | 2.36 |
| 13 | 5 | 1 | 8.08 | 0.50 | | | | | |

APPENDIX D4

The observed structure amplitudes and errors for $SrTiO_3$ at $112^oK$ as used in the refinement of the parameters in Table 4.5.2.

Those reflections with $h^2 + k^2 + \ell^2 < 40$ are included for completeness; they were not used in the refinements.

| h | k | l | $F_{obs}$ | $\sigma(F_{obs})$ | h | k | l | $F_{obs}$ | $\sigma(F_{obs})$ |
|---|---|---|---|---|---|---|---|---|---|
| 0 | 0 | 10 | 14.28 | 0.40 | 1 | 11 | 1 | 15.08 | 0.23 |
| 0 | 1 | 0 | 4.44 | 0.04 | 1 | 12 | 0 | 5.58 | 0.34 |
| 0 | 2 | 0 | 11.96 | 0.29 | 1 | 12 | 1 | 3.26 | 0.26 |
| 0 | 3 | 0 | 5.95 | 0.08 | 1 | 12 | 4 | 5.45 | 0.17 |
| 0 | 4 | 0 | 11.45 | 0.11 | 1 | 13 | 0 | 3.32 | 0.34 |
| 0 | 5 | 0 | 6.98 | 0.11 | 1 | 13 | 1 | 14.51 | 0.25 |
| 0 | 6 | 0 | 12.52 | 0.14 | 1 | 13 | 4 | 2.47 | 0.31 |
| 0 | 7 | 0 | 7.84 | 0.13 | 1 | 14 | 0 | 4.98 | 0.46 |
| 0 | 8 | 0 | 12.84 | 0.17 | 1 | 14 | 1 | 3.67 | 0.24 |
| 0 | 8 | 7 | 7.31 | 0.22 | 1 | 14 | 5 | 3.43 | 0.39 |
| 0 | 9 | 0 | 9.10 | 0.17 | 1 | 15 | 1 | 13.23 | 0.31 |
| 0 | 9 | 3 | 3.94 | 0.16 | 1 | 16 | 0 | 4.32 | 0.54 |
| 0 | 10 | 0 | 12.87 | 0.21 | 1 | 16 | 1 | 3.91 | 0.33 |
| 0 | 11 | 0 | 8.82 | 0.26 | 1 | 16 | 3 | 3.74 | 0.37 |
| 0 | 11 | 2 | 9.39 | 0.22 | 2 | 1 | 1 | 3.54 | 0.07 |
| 0 | 11 | 4 | 9.40 | 0.24 | 2 | 2 | 2 | 12.32 | 0.12 |
| 0 | 11 | 8 | 8.54 | 0.29 | 2 | 3 | 0 | 6.39 | 0.07 |
| 0 | 12 | 0 | 12.11 | 0.24 | 2 | 4 | 0 | 12.15 | 0.12 |
| 0 | 12 | 1 | 5.49 | 0.26 | 2 | 4 | 2 | 12.36 | 0.12 |
| 0 | 12 | 5 | 5.80 | 0.42 | 2 | 5 | 2 | 7.02 | 0.11 |
| 0 | 12 | 9 | 6.61 | 0.46 | 2 | 6 | 0 | 12.91 | 0.13 |
| 0 | 12 | 11 | 6.30 | 0.46 | 2 | 6 | 2 | 12.73 | 0.13 |
| 0 | 13 | 0 | 9.10 | 0.25 | 2 | 6 | 3 | 6.75 | 0.13 |
| 0 | 13 | 2 | 9.17 | 0.29 | 2 | 6 | 4 | 13.73 | 0.14 |
| 0 | 14 | 0 | 11.44 | 0.27 | 2 | 6 | 5 | 7.26 | 0.09 |
| 0 | 14 | 5 | 4.79 | 0.53 | 2 | 6 | 6 | 14.54 | 0.17 |
| 0 | 15 | 0 | 8.59 | 0.34 | 2 | 7 | 0 | 7.91 | 0.14 |
| 0 | 16 | 0 | 9.19 | 0.38 | 2 | 8 | 0 | 13.47 | 0.17 |
| 0 | 16 | 3 | 3.93 | 1.09 | 2 | 8 | 7 | 7.25 | 0.22 |
| 1 | 0 | 0 | 4.48 | 0.04 | 2 | 9 | 2 | 8.49 | 0.20 |
| 1 | 0 | 1 | 3.85 | 0.04 | 2 | 9 | 4 | 8.66 | 0.19 |
| 1 | 1 | 0 | 3.51 | 0.04 | 2 | 9 | 8 | 7.53 | 0.27 |
| 1 | 1 | 1 | 11.27 | 0.11 | 2 | 10 | 0 | 12.93 | 0.19 |
| 1 | 2 | 1 | 3.61 | 0.06 | 2 | 10 | 1 | 6.14 | 0.23 |
| 1 | 3 | 0 | 3.91 | 0.09 | 2 | 11 | 2 | 8.66 | 0.23 |
| 1 | 3 | 1 | 12.00 | 0.12 | 2 | 12 | 0 | 11.80 | 0.23 |
| 1 | 3 | 2 | 3.85 | 0.08 | 2 | 12 | 1 | 5.31 | 0.18 |
| 1 | 4 | 0 | 5.92 | 0.09 | 2 | 12 | 5 | 5.13 | 0.34 |
| 1 | 4 | 1 | 2.76 | 0.05 | 2 | 12 | 9 | 6.49 | 0.41 |
| 1 | 5 | 0 | 3.77 | 0.05 | 2 | 13 | 2 | 9.17 | 0.24 |
| 1 | 5 | 1 | 13.17 | 0.13 | 2 | 13 | 4 | 9.14 | 0.33 |
| 1 | 6 | 0 | 5.90 | 0.13 | 2 | 14 | 0 | 10.96 | 0.30 |
| 1 | 7 | 0 | 3.93 | 0.08 | 2 | 15 | 0 | 9.57 | 0.24 |
| 1 | 7 | 1 | 14.70 | 0.15 | 2 | 15 | 2 | 8.13 | 0.43 |
| 1 | 7 | 5 | 16.64 | 0.17 | 2 | 16 | 0 | 9.37 | 0.45 |
| 1 | 7 | 6 | 1.72 | 0.32 | 2 | 16 | 0 | 7.83 | 0.37 |
| 1 | 8 | 0 | 6.02 | 0.17 | 3 | 0 | 0 | 5.82 | 0.08 |
| 1 | 8 | 2 | 5.92 | 0.10 | 3 | 0 | 2 | 6.94 | 0.07 |
| 1 | 9 | 0 | 3.78 | 0.12 | 3 | 1 | 0 | 3.94 | 0.08 |
| 1 | 9 | 1 | 15.41 | 0.19 | 3 | 1 | 1 | 12.40 | 0.12 |
| 1 | 9 | 3 | 15.55 | 0.20 | 3 | 1 | 2 | 3.75 | 0.08 |
| 1 | 10 | 0 | 5.76 | 0.26 | 3 | 3 | 3 | 15.84 | 0.16 |
| 1 | 10 | 6 | 5.62 | 0.17 | 3 | 4 | 2 | 6.68 | 0.08 |
| 1 | 10 | 7 | 1.32 | 0.70 | 3 | 5 | 1 | 13.95 | 0.14 |
| 1 | 11 | 0 | 3.56 | 0.24 | 3 | 6 | 2 | 6.55 | 0.13 |

| h | k | l | $F_{obs}$ | $\sigma(F_{obs})$ | h | k | l | $F_{obs}$ | $\sigma(F_{obs})$ |
|---|---|---|---|---|---|---|---|---|---|
| 3 | 6 | 6 | 6.73 | 0.13 | 4 | 14 | 0 | 9.78 | 0.32 |
| 3 | 7 | 0 | 3.35 | 0.12 | 4 | 14 | 7 | 4.71 | 0.63 |
| 3 | 7 | 1 | 14.90 | 0.15 | 4 | 15 | 0 | 8.71 | 0.26 |
| 3 | 8 | 0 | 5.99 | 0.10 | 4 | 15 | 2 | 8.38 | 0.09 |
| 3 | 8 | 2 | 6.23 | 0.14 | 4 | 15 | 4 | 7.99 | 0.31 |
| 3 | 8 | 4 | 6.43 | 0.16 | 4 | 16 | 0 | 8.41 | 0.42 |
| 3 | 9 | 3 | 14.87 | 0.19 | 5 | 0 | 0 | 7.15 | 0.12 |
| 3 | 9 | 4 | 2.73 | 0.16 | 5 | 0 | 4 | 7.90 | 0.11 |
| 3 | 9 | 5 | 15.86 | 0.19 | 5 | 1 | 0 | 3.79 | 0.12 |
| 3 | 9 | 6 | 1.59 | 0.46 | 5 | 1 | 1 | 13.76 | 0.14 |
| 3 | 9 | 7 | 15.06 | 0.23 | 5 | 1 | 5 | 17.19 | 0.17 |
| 3 | 10 | 4 | 5.80 | 0.20 | 5 | 2 | 2 | 7.29 | 0.11 |
| 3 | 10 | 5 | 1.24 | 0.28 | 5 | 2 | 5 | 3.45 | 0.13 |
| 3 | 10 | 8 | 5.40 | 0.22 | 5 | 3 | 1 | 14.21 | 0.14 |
| 3 | 10 | 9 | 1.69 | 0.59 | 5 | 4 | 4 | 7.57 | 0.14 |
| 3 | 11 | 0 | 3.46 | 0.20 | 5 | 4 | 5 | 2.94 | 0.12 |
| 3 | 11 | 1 | 14.90 | 0.22 | 5 | 5 | 1 | 15.01 | 0.15 |
| 3 | 11 | 3 | 14.34 | 0.21 | 5 | 5 | 2 | 3.69 | 0.12 |
| 3 | 11 | 6 | 1.45 | 0.70 | 5 | 5 | 4 | 2.82 | 0.11 |
| 3 | 13 | 3 | 14.12 | 0.26 | 5 | 5 | 5 | 16.11 | 0.16 |
| 3 | 16 | 3 | 3.32 | 0.51 | 5 | 6 | 4 | 7.04 | 0.13 |
| 4 | 0 | 0 | 11.44 | 0.11 | 5 | 7 | 0 | 3.83 | 0.10 |
| 4 | 0 | 1 | 5.99 | 0.09 | 5 | 7 | 2 | 3.61 | 0.14 |
| 4 | 0 | 2 | 12.38 | 0.12 | 5 | 7 | 5 | 15.74 | 0.20 |
| 4 | 1 | 1 | 2.63 | 0.09 | 5 | 7 | 6 | 0.62 | 1.10 |
| 4 | 1 | 4 | 6.52 | 0.08 | 5 | 8 | 0 | 6.44 | 0.12 |
| 4 | 2 | 2 | 12.97 | 0.13 | 5 | 9 | 0 | 3.37 | 0.18 |
| 4 | 2 | 3 | 7.03 | 0.08 | 5 | 9 | 1 | 14.73 | 0.19 |
| 4 | 3 | 4 | 7.05 | 0.11 | 5 | 9 | 5 | 14.99 | 0.21 |
| 4 | 4 | 1 | 6.15 | 0.08 | 5 | 10 | 2 | 6.31 | 0.20 |
| 4 | 4 | 3 | 6.58 | 0.13 | 5 | 11 | 0 | 3.56 | 0.25 |
| 4 | 4 | 4 | 13.94 | 0.14 | 5 | 11 | 1 | 14.64 | 0.22 |
| 4 | 5 | 0 | 7.24 | 0.11 | 5 | 11 | 5 | 14.40 | 0.24 |
| 4 | 5 | 4 | 7.39 | 0.11 | 5 | 13 | 0 | 3.52 | 0.39 |
| 4 | 6 | 4 | 13.77 | 0.16 | 5 | 13 | 7 | 12.01 | 0.30 |
| 4 | 6 | 5 | 7.18 | 0.12 | 5 | 14 | 6 | 4.36 | 0.34 |
| 4 | 7 | 0 | 7.73 | 0.12 | 5 | 15 | 1 | 12.34 | 0.31 |
| 4 | 7 | 2 | 7.69 | 0.13 | 5 | 15 | 5 | 10.92 | 0.31 |
| 4 | 7 | 4 | 8.03 | 0.12 | 6 | 0 | 0 | 12.65 | 0.13 |
| 4 | 8 | 1 | 5.80 | 0.20 | 6 | 0 | 1 | 6.05 | 0.11 |
| 4 | 8 | 4 | 13.24 | 0.21 | 6 | 1 | 1 | 1.41 | 0.21 |
| 4 | 8 | 5 | 6.81 | 0.28 | 6 | 1 | 6 | 6.56 | 0.11 |
| 4 | 9 | 0 | 8.27 | 0.11 | 6 | 2 | 0 | 12.79 | 0.13 |
| 4 | 9 | 4 | 8.13 | 0.20 | 6 | 2 | 2 | 13.06 | 0.13 |
| 4 | 9 | 6 | 7.75 | 0.23 | 6 | 2 | 3 | 6.97 | 0.14 |
| 4 | 9 | 8 | 7.16 | 0.26 | 6 | 3 | 2 | 6.67 | 0.17 |
| 4 | 10 | 0 | 12.98 | 0.21 | 6 | 4 | 2 | 13.12 | 0.14 |
| 4 | 10 | 1 | 5.73 | 0.32 | 6 | 4 | 4 | 14.08 | 0.16 |
| 4 | 10 | 2 | 12.60 | 0.19 | 6 | 5 | 2 | 6.93 | 0.09 |
| 4 | 10 | 5 | 6.68 | 0.26 | 6 | 6 | 1 | 5.95 | 0.10 |
| 4 | 10 | 7 | 6.95 | 0.27 | 6 | 6 | 2 | 13.42 | 0.17 |
| 4 | 10 | 9 | 7.03 | 0.30 | 6 | 6 | 3 | 6.49 | 0.14 |
| 4 | 12 | 0 | 11.50 | 0.24 | 6 | 6 | 6 | 12.49 | 0.19 |
| 4 | 12 | 7 | 5.69 | 0.48 | 6 | 7 | 6 | 7.38 | 0.24 |
| 4 | 13 | 4 | 8.34 | 0.22 | 6 | 8 | 0 | 12.38 | 0.18 |

| h | k | l | $F_{obs}$ | $\sigma(F_{obs})$ | h | k | l | $F_{obs}$ | $\sigma(F_{obs})$ |
|---|---|---|---|---|---|---|---|---|---|
| 6 | 8 | 1 | 6.10 | 0.29 | 8 | 4 | 1 | 6.29 | 0.20 |
| 6 | 8 | 5 | 6.26 | 0.26 | 8 | 4 | 3 | 6.44 | 0.15 |
| 6 | 9 | 3 | 6.88 | 0.34 | 8 | 4 | 4 | 13.53 | 0.21 |
| 6 | 10 | 0 | 12.19 | 0.24 | 8 | 5 | 4 | 6.69 | 0.17 |
| 6 | 10 | 3 | 4.93 | 0.28 | 8 | 5 | 6 | 6.33 | 0.18 |
| 6 | 12 | 0 | 11.17 | 0.26 | 8 | 5 | 8 | 6.34 | 0.17 |
| 6 | 12 | 1 | 5.26 | 0.35 | 8 | 6 | 0 | 12.92 | 0.18 |
| 6 | 12 | 2 | 10.74 | 0.15 | 8 | 6 | 1 | 5.96 | 0.15 |
| 6 | 12 | 3 | 5.23 | 0.36 | 8 | 7 | 0 | 7.12 | 0.14 |
| 6 | 12 | 4 | 10.34 | 0.25 | 8 | 7 | 2 | 6.97 | 0.16 |
| 6 | 12 | 5 | 5.50 | 0.33 | 8 | 8 | 0 | 12.57 | 0.21 |
| 6 | 12 | 7 | 3.83 | 0.61 | 8 | 8 | 1 | 5.98 | 0.30 |
| 6 | 13 | 2 | 8.66 | 0.24 | 8 | 8 | 2 | 11.87 | 0.24 |
| 6 | 14 | 0 | 9.41 | 0.30 | 8 | 8 | 5 | 6.44 | 0.33 |
| 6 | 14 | 1 | 4.93 | 0.56 | 8 | 10 | 0 | 11.25 | 0.24 |
| 6 | 15 | 2 | 8.34 | 0.21 | 8 | 10 | 1 | 5.76 | 0.34 |
| 7 | 0 | 0 | 7.99 | 0.15 | 8 | 10 | 6 | 9.44 | 0.27 |
| 7 | 0 | 3 | 3.84 | 0.10 | 8 | 10 | 8 | 8.74 | 0.20 |
| 7 | 0 | 4 | 8.69 | 0.11 | 8 | 11 | 8 | 6.32 | 0.29 |
| 7 | 0 | 5 | 3.95 | 0.10 | 8 | 12 | 0 | 10.34 | 0.28 |
| 7 | 0 | 7 | 3.29 | 0.20 | 8 | 12 | 4 | 8.99 | 0.26 |
| 7 | 1 | 0 | 4.06 | 0.18 | 8 | 12 | 5 | 4.77 | 0.58 |
| 7 | 1 | 1 | 14.67 | 0.15 | 8 | 12 | 6 | 8.95 | 0.27 |
| 7 | 2 | 0 | 8.36 | 0.14 | 8 | 12 | 7 | 5.87 | 0.44 |
| 7 | 2 | 2 | 7.81 | 0.11 | 8 | 13 | 0 | 7.80 | 0.21 |
| 7 | 2 | 4 | 8.00 | 0.12 | 8 | 14 | 0 | 7.78 | 0.59 |
| 7 | 2 | 5 | 3.73 | 0.16 | 8 | 14 | 3 | 4.35 | 0.82 |
| 7 | 3 | 1 | 14.66 | 0.15 | 9 | 0 | 0 | 8.95 | 0.19 |
| 7 | 4 | 4 | 8.09 | 0.12 | 9 | 0 | 4 | 8.77 | 0.10 |
| 7 | 5 | 1 | 15.03 | 0.18 | 9 | 1 | 0 | 3.59 | 0.21 |
| 7 | 5 | 5 | 15.81 | 0.18 | 9 | 1 | 1 | 15.19 | 0.19 |
| 7 | 6 | 1 | 1.57 | 0.41 | 9 | 2 | 2 | 8.57 | 0.20 |
| 7 | 6 | 5 | 1.71 | 0.35 | 9 | 2 | 4 | 9.05 | 0.19 |
| 7 | 6 | 6 | 7.20 | 0.19 | 9 | 3 | 0 | 3.68 | 0.11 |
| 7 | 7 | 0 | 3.66 | 0.16 | 9 | 3 | 1 | 15.53 | 0.19 |
| 7 | 7 | 7 | 14.89 | 0.24 | 9 | 3 | 3 | 15.41 | 0.19 |
| 7 | 9 | 1 | 15.14 | 0.20 | 9 | 3 | 9 | 14.53 | 0.29 |
| 7 | 9 | 5 | 14.12 | 0.23 | 9 | 4 | 3 | 2.89 | 0.24 |
| 7 | 9 | 7 | 13.58 | 0.26 | 9 | 4 | 6 | 8.10 | 0.26 |
| 7 | 10 | 0 | 7.12 | 0.21 | 9 | 5 | 0 | 3.35 | 0.18 |
| 7 | 10 | 7 | 0.92 | 1.08 | 9 | 5 | 1 | 14.97 | 0.19 |
| 7 | 11 | 1 | 14.65 | 0.24 | 9 | 5 | 3 | 15.12 | 0.19 |
| 7 | 13 | 3 | 12.08 | 0.30 | 9 | 5 | 5 | 15.44 | 0.20 |
| 7 | 13 | 7 | 11.65 | 0.33 | 9 | 7 | 1 | 14.34 | 0.21 |
| 8 | 0 | 0 | 13.21 | 0.17 | 9 | 7 | 3 | 14.71 | 0.22 |
| 8 | 0 | 1 | 5.76 | 0.16 | 9 | 7 | 5 | 13.97 | 0.25 |
| 8 | 0 | 2 | 13.05 | 0.16 | 9 | 7 | 7 | 14.13 | 0.23 |
| 8 | 0 | 3 | 6.38 | 0.12 | 9 | 8 | 2 | 7.40 | 0.19 |
| 8 | 0 | 5 | 7.12 | 0.12 | 9 | 8 | 4 | 7.47 | 0.21 |
| 8 | 0 | 8 | 13.39 | 0.24 | 9 | 8 | 6 | 7.03 | 0.21 |
| 8 | 1 | 1 | 0.32 | 1.25 | 9 | 9 | 3 | 13.57 | 0.24 |
| 8 | 1 | 8 | 5.88 | 0.17 | 9 | 9 | 9 | 12.81 | 0.33 |
| 8 | 2 | 1 | 5.39 | 0.10 | 9 | 11 | 7 | 11.70 | 0.30 |
| 8 | 2 | 8 | 13.29 | 0.20 | 9 | 13 | 1 | 12.16 | 0.34 |
| 8 | 3 | 2 | 6.32 | 0.13 | 10 | 0 | 0 | 13.06 | 0.20 |

| h | k | l | $F_{obs}$ | $\sigma(F_{obs})$ | h | k | l | $F_{obs}$ | $\sigma(F_{obs})$ |
|---|---|---|---|---|---|---|---|---|---|
| 10 | 0 | 7 | 6.76 | 0.24 | 12 | 2 | 1 | 4.66 | 0.39 |
| 10 | 0 | 10 | 10.65 | 0.38 | 12 | 2 | 6 | 11.35 | 0.25 |
| 10 | 1 | 0 | 5.79 | 0.15 | 12 | 3 | 6 | 5.13 | 0.22 |
| 10 | 1 | 1 | 1.95 | 0.41 | 12 | 4 | 0 | 11.50 | 0.23 |
| 10 | 1 | 4 | 5.60 | 0.16 | 12 | 4 | 1 | 4.63 | 0.34 |
| 10 | 1 | 8 | 5.49 | 0.22 | 12 | 4 | 6 | 10.44 | 0.33 |
| 10 | 2 | 1 | 5.61 | 0.15 | 12 | 4 | 8 | 8.90 | 0.35 |
| 10 | 2 | 4 | 12.77 | 0.21 | 12 | 5 | 0 | 5.46 | 0.22 |
| 10 | 2 | 5 | 6.41 | 0.25 | 12 | 5 | 2 | 5.53 | 0.24 |
| 10 | 3 | 6 | 5.71 | 0.16 | 12 | 5 | 6 | 5.38 | 0.23 |
| 10 | 4 | 0 | 12.51 | 0.21 | 12 | 5 | 8 | 5.15 | 0.22 |
| 10 | 4 | 3 | 5.60 | 0.33 | 12 | 5 | 10 | 4.67 | 0.37 |
| 10 | 4 | 8 | 11.17 | 0.25 | 12 | 6 | 0 | 11.78 | 0.24 |
| 10 | 5 | 4 | 6.00 | 0.22 | 12 | 6 | 3 | 9.27 | 0.33 |
| 10 | 6 | 0 | 11.93 | 0.21 | 12 | 7 | 3 | 1.68 | 0.51 |
| 10 | 6 | 1 | 5.46 | 0.38 | 12 | 7 | 4 | 5.72 | 0.20 |
| 10 | 6 | 8 | 10.13 | 0.27 | 12 | 7 | 5 | 2.21 | 0.62 |
| 10 | 7 | 4 | 6.43 | 0.20 | 12 | 7 | 6 | 5.92 | 0.19 |
| 10 | 8 | 0 | 11.40 | 0.26 | 12 | 7 | 8 | 5.35 | 0.29 |
| 10 | 8 | 3 | 5.66 | 0.34 | 12 | 8 | 0 | 9.76 | 0.38 |
| 10 | 8 | 8 | 9.82 | 0.46 | 12 | 9 | 0 | 5.99 | 0.22 |
| 10 | 9 | 4 | 6.52 | 0.18 | 12 | 9 | 2 | 5.68 | 0.30 |
| 10 | 10 | 0 | 10.39 | 0.26 | 12 | 10 | 0 | 8.86 | 0.23 |
| 10 | 11 | 2 | 7.00 | 0.18 | 12 | 10 | 1 | 5.53 | 0.46 |
| 10 | 11 | 6 | 6.47 | 0.23 | 12 | 11 | 0 | 5.93 | 0.31 |
| 10 | 12 | 0 | 8.53 | 0.39 | 12 | 11 | 1 | 1.77 | 1.02 |
| 10 | 12 | 5 | 5.24 | 0.48 | 13 | 0 | 0 | 9.50 | 0.29 |
| 11 | 0 | 0 | 9.06 | 0.23 | 13 | 0 | 2 | 9.15 | 0.29 |
| 11 | 0 | 2 | 9.19 | 0.23 | 13 | 0 | 5 | 2.78 | 0.48 |
| 11 | 0 | 3 | 3.43 | 0.27 | 13 | 0 | 8 | 7.56 | 0.43 |
| 11 | 0 | 4 | 9.19 | 0.25 | 13 | 1 | 0 | 3.34 | 0.62 |
| 11 | 1 | 0 | 3.95 | 0.29 | 13 | 1 | 1 | 14.88 | 0.31 |
| 11 | 1 | 1 | 15.32 | 0.21 | 13 | 2 | 2 | 9.54 | 0.25 |
| 11 | 1 | 5 | 15.47 | 0.22 | 13 | 2 | 4 | 9.09 | 0.27 |
| 11 | 1 | 11 | 13.57 | 0.30 | 13 | 2 | 6 | 8.14 | 0.32 |
| 11 | 2 | 2 | 9.03 | 0.22 | 13 | 3 | 3 | 14.29 | 0.26 |
| 11 | 2 | 10 | 7.42 | 0.44 | 13 | 4 | 1 | 2.65 | 0.43 |
| 11 | 3 | 1 | 15.32 | 0.22 | 13 | 4 | 4 | 8.56 | 0.27 |
| 11 | 3 | 3 | 15.24 | 0.21 | 13 | 7 | 3 | 12.62 | 0.35 |
| 11 | 4 | 3 | 2.22 | 0.28 | 13 | 7 | 5 | 12.41 | 0.32 |
| 11 | 5 | 0 | 3.16 | 0.23 | 13 | 7 | 7 | 11.39 | 0.36 |
| 11 | 5 | 5 | 14.73 | 0.23 | 13 | 9 | 1 | 11.49 | 0.36 |
| 11 | 6 | 10 | 6.69 | 0.38 | 14 | 0 | 0 | 11.05 | 0.29 |
| 11 | 7 | 1 | 14.42 | 0.23 | 14 | 0 | 5 | 4.37 | 0.38 |
| 11 | 8 | 0 | 7.99 | 0.20 | 14 | 1 | 0 | 4.78 | 0.28 |
| 11 | 8 | 8 | 7.01 | 0.43 | 14 | 1 | 1 | 3.26 | 0.88 |
| 11 | 9 | 7 | 12.18 | 0.33 | 14 | 1 | 6 | 4.39 | 0.42 |
| 11 | 11 | 1 | 11.82 | 0.28 | 14 | 2 | 0 | 10.94 | 0.29 |
| 11 | 11 | 6 | 1.60 | 1.01 | 14 | 3 | 3 | 3.80 | 0.73 |
| 12 | 0 | 0 | 12.08 | 0.24 | 14 | 4 | 0 | 10.69 | 0.38 |
| 12 | 0 | 1 | 5.14 | 0.20 | 14 | 5 | 1 | 2.95 | 0.38 |
| 12 | 1 | 1 | 2.85 | 0.47 | 14 | 6 | 0 | 9.96 | 0.19 |
| 12 | 1 | 6 | 5.57 | 0.21 | 14 | 6 | 5 | 4.61 | 0.59 |
| 12 | 1 | 10 | 4.98 | 0.32 | 14 | 7 | 4 | 4.76 | 0.35 |
| 12 | 2 | 0 | 12.47 | 0.25 | 14 | 8 | 0 | 8.47 | 0.20 |

| h | k | l | $F_{obs}$ | $\sigma(F_{obs})$ | h | k | l | $F_{obs}$ | $\sigma(F_{obs})$ |
|---|---|---|---|---|---|---|---|---|---|
| 15 | 0 | 0 | 9.27 | 0.42 | 15 | 5 | 5 | 11.38 | 0.32 |
| 15 | 0 | 2 | 9.39 | 0.27 | 16 | 0 | 0 | 9.15 | 0.43 |
| 15 | 0 | 4 | 9.19 | 0.31 | 16 | 1 | 0 | 3.82 | 0.47 |
| 15 | 1 | 0 | 2.93 | 0.56 | 16 | 1 | 1 | 4.54 | 0.52 |
| 15 | 1 | 1 | 14.19 | 0.33 | 16 | 2 | 0 | 9.40 | 0.47 |
| 15 | 2 | 2 | 9.09 | 0.21 | 16 | 2 | 1 | 3.67 | 0.46 |
| 15 | 2 | 4 | 8.73 | 0.38 | 16 | 3 | 0 | 4.17 | 0.38 |
| 15 | 2 | 6 | 8.35 | 0.34 | 16 | 3 | 1 | 4.26 | 0.40 |
| 15 | 4 | 4 | 8.49 | 0.31 | 16 | 3 | 3 | 3.62 | 0.47 |
| 15 | 5 | 1 | 12.70 | 0.35 | 16 | 4 | 0 | 9.06 | 0.21 |

APPENDIX D5

The observed structure amplitudes and errors for $RbCaF_3$ at room temperature as used in the refinement of the parameters in Table 4.6.1.

| h | k | l | $F_{obs}$ | $\sigma(F_{obs})$ | h | k | l | $F_{obs}$ | $\sigma(F_{obs})$ |
|---|---|---|---|---|---|---|---|---|---|
| 1 | 1 | 1 | 73.35 | 1.13 | 8 | 2 | 1 | 15.24 | 0.23 |
| 2 | 1 | 0 | 14.93 | 0.22 | 8 | 2 | 2 | 26.39 | 0.39 |
| 2 | 1 | 1 | 29.80 | 0.45 | 8 | 3 | 0 | 12.55 | 0.23 |
| 2 | 2 | 0 | 104.80 | 1.57 | 8 | 3 | 2 | 11.39 | 0.19 |
| 2 | 2 | 1 | 15.54 | 0.24 | 8 | 3 | 3 | 17.38 | 0.26 |
| 3 | 1 | 1 | 58.32 | 0.86 | 8 | 4 | 0 | 21.32 | 0.32 |
| 3 | 3 | 1 | 42.93 | 0.65 | 8 | 4 | 1 | 11.33 | 0.28 |
| 3 | 3 | 2 | 20.72 | 0.31 | 8 | 4 | 4 | 14.13 | 0.50 |
| 3 | 3 | 3 | 30.65 | 0.46 | 8 | 6 | 0 | 13.67 | 0.21 |
| 4 | 2 | 1 | 16.62 | 0.25 | 8 | 6 | 1 | 8.06 | 0.12 |
| 4 | 2 | 2 | 69.56 | 1.04 | 8 | 6 | 6 | 7.30 | 1.45 |
| 4 | 3 | 0 | 9.91 | 0.15 | 8 | 8 | 0 | 8.96 | 0.17 |
| 4 | 3 | 3 | 24.24 | 0.36 | 8 | 8 | 3 | 4.41 | 0.54 |
| 4 | 4 | 0 | 56.29 | 0.84 | 8 | 8 | 8 | 3.24 | 0.31 |
| 4 | 4 | 1 | 15.54 | 0.24 | 9 | 4 | 3 | 6.22 | 0.57 |
| 4 | 4 | 2 | 50.88 | 0.76 | 10 | 1 | 0 | 13.68 | 0.21 |
| 4 | 4 | 3 | 10.69 | 0.17 | 10 | 1 | 1 | 18.61 | 0.29 |
| 5 | 1 | 1 | 33.69 | 0.51 | 10 | 2 | 1 | 12.04 | 0.18 |
| 5 | 3 | 0 | 13.98 | 0.21 | 10 | 2 | 2 | 15.97 | 0.24 |
| 5 | 3 | 1 | 23.23 | 0.35 | 10 | 4 | 1 | 9.09 | 0.23 |
| 5 | 3 | 2 | 15.36 | 0.54 | 10 | 5 | 0 | 7.44 | 0.11 |
| 5 | 4 | 1 | 19.70 | 0.30 | 10 | 5 | 3 | 8.90 | 0.37 |
| 5 | 4 | 3 | 17.00 | 0.26 | 10 | 6 | 6 | 5.50 | 1.29 |
| 5 | 5 | 1 | 10.07 | 0.15 | 10 | 7 | 2 | 4.43 | 0.20 |
| 5 | 5 | 3 | 5.26 | 0.19 | 10 | 7 | 7 | 3.11 | 0.47 |
| 5 | 5 | 4 | 13.58 | 0.21 | 10 | 8 | 0 | 5.32 | 0.24 |
| 6 | 1 | 0 | 18.55 | 0.28 | 10 | 8 | 4 | 3.95 | 0.27 |
| 6 | 3 | 0 | 12.65 | 0.19 | 10 | 8 | 6 | 3.44 | 0.55 |
| 6 | 3 | 3 | 23.02 | 0.35 | 10 | 9 | 3 | 3.42 | 0.15 |
| 6 | 4 | 0 | 35.39 | 0.53 | 10 | 10 | 0 | 3.31 | 0.21 |
| 6 | 4 | 1 | 13.56 | 0.21 | 12 | 1 | 1 | 11.55 | 0.18 |
| 6 | 4 | 2 | 31.79 | 0.48 | 12 | 2 | 1 | 8.89 | 0.13 |
| 6 | 4 | 3 | 10.16 | 0.15 | 12 | 3 | 1 | 9.12 | 0.14 |
| 6 | 5 | 1 | 18.62 | 0.28 | 12 | 3 | 3 | 7.65 | 0.30 |
| 6 | 6 | 1 | 10.14 | 0.15 | 12 | 4 | 1 | 6.57 | 0.19 |
| 6 | 6 | 4 | 15.39 | 0.23 | 12 | 5 | 2 | 4.96 | 0.20 |
| 7 | 1 | 1 | 15.17 | 0.22 | 12 | 5 | 3 | 5.59 | 0.29 |
| 7 | 2 | 1 | 9.18 | 0.14 | 12 | 6 | 0 | 4.99 | 0.09 |
| 7 | 3 | 1 | 9.31 | 0.23 | 12 | 6 | 6 | 2.59 | 0.67 |
| 7 | 3 | 2 | 9.33 | 0.28 | 12 | 7 | 1 | 3.63 | 0.33 |
| 7 | 3 | 3 | 4.72 | 0.34 | 12 | 7 | 3 | 3.38 | 0.17 |
| 7 | 4 | 1 | 11.13 | 0.28 | 12 | 8 | 2 | 1.67 | 1.03 |
| 7 | 4 | 3 | 10.79 | 0.27 | 14 | 1 | 0 | 6.63 | 0.16 |
| 7 | 5 | 1 | 2.46 | 0.19 | 14 | 2 | 2 | 5.87 | 0.13 |
| 7 | 5 | 4 | 9.53 | 0.16 | 14 | 3 | 0 | 5.39 | 0.14 |
| 7 | 6 | 5 | 8.55 | 0.24 | 14 | 3 | 2 | 4.26 | 0.38 |
| 7 | 7 | 2 | 7.96 | 0.39 | 14 | 3 | 3 | 4.33 | 0.13 |
| 7 | 7 | 4 | 6.88 | 0.38 | 14 | 4 | 0 | 4.31 | 0.18 |
| 8 | 1 | 0 | 16.79 | 0.25 | 14 | 4 | 2 | 4.14 | 0.15 |

APPENDIX D6

The observed structure amplitudes and errors for $KMnF_3$ at room temperature as used in the refinement of the parameters in Table 4.7.1.

| h | k | l | $F_{obs}$ | $\sigma(F_{obs})$ | h | k | l | $F_{obs}$ | $\sigma(F_{obs})$ |
|---|---|---|---|---|---|---|---|---|---|
| 0 | 1 | 0 | 29.95 | 0.30 | 3 | 2 | 3 | 62.35 | 0.63 |
| 0 | 2 | 0 | 153.30 | 1.53 | 3 | 3 | 0 | 73.79 | 0.74 |
| 0 | 3 | 0 | 54.07 | 0.54 | 3 | 3 | 2 | 62.75 | 0.63 |
| 0 | 4 | 0 | 131.75 | 1.32 | 3 | 3 | 3 | 163.04 | 1.64 |
| 0 | 5 | 0 | 76.78 | 0.76 | 3 | 4 | 0 | 34.60 | 0.44 |
| 0 | 6 | 0 | 79.33 | 0.79 | 3 | 4 | 1 | 33.15 | 0.43 |
| 0 | 8 | 0 | 35.45 | 0.81 | 3 | 4 | 2 | 33.85 | 0.50 |
| 1 | -1 | 1 | 191.29 | 1.91 | 3 | 4 | 3 | 36.24 | 0.50 |
| 1 | 0 | 0 | 30.12 | 0.30 | 3 | 5 | 0 | 65.36 | 0.66 |
| 1 | 0 | 1 | 73.00 | 0.73 | 3 | 5 | 1 | 142.01 | 1.42 |
| 1 | 1 | 0 | 74.86 | 0.75 | 3 | 5 | 2 | 57.21 | 0.57 |
| 1 | 1 | 1 | 190.83 | 1.91 | 3 | 6 | 0 | 20.07 | 0.73 |
| 1 | 2 | 0 | 26.11 | 0.26 | 3 | 6 | 1 | 8.82 | 1.61 |
| 1 | 2 | 1 | 61.93 | 0.62 | 3 | 6 | 2 | 19.97 | 1.14 |
| 1 | 3 | 0 | 76.62 | 0.77 | 3 | 6 | 3 | 13.95 | 2.03 |
| 1 | 4 | 0 | 17.53 | 0.38 | 3 | 7 | 2 | 46.26 | 0.77 |
| 1 | 4 | 1 | 28.14 | 0.34 | 3 | 8 | 0 | 6.16 | 3.92 |
| 1 | 5 | 0 | 76.16 | 0.76 | 3 | 8 | 2 | 11.06 | 2.39 |
| 1 | 5 | 1 | 169.20 | 1.69 | 4 | 0 | 0 | 133.23 | 1.34 |
| 1 | 6 | 0 | 6.89 | 1.33 | 4 | 0 | 1 | 17.06 | 0.39 |
| 1 | 8 | 1 | 11.21 | 2.08 | 4 | 0 | 2 | 117.33 | 1.17 |
| 2 | -2 | 2 | 143.36 | 1.44 | 4 | 0 | 3 | 34.69 | 0.41 |
| 2 | 0 | 0 | 153.92 | 1.54 | 4 | 0 | 4 | 78.48 | 0.78 |
| 2 | 0 | 1 | 25.87 | 0.26 | 4 | 1 | 0 | 17.33 | 0.37 |
| 2 | 0 | 2 | 148.87 | 1.49 | 4 | 1 | 1 | 27.84 | 0.37 |
| 2 | 1 | 0 | 25.94 | 0.26 | 4 | 1 | 4 | 16.92 | 0.91 |
| 2 | 1 | 1 | 61.40 | 0.61 | 4 | 2 | 0 | 117.36 | 1.17 |
| 2 | 1 | 2 | 23.50 | 0.28 | 4 | 2 | 1 | 17.50 | 0.47 |
| 2 | 2 | 0 | 154.39 | 1.55 | 4 | 2 | 2 | 104.56 | 1.04 |
| 2 | 2 | 1 | 23.49 | 0.26 | 4 | 2 | 4 | 67.74 | 0.68 |
| 2 | 2 | 2 | 141.73 | 1.42 | 4 | 3 | 0 | 34.92 | 0.41 |
| 2 | 3 | 0 | 48.26 | 0.48 | 4 | 3 | 1 | 33.00 | 0.41 |
| 2 | 3 | 1 | 63.71 | 0.64 | 4 | 3 | 2 | 34.59 | 0.48 |
| 2 | 3 | 2 | 44.21 | 0.44 | 4 | 3 | 3 | 36.05 | 0.54 |
| 2 | 4 | 0 | 117.07 | 1.17 | 4 | 3 | 4 | 28.63 | 0.57 |
| 2 | 4 | 1 | 16.42 | 0.55 | 4 | 4 | 0 | 80.21 | 0.80 |
| 2 | 4 | 2 | 103.65 | 1.03 | 4 | 4 | 0 | 79.12 | 0.79 |
| 2 | 5 | 0 | 69.74 | 0.69 | 4 | 4 | 0 | 79.01 | 0.79 |
| 2 | 5 | 1 | 63.96 | 0.64 | 4 | 4 | 0 | 78.95 | 0.79 |
| 2 | 5 | 2 | 63.82 | 0.64 | 4 | 4 | 0 | 77.86 | 0.78 |
| 2 | 6 | 0 | 65.98 | 0.66 | 4 | 4 | 0 | 78.88 | 0.79 |
| 2 | 6 | 1 | 8.26 | 1.98 | 4 | 4 | 0 | 79.37 | 0.79 |
| 2 | 8 | 1 | 2.46 | 12.55 | 4 | 4 | 0 | 78.84 | 0.79 |
| 2 | 8 | 2 | 20.84 | 1.81 | 4 | 4 | 0 | 78.35 | 0.78 |
| 3 | -3 | 3 | 160.57 | 1.61 | 4 | 4 | 0 | 79.51 | 0.79 |
| 3 | 0 | 0 | 53.73 | 0.54 | 4 | 4 | 0 | 79.00 | 0.79 |
| 3 | 0 | 1 | 76.84 | 0.77 | 4 | 4 | 0 | 77.35 | 0.77 |
| 3 | 0 | 2 | 46.97 | 0.47 | 4 | 4 | 1 | 16.90 | 0.67 |
| 3 | 0 | 3 | 73.74 | 0.74 | 4 | 4 | 2 | 66.40 | 0.67 |
| 3 | 1 | 0 | 77.05 | 0.77 | 4 | 4 | 3 | 27.39 | 0.63 |
| 3 | 2 | 0 | 47.85 | 0.48 | 4 | 5 | 0 | 49.79 | 0.59 |
| 3 | 2 | 1 | 64.48 | 0.65 | 4 | 5 | 1 | 38.40 | 0.59 |
| 3 | 2 | 2 | 44.62 | 0.45 | 4 | 5 | 2 | 47.41 | 0.60 |

| h | k | l | $F_{obs}$ | $\sigma(F_{obs})$ | h | k | l | $F_{obs}$ | $\sigma(F_{obs})$ |
|---|---|---|---|---|---|---|---|---|---|
| 4 | 5 | 3 | 36.25 | 0.69 | 6 | 0 | 4 | 34.33 | 0.71 |
| 4 | 5 | 4 | 36.45 | 0.65 | 6 | 0 | 6 | 10.47 | 2.53 |
| 4 | 6 | 0 | 35.58 | 0.71 | 6 | 1 | 0 | 8.23 | 1.31 |
| 4 | 6 | 1 | 16.20 | 1.90 | 6 | 1 | 6 | 12.37 | 1.56 |
| 4 | 6 | 2 | 27.52 | 1.43 | 6 | 2 | 0 | 63.91 | 0.64 |
| 4 | 6 | 3 | 20.28 | 1.11 | 6 | 2 | 1 | 8.32 | 1.67 |
| 4 | 6 | 4 | 15.14 | 1.45 | 6 | 2 | 6 | 6.09 | 3.08 |
| 4 | 7 | 0 | 47.84 | 0.75 | 6 | 3 | 0 | 18.11 | 1.01 |
| 4 | 7 | 1 | 35.21 | 0.79 | 6 | 3 | 1 | 7.05 | 2.88 |
| 4 | 7 | 3 | 31.64 | 0.86 | 6 | 3 | 2 | 19.81 | 0.78 |
| 4 | 8 | 0 | 11.72 | 4.31 | 6 | 3 | 3 | 12.70 | 1.45 |
| 4 | 8 | 1 | 1.47 | 25.88 | 6 | 3 | 6 | 17.31 | 1.97 |
| 4 | 8 | 2 | 1.50 | 23.20 | 6 | 4 | 0 | 34.94 | 0.78 |
| 5 | 0 | 0 | 76.09 | 0.76 | 6 | 4 | 1 | 13.97 | 1.30 |
| 5 | 0 | 1 | 74.49 | 0.74 | 6 | 4 | 2 | 28.83 | 0.72 |
| 5 | 0 | 2 | 68.75 | 0.68 | 6 | 4 | 3 | 21.28 | 0.97 |
| 5 | 0 | 3 | 66.18 | 0.66 | 6 | 4 | 4 | 17.70 | 1.66 |
| 5 | 0 | 4 | 50.40 | 0.58 | 6 | 5 | 0 | 28.36 | 0.75 |
| 5 | 0 | 5 | 50.98 | 0.66 | 6 | 5 | 2 | 27.43 | 1.19 |
| 5 | 1 | 0 | 75.42 | 0.75 | 6 | 5 | 3 | 15.99 | 1.65 |
| 5 | 1 | 1 | 164.18 | 1.65 | 6 | 5 | 5 | 15.32 | 1.77 |
| 5 | 1 | 5 | 96.62 | 0.97 | 6 | 6 | 0 | 8.95 | 2.13 |
| 5 | 2 | 0 | 68.79 | 0.68 | 6 | 6 | 1 | 14.08 | 1.92 |
| 5 | 2 | 1 | 63.68 | 0.63 | 6 | 6 | 2 | 10.32 | 2.75 |
| 5 | 2 | 2 | 63.04 | 0.63 | 6 | 6 | 3 | 16.57 | 1.85 |
| 5 | 2 | 5 | 46.00 | 0.64 | 6 | 7 | 1 | 15.49 | 1.79 |
| 5 | 3 | 0 | 65.12 | 0.65 | 7 | 0 | 1 | 58.99 | 0.59 |
| 5 | 3 | 1 | 140.07 | 1.40 | 7 | 0 | 2 | 65.64 | 0.66 |
| 5 | 3 | 2 | 56.32 | 0.56 | 7 | 0 | 3 | 49.57 | 0.85 |
| 5 | 3 | 5 | 78.15 | 0.78 | 7 | 0 | 5 | 33.89 | 0.95 |
| 5 | 4 | 0 | 49.62 | 0.54 | 7 | 1 | 0 | 60.09 | 0.65 |
| 5 | 4 | 1 | 37.21 | 0.60 | 7 | 3 | 2 | 43.29 | 0.73 |
| 5 | 4 | 2 | 45.99 | 0.65 | 7 | 4 | 0 | 45.52 | 0.86 |
| 5 | 4 | 3 | 35.17 | 0.32 | 7 | 4 | 1 | 32.62 | 0.97 |
| 5 | 4 | 4 | 36.85 | 0.77 | 7 | 4 | 3 | 28.72 | 0.95 |
| 5 | 4 | 5 | 32.22 | 0.93 | 7 | 5 | 0 | 33.11 | 0.91 |
| 5 | 5 | 0 | 56.03 | 0.68 | 7 | 5 | 2 | 28.78 | 1.21 |
| 5 | 5 | 1 | 95.19 | 0.95 | 7 | 6 | 1 | 18.39 | 1.37 |
| 5 | 5 | 2 | 43.63 | 0.89 | 8 | 0 | 0 | 30.81 | 0.87 |
| 5 | 5 | 3 | 78.41 | 0.79 | 8 | 0 | 2 | 24.25 | 1.19 |
| 5 | 5 | 4 | 30.09 | 0.99 | 8 | 0 | 3 | 7.73 | 3.58 |
| 5 | 6 | 0 | 27.53 | 0.93 | 8 | 0 | 4 | 8.33 | 4.38 |
| 5 | 6 | 2 | 25.56 | 0.91 | 8 | 1 | 0 | 7.74 | 2.80 |
| 5 | 6 | 3 | 16.53 | 1.23 | 8 | 1 | 1 | 9.24 | 1.41 |
| 5 | 6 | 5 | 16.52 | 1.55 | 8 | 2 | 0 | 24.50 | 1.17 |
| 5 | 7 | 0 | 34.59 | 1.19 | 8 | 2 | 1 | 7.48 | 3.44 |
| 5 | 7 | 2 | 33.70 | 1.13 | 8 | 2 | 2 | 15.92 | 1.84 |
| 6 | 0 | 0 | 76.74 | 0.77 | 8 | 3 | 0 | 7.67 | 3.40 |
| 6 | 0 | 1 | 7.93 | 0.89 | 8 | 3 | 2 | 4.90 | 3.40 |
| 6 | 0 | 2 | 62.56 | 0.63 | 8 | 4 | 0 | 10.85 | 1.48 |
| 6 | 0 | 3 | 18.04 | 1.02 | 8 | 4 | 1 | 12.04 | 1.80 |
| 6 | 0 | 3 | 20.17 | 1.44 | 8 | 4 | 2 | 9.95 | 3.11 |

REFERENCES


Aleksandrov, K S, Reshchikova, L M and Beznosikov, B V, (1966), Phys Stat Solidi 18, K17.

Almairac, R, Rousseau, M, Gesland, J Y, Nouet, J and Hennion, B, (1977), J Phys, Paris 38, 1429.

Anderson, P W, (1960) in 'Fizika dielektrkov' ed G I Shanki (Moscow : Acad Sci USSR).

Arndt, U W and Willis, B T M, (1966), 'Single Crystal Diffractometry' (Cambridge : University Press).

Bacon, G E, (1974) in 'Int Tables for X-Ray Crystallography', vol IV, eds J A Ibers and W C Hamilton (Birmingham : Kynoch).

Bacon, G E, (1975), 'Neutron Diffraction' (Oxford : University Press).

Barton, D E and Dennis, K E, (1952), Biometrika 39, 425.

Becker, P J and Coppens, P, (1974), Acta Cryst A30, 129, 148.

Becker, P J and Coppens, P, (1975), Acta Cryst A31, 417.

Bell, R O and Rupprecht, G, (1963), Phys Rev 129, 90.

Bruce, A D, (1978) in 'Solitons and Condensed Matter Physics', eds A R Bishop and T Schneider (Berlin, Heidelberg : Springer-Verlag).

Bruce, A D and Cowley, R A, (1973), J Phys C6, 2422.

Bruce, A D and Schneider, T, (1977), Phys Rev B16, 3991.

Bruce, A D and Cowley, R A, (1979), Adv Phys in press.

Bruce, A D, Müller, K A and Berlinger, W, (1979), Phys Rev Lett 42, 185.

Bruce, A D, Taylor, W and Murray, A F, (1979a), submitted to J Phys C.

Bulou, A, Ridou, C, Rousseau, M, Nouet, J and Hewat, A W, (1979), to be published.

Busing, W R, Martin, K O and Levy, H A, (1962), Report No ORNL-TM-305, Oak Ridge Nat Lab, Oak Ridge, Tennessee.

Buzaré, J Y, Rousseau, J J and Fayet, J C, (1977), J Phys, Paris 38, L445.

Chambers, J M, (1967), Biometrika 54, 367.

Cochran, W, (1960), Adv Phys 9, 387.

Coppens, P and Hamilton, W C, (1970), Acta Cryst A26, 71.

Courtens, E, (1972), Phys Rev Lett 29, 1380.

Cowley, R A, Axe, J D and Iizumi, M, (1976), Phys Rev Lett 36, 806.

Cruickshank, D W J, Pilling, D E, Bujosa, A, Lovell, F M and Truter, M R, (1961) in 'Computing Methods in the Phase Problem in X-ray Crystal Analysis', eds R Pepinsky, J M Roberts and J C Speakman (Oxford : Pergamon).

Edgeworth, F Y, (1905), Trans Camb Phil Soc Math Phys Sci 20, 36, 113.

Field, D W, (1976), Phys Stat Sol (a)36, 597.

Fujii, Y, Hoshino, S, Yamada, Y and Shirane, G, (1974), Phys Rev B9, 4549.

Halperin, B I and Varma, C M, (1976), Phys Rev B14, 4030.

Hamilton, W C, (1965), Acta Cryst 18, 502.

Harada, J, Sakata, M, Hoshino, S and Hirotsu, S, (1976), J Phys Soc Jap 40, 212.

Hastings, J B, Shapiro, S M and Frazer, B C, (1978), Phys Rev Lett 40, 237.

Heidemann, A and Wettengel, H, (1973), Z Phys 258, 429.

Hirotsu, S and Sawada, S, (1969), Phys Lett A28, 762.

Hirotsu, S and Sawada, S, (1973), Solid State Comm 12, 1003.

James, R W and Brindley, G W, (1928), Proc Roy Soc A121, 155.

Johnson, C K, (1969), Acta Cryst A25, 187.

Johnson, C K, (1970) in 'Thermal Neutron Diffraction', ed B T M Willis (London : Oxford U P).

Kjems, J K, Shirane, G, Müller, K A and Scheel, H J, (1973), Phys Rev B8, 1119.

te the W's in Eq. (1) in terms of the phonon normal coordinates A(q j)

$$W_\alpha(O_\alpha|q) = \sum_j \sqrt{\hbar/2m_O\omega(q\ j)}\ \tilde{f}_\alpha(O_\alpha|q\ j)A(q\ j), \quad (4)$$

with the renormalized shell eigenvectors

$$\tilde{\mathbf{f}}_\lambda = M^{+1/2}(S_o+\Delta)^{-1}\ T_o^{\dagger} M^{-1/2}\tilde{\mathbf{e}}_\lambda\ . \quad (5)$$

After the factorization involved in the Hartree approximation and the use of Eq. (4), Eq. (1) becomes

$$\Phi_H = (\hbar/4N)\sum_{\lambda\lambda'}(C_{\lambda\lambda'}/\omega_\lambda\omega_{\lambda'})A_\lambda A_{\bar{\lambda}}A_{\lambda'}A_{\bar{\lambda}'}\ , \quad (6)$$

where the 4th order phonon-phonon coupling coefficients are

$$C_{\lambda\lambda'} = (K_{OB,B}\hbar/4m_O^2)\sum_\alpha f_\alpha^2(O_\alpha|\lambda)f_\alpha^2(O_\alpha|\lambda'). \quad (7)$$

The ferroelectric mode, $(0,T_1 0)$, is most strongly coupled with the $T_1 0$ and TA modes in (100) and (110) directions. These couplings are strongly q-dependent, as it is shown in Fig, 2 for q ∥ (100) in $KTaO_3$.

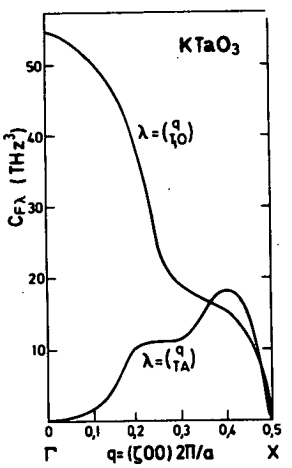


Fig. 2. q-dependence, in [100]-direction, of the coupling coefficients $C_{F\lambda}$ between the ferroelectric, F= $(\vec{0},T_1 0)$, and the TA and $T_1 0$ modes in $KTaO_3$.

The non linear dipolar interaction, Eq. (1), corresponds to a very delocalized 4th order effective interionic potential, in contrast with previous attempts to explain the ferroelectric soft mode behaviour in $ABO_3$ perovskites by considering anharmonic extensions of the short range interionic forces, particularly those between the O and B ions[6,7]. The displacement amplitudes W are related to those corresponding to the cores, U, in the same way as f to e, Eq. (5). If Φ, Eq. (1), is factorized as in the Hartree approximation, the W's are expressed in terms of the U's, and these are transformed to the direct lattice, the following biquadratic effective interionic potential results:

$$\Phi_{ef} = (K_{OB,B}/12)\{\frac{1}{2}\sum_{ii'}(u_i-u_{i'})\varphi(i\ i')(u_i-u_{i'})\}^2 \quad (8)$$

where i ≡ (κℓ), and the 3x3 matrices $\varphi(i\ i')$ are given by

$$\varphi_{\beta\beta'}(i\ i') = \frac{1}{N}\sum_{\alpha q} A_{\alpha\beta}(O_\alpha\kappa|q)A_{\alpha\beta'}(O_\alpha\kappa'|q) \times \times \cos(\mathbf{q}.\mathbf{r}_{i\ i'}) \quad (9)$$

Here A is the matrix $(S_o+\Delta)^{-1}\ T_o^{\dagger}$. The coefficients $\varphi_{\beta\beta'}(i\ i')$ have been calculated for several next nearest neighbours around each ion type. The most important correlations occur among the O and B ions which lie on a line parallel to one of the principal symmetry directions. For these ions the correlations between displacements parallel to the considered line are at least one order of magnitude stronger than those between transverse displacements. In Fig. 3 we show the range of these relevant correlations in $KTaO_3$.

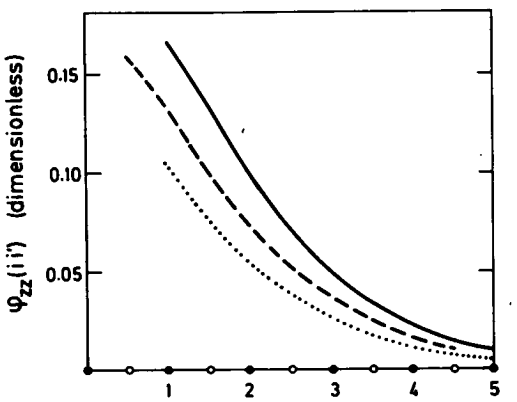


Fig. 3. The coefficients $\varphi_{zz}(ii')$ for the ion pairs (B,B) (full line), (B, 0) (dashed line) and (0,0) (dotted line) lying on the z-axis. On the abscissa the positions of the succecessive neighbours of an ion (B or 0) placed at the origin are indicated.

The anharmonic extensions of the O-B and O-A interionic force constants determined by constraining the model to fit various anharmonic properties, have been shown to describe satisfactorily the softening of the $R_{25}$ mode in $SrTiO_3$[6]. In attempting to fit the temperature dependence of the ferroelectric mode, however, an unreasonably strong 4th order O-B interaction had to be considered in order to overcompensate the negative contribution of the 3rd order anharmonicity. As a consequence of this choice, anharmonic properties which depend on the Ti-O interaction are not described satisfactorily[6]. Now, a non-linear intraionic oxygen polarizability leads to a consistent description of the Raman scatte-

ring and all the phonon interactions related to the ferroelectric soft mode not only in $SrTiO_3$ but also in $KTaO_3$, where no $R_{25}$ soft mode has been observed. We believe, therefore, that the interionic anharmonicities are indeed responsible for those soft modes corresponding to the rotations of the octahedra, which appear also in non-oxidic perovskites, but that the effects of these anharmonicities on the ferroelectric soft mode nearly cancel out, so that the non-linear oxygen polarizability becomes the dominating mechanism in this case. This explains the appearance of ferroelectric soft mode behaviour in oxydic perovskites only. Moreover, the fact that this behaviour is observed only in those crystals with a transition metal ion centered in the oxygen octahedra supports the idea that the oxygen polarizability is anisotropically enhanced due to hybridization between oxygen p-states and transition metal d-states[3]. It is interesting to note that this type of hybridization has been shown[8] to be responsible for phonon anomalies which lead to superconducting transitions in cubic carbides and nitrides with the same transition metal ions ($Ti^{4+}$, $Zr^{4+}$, $Nb^{5+}$, $Ta^{5+}$).

Summarizing, the pathological behaviour of the oxygen polarizability, which leads to strong Raman scattering in oxides, is, in addition, the origin of phonon-phonon interactions in the perovskites which explains the appearance of ferroelectricity in these structures. A self-consistent treatment of these interactions gives a satisfactory description of the phonons in the incipient ferroelectrics $SrTiO_3$ and $KTaO_3$ down to $0^{\circ}K$.

## REFERENCES


1. For recent summaries see: SCOTT, J.F., Rev. Mod. Phys. 46, 83 (1974; GILLIS, N.S. in " Dynamical Properties of Solids", Vol. 2, ed. G.K. Horton and A.A. Maradudin (North-Holland, Amsterdam, 1975), p. 105
2. PYTTE, E., Phys. Rev. B 5, 3758 (1972); CHAVES, A.S., BARETTO, F.C.S. and RIBEIRO, L.A.A., Phys. Rev. Lett. 37, 618 (1976)
3. MIGONI, R., BILZ, H. and BÄUERLE, D., Phys. Rev. Lett. 37, 1155 (1976)
4. For a review on the shell model formalism see: COCHRAN, W., Crit. Rev. Sol. St. Sci. 2, 1 (1971)
5. COMES, R. and SHIRANE, G., Phys. Rev. B 5, 1886 (1972)
6. COWLEY, R.A., Phil Mag. 11, 673 (1965); BRUCE, A.D. and COWLEY, R.A., J. Phys. C 6, 2422 (1973).
7. HÜLLER, A., Z. Phys. 220, 145, (1969)
8. HANKE, W., HAFNER, J. and BILZ H., Phys. Rev. Lett. 37, 1560 (1976)


---

# HIGH-RESOLUTION (DIRECT SPACE) STUDIES OF ANHARMONIC MOTION ASSOCIATED WITH THE STRUCTURAL PHASE TRANSITION IN $SrTiO_3$


G.M. Meyer, R.J. Nelmes and J. Hutton
Department of Physics, Edinburgh University,
Mayfield Road, Edinburgh 9, Scotland.



Data have been collected at room temperature on $SrTiO_3$ to a high resolution limit of $\sin\Theta_{max}/\lambda = 1.2$ $\AA^{-1}$ on a four-circle neutron diffractometer. The harmonic (2nd order) and anharmonic (4th order) thermal parameters have been refined within the approximation of the truncated cumulant expansion. The motions of the strontium and titanium atoms are found to have isotropic mean-square amplitudes —— $U(Sr) = 0.0054(1)$ $\AA^2$ and $U(Ti) = 0.0035(2)$ $\AA^2$ —— with no significant (anharmonic) fourth-cumulant terms. The oxygens have very anisotropic harmonic thermal parameters —— $U_{11} = 0.0125(3)$ $\AA^2$ and $U_{33} = 0.0058(3)$ $\AA^2$ —— with a large, predominantly isotropic, fourth-cumulant term $a^I = 0.0069(8)$ $\AA^4$. A comparison is made with $KMnF_3$ in which the fourth-order cumulant terms on the fluorine atoms display tetragonal components. The relevance of these results to recent models of phase transitions is discussed.


## 1. INTRODUCTION

Many of the classical structural phase transitions of the soft-mode, displacive type have been found more recently to be associated with low-frequency, heavily-damped response and highly anisotropic dynamics (e.g. the soft mode heavily damped well above the transition, the

ıch-debated central peak, strongly structured ffuse scattering). Models put forward to xplain these phenomena (e.g. Lambert-Comès[1] in elation to structured diffuse scattering, and ıe more general microdomain picture proposed Krumhansl and Schrieffer[2]) imply that even ır such displacive systems the time-averaged tructure of the high-temperature phase is a sordered one — with atoms occupying an array sites like that obtained by operating on the w-temperature structure with the high-temperture symmetry.

If the displacement of sites from the an position obtained in this way from the lly saturated low-temperature order paraeter is $\delta_o$, then the actual displacement, $\delta$, ay be anywhere in the range $0 \leqslant \delta \leqslant \delta_o$. The agnitude of $\delta$ is expected to increase from ero as the temperature falls and inter-atomic ynamic correlations extend[3].

One attractive line of attack on the roblem of testing the predictions of such odels for real systems is to do careful conentional crystal structure studies — measurng $S(\underline{Q},\omega=0)$. The latter transforms to $G(\underline{r},t)dt$ directly (where $G(\underline{r},t)$ is the timeependent pair-correlation function). Making nly the assumption of separable scatterers in periodic lattice one extracts $\int\rho(\underline{r},t)dt$, the ime-averaged scattering density. The advantge of this procedure is that it makes no ssumptions whatever about the dynamics of the ystem. Our argument then is that if $\delta \neq 0$ the robability distribution function (p.d.f.) for ne atom(s) concerned ($\equiv \int\rho(\underline{r},t)dt$ in the egion of the atom(s)) will be disordered: hat is, the p.d.f. will be made up of normal ingle-peaked, quasi-harmonic distributions entred on each of the sites. Whether or not nese peaks can be resolved depends on the size f $\delta$ relative to thermal amplitudes and on the esolution to which the p.d.f. is determined. vidently it will generally be necessary to ork to very high resolution.

We report here on an investigation of he p.d.f. of oxygen in $SrTiO_3$ at room temprature. $SrTiO_3$ undergoes a cubic to etragonal transition at $\sim$ 105 K. The change n structure at this transition is known to be rincipally a small rotation of the oxygen octaedra around one of the four-fold axes of the ubic phase; the oxygen displacement, $\delta_o$, is 0.1 Å.

The 'classical' structure of $SrTiO_3$ in its ubic phase (space group Pm3m) is shown in igure 1A. Applying the cubic symmetry to otations of the oxygen octahedra about all the our-fold axes leads to disordering of the type hown in Figure 1B.

## 2. EXPERIMENTAL DETAILS

The sample was a strain-free, flux-grown, ingle crystal of $SrTiO_3$, of approximate imensions 5 mm by 2 mm by 1 mm, kindly supplied y Dr. H.J. Scheel of I.B.M., Zurich.

The experiment was carried out at room emperature on the D8 four-circle neutron

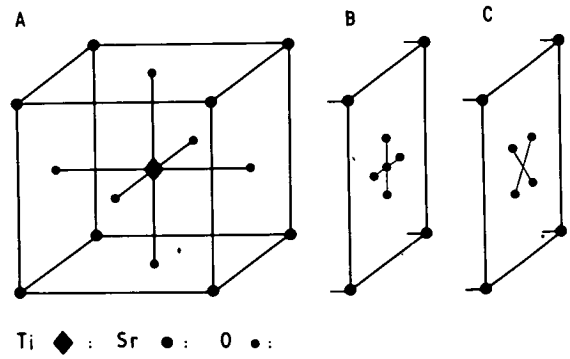


Figure 1. The structure of cubic $SrTiO_3$(A) and possible disordered arrays (exaggerated) for oxygen (B and C).

diffractometer at the Institut Laue-Langevin (I.L.L.), Grenoble. Three equivalents of each independent reflection were measured out to a limit of $\sin\theta/\lambda = 1.2$ Å$^{-1}$ ($\lambda = 0.72$ Å). Standard reflections were measured regularly and the intensity of each was within two standard deviations of the mean value. The full data-set was symmetry-averaged to yield 112 independent reflections. Estimated standard deviations (e.s.d.'s), for weighting subsequent least-squares refinements, were obtained from counting statistics — except for 19 of the low-angle strong reflections (h, k and $\ell$ all even or all odd) which had one or more of the three equivalents differing by more than would be expected from counting statistics. The e.s.d.'s for these were taken from the spread found in the three values. The (111) reflection was later found to be very highly extinguished and was omitted from the data-set used in refinements.

Corrections for thermal diffuse scattering were not made: the corrections at this neutron wavelength are complicated because the neutron velocity is approximately that of the transverse acoustic phonons. However the phonon velocities are quite large, so the corrections would not be expected to alter qualitatively the parameters obtained from the fitting.

## 3. REFINEMENTS

A standard crystallographic least-squares program, modified to refine an isotropic extinction parameter and third- and fourth-cumulant parameters, was used in all the refinements. The addition of third and fourth cumulants[4] modifies the conventional Gaussian Debye-Waller factor by multiplication with third- and fourth-order exponential terms

$$\exp(-W) = \exp(i^2\Sigma h_j h_k K^{jk}) \times \exp(i^3\Sigma h_j h_k h_\ell K^{jk\ell}) \times \exp(i^4\Sigma h_j h_k h_\ell h_m K^{jk\ell m})$$

where the summations are over $j,k,\ell,m = 1,2,3$. The h's are $h^M/a$, where $h^M$ are Miller indices

and a is the unit-cell dimension. $K^{jk\ell}$ and $K^{jk\ell m}$ are the terms of the third- and fourth-order cumulant tensors respectively. The program refines these parameters along with the parameters $K^{jk}$ of the second-order cumulant tensor. The latter is described in this paper in terms of the mean-square amplitudes $U_{jk} = K^{jk}/2\pi^2$ (or simply U for the isotropic case).

The atoms of $SrTiO_3$ have no non-zero third cumulants (because of atomic site symmetry). The fifteen terms in the general fourth-cumulant tensor are reduced to two independent terms in the cases of strontium and titanium and to four independent terms in the case of the oxygen atoms.

Three refinements, I, II and III, were carried out, the refined parameters in each case being:

I) a scale factor, an isotropic extinction parameter and harmonic thermal parameters (i.e. second cumulants) on all atoms;

II) as for I) but in addition fourth-cumulant parameters on oxygen atoms only;

III) as for I) but in addition fourth-cumulant parameters on all the atoms.

The addition of fourth-cumulant parameters on the oxygen atoms was found to result in a very highly significant improvement in the fit to the data. In the notation of Hamilton[5], the R-factor ratio of the weighted residuals for models I and II is $\mathcal{R} = 1.7$. The 99.99% significance point of the distribution of $\mathcal{R}$ for the relevant degrees of freedom is 1.1, so the improvement in fit with the addition of fourth-cumulant parameters on the oxygens is significant well beyond the 99.99% level. In contrast the addition of fourth-cumulant parameters on the strontium and titanium atoms (model III) was not significant even at the 50% level.

TABLE 1. The thermal parameters for $SrTiO_3$. The models, I and II, are described in the text. The U's are (harmonic) second cumulants (mean-square amplitudes) in $Å^2$; $U_{11}(0)$ is the amplitude in the Sr-O plane, and $U_{33}(0)$ along the Ti-O direction. The K's are (anharmonic) fourth cumulants on the oxygen in $Å^4$. Estimated standard deviations on refined values are given in parentheses.

| | Harmonic model (I) | Anharmonic model (II) | Calculated values[6] |
|---|---|---|---|
| U(Sr) | 0.0052(2) | 0.0054(1) | 0.0062 |
| U(Ti) | 0.0040(2) | 0.0035(2) | 0.0032 |
| $U_{11}(0)$ | 0.0101(2) | 0.0125(3) | 0.0102 |
| $U_{33}(0)$ | 0.0039(2) | 0.0058(3) | 0.0035 |
| $K^{1111} = K^{2222}$ | | 0.0076(8) | |
| $K^{3333}$ | | 0.0057(7) | |
| $K^{1122}$ | | 0.0023(4) | |
| $K^{2233} = K^{3311}$ | | 0.0023(2) | |

The results for models I and II are shown in Table 1. Stirling[6] has fitted harmonic, but deformable, shell models to the phonon dispersion curves in $SrTiO_3$. From these models he calculated the thermal parameters shown in Table 1. It is seen that there is good agreement between his calculations and our results. (It is not obvious that either of our refinements should produce the same results as Stirling's calculations since the agreement is dependent on the form and extent of the anharmonicity in $SrTiO_3$.)

## 4. OXYGEN PROBABILITY DISTRIBUTION FUNCTION

The probability distribution function (p.d.f.) of an atom is the Fourier Transform of its Debye-Waller factor. If the cumulant terms higher than second-order are small, an approximation to the transform is given by the Edgeworth expansion[4] about the harmonic p.d.f. (as determined in refinement I). When this is done for the oxygen atoms, we find that the ripples from truncating the Edgeworth expansion at the fourth-order terms are so severe that a significant proportion of the resulting approximate p.d.f. is negative. And it is not possible to transform the Debye-Waller factor (as approximated by the second and fourth cumulants) numerically since, with the cumulant parameters found in this case, it falls to only $\sim 0.5$ (from unity at the origin of reciprocal space) before increasing indefinitely at large reciprocal lattice vectors (beyond the range of our present measurements). Some other method must then be found to describe either the Debye-Waller factor or the p.d.f. more realistically; and at present it is not possible to say more about the oxygen p.d.f. than that it is very significantly non-Gaussian and that the perturbation seems (see below) to be principally isotropic.

## 5. DISCUSSION

It is instructive to decompose the oxygen fourth cumulants into tensors of decreasing symmetry[8] —— isotropic, cubic and tetragonal.

TABLE 2. Values for the oxygen and fluorine fourth cumulants when decomposed into symmetry elements (in $Å^4$).

| Component | | O in $SrTiO_3$ | F in $KMnF_3$ |
|---|---|---|---|
| Isotropic | $a^I$ | 0.0069(8) | -0.0017(41) |
| Cubic | $a^C$ | 0.0000(6) | 0.0023(34) |
| Tetragonal | $a^T$ | 0.0006(5) | -0.0032(19) |
| | $j^T$ | 0.0000(2) | 0.0035(15) |

The result of doing this is shown in Table 2 column 1. It is seen that only the isotropic term defined as[8]

$$a^I = \frac{(2K^{1111} + K^{3333}) + 2(2K^{3311} + K^{1122})}{5}$$

is significant. This is of interest in view of the work of Bruce and Cowley[7], which extends the harmonic model fitting of Stirling[6] to include anharmonic force constants. The free energy they obtain for $SrTiO_3$ suggests that

there are two different competing superpositions of the three-fold degenerate soft mode in the cubic phase. (The parameter $A_n$ in equation 14 of that paper is small.) Thus, although $SrTiO_3$ has the same tetragonal structure as $KMnF_3$ below $T_c$ (a rotation of the oxygen octahedra about a <100> axis), the crystal is 'unaware' of this above $T_c$ and there is competition from the superposition which condenses in the rhombohedral $LaAlO_3$ structure (a rotation of the oxygen octahedra about a <111> axis). The latter distortion would correspond to a dynamic disorder in the cubic phase of the type shown in Figure 1C. So, if $\delta \neq 0$, the oxygens in $SrTiO_3$ may show a mixture of the distributions illustrated in Figures 1B and 1C and thus be disordered over nine sites —— a quasi-isotropic distribution, at least in the Sr——O plane.

It is also of interest to compare the $SrTiO_3$ refinements with refinements of a preliminary experiment on $KMnF_3$ performed under similar conditions (but with fewer reflections and collected to less precision). The $KMnF_3$ results are shown in Table 3. The salient features are:

TABLE 3. The thermal parameters for $KMnF_3$. The models, I and II, are as for $SrTiO_3$. The units and symbols are as explained in the legend to Table 1 —— with Sr, Ti and O replaced, respectively, by K, Mn and F.

| | Harmonic model (I) | Anharmonic model (II) |
|---|---|---|
| U(K) | 0.0187(3) | 0.0185(5) |
| U(Mn) | 0.0066(2) | 0.0067(5) |
| $U_{11}$(F) | 0.0344(2) | 0.0340(4) |
| $U_{33}$(F) | 0.0068(2) | 0.0080(4) |
| $K^{1111} = K^{2222}$ | | -0.0026(36) |
| $K^{3333}$ | | 0.0070(20) |
| $K^{1122}$ | | -0.0088(32) |
| $K^{2233} = K^{3311}$ | | 0.0018(12) |

1) the significantly larger harmonic terms on all atoms (in comparison to $SrTiO_3$);
2) a large anisotropy in the fluorine harmonic parameters (similar to oxygen);
3) a lack of anharmonicity on the potassium and manganese atoms (similar to strontium and titanium), and significant anharmonicity on the fluorine;
4) but, in contrast to the oxygen atoms in $SrTiO_3$, the fluorine atoms in $KMnF_3$ exhibit non-isotropic anharmonicity. On decomposing the fourth-cumulant tensors (see Table 2) only the tetragonal components[8]

$$a^T = \frac{(K^{1111} - K^{3333})}{3} \quad \text{and} \quad j^T = \frac{(K^{3311} - K^{1122})}{3}$$

appear significant (at the accuracy to which the data are collected). This possibly suggests that $KMnF_3$ is more dominated by the superposition which would generate disorder of the type shown in Figure 1B. (As far as the authors are aware, no anharmonic lattice-dynamic calculations have been made for $KMnF_3$, so the parameter $A_n$ (Bruce and Cowley, equation 14) is unknown.)

In conclusion we reiterate and emphasise that we are not yet able to derive a p.d.f. for anharmonicity as large as that found on the oxygen of $SrTiO_3$ (and the fluorine of $KMnF_3$). So we cannot say whether our results, in their present form, suggest $\delta \neq 0$. We are currently investigating a more realistic description of the p.d.f. and developing the techniques of incorporating this into least-squares refinement. These methods will be used on much higher resolution (sin $\theta/\lambda$ limit $\simeq 2.2$ Å$^{-1}$) $SrTiO_3$ data recently collected at 115 K on the D9 four-circle diffractometer at the I.L.L. In the future we hope to compare the results with similar very high-resolution data from other 'antiferroelectric' perovskites.

We are most grateful to Dr. H.J. Scheel of I.B.M., Zurich, for providing the specimen crystal, to Dr. M.S. Lehmann and Mr. J. Allibon of I.L.L., Grenoble, for generous assistance with the experiment and to Dr. A.D. Bruce of this Department for many lively discussions. We would like to acknowledge the support of the Science Research Council for a Research Fellowship (GMM), a Research Studentship (JH) and use of the facilities of I.L.L., Grenoble.

## REFERENCES

1. For example COMÈS, R., LAMBERT, M. and GUINIER, A., Acta Cryst. A26, 244 (1970); DÉNOYER, F., COMÈS, R. and LAMBERT, M., Solid State Comm. 8, 1979 (1970).
2. KRUMHANSL, J.A. and SCHRIEFFER, J.R., Phys. Rev. B11, 3535 (1975).
3. BRUCE, A.D. and SCHNEIDER, T., Phys. Rev. B, to be published.
4. JOHNSON, C.K. in Thermal Neutron Scattering ed. B.T.M. Willis, Oxford University Press, 132 (1970).
5. HAMILTON, W.C., Acta Cryst. 18, 502 (1965).
6. STIRLING, W.G., J. Phys. C, 5, 2711 (1972).
7. BRUCE, A.D. and COWLEY, R.A., J. Phys. C.6, 2422 (1973).
8. THORNLEY, F.R. Unpublished work.

# LATTICE DYNAMICAL PROPERTIES OF DISORDERED OR UNSTABLE LATTICES

K. L. Ngai and T. L. Reinecke
Naval Research Laboratory, Washington, D. C. 20375, USA

A model based on local structural excitations can account for many unusual lattice properties of systems with disorder or lattice instability. Such systems include nonstoichiometric ferroelectrics, binary and ternary superconductors, amorphous semiconductors, and ionic conductors. The effects of the interaction between phonons and local structural excitations on the lattice properties are obtained and discussed.

## 1. INTRODUCTION

Recently we have studied the lattice dynamical properties of several different classes of noncrystalline or disordered solids. These include (i) the insulating non-stoichiometric ferroelectrics in the tetragonal tungsten bronze T1 structure,[1] (e.g. $Sr_{1-x}Ba_xNb_2O_6$ (SBN), and $Ba_{4+x}Na_{2-2x}Nb_{10}O_{30}$), (ii) binary and ternary superconductors with structural instabilities,[2,3] (iii) amorphous semiconductors and insulators,[4] and (iv) Na β-alumina, a typical superionic conductor.[5] In these systems there are invariably some "anomalous" lattice dynamical and thermodynamical properties which cannot be understood on the basis of crystalline lattice dynamics. We have recently contributed to the fundamental understanding of various aspects of the anomalous behavior of these materials, by identifying a physical ingredient which is common to all of these "disordered" solids.

The common characteristic of these systems is the existence of what can be called "local structural excitations"[1-5] which interact with the lattice and give rise to the "anomalous" lattice properties. The local structural excitations are known in the literature by several names including "local rearrangement modes,"[4] "disorder modes,"[5] "Anderson Halperin Varma-Phillips tunneling centers,"[6] "local structural excitations"[2,3] and "configuration tunneling excitations."[1] For example, in amorphous semiconductors and insulators it was suggested[6] that, due to the structural disorder, a group of atoms can be excited from one configuration to another separated by an energy barrier. These AHV-Phillips tunneling excitations[6] account for the observed linear specific heat[7] and other lattice properties of such materials. Another possible source for such excitations in amorphous systems are the two-electron states[8] in the energy gap.

Consider the tetragonal tungsten bronze structure ferroelectrics[1,9] such as SBN or the isostructural T1 superconducting tungsten bronze compound[3] $Na_xWO_3$. The network of distorted $NbO_6$ (or $WO_3$) octahedra are connected in such a way that there are pentagonal and square tunnels which are occupied randomly by the Ba and Sr ions of SBN, and Na ions of $Na_xWO_3$. The structures of these materials are unusual because there are other structural phases such as the T2 separated from T1 by a small energy. There exists a geometrical operation[1,10] by which a local group of octahedra form a local T2 defect in T1 structure. Hence, locally, each group of four corner-sharing octahedra have (at least) two free-energy states corresponding to the local T1 and T2 states; they are separated by a barrier due to the electronic bonding changes involved.[1] We have called the excitations between these two local states "configurational tunneling excitations" (CTEs).[1]

"High" $T_c$ superconductors such as sputtered films, the A-15s, and binary and ternary compounds and alloys, are often characterized by the existence of structural instabilities, by the presence of more than one phase, by defects, and by structural disorder and nonstoichiometry. Again there is the possibility of the existence of more than one local structural state.[2,3] Excitations between the two local states then constitute the "local structural excitations" in these materials.[2,3]

As a final example consider Naβ-alumina, a typical fast ion conductor. It was first suggested by us[5] that the $Na^+$ ionic motion involves cooperative changes in position and energy of varying numbers of ions and atoms in clusters of different configurations; these cooperative effects in turn can give rise to excitations between two (or more) of the ionic cluster configurations with an accompanying spectrum of excitation energies which constitute the local structural excitations. We have deduced the existence of a smooth power low density of states of these modes from the low frequency ($\lesssim 10^{11}$Hz) conductivity of Na-β alumina.[5] Such modes lead naturally to a linear specific heat, and indeed such a linear specific heat in β-alumina was later observed experimentally.[11]

Thus local structural excitations occur widely in disordered systems but are not present in crystalline solids. The effects of these excitations on the lattice dynamical properties are therefore of great interest.

## 2. LATTICE DYNAMICAL EFFECTS ARISING FROM LOCAL STRUCTURAL EXCITATIONS

The physical effects of "local structural excitations" (LSEs) arise mainly from the two lowest lying states. Thus for simplicity we consider only these two states separated by energy $\Delta_j$ spanned by the Pauli spin operators $\vec{\sigma}_j$. We consider a distribution of isolated LSEs interacting with the harmonic phonons by means of

GLOSSARY OF COMMONLY USED SYMBOLS AND ABBREVIATIONS

| | |
|---|---|
| $a_{n\ell j}$ | an $n^{th}$-order F.I. parameter associated with an ion on m3m site symmetry |
| b(X) | the coherent neutron scattering length of ion X |
| $b_{n_z nmp}$ | an $(n_z+n)^{th}$-order F.I. parameter associated with an ion on 4/mmm site symmetry |
| $d^i$ | a fourth-order orthogonal-cumulant parameter |
| EPR | electron paramagnetic resonance |
| $F_{calc}(\underline{Q})$ | a calculated structure amplitude |
| $F_{obs}(\underline{Q})$ | an observed structure amplitude |
| F.I. | Fourier-invariant |
| I.L.L. | Institut Laue-Langevin, Grenoble |
| m.s.a. | mean-square amplitude |
| p.d.f. | probability density function |
| p.w.a. | partial weights analysis |
| $P_i(\underline{r})$ | the probability density of ion i at $\underline{r}$ |
| $\underline{Q}$ | a vector of the reciprocal lattice |
| $\underline{r}$ | the ionic displacement from the mean position |
| R | the residual |
| $R_w$ | the weighted residual |

Kobayashi, H, (1978), 'Modeling and Analysis', IBM Systems Programming Series (Reading, Mass : Addison Wesley).

Krumhansl, J A and Schrieffer, J R, (1975), Phys Rev B11, 3535.

Kurittu, J and Merisalo, M, (1977), Report Series in Physics, HU-P-132, University of Helsinki.

Kurki-Suonio, K, (1977), Israel J Chem 16, 115, 132.

Kurki-Suonio, K, Merisalo, M and Peltonen, H, (1979), Phys Scripta 19, 57.

Lipson, H and Cochran, W, (1966), 'The Determination of Crystal Structures' (London : Bell).

Lonsdale, K, (1962) in 'Fifty Years of X-Ray Diffraction', ed P P Ewald (Utrecht : Oosthoek).

Maetz, J, Müllner, M, Jex, H and Peters, K, (1978), Solid State Comm 28, 555.

Maradudin, A A and Flinn, P A, (1963), Phys Rev 129, 2529.

Mel'nikova, C V, Aleksandrov, K S, Anistratov, A T and Beznosikov, B V, (1977), Sov Phys Sol State 19, 18.

Merisalo, M and Larsen, F K, (1977), Acta Cryst A33, 351.

Merisalo, M and Järvinen, M, (1978), Phil Mag B37, 233.

Merisalo, M and Kurittu, J, (1978), J Appl Cryst 11, 179.

Minkiewicz, V J, Fujii, Y and Yamada, Y, (1970), J Phys Soc Jap 28, 443.

Møller, C K, (1959), Mat Fys Medd Danske Vidensk Selsk 32, No 2, 1.

Müller, K A and Berlinger, W, (1971), Phys Rev Lett 26, 13.

Nelmes, R J, (1979), to be published in Ferroelectrics.

Nelmes, R J, (1979a), submitted to Acta Cryst.

Pawley, G S, (1971) in 'Advances in Structure Research by Diffraction Methods', vol IV, eds W Hoppe and R Mason (Oxford : Pergamon).

Prager, P R and Harvey, G G, (1975), Acta Cryst A31, 780.

Ridou, C, Rousseau, M and Freund, A, (1977), J Phys, Paris 38, L 359.

Riste, T, Samuelson, E J, Otnes, K and Feder, J, (1971), Solid State Comm 9, 1455.

Rossmanith, E, (1977), Acta Cryst A33, 593.

Rousseau, M, (1977), Thesis, Le Mans.

Rousseau, M, (1979), J Phys, Paris 40, L439.

Rousseau, M, Nouet, J and Zarembowitch, A, (1974), J Phys Chem Solids 35, 921.

Rousseau, M, Nouet, J and Almairac, R, (1977), J Phys, Paris 38, 1423.

Sakata, M, Harada, J, Rouse, K D and Cooper, M J, (1978), Acta Cryst A34, S284.

Sakata, M, Harada, J, Cooper, M J and Rouse, K D, (1979), submitted to Acta Cryst.

Schneider, T and Stoll, E, (1976), Phys Rev B13, 1216.

Schwartz, K D and Elbaum, C, (1970), Phys Rev B1, 1512.

Shapiro, S M, Axe, J D, Shirane, G and Riste, T, (1972), Phys Rev B6, 4332.

Shirane, G, Minkiewicz, V J and Linz, A, (1970), Solid State Comm 8, 1941.

Sirotin, Y I, (1964), Sov Phys Dokl 8, 652.

Stewart, J M, (1972), The X-Ray System - Version of June 1972. Tech Report TR-192, Computer Science Center, University of Maryland.

Stirling, W G, (1972), J Phys C5, 2711.

Thornley, F R and Nelmes, R J, (1974), Acta Cryst A30, 748.

Thornley, F R, Kennedy, N S J and Nelmes, R J, (1976), J Phys C9, 681.

Torberg-Jensen, N, (1969), J Chem Phys 50, 559.

Truter, M R, Cruickshank, D W J and Jeffrey, G A, (1960), Acta Cryst 13, 855.

Wallace, D L, (1958), Ann math Stat 29, 635.

Willis, B T M, (1969), Acta Cryst A25, 277.

Zachariasen, W H, (1967), Acta Cryst 23, 558.

Cooper, M J, Rouse, K D and Willis, B T M, (1968), Acta Cryst A24, 484.

Cooper, M J and Sakata, M, (1979), Acta Cryst A35, 989.

Dawson, B, (1967), Proc Roy Soc 298, 255.

Dawson, B, (1967a), Proc Roy Soc 298, 264.

Dawson, B, Hurley, A C and Maslen, V W, (1967), Proc Roy Soc 298, 289.

Dawson, B and Willis, B T M, (1967), Proc Roy Soc 298, 307.

Koester, L, (1977) in 'Springer Tracts in Modern Physics', vol 80, ed G Höhler (Berlin, Heidelberg : Springer-Verlag).

Rae, A D, (1975), Acta Cryst A31, 334.

PUBLICATIONS

(i) High Resolution (Direct Space) Studies of Anharmonic Motion Associated with the Structural Phase Transition in $SrTiO_3$. G M Meyer, R J Nelmes and J Hutton, (1978), Proc Int Conf Lattice Dynamics, Paris 1977, ed M E Balkanski (Paris : Flammarion), 652.

(ii) High Resolution Structural Studies of Perovskites in Relation to the Nature of their Structural Phase Transitions. J Hutton, G M Meyer and R J Nelmes, (1978), Acta Cryst, A34, S303.

(iii) The Pressure and Temperature Dependence of the Structure of Paraelectric (Tetragonal) $KH_2PO_4$ and $KD_2PO_4$. R J Nelmes, G M Meyer, E Baharie and J Hutton, (1978), Acta Cryst, A34, S314.

(iv) High-resolution Studies of Cubic Perovskites by Elastic Neutron Diffraction : $CsPbCl_3$. J Hutton, R J Nelmes, G M Meyer and V R Eiriksson, (1979), J Phys C in press.

| | |
|---|---|
| Sc | the overall scaling factor |
| T | the absolute temperature |
| $T_c$ | the cubic → tetragonal phase transition temperature |
| TDS | thermal diffuse scattering |
| $u^{jk}$ | the (j,k) element of the mean-square vibrational amplitude tensor |
| $V(\underline{r})$ | the one-particle ionic potential at $\underline{r}$ |
| $w_i$ | the weight assigned to the $i^{th}$ $F_{obs}(\underline{Q})$ |
| $W_i(\underline{Q})$ | the temperature factor at $\underline{Q}$ |
| $\alpha$ | the quantity used in the correction of the measured intensity for the effects due to TDS |
| $\alpha_s$ | the significance level used in the ratio tests |
| $\delta$ | the local order parameter |
| $\xi$ | the 'factor of scepticism' |
| $\theta_B$ | the Bragg angle |
| $\lambda$ | the incident wavelength |
| $\sum w\Delta^2$ | the weighted sum of squares |
| $\sigma(F_{obs})$ | the standard deviation of $F_{obs}$ |